



Pan, Zhongyin (2015) *Modelling and design of ultrasonic bone cutting blades*. PhD thesis.

<http://theses.gla.ac.uk/7211/>

Copyright and moral rights for this thesis are retained by the author

A copy can be downloaded for personal non-commercial research or study

This thesis cannot be reproduced or quoted extensively from without first obtaining permission in writing from the Author

The content must not be changed in any way or sold commercially in any format or medium without the formal permission of the Author

When referring to this work, full bibliographic details including the author, title, awarding institution and date of the thesis must be given

# MODELLING AND DESIGN OF ULTRASONIC BONE CUTTING BLADES

Zhongyin Pan

A thesis for the degree of Doctor of Philosophy (PhD)

Submitted to the School of Engineering,  
College of Science and Engineering,  
University of Glasgow

December, 2015

# Abstract

Ultrasonic cutting technology has been introduced for surgical applications since the 1950s. Ultrasonic bone cutting applies high frequency mechanical vibration of a blade tuned at a specific frequency to make incision on human hard tissues. It offers advantages such as improved safety, smooth and precise cutting. To facilitate the design of high performance surgical ultrasonic bone cutting blades, this thesis is devoted to the modelling and designing of ultrasonic blades with an attempt to better understand the dynamic characteristics of blade and improve the conventional design method.

A non-coupled vibration analytical model which deals with four modes of vibration, including longitudinal oscillation, flexural bending, lateral bending, and torsional vibration of ultrasonic blades, was proposed based on one-dimensional theories. The model allows the estimation of the modal parameters of a blade without establishing a 3D model. The experimental study of this model using a uniform beam and a sectional ultrasonic blade showed that the model predicted the modal frequencies of these structures with satisfactory accuracy. This suggested that the analytical model can be used as an alternative method to FEA in the characterisation of ultrasonic blades.

Two coupled models, a parametric vibration model and a longitudinal-bending coupled vibration model, were proposed to study the coupled vibration of ultrasonic blades. The parametric vibration model formulated the coupled vibration using a lumped mass beam. This enabled the investigation of interaction between the vibration modes based on a simple one-dimensional structure. However, this model resulted in governing equations of considerable complexity, which were considered to be more suitable for the purpose of theoretical study instead of performance prediction. In addition, a longitudinal-bending coupled model was proposed in this study with an attempt to understand a type of coupled vibration that is commonly observed in ultrasonic blades of beam-like profile. The model was established by introducing an extra rotation moment in the one-dimensional bending equation. Two numerical iteration approaches, with their implementation and error analysis detailed, were proposed to solve this model.

An optimal design method was proposed in this study with an aim to improve the conventional design process of ultrasonic blades by applying mathematical algorithms instead of the designers' experience and intuition to optimise the design. The method was introduced based on the concept of performance indicators that measure specific physical characteristics of a blade using mathematical functions. Four kinds of indicators, the frequency based, gain based, displacement based and stress based indicators, which evaluate the main dynamic characteristics of ultrasonic blades, were detailed in this study. The process of the optimal design method consists of three major stages: formulation, optimisation and verification. The concept of the proposed method is to maximise the blade performance through the optimisation of the performance indicators. This can improve the quality of design by making sure the most desired characteristics are achieved in the blade. A software toolkit was developed using the Abaqus script interface and Python language in order to apply this method in the design of ultrasonic blades.

Five ultrasonic bone cutting blades with different types of cutting edges were designed using either the conventional or the optimal design method. These blades were subjected to ultrasonic cutting tests under various cutting conditions. Ultrasonic cutting performed on biomechanical samples, ovine femur and rat bones showed that the blades were capable of making incisions on bones without the requirement of large applied force. Positive linear correlation between the applied force and the cutting speed was found in the ultrasonic cutting carried out under static applied force, and positive linear relationship between the applied force and the surface temperature was observed in the ultrasonic cutting carried out under sliding motion. The presence of elevated temperatures in the cutting tests suggested that the blades require the application of cooling in ultrasonic bone cutting. The study confirmed that the proposed optimal design method was an effective design approach. The blades were designed with expected vibration characteristics and satisfactory cutting performance.



# Acknowledgement

**Those who sow with tears will reap with songs of joy.**

——Psalm 126:5

When I finally completed the writing of this thesis, the images of my PhD study, which were filled with the hard working hours, disappointed moments, joy of success and even cries, jumped out from my memory again, reminding me the past years of my life. I realised I was such a blessed person who not only reaped a degree but had also found peace, love and joy during this period. I would like to dedicate this thesis to all those who have helped, supported and loved me in my life, especially in my tough times.

First and foremost, I would like to express my sincerest gratitude to my supervisor Prof. Lucas. This thesis would not have come to existence without her patience, encouragement and guidance in the past years.

Thanks are extended to Dr. Ganilova for her contribution in my research and her help in the language correction. Also thanks to Prof. Cartmell, who gave me useful suggestions on math and modelling.

Thanks are expressed to Prof. Hu, my MSc supervisor in China. His encouragement gave me confidence to pursue a PhD degree.

I would like to thank my colleagues in the University of Glasgow, and my friends in Glasgow and Edinburgh. My study and life would have been very difficult and dull without them.

Finally, I would like to give my special thanks to my family—my parents, my sister, and especially my beloved wife. Their support is the power moving me forward in my life. The completion of my study would be unimaginable without their love and sacrifice.

Thanks to all!

# Contents

<b>Abstract</b> .....	<b>I</b>
<b>Acknowledgement</b> .....	<b>III</b>
<b>Contents</b> .....	<b>IV</b>
<b>List of Tables</b> .....	<b>VII</b>
<b>List of Figures</b> .....	<b>VIII</b>
<b>Chapter 1 Introduction</b> .....	<b>1</b>
1.1 Introduction.....	1
1.2 Ultrasound and Power Ultrasonics.....	2
1.2.1 The Field of Ultrasonics.....	2
1.2.2 Early History of Ultrasound.....	3
1.2.3 Effects of High Power Ultrasound .....	6
1.3 Industry Applications of High Power Ultrasonics .....	7
1.3.1 Ultrasonic Cleaning .....	7
1.3.2 Metal/Plastic Welding.....	8
1.3.3 Ultrasonic Assisted Machining .....	8
1.3.4 Ultrasonic Cutting .....	9
1.4 Bone Cutting in Surgery .....	13
1.4.1 Structure of Bone .....	13
1.4.2 Heat Generation and Thermal Damage of Bone.....	14
1.4.3 Conventional Bone Cutting Instruments.....	15
1.4.4 Ultrasonic Bone Cutting Technology .....	16
1.5 Design and Characterisation of Ultrasonic Cutting Blades .....	20
1.5.1 Ultrasonic Cutting System .....	20
1.5.2 Modelling and Analysis .....	22
1.5.3 Design of Ultrasonic Components .....	25
1.5.4 Design of Ultrasonic Blades .....	29
1.5.5 The Method of Optimal Design .....	31
1.6 Summary of Work.....	33
<b>Chapter 2 Analytical Modelling of Ultrasonic Blades Operating in a Single Mode of Vibration</b> .....	<b>35</b>
2.1 Introduction.....	35
2.1.1 Characterising Vibration Parameters and One-Dimensional Theories .....	35
2.1.2 Modelling of Longitudinal Vibration.....	36
2.1.3 Modelling of Bending Vibration.....	37
2.1.4 Modelling of Torsional Vibration.....	38
2.2 One-Dimensional Theories and Vibration Equations .....	39
2.2.1 Theory of Longitudinal Vibration.....	39

2.2.2 Theory of Bending Vibration.....	42
2.2.3 Theory of Torsional Vibration.....	44
2.3 Modelling of Ultrasonic Blades.....	46
2.3.1 Shape Parameters and Shape Functions.....	46
2.3.2 Finite Difference Method.....	49
2.3.3 Modelling of Longitudinal and Torsional Vibration.....	51
2.3.4 Modelling of Bending Vibration.....	55
2.4 Case Study and Results.....	60
2.4.1 Case Study of a Uniform Beam.....	60
2.4.2 Case Study of an Ultrasonic Blade.....	66
2.5 Summary.....	70
<b>Chapter 3 Analytical Modelling of Ultrasonic Blades Operating in Coupled Vibration.....</b>	<b>72</b>
3.1 Introduction.....	72
3.1.1 Coupled Vibration in Ultrasonic System and Beam-Like Structures.....	72
3.1.2 Parametric and Auto-Parametric Vibration of Beam-Like Systems.....	74
3.1.3 Other Research on the Coupled Vibration of Beam-Like Systems.....	75
3.2 A Model for Parametric Excited Cantilever Beams.....	77
3.2.1 Assumptions and Representation of the Problem.....	77
3.2.2 System Energy and Equation of Motion.....	81
3.2.3 Discussion.....	83
3.3 A Model for Longitudinal-Bending Coupled Vibration.....	84
3.3.1 Basic Assumptions and Coupled Dynamic Equation.....	85
3.3.2 Finite Difference Method and Solution.....	86
3.3.3 High Order Finite Difference Method (27-Point Stencil) and Solution .....	92
3.3.4 Error Analysis and Comparison of the Finite Difference Methods.....	99
3.3.5 Case Study.....	102
3.3.6 Discussion.....	104
3.4 Summary.....	106
<b>Chapter 4 Blade Performance Indicators and Optimal Design Method.....</b>	<b>108</b>
4.1 Introduction.....	108
4.1.1 The Conventional Method and Design Strategies.....	108
4.1.2 The Application of Optimisation in the Design of Ultrasonic Devices .....	110
4.2 Blade Performance Indicators.....	113
4.2.1 The Concept of Performance Indicators.....	113
4.2.2 Frequency Based Indicators.....	116
4.2.3 Gain Based Indicators.....	118
4.2.4 Displacement Based Indicators.....	119
4.2.5 Stress Based Indicators.....	121
4.2.6 Other Types of Indicators.....	123

4.2.7 Summary .....	123
4.3 Optimisation Algorithms .....	124
4.3.1 Exhaustive Search and Graphic Method .....	125
4.3.2 Linear Programming Problem and Simplex Method .....	125
4.3.3 Genetic Algorithm .....	127
4.3.4 Simulated Annealing Algorithm .....	129
4.3.5 Multi-objective Optimisation .....	131
4.4 Proposal of an Optimal Design Method .....	132
4.4.1 Formulation of the Problem .....	133
4.4.2 Optimisation .....	137
4.4.3 Blade Verification .....	137
4.4.4 Implementation and Programming .....	138
4.5 Summary .....	143
<b>Chapter 5 Design of Ultrasonic Cutting Blades and Experiments .....</b>	<b>146</b>
5.1 Introduction .....	146
5.2 Blade Designed Using Conventional Method .....	147
5.2.1 Blade I: Blade with Sharp Cutting Edge .....	147
5.2.2 Blade II: Blade with Serrated Cutting Edge .....	166
5.2.3 Summary .....	173
5.3 Blade Designed Using Optimal Method .....	175
5.3.1 Blade III: Blade Shape and Geometry Parameters .....	175
5.3.2 Blade Performance Indicators .....	177
5.3.3 Calculation and Result Discussion .....	182
5.3.4 Experimental Verification .....	190
5.3.5 Ultrasonic Cutting Test .....	193
5.3.6 Summary .....	212
5.4 Discussion .....	214
<b>Chapter 6 Conclusions and Further Work .....</b>	<b>218</b>
6.1 Conclusions .....	218
6.1.1 Analytical Modelling of Ultrasonic Blades .....	218
6.1.2 Proposal of the Optimal Design Method .....	220
6.1.3 Design of Ultrasonic Bone Cutting Blades .....	221
6.2 Further Work .....	223
<b>Appendix .....</b>	<b>225</b>
A.1 Undetermined Coefficient Method .....	225
A.2 Selected Matlab Script for One Dimensional Analytical Modelling .....	227
A.3 Selected Matlab Script for Longitudinal-Bending Coupled Analytical Modelling .....	235
A.4 Selected Python Script of Optimal Design Toolkit .....	238
<b>Publications .....</b>	<b>247</b>
<b>Reference .....</b>	<b>248</b>

# List of Tables

Table 3.1 Conditions and Settings of Analysis .....	102
Table 4.1 Frequency Based Indicators .....	117
Table 4.2 Gain Based Indicators .....	119
Table 4.3 Displacement Based Indicators.....	120
Table 4.4 Stress Based Indicators .....	122
Table 4.5 Summary of Indicators.....	124
Table 4.6 Main Files of the Optimal Design Library.....	141
Table 5.1 Properties of Ti90Al6V4 .....	149
Table 5.2 Results of FEA (Mode Shapes and Modal Frequencies).....	151
Table 5.3 Results of EMA and Comparison with FEA .....	158
Table 5.4 Material Properties of Biomechanical Material and Bones .....	160
Table 5.5 Results of FEA (Mode Shapes and Modal Frequencies).....	168
Table 5.6 Results of EMA and Comparison with FEA .....	172
Table 5.7 Blade Geometry Parameters .....	176
Table 5.8 Performance Indicators .....	178
Table 5.9 Input for Stress Analysis.....	180
Table 5.10 Constraints of Indicators/Parameters .....	182
Table 5.11 Parameters and Indicators of the Optimal Design .....	187
Table 5.12 Results of Modal Analysis.....	188
Table 5.13 Results of EMA and Comparison with FEA .....	192
Table 5.14 Mechanical Properties of Biomechanical Material [255] .....	198
Table 5.15 Standard Deviation and Relative Error .....	200
Table 5.16 Correlation Coefficients and Model Parameters.....	201
Table 5.17 Correlation Coefficients and Average Temperature .....	203
Table 5.18 Cutting Settings.....	206
Table 5.19 Correlation Coefficients and Model Parameters.....	210
Table 5.20 Ultrasonic Cutting Tests .....	213
Table 5.21 Ultrasonic Blades.....	214

# List of Figures

Figure 1.1 Ultrasonic Cleaning.....	8
Figure 1.2 Ultrasonic Food Cutting .....	11
Figure 1.3 Structure of Bone [58].....	14
Figure 1.4 Bone Cutting Tools.....	15
Figure 1.5 Commercial Ultrasonic Cutting Device and Tool Tip (Mectron, Micropiezo S [39]).....	19
Figure 1.6 Ultrasonic System, Acoustic Unit .....	21
Figure 1.7 Representation of One-dimensional Structure.....	25
Figure 1.8 Conventional Design Process of Ultrasonic Blades .....	29
Figure 2.1 Longitudinal Vibration of a Beam.....	40
Figure 2.2 Bending Vibration of a Beam.....	42
Figure 2.3 Torsional Vibration of a Beam .....	44
Figure 2.4 Sectional Blade.....	47
Figure 2.5 Shape of Cross-section .....	47
Figure 2.6 Prandtl Function .....	49
Figure 2.7 Profile of the Uniform Beam.....	60
Figure 2.8 Finite Element Analysis of Uniform Beam.....	62
Figure 2.9 Manufactured Uniform Beam.....	62
Figure 2.10 Experimental Modal Analysis .....	63
Figure 2.11 Shape of the Blade.....	66
Figure 2.12 Functions of Cross-section Area and Moment of Area .....	67
Figure 2.13 Manufactured Blade .....	68
Figure 2.14 Measured Points in EMA .....	68
Figure 3.1 The Representation of the Problem .....	78
Figure 3.2 Component displacement and Euler angles.....	79
Figure 3.3 Coupled Longitudinal and Bending Vibration .....	84
Figure 3.4 Structure with Coupled Bending and Longitudinal Vibration .....	85
Figure 3.5 Stencil of Difference Equation .....	89
Figure 3.6 27-Points Stencil.....	94
Figure 3.7 Stencil for Case of $i=0$ .....	97

Figure 3.8 Stencil for Case of $i=m$ .....	97
Figure 3.9 Excitation and Initial Bending.....	102
Figure 3.10 Amplitude of Bending over Time.....	103
Figure 3.11 Displacement of End Point (with Longitudinal Vibration).....	104
Figure 3.12 Overlay of Bending Shape.....	104
Figure 4.1 Ultrasonic Blade .....	116
Figure 4.2 Modal Distance Indicators.....	117
Figure 4.3 The Optimal Design Method.....	134
Figure 4.4 Geometry Parameters .....	135
Figure 4.5 Blade Shape and Parameters .....	135
Figure 4.6 Abaqus Scripting Interface.....	139
Figure 4.7 Screenshot of the Development Environment.....	140
Figure 4.8 Modules of the Optimal Design Package .....	141
Figure 4.9 Interaction between Modules and Abaqus .....	142
Figure 4.10 GUI of Abaqus Plug-in.....	142
Figure 5.1 Profile and Shape of the Sharp Cutting Edge.....	147
Figure 5.2 Shape of the Blade.....	148
Figure 5.3 Design Procedure.....	150
Figure 5.4 Finite Element Model of the Blade .....	150
Figure 5.5 Amplitude of Longitudinal Displacement.....	152
Figure 5.6 Model for Stress Analysis .....	153
Figure 5.7 Mises Stress in Blade.....	154
Figure 5.8 Normalised Stress Distribution, Mises Stress .....	154
Figure 5.9 Manufactured Blade .....	155
Figure 5.10 Result of Impedance Analysis .....	156
Figure 5.11 Measure Points on Blade.....	157
Figure 5.12 Overlay of FRFs .....	157
Figure 5.13 Ultrasonic Devices and Cutting Sample.....	160
Figure 5.14 Calibration of Material Emissivity.....	161
Figure 5.15 Cutting Test, Biomechanical Material.....	162
Figure 5.16 Sheep Femur.....	163
Figure 5.17 Ultrasonic Bone Cutting, Manually Performed.....	164
Figure 5.18 Test Rig and Bone Sample .....	164

Figure 5.19 Ultrasonic Bone Cutting, Test Rig .....	165
Figure 5.20 Serrated Cutting Edge.....	166
Figure 5.21 Blade II with Serrated Cutting Edges.....	167
Figure 5.22 Normalised Displacement .....	169
Figure 5.23 Stress in Blade II .....	169
Figure 5.24 Normalised Stress Distribution.....	170
Figure 5.25 Manufactured Blade .....	170
Figure 5.26 Result of Impedance Analysis .....	171
Figure 5.27 Overlay of Transfer Functions, Magnitude .....	172
Figure 5.28 Broken Blade .....	173
Figure 5.29 Blade Profile and Geometry Parameters .....	176
Figure 5.30 Modal Distance and Mode Coupling.....	178
Figure 5.31 FRF and Width of the Peak (Blade I, Tip, Longitudinal Direction).....	179
Figure 5.32 Input for Stress Analysis .....	180
Figure 5.33 Calculation Procedure .....	183
Figure 5.34 Optimisation Space and Tuned Surface .....	183
Figure 5.35 Modal Distance ( $M_A$ ).....	184
Figure 5.36 Maximum (Mises) Stress ( $S_A$ ) .....	185
Figure 5.37 Gains of Blade .....	186
Figure 5.38 Qualified and Optimal Design (Superimposing on Values of $S_A$ ).....	187
Figure 5.39 Model of the Optimal Design.....	188
Figure 5.40 Normalised Displacement .....	189
Figure 5.41 Stress Distribution (Under Multi-Component Excitation).....	189
Figure 5.42 Normalised Stress Distribution (Under Multi-Component Excitation)ll	189
Figure 5.43 Manufactured Blade .....	190
Figure 5.44 Result of Impedance Analysis .....	190
Figure 5.45 EMA Grid Points on Blade III (Serrations not Shown) .....	191
Figure 5.46 Result of Impedance Analysis .....	191
Figure 5.47 Manufactured blades .....	194
Figure 5.48 Experimental Setup .....	195
Figure 5.49 Test Rig .....	195
Figure 5.50 Cutting Angles.....	196
Figure 5.51 Measurement of Temperature Inside the Sample.....	196
Figure 5.52 Biomechanical Test Sample .....	197



Figure 5.53 Cutting Speed .....	200
Figure 5.54 Surface Temperature .....	202
Figure 5.55 Internal Temperature .....	203
Figure 5.56 Internal Temperature vs Cutting Depth & Time .....	203
Figure 5.57 Test Rig .....	204
Figure 5.58 Experimental Setup .....	205
Figure 5.59 Cutting Setting.....	206
Figure 5.60 Incisions under Different Cutting Settings .....	207
Figure 5.61 Cutting Temperature Measurement.....	208
Figure 5.62 Cutting Temperature.....	209
Figure 5.63 Ultrasonic Cutting of Rat Bones.....	210
Figure 5.64 Bone Samples after Cutting.....	211
Figure 5.65 Temperature Measurement (Serrated Blade).....	212

# Chapter 1

## Introduction

### 1.1 Introduction

Ultrasonic cutting applies the vibration of a blade (or blades) tuned at the frequency range of 20-100kHz in the cutting process. This technology provides a way of cutting materials for various industrial and medical applications. It offers a number of advantages, including enhanced accuracy and smooth operation, over the traditional cutting methods [1-3]. Food processing is among the applications where ultrasonic cutting technology has been well established. The introduction of ultrasonic vibration improves the cutting quality and efficiency significantly, especially for fragile and sticky foodstuffs [4, 5]. The use of ultrasonic cutting has also increased rapidly in surgery applications [6, 7]. It has been a widely accepted procedure in dentistry, where a number of commercial products are available [8, 9]. Clinical applications have shown that this technology improves the cutting precision and reduces the risk of tissue injury [2, 7, 10]. However, for surgical applications where deep incisions in hard tissues are required, it could still be a challenge to apply ultrasonic cutting in surgery operations due to the difficulty of cutting and the risk of thermal damage [8, 11-13]. To overcome this, the blade should be carefully designed in a way that enhances the cutting performance while reducing the temperature of cutting. As the blade performance relies closely on the dynamic behaviour of the blade, it is necessary to model and characterise the vibration of the blade during its design process in order to obtain a satisfactory design for a specific surgical application [1, 14, 15].

This thesis is devoted to the study of modelling and design strategies of ultrasonic bone cutting blades used for surgery procedures. The research is based on the analysis of dynamic characteristics and experimental tests of ultrasonic blades. The main aims of the study are as follows:

- (1) Investigate analytical approaches of modelling the vibration characteristics, such as modal frequencies and mode shapes, of typical ultrasonic bone cutting blades.
- (2) Model the coupled vibration of blades of slender shape.

- (3) Provide a strategy to optimise the performance of a design based on the analysis of dynamic characteristics.
- (4) Design ultrasonic bone cutting blades and verify the proposed strategies.

## **1.2 Ultrasound and Power Ultrasonics**

### **1.2.1 The Field of Ultrasonics**

Ultrasound is the term used for sound waves with a frequency greater than the limit of human hearing. It is essentially high frequency mechanical vibration travelling through fluids or solids. The lower frequency limit of ultrasound technology is usually 18-20kHz and the upper limit can be as high as gigahertz. The application and investigation of ultrasound is referred to as Ultrasonics, which is a branch of acoustics studying the generation and use of high frequency inaudible acoustic.

The field of Ultrasonics is broad, covering a large number of diverse topics such as medicine, underwater sound, chemical, electrical, and other engineering applications. In terms of the intensity of the soundwave applied, ultrasonics may be divided into two broad categories: low intensity ultrasonics and high intensity ultrasonics [16]. Due to the diversity of applications, it is difficult to define a clear cut limit between high and low intensity ultrasonics. Nevertheless, the sound wave intensity in low intensity applications, depending on the medium, is usually 0.1-1 W/cm<sup>2</sup> [17, 18]. The low intensity sound wave usually does not change the physical characteristics of the material or medium in the application. Typical examples of such applications include non-destructive testing and ultrasonic imaging. As the intensity levels are low, the power levels applied in the transducers are often low, typically in the range of milliwatt [16].

High intensity ultrasonics, on the other hand, usually applies ultrasound of considerably high intensity, from several to hundreds of watts per square centimetres. In accordance with the intensity value of sound wave, the power levels applied in the ultrasonic transducers can be in the range of tens, hundreds or even thousands of watts. Therefore this field is also referred to as high power ultrasonics in this thesis. The sound wave in such applications is typically applied with an aim to induce physical actions (such as cleaning or mechanical movement), or cause permanent physical, biological or chemical properties changes in the material or medium [16, 17]. This

technology was introduced after World War II and has found applications in numerous areas in industry and health care [19-24]. Typical applications of high intensity ultrasonics in industry include ultrasonic welding [25], cleaning [26], soldering [27] and machining [28], where the processing is done more effectively compared to conventional methods as a result of the ultrasonic vibration [16]. Another rapidly developing area in high intensity ultrasonics are medical applications, such as ultrasonic bone cutting [2, 13, 29], soft tissue cutting [6, 30], drug delivery [18], and High-Intensity Focused Ultrasound (HIFU) [31]. Applications such as ultrasonic cutting and welding utilizes waves with frequencies in the low end of ultrasound, usually between 18kHz to 100kHz [3, 22, 32]. Whereas for applications such as HIFU, the frequency of the sound wave may be above 1MHz [31].

### **1.2.2 Early History of Ultrasound**

The fundamental science of vibration was formulated during the 17th century as a result of the contribution made by numerous researchers including Giovanni Battista Benedetti, Galileo Galilei, Isaac Newton, Joseph Sauveur [33]. By the end of the 17th century, scientists were able to predict the vibration frequencies of a string and study the sound waves in the air. However, the concept of the existence of sound with frequency above the hearing limit of human was unheralded in the literature. An important advancement was seen in 1794, when the Italian priest and physiologist Lazzaro Spallanzani provided experimental evidence for the first time in history that non-audible sound exists in the nature. He found that blinded bats were able to navigate themselves around obstacles in the dark. The work led him to conclude that the bats used sound waves instead of sight to direct the flight [20, 34].

By the 1800s, people had accepted the concept that there exists sound waves which are outside the frequency range of human hearing but may be detected by some animals. In the 1830s, French physicist Félix Savart constructed an acoustical device known as Savart wheel to investigate the thresholds of human audibility. The device used a spinning toothed wheel and a card to produce sound of up to 24kHz. This was considered the first time in history that ultrasound was generated using an artificial way. Meanwhile, whistles using the stream of air flow to produce high frequency sound waves made their appearance during the 1800s. The most well known design among them was the Galton's whistle invented by English scientist Francis Galton in

1876 [20]. The whistle was capable of generating ultrasound that is inaudible to human being but can be detected by animals such as cats and small dogs. This invention is often regarded as the birth of ultrasonics.

The major breakthrough in ultrasonics came in 1880, when French physicists Pierre Curie and his brother Jacques Curie discovered the piezoelectric effect in certain crystals such as quartz and Rochelle salt (sodium potassium tartrate tetrahydrate). The Curie brothers observed that the crystals generated electric potential when being compressed. Later on physicist Gabriel Lippman mathematically deduced that the reverse effect of establishing a mechanical stress in such material could be achieved by applying a voltage on the material. The theory was quickly verified experimentally by the Curie brothers. Thus, it was then possible to sense and generate high frequency ultrasound using the piezoelectric and anti-piezoelectric effect, which spurred the research and development of ultrasonics [20].

The earliest technological application of ultrasonics was the underwater sonar detection systems. During World War I, in particular after the sinking of the Titanic, there was strong desire to develop underwater navigation system. An early design of echo sonar was patented by English meteorologist Lewis Richardson, and the first working sonar was built by Reginald Fessenden, a Canadian born American engineer, in the U.S. in 1914. The Fessenden sonar used a moving-coil electromagnetic oscillator to emit and sense sound waves underwater. It was capable of detecting an iceberg two miles away but could not resolve the direction precisely [20]. Yet the most important contribution made for the ultrasonic sonar system was accredited to eminent French physicist Paul Langevin. Shortly after the outbreak of World War I, a young Russian engineer, Constantin Chilowsky, proposed a submarine detection device inspired by Richardson's patent and Fessenden's sonar. The proposal was forwarded to Langevin, who replaced the magnetic transducer in the original proposal with an improved solution. The idea of using anti-piezoelectric effect to generate ultrasound was discarded at first but was resurrected after the improvement of crystal preparation and the availability of advanced electrical components. Langevin conceived a new kind of transducer design, referred to as the Langevin transducer, which adopted the steel-quartz-steel sandwich structure. This design considerably enhanced the radiated energy of the transducer and improved the performance of

ultrasonic echo ranging devices. Langevin's work was considered to be a milestone of modern science of ultrasonics.

After World War I, research on ultrasonics flourished. In addition to underwater detection, applications of ultrasound had extended to physical therapy and industry. Meanwhile, people started to observe the biological effects and the destructive capability of high intensity ultrasound. During Langevin's first tests of his new transducers, small fish were found killed by the sound wave. Among those who witnessed this phenomenon was the famous American physicist Robert W. Wood. Wood recorded in his notes that the high intensity ultrasound caused millions of tiny air bubbles in the water and killed fish swimming into the sound beam [35]. After returning to the U.S in 1918, Wood collaborated with American scientist Alfred L. Loomis to study whether Langevin's work would offer a wider scope for the research in biology, physics and chemistry. They used a high power ultrasonic transducer to investigate the effects of high intensity ultrasound in various conditions, which resulted in a series of exciting findings. In 1927, they published a paper reporting their observation of experiments [36]. The effects include: radiation pressures of notably large magnitude, causing burning of wood with oscillating rods, drilling and etching through glass, internal heating of solids and liquids, formation of fogs, destruction of unicellular organisms and blood cells, killing or causing harm to fish, frogs and mice. Among these, the significant phenomenon closely related to ultrasonic cutting was that the energy transmitted through an oscillating rod was capable of achieving incision in considerably hard materials.

Wood and Loomis' work in 1927 was regarded as a landmark in power ultrasonics. Before 1927, few publications were identified on power ultrasonics. However, during 1927-1939, at least 150 papers were released, addressing dispersion, emulsification, coagulating action, chemical and biological effects of high intensity ultrasound [20]. These studies led to a number of proposals to apply high power ultrasound in medical and industrial applications. During the same time, research on other aspects of ultrasonics flourished as well. Bibliographic listing of studies on the physics and engineering applications of ultrasonics reached more than 6,000 by the mid 1950s [19]. Ultrasonics had become an extensively deployed technology in applications including drilling, welding, sterilization, degreasing and medical therapy.

### 1.2.3 Effects of High Power Ultrasound

The application of power ultrasonics relies on various effects of high power ultrasound to change the properties of the material. For ultrasonic bone cutting, although the details of the cutting mechanism remains unclear due to the complexity of material properties and the interaction between the bone and the tool, the cutting action was considered to be achieved by a combination of effects including cavitation, thermal and direct mechanical actions [6].

Cavitation is a phenomenon associated with intense oscillating acoustic field in liquid, where cavitation bubbles are generated, expand and collapse. These cavitation bubbles exhibit complex dynamic behaviour, including shock waves and acoustic emissions, jet-like ejection, high pressure and high temperature [37]. It is observed that the behaviour of the cavitation bubbles is sensitive to the characteristics of biomaterial [38]. The cavitation may induce considerable mechanical effects due to its violent nature and the large energy density in the collapsing cavitation bubbles. This phenomenon can contribute to the removal of material during ultrasonic cutting.

Thermal effect is another significant phenomenon found in high power ultrasonic applications. The contact friction between the surface of ultrasonic tools and the material is an important cause responsible for the generation of heat. In addition, other effects such as cavitation and deformation of material are also sources of heat generation. The thermal effect results in temperature rising during ultrasonic cutting, which could cause damage in the material. Cardoni et al. [12] illustrated that it is possible to reduce the cutting temperature by improving the profile of ultrasonic blades. Apart from that, optimisation of cutting parameters, such as cutting speed and applied force, could bring down the cutting temperature in certain applications [39].

In addition, direct mechanical actions are also substantially responsible for the removal of material in ultrasonic cutting. When high frequency oscillating blades contact with the cutting material, the fast moving tool tips cause direct impact and shear force, resulting in cracking, fragmentation and other effects [30, 40-44]. It is reported that the cutting mechanism varies between different kinds of material depending on their structure and properties. Shear force, pressure wave components and acoustic streaming are considered to be the phenomena predominantly related to ultrasonic vibration in the cutting of soft tissues [6, 30, 41]. For hard tissue and brittle

material, the cutting process may be partly ascribed to fracture or crack propagation induced by the mechanical impact. Smith et al. [44] proposed that the cutting mechanism in friable materials is essentially controlled crack propagation associated with the vibration mode of the ultrasonic blade. This assumption inspired the development of an FE model with an aim to better understand the cutting process. A similar concept was adopted by MacBeath [39] to investigate the cutting process of bone. These studies provided useful information to optimise the critical vibration parameters of ultrasonic cutting.

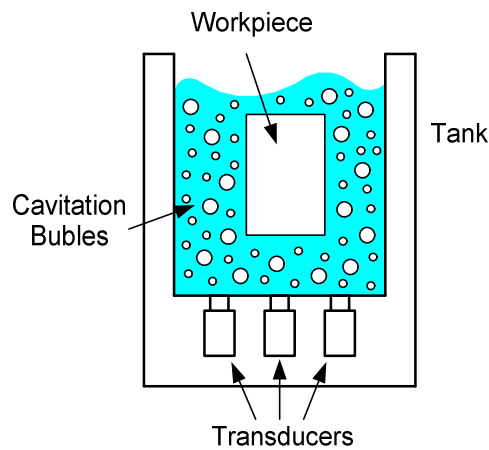
### **1.3 Industry Applications of High Power Ultrasonics**

High power ultrasonics has been used in a wide variety of industrial applications and medical procedures. Established applications of power ultrasonics in industry include ultrasonic cleaning, metal/plastic welding, chemical processing, metal/plastic forming and ultrasonic machining [45]. With the advancement of technologies, more applications, such as food/tissue cutting, ultrasonic motor and ultrasonic levitation, have emerged.

#### **1.3.1 Ultrasonic Cleaning**

Ultrasonic cleaning, which dates back to the 1940s, is one of the earliest applications of power ultrasonics that is available commercially [20, 45]. The classic definition of ultrasonic cleaning is the application of high intensity ultrasound to facilitate the removal of foreign loosely held contaminants on the surface of items such as industry components and jewellery. It is one of the most efficient non-abrasive cleaning method which can remove complex contaminants without damaging the surface of the workpiece or compromising the integrity [26]. Figure 1.1 illustrates a basic setup of an ultrasonic cleaner. The workpiece to be processed is placed in a tank filled with cleaning liquid. Ultrasonic transducers are fixed outside the vessel or are attached to a diaphragm that contacts with the liquid, which enables the transmission of high intensity ultrasound from the transducers into the liquid. During cleaning process, the contaminants on the surface of the workpiece can be removed under combined effects induced by the sound wave, such as cavitation and micro-streaming [26].





**Figure 1.1 Ultrasonic Cleaning**

### **1.3.2 Metal/Plastic Welding**

Ultrasonic welding can be applied to metal or plastic. For metal, the application is a solid-state joining process that utilises high frequency shear vibration under longitudinal pressure to bond metal sheets or plates together. By applying high power ultrasonic vibration in the welding processing, the energy delivered to the metal is capable of causing macroslip and microslip in the material to join the surface layers of the metal. This technology has been used in the industry to join electrical contacts or fabricate products such as heat exchangers [21, 22, 25].

On the other hand, ultrasonic plastic welding utilises the combined effects of mechanical vibration, pressure and thermal energy, usually generated by ultrasonic vibration of up to 90kHz in frequency, to melt and join the plastic at the designated point. The process has been used in numerous applications, such as toy manufacturing, to replace glue or mechanical fasteners [21, 25].

### **1.3.3 Ultrasonic Assisted Machining**

Ultrasonic assisted machining applies ultrasonic vibration on conventional machining process with an attempt to improve the quality of machining. Babitsky et al. [46, 47] reported the application of imposed ultrasonic vibration in the machining of aviation materials. On the basis of a conventional turning machine, high frequency mechanical oscillation (20kHz) in the feed direction was imposed on the cutting tool through an ultrasonic transducer and an auto-resonant control system. By machining two nickel-based alloys used in modern aviation industry, Inconel-718 and C263, it is shown that

the surface quality was enhanced significantly as a result of the ultrasonic vibration. Comparing to the conventional cutting approach, the presented method achieved a roughness improvement of up to 40%. In a later study, Jin and Murakawa [32] proposed an improved design for the ultrasonic cutting tools to avoid tool chipping in such applications. By manufacturing the tools with high rigidity material and improving the shape of the cutting edge, it is expected that the tool life can be prolonged considerably.

Kim and Choi [48] investigated the micro-surface machining of optical plastics using an ultrasonically excited cutting tool. It is reported that when the depth of cutting was less than  $2.7\mu\text{m}$ , ultrasonic cutting was capable of achieving ductile cut surface on optical parts with improvements in both waviness and roughness of the machining. This suggested that the ultrasonic cutting could be used as an alternative method to conventional grinding and polishing in the manufacture of high precision optical components.

#### **1.3.4 Ultrasonic Cutting**

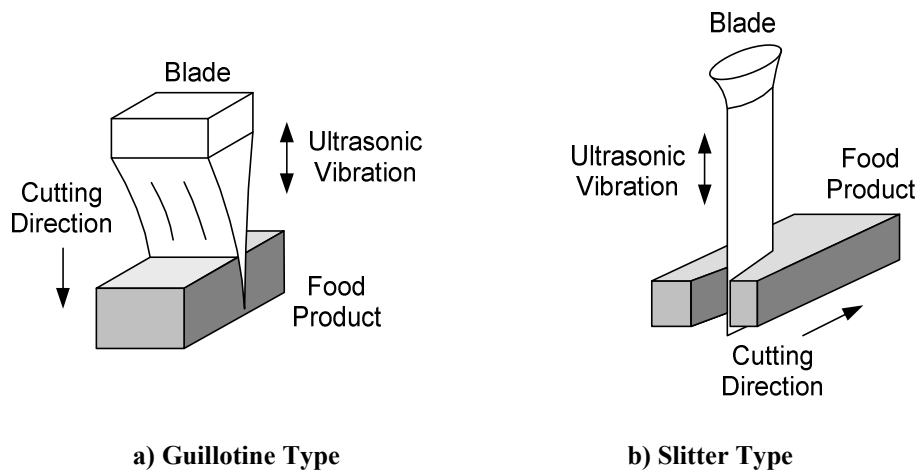
Ultrasonic cutting is an established application of ultrasound in industry. This technology can be used to process material such as food, metal, glass and plastics. Although ultrasonic cutting may be conducted with the aid of abrasive, this section reviews only those applications that rely on the direct contact between a blade vibrating ultrasonically and the workpiece to achieve incision.

##### **(1) Ultrasonic Food Cutting**

Ultrasonic cutting has been used commercially in the food production industry to facilitate the preparation of large volume of food such as pastries, confectionery and cheese. For goods which are brittle and contain layers of different consistencies, they are often difficult to cut by conventional approaches such as guillotine or rotating saw, as the material may collapse or crumble during the process. In addition, for the sticky products, such as confectionery, the cutting tools used in the conventional methods are more likely to be smeared by food adhering, which increases the possibility of cutting jams and halting of production [49].

Ultrasonic food processing utilises a blade oscillating ultrasonically instead of a conventional knife to process the food. Conventionally, to avoid the shattering and deformation of food, specialised processing such as freezing is usually needed prior to the cutting of products, which reduces processing efficiency and increases costs. Such a procedure, however, is not required in ultrasonic cutting [49]. In addition, this technology provides unique advantages, including prevention of food adherence on tool surface and reduction of product waste [4], in the processing of products that are conventionally difficult to cut, such as sticky confectionary. As a result, the application of ultrasonic cutting technology, either on a large scale automatic production line or on a single machine, can facilitate the production and reduce the maintenance costs [5].

In terms of the way the vibration is applied during the cutting, the processing can be classified into two types: the guillotine and the slitter, where the ultrasonic excitation is applied parallel and perpendicular to the direction of cutting respectively, as illustrated in Figure 1.2. In the guillotine type cutting, the blade tip is used as the cutting edge, where the vibration amplitude is usually evenly distributed along the blade width. On the other hand, in the slitter type cutting, the edges on the sides of the blade are used for cutting, where vibration amplitude is non-uniformly distributed along the edge. This could result in difference in cutting effect along the excitation direction and should therefore be taken into consideration in blade design [49]. The selection of these cutting methods should be determined according to the design of machine and the properties of the food product [5]. For example, for crumble products which may be more vulnerable to vertical forces, the slitter type cutting could be a preferred option. In either application, the introduction of high frequency vibration results in low frictional surface and enhanced cutting performance, which improves the quality of processing by avoiding adhering and damage of food [50]. This method is capable of making clean incision even for sticky products.



**Figure 1.2 Ultrasound Food Cutting**

In view of the advantages of incorporating ultrasonic vibration in food processing, numerous studies have been devoted to the characterisation of cutting performance and the design of ultrasonic food cutting devices. Schneider et al. [51] overviewed the process of ultrasonic food cutting. The investigation confirmed that the introduction of high frequency mechanical vibration resulted in low friction on the blade surface which reduced the so called "adhesion conditioned shearing" and tool fouling. In addition, reduction of separation force was reported causing by concentration of local energy around the cutting zone. In a later study, the energy consumption during ultrasonic food cutting was investigated by Schneider et al [52]. It showed that excitation of higher frequency resulted in increased power demand, which may also result in loss of quality in food. Apart from this, cutting of non-porous food rich in water and fat required less energy than porous food. Other factors such as absorption properties of the products and coupling conditions of the cutting were also responsible for the energy consumption. Similar work was done by Arnold et al. [3] where a guillotine type ultrasonic blade tuned at 40kHz with an amplitude of  $12\mu\text{m}$  was used to cut different cheese varieties. The investigation showed that increasing vibration amplitude in the blade had a positive effect on the improvement of cutting quality. However, the improvement was less significant if the ultrasonic excitation was at a high level. Also the role the composition of cheese played during the processing was of considerable importance to the quality of cutting. An inverse relationship was observed between the requirement of energy and the ratio of moisture/solids-non-fat. Schneider and Arnold's work illustrated that to maximize the performance of an

ultrasonic cutting system, it is necessary to take into account various factors, such as cutting parameters and properties of the material, in the design of ultrasonic tools.

McCulloch [53] studied the design of ultrasonic food cutting devices. A method of modelling the interaction between the ultrasonic blade and the cutting material was proposed based on finite element analysis, providing a way to understand the mechanism of the cutting process. The key techniques of this method included incorporating thermo-mechanical finite element models in the analysis and extracting the properties of food material experimentally. The study suggested that it is possible to estimate the optimal cutting parameters during the design process of ultrasonic food cutting blades, which allows the user to further improve the performance of ultrasonic cutting systems.

## **(2) Other Application of Ultrasonic Cutting**

In addition, applications of ultrasonic cutting have been reported in the processing of wood, metal and plastics. Sinn et al. [54] applied an ultrasonic apparatus in the cutting of wood. A wedge shape cutting knife was mounted on a device tuned longitudinally at 20kHz. This apparatus was used to machine the softwood and hardwood in both dry and wet conditions. It is reported that considerably reduced cutting force, up to 50% lower than the conventional method, was achieved in the tests with vibration amplitude of only  $8\mu\text{m}$ . This was considered to be caused by the reduction of contact friction between the surfaces of the knife and the wood. An attempt to cut stacked paper using a longitudinally excited ultrasonic guillotine was made by Deibel et al [55]. Vibration parallel to the direction of cutting was imposed on the cutting knife by an ultrasonic transducer. The cutting process was simulated by a dynamic model, which provided an insight into the key parameters of cutting, including the contact ratio, compression ratio and dynamic force. The results were confirmed by experiments, concluding that the dynamic forces introduced by the ultrasonic vibration resulted in more effective cutting.

Babitsky et al. [46, 47] reported the application of imposed ultrasonic vibration in the machining of aviation materials. On the basis of a conventional turning machine, high frequency mechanical oscillation (20kHz) in the feed direction was imposed on the cutting tool through an ultrasonic transducer and an auto-resonant control system. By

machining two nickel-based alloys used in modern aviation industry, Inconel-718 and C263, it is shown that the surface quality was enhanced significantly as a result of the ultrasonic vibration. Comparing to the conventional cutting approach, the presented method achieved a roughness improvement of up to 40%. In a later study, Jin and Murakawa [32] proposed an improved design for the ultrasonic cutting tools to avoid tool chipping in such applications. By manufacturing the tools with high rigidity material and improving the shape of the cutting edge, it is expected that the tool life can be prolonged considerably.

Kim and Choi [48] investigated the micro-surface machining of optical plastics using an ultrasonically excited cutting tool. It is reported that when the depth of cutting was less than  $2.7\mu\text{m}$ , ultrasonic cutting was capable of achieving ductile cut surface on optical parts with improvements in both waviness and roughness of the machining. This suggested that the ultrasonic cutting could be used as an alternative method to conventional grinding and polishing in the manufacture of high precision optical components.

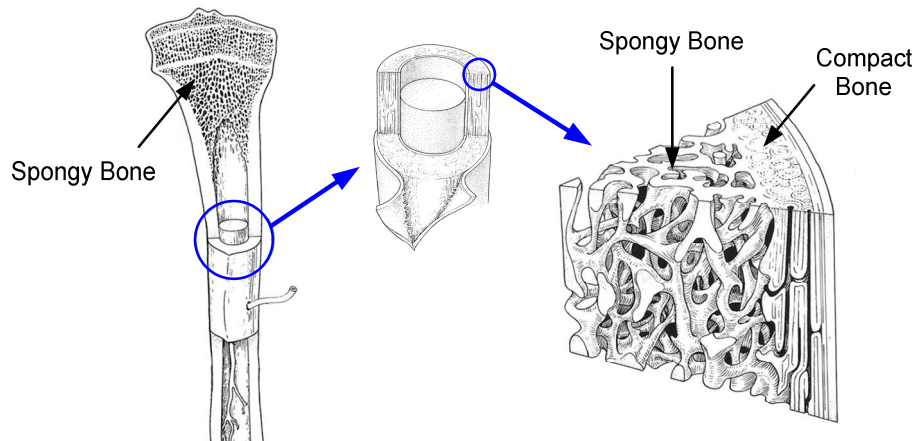
## **1.4 Bone Cutting in Surgery**

Applications of high power ultrasonics have also emerged in medical applications. Among them is ultrasonic bone cutting. The cutting of human hard tissues such as bones is an important operation in surgery, especially in osteotomy. However, it can be a challenge for surgeons to perform precise and safe operation due to the hardness of the tissues.

### **1.4.1 Structure of Bone**

Bones are in fact complicated composite materials consist of various kinds of tissues, including crystals of mineral and protein. This provides both strength and resilience so that the skeleton can absorb impact without breaking. The structure and composition of a bone depends on numerous factors such as physiological function, skeletal site, age and sex of the body [56]. Figure 1.3 illustrates the structure of a human long bone. In the simplest form, the bone can be regarded as made up of two layers. The outer layer is a dense and rigid tissue referred to as compact or cortical bone. This layer is hard and provides adequate strength for the bone to withstand forces. For an adult human body, the compact bone accounts for 80% of the skeleton.

As a result of its hardness, considerable difficulties may be encountered when cutting this tissue. Beneath the outer layer is the spongy tissue referred to as cancellous or trabecular bone. The cancellous bone is less dense and has lower strength than the compact bone. Thereby this layer is less difficult to cut than the outer layer.



**Figure 1.3 Structure of Bone [58]**

#### **1.4.2 Heat Generation and Thermal Damage of Bone**

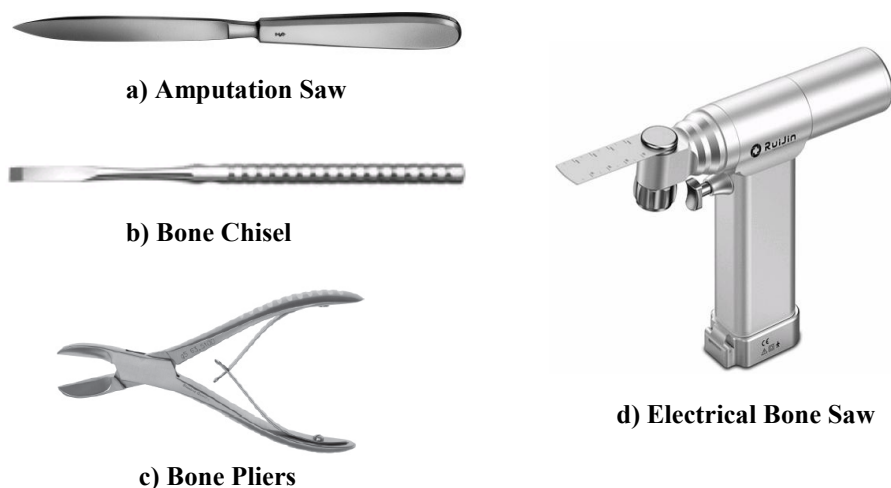
In operations such as bone cutting and drilling, heat generation can be caused by friction between the tool and tissue and shearing of the material [59]. For conventional osteotomy such as bone drilling, the factors influence the heat generation include the speed of cutting/drilling [60, 61], applied force [62, 63], irrigation [64, 65], and design of the cutting device [66]. To reduce the generation of excessive heat during the operation, methods of cooling the cutting tool are usually required [67]. For ultrasonic bone cutting, the heat generation can be affected by the frequency and amplitude of vibration [68], applied force [69], and design of the cutting profile [12]. In addition, heat induction can also increase as the duration of cutting process is increased [65, 70].

For either spongy or compact bone, if the tissue is subjected to elevated temperature during the cutting process, irreparable thermal damage or necrosis may occur in the bone, which can cause negative effects for the operation and prolong the recovery time for the patient [71]. The highest temperature the bone tissues can suffer depends on the condition of the bone and the duration of heating. Generally, bone necrosis is most likely to occur at a temperature threshold of 50°C-70°C. Lundskog [11] showed that cellular necrosis can occur if bone is exposed at 50°C for longer than 30 seconds.

Study conducted by Mortiz and Henrique [72] observed immediate damage in epithelial cells exposed to a temperature of 70°C. Although it may be acceptable for the bone to suffer higher temperature if it is only exposed to elevated temperatures for a very short period of time [11, 59], it is suggested 55°C can be used as a threshold [71] as this temperature would be sufficient for a bone to suffer serious damage if the tissue is exposed to the heat for longer than 30-60 seconds.

### 1.4.3 Conventional Bone Cutting Instruments

Conventionally, bones are cut by hand operated tools such as bone pliers, chisels and saws, as well as by electrically or pneumatically driven devices, such as electric bone saws, as illustrated in Figure 1.4. The hand operated bone cutters that are still being used today can be dated back to the 17th or 18th century, most of which were initially inspired by the tools used in wood industry [13]. One of the main disadvantages of these cutters is that they require the operator to exert considerable physical effort to perform cutting on hard bones. This not only introduces difficulties for the operation but also increases the hazard of causing damage to the surrounding soft tissues. Nevertheless, such tools have been used by surgeons for centuries and they were satisfactory equipments when osteotomy was limited to amputations [13].



**Figure 1.4 Bone Cutting Tools**

Powered bone cutting tools, such as electrical bone saws, take advantage of high speed mechanical motion, either rotary, reciprocal or oscillatory movements, to achieve deep incisions in bone. These tools can reduce the physical effort of surgeons in bone cutting and increase the speed of cutting. However, the fast movement of the



mechanical components in such tools can cause vibration and noise in the operation, introducing inconvenience for surgeons to perform precise incision.

#### **1.4.4 Ultrasonic Bone Cutting Technology**

##### **(1) Features of Ultrasonic Bone Cutting Technology**

Ultrasonic cutting technology has been introduced for surgical applications since the 1950s. Ultrasonic bone cutting applies high frequency mechanical vibration of a blade tuned at a specific frequency to make incision on hard tissues. The main advantages of this technology are as follows [9, 73-75]:

- (1) Low bleeding. The basic mechanism of coagulation in ultrasonic cutting is regarded to be the denaturation of protein under the combined effects of frictional heat and ultrasonic energy [76-78], which seals the vessels around the cutting site and reduce bleeding [79]. Both the cutting and coagulation processes may be controlled by altering the vibration parameters of the ultrasonic cutting devices [78].
- (2) Smooth and precise cutting. Limited vibration amplitude (normally less than 200 $\mu$ m) and low cutting force allows the operator to control the cutting procedure precisely [2, 13].
- (3) Selectively cutting and reduced risk of soft tissue damage. The effect of ultrasonic cutting varies between different kinds of tissues [6]. Taking advantage of this, ultrasonic cutting devices can further benefit from the capability of selectively cutting. Beziat et al. [10], Yaman and Suer [80], and Labanca et al.[7] showed in surgical operation cases that the ultrasonic devices designed for mineralised tissue cutting were capable of making incisions in hard tissues effectively while leaving surrounding soft tissues intact. A worst case scenario study was reported by Schaeren et al.[81], where nerve tissue was exposed to prolonged and direct contact with an ultrasonic bone cutting device. It showed that the cutting device did not dissect the soft tissue, and the structural and functional damage induced in the tissue was limited. The application of such devices may minimise the injury of soft tissues in osteotomy.

The ultrasonic bone cutting devices can have similar structure as the tools used in ultrasonic food cutting. However they are usually designed with additional features, such as functions of irrigation, to meet the requirements of medical procedures.

## **(2) Research and Development**

The earliest attempts of applying ultrasonic technology in the cutting of human hard tissues were made in dentistry. In 1953, Catuna [74] reported the application of ultrasound in the preparation of tooth cavities for restoration. Initially, industrial devices, such as impact grinders, were used to generate ultrasonic vibration and complete the operation. After a series of successful experiments, specialised apparatus were designed as a new type of surgical tools [73]. However, these ultrasonic devices, compared to conventional electrical or pneumatic powered dental units, were cumbersome and expensive. As a result, although the ultrasonic technology was considered to be of numerous advantages, including reduced tissue heating, low applied pressure during operation, and improved patient experience [73-75], its commercialisation in surgical application was limited in the 1950s.

Nevertheless, the possibility of using ultrasonic vibration in the cutting of bone continued to be explored. Zinner [82] suggested an improved ultrasonic instrument, equipped with a scaling tip in its probe-like design, to be applied together with water coolant for the removal of teeth plaque and calculus in dentistry. Vang patented a surgical scalpel device in 1955 which used longitudinal vibration of 6kHz-12kHz to cut biological materials [83]. Although the working frequency of this device was below the ultrasonic range, Vang's design demonstrated the concept of using high frequency mechanical vibration to facilitate surgical procedures. This invention was later improved by Shaefer in 1958, replacing the initial solenoid-magnet transducer design with a piezo-electric assembly [13]. Sawyer further improved Vang's design in 1974 and filed a patent for an electrical ultrasonic knife [13].

The first ultrasonic bone cutting device used for bone surgery was designed by Loschilov [24], referred to as URSK-7N. It utilised the effect of magnetostriction to convert electrical excitation into ultrasonic vibration at the frequency range 25kHz-30kHz. An ultrasonic booster (horn) was used to amplify the mechanical vibration, generating output of 50 $\mu$ m. To facilitate cutting in different surgical procedures, end

effectors of various shapes, such as scalpel or saw, could be fitted as required. After completing a large number of clinical operations with this apparatus in 1969-1971, Volkov [24] concluded that it simplified the orthopaedic operations by enabling the surgeons to perform precision cutting of just two centimetres in size.

Mararow [84] and McFall et al. [85] conducted animal based studies in order to compare the performance of pneumatic and electric powered burs and saws to an ultrasonic cutting apparatus. The studies confirmed that the ultrasonic device could improve the precision of cutting and reduce the possibility of soft tissue damage. Although both Mararow and McFall reported that slower rate of healing was found on the incisions made by the ultrasonic device, the sites healed normally within the period of the experiments. McFall also commented that the introduction of saline during the cutting process could reduce the time of healing. In a later study, Horton et al. [86] investigated the cutting capability of an ultrasonic instrument which used the chisel-like action to remove bone material. Incisions on dog alveolar bone were made in a clinical procedure using both the ultrasonic apparatus and a conventional rotary bur. Post-operation histological observation of the bone suggested that the ultrasonic instrument resulted in rougher cutting surface than the rotary bur. However higher healing rate was found in the case of ultrasonic cutting. Similarly, comparison between an ultrasonic saw and an oscillating saw was done by Aro et al. [43], stating that smoother and more precise incision was achieved in the ultrasonic cutting. Based on the dog experiments, Horton et al. [29] evaluated the ultrasonic instruments in surgical applications including teeth removal and osseous management in periodontal therapy. Positive conclusions were drawn towards the application of the ultrasonic technology. In addition to the improved control and enhanced cutting precision, ultrasonic cutting was found to be without postoperative sequelae and of minimal discomfort. Horton and Aro's work suggested that the ultrasonic apparatus were most useful in the cutting of small bones. Nevertheless, a series of disadvantages with the ultrasonic devices were reported, including inconvenience in the operation due to the size of the apparatus and the need to configure the optimal operation frequency. Apart from that, the application of ultrasonic technology did not improve the operation time as the cutting efficiency of the ultrasonic chisel and saw was slightly lower than conventional tools.

Khambay and Walmsley [87, 88] developed an ultrasonic bone chisel which had a similar design as Horton's apparatus [86]. The device used a straight cutting tip shaped as a chisel and tuned longitudinally in order to allow the tool to take full advantage of the ultrasonic vibration. It was designed to perform bone cutting which was generally completed by conventional tools such as rotary drills or burs. The in-vitro tests showed that the ultrasonic chisel achieved a cutting rate of 26-110mm/min while the rotary bur was capable of achieving a higher rate of 48-185mm/min. Though the cutting efficiency was lower than conventional tools, the ultrasonic chisel only required a longitudinal force of 1.48-3.22N to be exerted during cutting, allowing operation performing in a comfortable and precise way.

More recently, a large number of commercial ultrasonic surgical cutting devices have become available, most of which are used for dentistry and osteotomy [39]. These products are currently produced by companies such as Mectron (Italy), Resista (Italy), BTI (Spain), Satelec (France), Electro Medical Systems (Switzerland) and NSK (Japan). Mectron s.p.a manufactures piezoelectric bone cutting devices, which are referred to as the PIEZOSURGERY® products and are claimed to be one of the best commercial bone cutting apparatus [39]. Figure 1.5 illustrates a product designed for dental surgeries. This device consists of a control unit and a handpiece attached with a changeable tool tip [39]. Longitudinal ultrasonic oscillation is generated and transmitted to the tool tip, allowing the operator to perform cutting on bone. As illustrated in Figure 1.5(b), a number of tool tips, designed with various shapes, are available for different purposes of cutting, which enable the application of this device for different types of oral operations, such as scaling, osteotomy and restoration.



**a) Device**

**b) Tool Tips**

**Figure 1.5 Commercial Ultrasonic Cutting Device and Tool Tip (Mectron, Micropiezo S [39])**

According to the product documents, the bone cutting tools operate at 25kHz-29kHz, with a displacement of 60-210 $\mu$ m amplitude at the cutting tip. Compared to other similar apparatus designed in the earlier years [86], these products are equipped with a hand-piece of reduced size and advanced configuration, which simplifies their operation and allows the performing of precise cutting. In addition, a solution for cooling and debris removing is offered, using a pneumatic pump to jet physiological sodium chloride to the ultrasonic cutting site. These features significantly enhance the performance of the products.

Despite the popular application of ultrasonic technology in dentistry procedures, challenges still exist in ultrasonic cutting when it is required to make deep incisions safely in large bones such as femur [39], one of which is the occurrence of high cutting temperature. Although cooling is usually applied during the cutting procedure, it is desired to design the ultrasonic cutting devices in a way that minimises the generation of heat while delivering satisfactory cutting performance. MacBeath [39] detailed the design process of ultrasonic blades based on FEA and EMA. FE models were used to evaluate the performance of a cutting blade as well as investigate the relationship between the applied load, cutting speed and the material. The results of the FEA were used to modify the geometry of the cutting tip with an attempt to lower the possibility of heat generation. MacBeath's work showed that a carefully designed blade geometry could reduce the cutting temperature in applications. In addition, it is possible to further enhance the ultrasonic cutting performance by optimising the cutting parameters including the cutting speed and applied load.

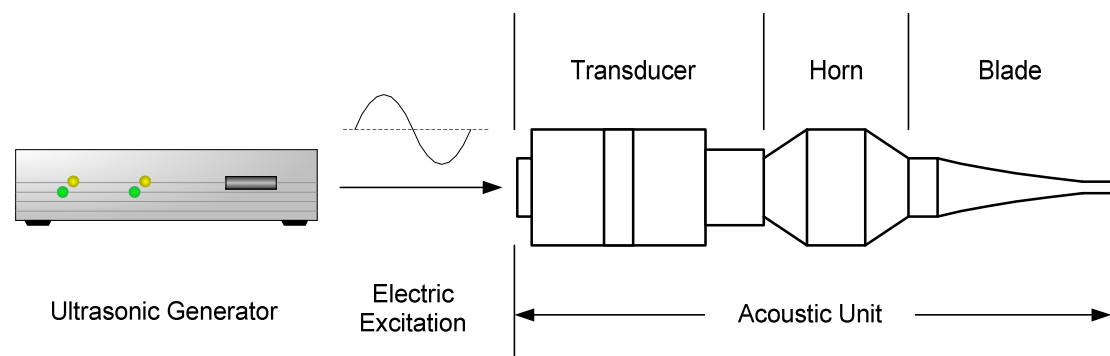
## **1.5 Design and Characterisation of Ultrasonic Cutting Blades**

This section introduces the methods and techniques used in the design and characterisation of ultrasonic cutting blades. This thesis focuses on the ultrasonic surgical cutting devices that are intended to achieve cutting in bone while minimising damage in the surrounding soft tissues. The research on relevant ultrasonic components such as horns will also be reviewed in this section.

### **1.5.1 Ultrasonic Cutting System**

Figure 1.6 illustrates a typical ultrasonic cutting system consisting of an ultrasonic generator, a transducer, a horn and an ultrasonic blade. The ultrasonic generator is

essentially a signal amplifier which outputs high power electrical excitation. This output is converted by the ultrasonic transducer into mechanical vibration. High power ultrasonic transducers are designed to output high power mechanical vibration at specified frequency. The excitation of such transducer is usually sharply tuned to the resonant frequency of the transducer in order to maximise its effect [91]. However, the resonance of the transducer is also affected by external factors such as the attached blade and applied load. The resonant frequency may be shifted during the cutting process as a result of the change of working conditions. For this reason, ultrasonic generators are usually equipped with automatic resonant control or frequency tracking system, which ensures the transducer be driven appropriately at its optimal working condition.



**Figure 1.6 Ultrasonic System, Acoustic Unit**

Ultrasonic blade is the working part of the acoustic unit. As it contacts with the cutting material directly and performs cutting, the performance of the whole cutting system is greatly determined by the characteristics of the blade. Unless specified otherwise, the ultrasonic cutting studied in this thesis is performed by ultrasonic blades excited longitudinally at the half wave-length mode. Generally, a properly designed ultrasonic blade should satisfy the following basic requirements:

- (1) The blade should be tuned at the correct frequency of the desired mode. Otherwise it may prevent the ultrasonic generator from driving the transducer properly.
- (2) The blade must have adequate strength to withstand the stress caused by high frequency deformation and the applied force during the cutting process.
- (3) In high power ultrasonic cutting, the required vibration amplitude at the cutting interface of a blade is usually larger than the output of the transducer [39].

Hence it is necessary to design the blade with appropriate gain in order to amplify the vibration.

- (4) The profile of the blade should be designed in a way that facilitates the cutting operation.

The design of an ultrasonic blade is a precise procedure involving thorough investigation of the characteristics and optimisation of critical dynamic parameters of the blade without compromising the performance and reliability. It used to be a time consuming and expensive process, where a blade was designed, manufactured and subjected to a series of fine tuning procedures before it was ready for operation and further tests. This try-and-test process relied heavily on experience and estimation. The blade would have to be redesigned if it fails to meet the requirements.

From the latter half of last century, with the advancement of techniques including finite element analysis (FEA) and experimental modal analysis (EMA), the design process of ultrasonic blades evolved into a more efficient and accurate procedure. FEA allows the designer to precisely examine the vibration characteristics of an ultrasonic blade without manufacturing a physical prototype. On the other hand, EMA enables accurate measurement of the actual modal parameters of a blade. These techniques significantly facilitate the design of modern ultrasonic blades.

### **1.5.2 Modelling and Analysis**

As an ultrasonic blade relies on high frequency mechanical vibration to achieve cutting, modelling and analysing its vibration characteristics are crucial in the design process. FEA is one of the most commonly used approaches to perform such analysis, and EMA is an experimental method to estimate the actual modal behaviour of an ultrasonic blade. Apart from them, analytical method can also be used to characterise the dynamic behaviour of ultrasonic blades. These methods enable the designers to evaluate the performance of an ultrasonic blade and make appropriate modification to improve the design.

#### **(1) Finite Element Analysis**

FEA is a numerical process that uses discrete elements to model an engineering system and obtain the approximation solutions of the analysis. The basic concept of

this method is to divide the structure into a collection of simple geometry, disjoint and non-overlapping elements. Each element is applied with a set of governing equations to simulate their responses in the real world problem. The elements are connected by applying appropriate boundary conditions, which resulted in a set of simultaneous algebraic equations. The solution of the whole system can then be obtained by numerically solving these equations.

Widely application of FEA in engineering has been enabled by the rapid advance of computer technology. High precision vibration and structure analysis can now be performed using FEA, allowing engineers to thoroughly evaluate and optimise their designs before prototyping and testing. This improves the design quality and reduces the cost of development. Commercial general purpose FEA packages, such as Abaqus and Ansys, are available on the market. With these software tools, FEA can be used in the design of ultrasonic devices to analyse their vibration modes and evaluate the material stress. Unless otherwise specified, the FEA carried out in this research is completed using the commercial multi-disciplinary package Abaqus V6.11-2.

## **(2) Experimental Verification**

In addition to analysis, it is also important to verify the simulation and estimate the actual characteristics of an ultrasonic device during the design process. This can be done by EMA, which is a powerful tool capable of revealing the inherent modal behaviour of a mechanical system experimentally. EMA made its appearance decades ago and has now been widely used in industry to investigate the dynamic behaviour of structures such as aircraft wings, bridges and precision mechanical components.

EMA is based on the concept that the vibration responses of a linear time invariant dynamic system can be represented as the combination of a set of harmonic motions referred to as the natural modes of vibration. The theory of EMA is established on the basis of the dynamic system model comprising stiffness, mass and damping properties. By taking into account the spatial distributions of these parameters, the dynamic behaviour of the structure can be described in terms of a set of normal partial differential equations, which can be reconstructed through the measurement of relationships between the excitation and the vibration responses at specific locations.

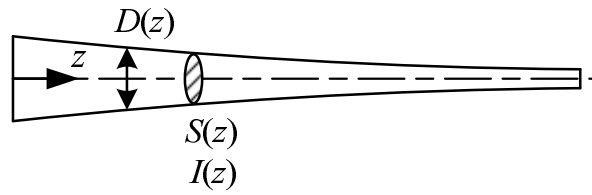


The relationship is usually a complex mathematical function known as frequency response function (FRF).

The experimental practice of EMA involves measuring the FRFs of a structure using appropriate approaches and deriving the modal model. For ultrasonic components, the FRFs are usually obtained under excitation of white noise (random signal), shock (impact testing), sine sweep or burst chirp. In this study, white noise is used as it requires relatively short testing time while providing adequate energy to excite the vibration modes. The vibration responses of the structure can be measured by a laser-vibrometer, which is capable of making non-contact measurements for small amplitude vibration. The modal parameters, including natural frequencies and mode shapes, can be extracted based on the obtained FRFs using method of curve fitting. They provide an insight into the actual dynamic characteristics of the structure and enable the designer to evaluate whether the expected performance is obtained.

### **(3) Analytical Modelling**

In addition to FEA, it is also possible to model the ultrasonic blades using other methods such as analytical models. Analytical modelling has been demonstrated to be an effective method in the design of ultrasonic horns [92-94]. This method treats a horn or other ultrasonic device as a one-dimensional structure of variable cross-section, which enables the application of one-dimensional theories to study the vibration characteristics of the horn. As suggested by the name, the one-dimensional theories are mainly used for the structure that has one dimension significantly larger than others. This feature allows the structure to be modelled using functions with a single variable [95, 96]. Figure 1.7 illustrates a rod with non-constant circular cross-sections, where the axial length of the rod is significantly larger than the diameters. Using one-dimensional modelling, this structure can be represented by functions that describe the properties of its cross-section, such as diameter  $D(z)$ , cross-section area  $S(z)$ , and moment of inertia  $I(z)$ . Based on these functions, the dynamic behaviour of the structure can be formulated with respect to  $z$ , only one variable.



**Figure 1.7 Representation of One-dimensional Structure**

According to the type of load and vibration, the structure can be treated as a bar, a beam or a shaft which deals with the longitudinal, bending and torsional vibration respectively. This provides a simple but feasible solution to model an ultrasonic blade in an analytical way. For certain types of profile, such as constant cross-section and tapered structure, closed form solutions of the model can be obtained. However, this may not be possible when the shape of the structure is complex. Instead, numerical methods can be used to compute the numerical solutions.

An advantage of the analytical modelling is that it does not require a 3D model to be generated and meshed before the calculation, which enables the application of this method in the case where detailed 3D models are not available or not necessary for analysis. Also it is expected that the one-dimensional analytical models can be computed in a faster way than 3D finite element models. Therefore it can be implemented as a fast estimation approach for applications which deal with the computation of a large number of ultrasonic blade designs. Moreover, comparing with general purpose FEA, the analytical method can be more flexible when introducing special non-linear vibration mechanisms in the modelling. Chapter 3 and Chapter 4 of this thesis will apply analytical models to study the vibration characteristics of ultrasonic blades.

### **1.5.3 Design of Ultrasonic Components**

Ultrasonic concentrators or horns are important components in power ultrasonic systems. For a longitudinally resonated ultrasonic cutting blade, a tapered or stepped half-wavelength horn is usually an essential part of its design. The earliest studies of half-wavelength horns were published in the 1950s. Balamuth [97] investigated the design of ultrasonic horns (referred to as "mechanical impedance transformers") based on theoretical analysis of the structure. The paper concluded that stepped horns could achieve better performance than exponentially tapered horns in terms of mechanical

impedance transformation. However, as the lateral deformation was ignored in the theory, it is necessary to keep the diameter of cross-section area less than a quarter wavelength in order to obtain accurate prediction. Similar work was reported by Merkulov [92]. Analytical and experimental analysis of various types of tapered horns were presented. It was shown that significantly larger gain could be achieved on catenoidal horns. However, the amplification was restricted by the strain limit of the horn material. In a later study, Merkulov and Kharitonov [93] investigated complex horns of multiple sections. It was demonstrated that such a design was capable of achieving considerably higher gain than the simple tapered shape. Due to the complexity of the profile, although the proposed analytical method predicted the gain of horns with satisfactory accuracy, differences between the theoretical and experimental resonant frequency were expected.

The above studies put forward "general" design strategies which compute the characteristics of a horn, such as resonant frequency or material stress, based on a given design. Their design process was established on a trial basis by repeating the design procedures until all characteristics meet the desired requirements. Alternatively, Eisner and Seager [98] presented another strategy which initially considered the required vibrational characteristics of a horn by constructing a wave function, from which the shape of the horn was derived at the following design stages.

The importance of incorporating appropriate boundary conditions in the mathematical model of a horn was pointed out by Jakubowski [99]. This paper introduced the concept of mechanical impedance and applied it to formulate the boundary conditions. The case study of an exponential horn and a cylindrical bar illustrated that by including the load conditions in the calculation, the transducer-horn system were designed more efficiently. Amza and Drimer [100] studied the design and construction of an ultrasonic horn by considering the mechanical force field in the structure. Amza investigated the choice of material for the horn manufacturing. It was shown that good results could be obtained using material such as titanium, duraluminium alloy, tool carbon steel, austenitic non-corrosive steel, Monel metal and grade carbon steel. To reduce the deviation between the prediction and the actual tuned frequency, a length correction factor was introduced during the calculation of vibration modes, which altered the vibration distribution and position of nodal points

in the solution. However, the physical meaning of the factor may be unclear in some cases.

In addition to the stepped and tapered horns, another type of horn called a block horn is used for ultrasonic process such as plastic welding. Such horns can have a wide cross-sectional area. At least one dimension of the output face is of similar size as the wavelength of ultrasound. Block horns are more efficient when distributing the ultrasonic energy over a wide area. Shoh [21] discussed the application of block horns which were first commercially used during the 1970s. However, the design of horns was not detailed in this paper. Derks [101] presented design strategies for block horns with an aim to optimise their performance by achieving uniform amplitude at the output surface. Several strategies, including avoiding the presence of other modes around the tuned frequency and incorporation of slots, were suggested.

Research on rectangular block horns used for plastic welding was reported by Adachi et al [102]. Vibration modes of horns with different slots were analysed by the finite element method. Adachi discussed the influence of the slot dimensions on the uniformity of output amplitude. A set of design rules was put forward with an attempt to achieve a flat longitudinal amplitude distribution at the output surface. Although a satisfactory design was obtained in the case studied, a more general design process was desired. In a later study, Adachi and Ueha [103] presented a novel design approach referred to as the method of wave-trapped horns. This technique modified the vibration mode by adding elastic components attached at the input face of the horn. The length of these components was adjusted until satisfactory uniformity of output amplitude was obtained. This method, however, may not be applicable for large horns as the improvements could be overwhelmed by effects of the lateral dimension.

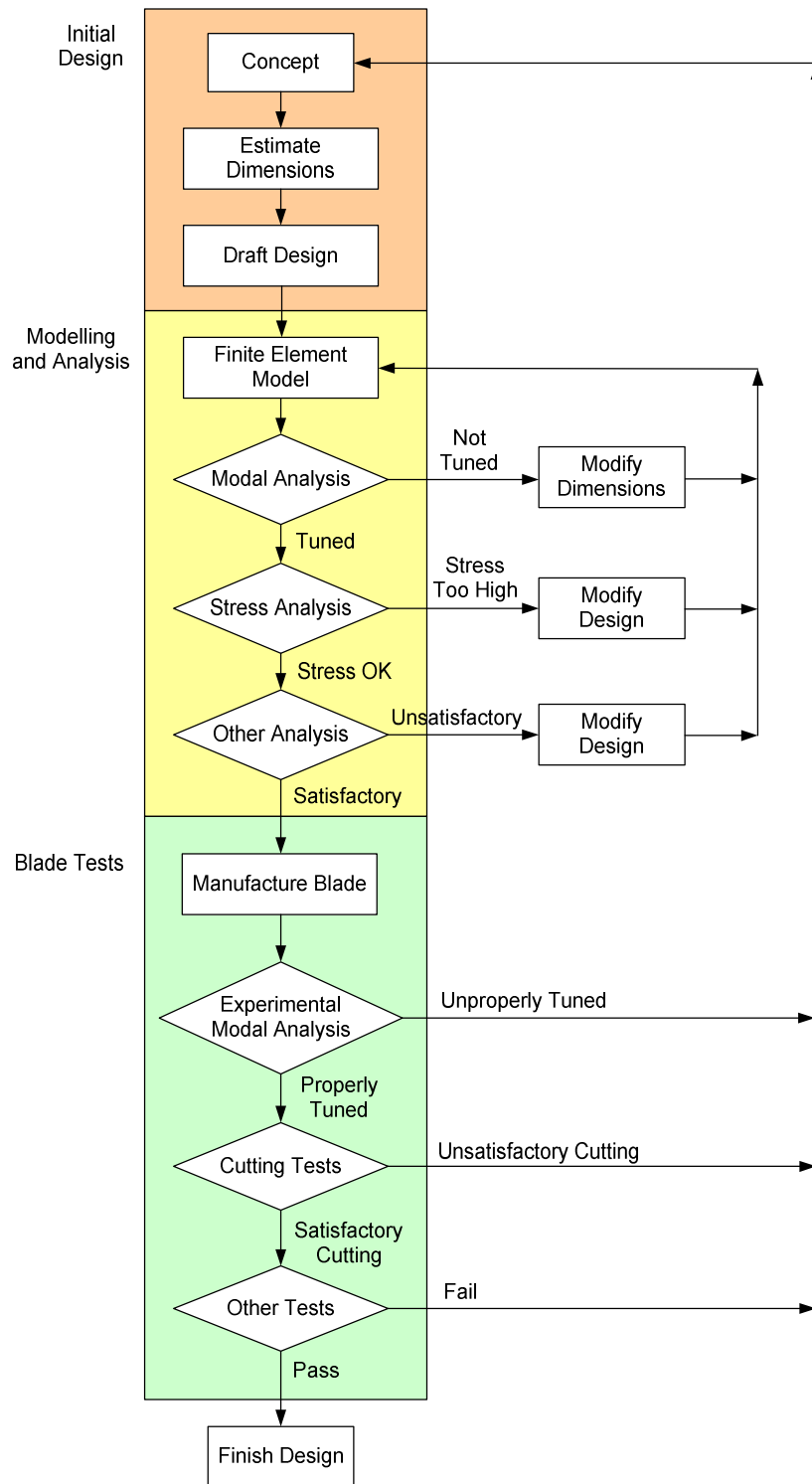
O'Shea [104] investigated the design of block horns using finite element analysis and showed that effective design of such ultrasonic components would not be possible without the identification of their modal parameters such as modal frequencies and mode shapes. In addition, Koike and Ueha [105] illustrated that the performance of the ultrasonic transducers/components could be studied through transient vibration analysis. Rather than taking into account the horn only, Koike investigated the full transducer-horn assembly using FEM and Newmark- $\beta$  method. The paper concluded that the main cause of fracture in unloaded tools could not be ascribed to transient

stress. Chapman and Lucas [106] presented the resonant frequency analysis of a thick cylindrical horn tuned in a radial mode. A combination of FEA, electronic speckle pattern interferometry (ESPI) and EMA was used to measure the horn's modal characteristics. This allowed the horn to be redesigned in a way that avoids the appearance of non-operational modes in the neighbourhood of the working frequency, reducing the occurrence of modal coupling behaviour. The study illustrated an example of design practise of ultrasonic components by applying advanced measuring techniques to validate finite element models. Cardoni [14] studied the dynamic characteristics of ultrasonic cutting devices, including half-wavelength and one-wavelength blades. It was demonstrated again that the EMA verified FE models, which enabled thorough stress and deformation inspection of ultrasonic devices, were of great importance in the design process. Cardoni also suggested that it is necessary to avoid bending vibration in order to improve the overall performance of the device.

Ultrasonic devices may be designed in a more complex form where multiple components are tuned as one assembly and are driven by the same ultrasonic transducer. This increases the efficiency of processing by allowing multiple operations, such as welding of multiple spots, to be completed simultaneously in one action. Apart from that, it simplifies the system setup and reduces the running cost by using only one set of driving and control circuits. However, such devices are characterised by complex modal behaviour, which is difficult to predict, and lower reliability. Rawson [49] discussed the application of multi-blade cutting systems in the food industry. It was illustrated that this kind of apparatus was capable of improving both the efficiency and quality of food processing. Cardoni [1, 14] detailed the design of a novel multi-blade ultrasonic cutting device. The study showed that complicated modal interaction behaviour could occur in the blade-horn assembly. The response of the excitation depended not merely on the vibration characteristics of the horn but on all attached blades as well. The study showed that the phenomenon of modal interaction and combination resonance could be improved by introducing slots and castellation in the horn design. However, it is difficult to obtain a set of general design rules for such types of ultrasonic devices.

### 1.5.4 Design of Ultrasonic Blades

Generally, the conventional design process of an ultrasonic blade includes three main parts: initial design, modelling and analysis, and blade tests [14, 39, 53]. Figure 1.8 illustrates the typical steps involving in the design process.



**Figure 1.8 Conventional Design Process of Ultrasonic Blades**

## **(1) Initial Design**

The starting point of the design process is an initial design concept, which is usually conceived according to the requirements of the application. In this stage, the basic features of the blade, such as the material, the type/shape of the blade, location of the cutting edge (e.g. on the tip of the blade for guillotine cutting or, on the sides of the blade for other types of cutting), and shape of cutting edge (with/without serration, sharp/blunt), are decided by considering the function of the blade and other design requirements.

The size, especially the length, of the blade can be estimated by taking into account the wavelength of ultrasound [14, 39, 53]. According to vibration and acoustic theories [95, 107, 108], for a uniform rod, the ultrasound wavelength in the material can be obtained by

$$\lambda = \frac{1}{2f} \sqrt{\frac{E}{\rho}} \quad (1.1)$$

where  $\lambda$  is the wavelength of ultrasound,  $f$  is vibration frequency,  $\rho$  is material density and  $E$  is Young's modulus. To enable properly excitation and achieve satisfactory vibration characteristics, an ultrasonic blade is usually design to be a half-wavelength or one-wavelength resonant structure [14, 39, 53]. Eq. (1.1) provides a simple way to estimate the rough length of the blade. For a half-wavelength blade, the length is approximately  $\lambda/2$  and for a one-wavelength blade this is  $\lambda$ . Based on this information, a draft design can be produced.

## **(2) Modelling and Analysis**

In the next stage, the draft design is modelled, analysed and refined with an aim to achieve the desired characteristics. The main analyses include modal analysis and stress analysis, which are usually performed using FEA. The basic objective is to make sure the design is resonant at the correct frequency without exceeding the tolerable stress. In addition, other analysis or simulation can also be carried out in this stage to study other characteristics of the design, such as heat generation and cutting effect.

The analysis will be followed by appropriate modification of the design and the design-analysis-modification cycle will be repeated a number of times until a satisfactory design is obtained. In the conventional design method, the modification is done by the designer based on the information obtained from the analysis, which is a job heavily relying on the designer's experience and intuition. It may take a number of trials before a satisfactory design is found. However, this may not be the best optimised design as it is difficult to examine all feasible solutions in the design process.

### **(3) Blade Tests**

As some degree of discrepancy is usually expected between the analysis and the real world problem, prototyping and testing are essential after a satisfactory design is obtained. The tests verify the actual performance of the blade, and provide useful information for analysis correction and design improvement. The characteristics of the blade that are difficult to model and analyse can also be studied in the tests.

EMA is a powerful approach to estimate the vibration characteristics of an ultrasonic blade experimentally. By identifying the vibration modes and their modal frequencies, EMA can be used to examine whether the blade can work stably in ultrasonic cutting. Cutting test is the way to evaluate the overall performance of the blade, where the prototype will be excited in normal working condition and perform cutting on test samples. The design process will complete if the blade exhibits the expected characteristics and meets the design requirements, otherwise appropriate improvements have to be made and the design process will restart.

#### **1.5.5 The Method of Optimal Design**

The proposal of the concept of optimisation can be dated back to as early as the days of Newton, Lagrange, and Cauchy [109]. However, it was not widely applied in engineering until World War II. This was partly due to the complexity of practical design problems and the limitation of calculation approaches up to that time. With the rapid advancement in computer technology, a large number of numerical optimisation algorithms emerged after the 1950s, which enabled the implementation and application of the optimal method in different kinds of realistic engineering problems.



Based on this advancement, optimal design is now an effective method in research and industry product development. The distinct characteristic of the optimisation method is that it uses mathematical algorithms in the design process to maximise the desired benefits and obtain the "best" design. Depending on the application and requirements, the "best" can mean that the system has the minimum energy consumption, largest output or lowest material stress. As the optimal design applies optimisation algorithms rather than the designers' experience or intuition to update the trial designs, the design can be done in a more reliable and effective way.

According to the nature of the problem, optimal design can be implemented using various procedures. However, the following basic stages are usually necessary for all applications [110-112]:

- (1) Formulation of the design problem.** In order to apply the relevant mathematical approaches in a real world case, the design problem must be represented in a mathematical way and be formulated into an optimisation problem. Generally, this can be done by constructing one or more objective functions to describe the goal of optimisation and defining the appropriate constraints to assign design requirements.
- (2) Evaluation of the design.** This is to compute the characteristics of the design and check the relevant performance according to the design requirements. Only those competent designs will be kept and updated for later stages.
- (3) Updating the design using optimisation algorithms.** Updated designs are generated by the optimisation algorithm in order to evaluate the improvement of the adjustment and search for better solutions. The design process is terminated when the optimal design is obtained or when other stop criteria are met.

The concept of optimal design can be applied in the design of ultrasonic blades. As optimisation algorithms enable the examination of a considerably large number of feasible designs, it is expected that the optimal design method can result in better design quality than the conventional design method. However, the main challenge of its application is how to formulate the problem of ultrasonic blade design in an appropriately way so that the optimisation can be implemented effectively. To study this issue, Chapter 5 and Chapter 6 will be devoted to the proposal, implementation and application of the optimal design method for ultrasonic bone cutting blades.

## 1.6 Summary of Work

Ultrasonic cutting offers a number of advantages over the traditional cutting methods for surgical bone cutting. As this technology relies on high frequency mechanical vibration of an ultrasonic blade to achieve cutting on bone, modelling and analysing the dynamic characteristics is crucial in the design of high performance ultrasonic surgical bone cutting blades. This thesis focuses on ultrasonic bone cutting devices that are intended to make incisions in bones with minimum damage on surrounding soft tissues. The study is devoted to the analytical modelling of the dynamic characteristics of ultrasonic blades and the proposal of an optimal blade design method.

This thesis formulates ultrasonic blades as one-dimensional structures, and studies both non-coupled vibration and coupled vibration of blades using one-dimensional theories. For non-coupled vibration, the modelling is based on the assumption that no interaction occurs between different modes of vibration. Therefore the blade can be characterised by studying its operation under a single mode of vibration using longitudinal, bending and torsional theories respectively. This study details the derivation of the analytical model and shows that the proposed method can be used as an alternative approach to FEA in the characteristics prediction of ultrasonic blades. Modelling coupled vibration is also discussed in this thesis. Two models, a parametric vibration model and a longitudinal-bending coupled vibration model, are proposed based on the one-dimensional theories by introducing mechanism of interaction between different modes of vibration.

The proposal, implementation and application of an optimal design method are discussed. The optimal design method is proposed as an improvement of the conventional design method based on the introduction of blade performance indicators. Four types of performance indicators are defined in this study, which enable the evaluation of main vibration characteristics of ultrasonic blades. The concept of the proposed method is to maximise the blade performance through the optimisation of the performance indicators. This can improve the quality of design by making sure the most desired characteristics are achieved in the blade.

Five ultrasonic blades with different cutting edges are designed in this study using either the conventional or the optimal design method. Tests of the blades suggest that satisfactory design with expected vibration characteristics can be obtained using the optimal design method, and the improvement of cutting performance can be further carried out based on the optimised design by incorporating the cutting edges that fit the most for a specific application. Ultrasonic cutting performed on biomechanical samples, ovine femur and rat bones shows that the blades are capable of making incisions on bones without the requirement of large applied force. Positive linear correlation between the applied force and the cutting speed is found in the ultrasonic cutting carried out under static applied force, and positive linear relationship between the applied force and the surface temperature is observed in the ultrasonic cutting carried out under sliding motion. The study confirms that the blades are designed with expected characteristics and satisfactory cutting performance.

# **Chapter 2**

## **Analytical Modelling of Ultrasonic Blades Operating in a Single Mode of Vibration**

### **2.1 Introduction**

Ultrasonic bone cutting relies on direct contact between a vibrating blade and the hard tissues to make incisions. Investigations have shown that the cutting performance of an ultrasonic blade is closely related to its dynamic characteristics [14, 39]. Modal parameters, including the natural frequencies and mode shapes, are among the most basic and important characteristics. For an ultrasonic blade to be properly fabricated, it is essential to inspect these parameters during the design process.

#### **2.1.1 Characterising Vibration Parameters and One-Dimensional Theories**

Finite element analysis (FEA) is a versatile and flexible method widely used during the development of ultrasonic devices to characterise the vibration parameters. Cardoni [14] applied FEA to investigate how the design of ultrasonic blades can determine their dynamic behaviour. Suggestions of design improvement were drawn based on the characterisation of modal frequencies, gain and stress. In later studies by McCulloch [53] and MacBeath [39], FEA was employed as the main tool in the design of ultrasonic food and bone cutting blades. Attempts were made to enhance the quality of analysis by improving the FE models and incorporating advanced material properties. Amin [113] calculated the tuned frequencies of horns using FEA whereby an optimisation procedure was proposed to design such devices. Zhang [114] applied FEA in the design of a micro-drill where longitudinal ultrasonic vibration is superimposed to assist the drilling process. This enabled the modelling of the flute type structure for precise eigenfrequency extraction. Applications were also presented by Lucas [42] and Alam [115] where the ultrasonic devices were modelled and analysed by FEA.

Although FEA offers an effective and flexible way to study the behaviour of ultrasonic blades, there may be limitations with this method in certain applications. Creation and meshing of 3D models are usually essential tasks of FEA in the design

of ultrasonic blade. However, these jobs can be time consuming in the early or conceptual stage of the design process where a detailed 3D model is not yet available or is unnecessary [14, 39, 53]. Instead, it may be more convenient to apply a simplified but fast method to estimate the critical parameters. Apart from that, as FEA is usually performed using commercial software packages, it can be difficult to introduce special coupling or non-linear effects in the analysis. In this case, an alternative solution can be modelling and investigating an ultrasonic blade analytically.

Taking into account the fact that the shape of a blade is usually slender and symmetric, it is possible to approximate it with a one-dimensional structure of variable cross-section as introduced in Section 1.5.2. According to vibration theories and previous studies, the longitudinal, bending (including bending along both the width and thickness directions) and torsional vibration are the basic modes of vibration that are most commonly observed in blades, horns or other ultrasonic components [14, 39, 53, 95, 107, 108]. For this reason, the modelling in this chapter will be conducted in terms of the modes of vibration using one-dimensional theories. The following sub-sections will review the relevant applications of one-dimensional theories presented in the literature.

### **2.1.2 Modelling of Longitudinal Vibration**

The tuned frequency and other modal parameters of longitudinal vibration can be calculated by treating the structure as a rod subjected to deformation along its longitudinal or axial direction. For special cases, such as a structure with uniform, linear or exponential cross-section area, the modal frequencies can be obtained directly by solving the governing equations of longitudinal vibration [92, 95, 96, 107, 116] which as a rule is the motion used for ultrasonic cutting. This can sometimes be facilitated by transforming the equation of motion into another analytical solvable representation [117]. Eisenberger [118] studied the exact solution of modal frequencies for variable cross-section bars. The function of the cross-section area was represented by polynomial variations and power series, which allowed the general solution of the dynamic axial stiffness and natural frequencies to be obtained. In theory, the method can be used to calculate all kinds of non-uniform bars as long as the cross-section area function is represented to the desired accuracy. However, its

implementation could be impractical or inconvenient for cases of complex non-uniformity. Instead of treating the structure as a whole body, some problems can be simplified using sectional representation. Li [119] discussed the exact solutions of the governing equations of longitudinal vibration using multiple sectional stepped non-uniform rods. The solution presented in the study was also applicable for other structures with a similar profile. However, for structures of complex shape, a closed form solution is usually difficult to obtain. Alternatively, numerical approaches can be applied to solve the vibration equations [92]. Merkulov [93] modelled complex ultrasonic horns by dividing them into two or several simple sections whereby the modal parameters of the whole component were obtained through a set of differential equations. However, this method concentrated on horns with circular cross-sections only. Also, the profile of the sections must be restricted to a few specified cases; otherwise difficulties may be encountered when solving the equations.

### **2.1.3 Modelling of Bending Vibration**

Using a similar concept, an ultrasonic blade or horn can be modelled as a beam in order to investigate its bending vibration. Due to causes such as manufacturing imperfection and non-linear behaviour, bending oscillation can exhibit even when a blade is excited longitudinally. However, unlike the longitudinal vibration, the bending motion is usually undesired in slender ultrasonic blades to avoid excessive stress. According to the classic Euler–Bernoulli beam theory, the governing equation of an ideal beam is a fourth order partial differential equation, which does not take into account the effects of rotary inertia and shear force. However, the ignored effects may become significant as the frequency of vibration is increased. In this case, the improved theories, such as the Timoshenko theory, would be more suitable [95, 96, 107, 116].

For certain simple tapered beams, closed form solutions of the bending vibration can be obtained. Ece [120] and Naguleswaran [121] computed the analytical solutions for beams with linear or exponential cross-section area. However, the approaches were not directly applicable for ultrasonic blades due to the complexity of the profile. In cases where exact analytical solutions are impossible to find, numerical methods can be applied. Tong [122] approximated a non-uniform and non-homogeneous beam using a number of uniform and homogeneous stepped beams. This method is flexible

when modelling complex structures. It should be treated as a numerical approach when a large number of stepped beams are used.

#### **2.1.4 Modelling of Torsional Vibration**

Ultrasonic blades or horns can be treated as a shaft structure when investigating their torsional vibration. The equation of motion in its simplest form can be obtained by considering the torsion of a uniform rod with a round cross-section [95, 107]. For other cases where non-circular cross-sections exist, it is necessary to introduce a correction factor in the equation in order to take into account the effects of distortion and warp during the torsion [123, 124]. Eisenberger [125, 126] presented an analytical method which was capable of obtaining exact form solutions of natural frequencies and dynamic stiffness matrix for torsional bars with variable cross-sections. Vet [127, 128] investigated the fundamental torsional vibration of beams with rectangular cross-sections and without boundary constraints using the Rayleigh-Ritz method. The kinetic distribution and potential energy of an elastic system was employed to determine the fundamental frequency of vibration. It showed that this was an effective method with good accuracy as long as an appropriate displacement function with adequate computing precision was used. Kulkarni [129] applied the Reissner method to determine the natural frequencies of torsional beams tapered in thickness and breadth. The procedure considered only the first two torsional modes based on a Reissner function. Results of satisfactory accuracy were obtained at fairly low computing costs. Augustyn [130] presented the equations of torsional motions for beams which had different types of cross-sections and boundary conditions, such as those with thin wall and rectangular cross-sections. These equations can be used as the analytical description of a number of structures widely used in practical applications. However, the study did not discuss the relevant solutions of the equations. Elwany [131] modelled the torsional vibration of a beam with rectangular cross-section in order to conduct optimisation in the design process. Some reasonable assumptions about deformation and stress were made, which enabled the application of the one-dimensional torsion theory. This method was of sufficient precision in the analysis of the dynamic characteristics of interest. Numerical solution and experimental results showed that the approach was effective in both modal frequency calculation and design optimisation.

The above studies show that it is a feasible solution to use one-dimensional theories to model and inspect the vibration of ultrasonic blades. The longitudinal, bending and torsional motion of a blade can be characterised by the relevant vibration theories respectively. This offers an alternative approach to extract the critical dynamic parameters of an ultrasonic blade during the design process.

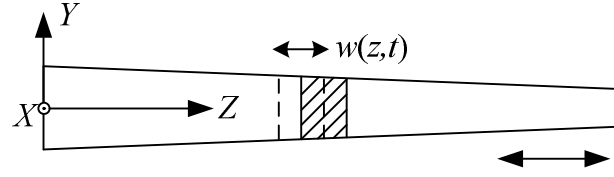
## **2.2 One-Dimensional Theories and Vibration Equations**

This section will present the fundamentals of the one-dimensional theories, which includes the vibration theories of the longitudinal, bending and torsional motion of a slender beam. It is assumed that these modes of vibration are independent of each other without the presence of any coupling effects. For each type of motion, the governing equation of vibration can be derived from a basic structure using one-dimensional theory. The concept of the modelling of an ultrasonic blade is to extend these governing equations so that the factor of variable cross-sections is taken into account. Thus, providing the shape of a blade is appropriately defined in terms of its cross-sections, the governing equations will be applicable to characterise the vibration of the blade.

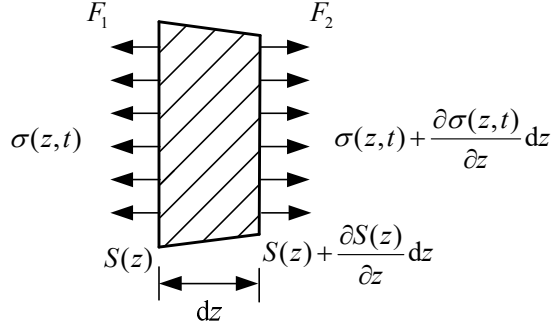
### **2.2.1 Theory of Longitudinal Vibration**

Figure 2.1(a) illustrates a bar vibrating along the longitudinal direction. It is assumed that the stress is uniformly distributed along the cross-section which remains flat in the deformation [92]. This is a satisfactory approximation when the vibration wavelength is considerably larger than the width of the beam [96]. As only the longitudinal vibration is studied in this theory, the motion is modelled with respect to  $w(z, t)$ , the displacement parallel to the longitudinal direction (axis  $Z$ ), neglecting any other contributing components of the deformation.





a) Longitudinal Vibration



b) An Element of the Beam

Figure 2.1 Longitudinal Vibration of a Beam

To obtain the governing equation of longitudinal vibration, a small beam element as illustrated in Figure 2.1(b) is considered. According to the stress analysis, the forces exerted on the faces of the element are obtained as [96]

$$F_1 = S(z)\sigma(z,t) \quad (2.1)$$

and

$$F_2 = [S(z) + \frac{\partial S(z)}{\partial z} dz][\sigma(z,t) + \frac{\partial \sigma(z,t)}{\partial z} dz] \quad (2.2)$$

where  $S(z)$  is the cross-section area and

$$\sigma(z,t) = E \frac{\partial w(z,t)}{\partial z} \quad (2.3)$$

is the stress on the cross-section,  $E$  is the modulus of elasticity,  $t$  is time. According to Newton's second law of motion, one obtains

$$F_2 - F_1 = \rho S(z) \frac{\partial^2 w(z,t)}{\partial t^2} dz \quad (2.4)$$

where  $\rho$  is the mass density of the material. By substituting Eq. (2.1) and (2.2) into Eq. (2.4) and, neglecting the infinitesimal of higher order, the governing equation of longitudinal vibration can be obtained in the following form

$$\frac{\partial}{\partial z} \left[ S(z) \frac{\partial w(z,t)}{\partial z} \right] = \frac{\rho S(z)}{E} \frac{\partial^2 w(z,t)}{\partial t^2} \quad (2.5)$$

It should be emphasised that this equation has already been taken into account the non-uniform shape of the beam by treating the cross-section area as a function.

Eq. (2.5) can be solved using the method of separation of variables by considering the harmonic vibration as

$$w(z,t) = \tilde{W}(z) [A \cos(\omega t) + B \sin(\omega t)] \quad (2.6)$$

where  $A$  and  $B$  are two constant vibration parameters,  $\omega$  is the circular frequency and  $\tilde{W}(z)$  is a time independent function known as the mode shape function [95, 96, 107, 116]. Substituting Eq. (2.6) into (2.5) yields

$$[S(z)\tilde{W}'(z)]' + \frac{\rho S(z)\omega^2}{E} \tilde{W}(z) = 0 \quad (2.7)$$

where prime denotes differentiation with respect to  $z$ . Eq. (2.7) is referred to as the equation of longitudinal mode shape function, where  $\tilde{W}(z)$  is an unknown function. As Eq. (2.7) is a second order differential equation, it is necessary to define two boundary conditions in order to obtain particular solutions. For the case of a half-wavelength ultrasonic blade, the free-free boundary conditions can be applied, which simulates the longitudinal tuning condition of the blade. In this case, the boundary conditions are given as of the form [95, 96, 107, 116]

$$\tilde{W}'(0) = 0 \quad (2.8)$$

$$\tilde{W}'(L) = 0 \quad (2.9)$$

In order to satisfy Eq. (2.7)-(2.9),  $\omega$  must be certain values known as the modal frequencies. Assigning one of such values for  $\omega$  in Eq. (2.7) will result in a group of general solutions for  $\tilde{W}(z)$ . These solutions are the associated mode shape functions of  $\omega$ , which are of similar form according to the theory of second order differential equations. Without losing generality, a particular solution obtained under a normalised input condition

$$\tilde{W}(0) = 1 \quad (2.10)$$

$$\tilde{W}'(0) = 0 \quad (2.11)$$

is defined as the normalised mode shape function of the associate  $\omega$ . Thus the modal frequencies and the normalised mode shape functions can be used to characterise the longitudinal vibration of the ultrasonic blade.

### 2.2.2 Theory of Bending Vibration

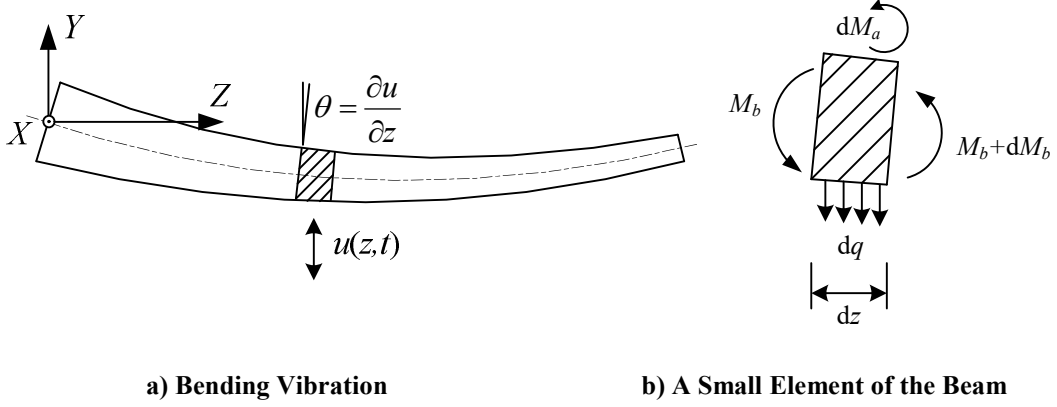


Figure 2.2 Bending Vibration of a Beam

In order to model the bending vibration of ultrasonic blades, an improved one-dimensional bending theory is presented. Figure 2.2(a) illustrates a beam in bending along its thickness direction, where  $\theta$  is the rotate angle and  $u(z,t)$  is the displacement along the axis of  $Y$ . For a small element of the beam as illustrated in Figure 2.2(b), according to the Euler–Bernoulli beam theory, the bending moment on its cross-section is given by

$$M_b = EI_x(z) \frac{\partial^2 u(z,t)}{\partial z^2} \quad (2.12)$$

where  $I_x(z)$  is the second moment of area to the axis of  $X$ . The inertia load on the element, which is associated with the translatory motion, is written as

$$dq = \rho S(z) \frac{\partial^2 u(z,t)}{\partial t^2} dz \quad (2.13)$$

The classic Euler–Bernoulli beam theory does not take into account the effects of shear force and rotary inertia. However, for a beam with a relatively large cross-section, these effects may become significant when the structure is performing high frequency vibration [95, 96, 107, 116]. Nevertheless, to simplify the problem, this

study only considers the influence of the rotary inertia. In this case, the moment of rotary inertia on the element is given as [96]:

$$dM_a = \rho I_x(z) \frac{\partial^3 u(z,t)}{\partial z \partial t^2} dz \quad (2.14)$$

The moments and load in Eq. (2.12)-(2.14) must be balanced, yielding

$$\frac{d^2}{dz^2} M_b dz - \frac{d^2}{dz^2} M_a dz + dq = 0 \quad (2.15)$$

Therefore,

$$\frac{d^2}{dz^2} [EI_x(z) \frac{\partial^2 u(z,t)}{\partial z^2}] - \frac{d}{dz} [\rho I_x(z) \frac{\partial^3 u(z,t)}{\partial z \partial t^2}] + \rho S(z) \frac{\partial^2 u(z,t)}{\partial t^2} = 0 \quad (2.16)$$

which is the governing equation of bending vibration. This equation has taken into account the case of non-uniform cross-sections by including the cross-section area and moment of area as functions.

To investigate the mode shapes and modal frequencies of the vibration, the method of separation of variables was applied to Eq. (2.16) [95, 96, 107, 116]. Defining the harmonic vibration as of the form

$$u(z,t) = \tilde{U}(z)[A \cos(\omega t) + B \sin(\omega t)] \quad (2.17)$$

where  $A$  and  $B$  are constant parameters of oscillation,  $\omega$  is the circular frequency and  $\tilde{U}(z)$  is a time independent function known as the mode shape function, and substituting Eq. (2.17) into Eq. (2.16) yields

$$[EI_x(z) \tilde{U}''(z)]'' + [\rho \omega^2 I_x(z) \tilde{U}'(z)]' - \rho \omega^2 S(z) \tilde{U}(z) = 0 \quad (2.18)$$

which is referred to as the equation of bending mode shape function. To further investigate its solution, it is necessary to define appropriate boundary conditions for Eq. (2.18). Although the ultrasonic blade is attached to the transducer, taking into account the fact that the amplitude of bending is relatively small, it is acceptable to apply free-free boundary conditions in this case, which simplifies the problem by ignoring the details of the attachment. According to the bending theory [95, 96, 107, 116], these boundary conditions are represented as of the form

$$\tilde{U}''(0) = 0, \quad \tilde{U}'''(0) = 0 \quad (2.19), (2.20)$$

$$\tilde{U}''(L) = 0, \quad \tilde{U}'''(L) = 0 \quad (2.21), (2.22)$$

Similar to the case of longitudinal vibration, to satisfy Eq. (2.18)-(2.22),  $\omega$  must be certain values known as modal frequencies. The general solutions of  $\tilde{U}(z)$  for a given modal frequency are the associated mode shape functions. Particularly, the solution obtained from a normalised input condition

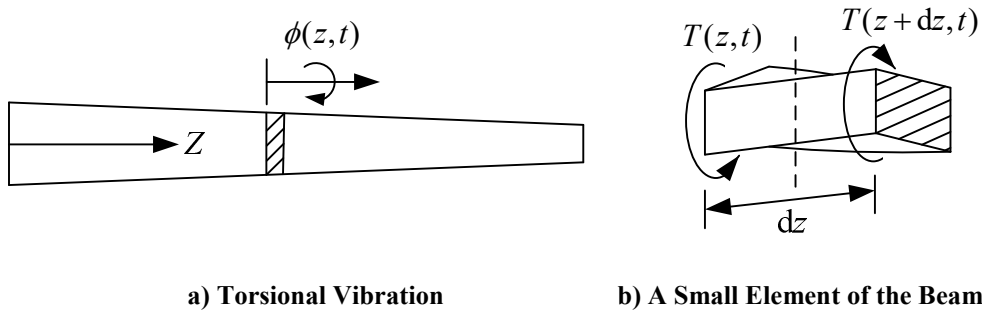
$$\tilde{U}(0) = 1, \quad \tilde{U}''(0) = 0 \quad (2.23), (2.24)$$

$$\tilde{U}''(L) = 0, \quad \tilde{U}'''(L) = 0 \quad (2.25), (2.26)$$

is defined as the normalised mode shape under the relevant modal frequency. The modal frequencies and the normalised mode shape functions are used to characterise the bending vibration of the ultrasonic blade.

Though the above equations were derived for the bending motion along the thickness direction of the beam, they are also applicable for bending along the breadth of the structure. Equations of the same form can be obtained by treating the breadth as the "thickness" of the beam, resulting in  $I_x(z)$  being replaced by  $I_y(z)$ , the second moment of area to the  $Y$  axis. However, a larger error should normally be expected in this case as the bending theory is of high accuracy only when the "thickness" is considerably smaller than the length of the beam.

### 2.2.3 Theory of Torsional Vibration



**Figure 2.3 Torsional Vibration of a Beam**

In addition to the longitudinal and bending theories, one-dimensional torsion theory was used to model the torsional vibration of an ultrasonic blade. Figure 2.3(a) illustrates a beam undertaking torsional motion, where  $\phi(z, t)$  is the torsion angle. For a small section on the beam, as illustrated in Figure 2.3(b), the torsion moment on the two planes of the element can be written as

$$T(z, t) = GJ_z(z) \frac{\partial \phi(z, t)}{\partial z} \quad (2.27)$$

$$T(z + dz, t) = G[J_z(z) + \frac{\partial J_z(z)}{\partial z} dz] \left( \frac{\partial \phi(z, t)}{\partial z} + \frac{\partial^2 \phi(z, t)}{\partial z^2} dz \right) \quad (2.28)$$

where  $G$  is the shear modulus,  $J_z(z)$  is the effective polar area moment for the cross-section, which has already taken into account the effect of distortion and warp for non-circular cross-sections.

The inertia force of rotation on the element is given by

$$dM_a(z) = \rho I_z(z) \frac{\partial^2 \phi(z, t)}{\partial t^2} \quad (2.29)$$

where  $I_z(z)$  is the second moment of area to the axis of  $Z$ . As this force is balanced by the torsion moments in Eq. (2.27) and (2.28), one obtains

$$T(z + dz, t) - T(z, t) = dM_a(z) dz \quad (2.30)$$

Therefore, applying Eq. (2.27)-(2.29) yields

$$\frac{\partial}{\partial z} \left[ J_z(z) \frac{\partial \phi(z, t)}{\partial z} \right] = \frac{\rho I_z(z)}{G} \frac{\partial^2 \phi(z, t)}{\partial t^2} \quad (2.31)$$

This is the governing equation of pure torsional vibration, which is essentially of similar form as the case of longitudinal vibration. Defining the harmonic vibration

$$\phi(z, t) = \tilde{\Phi}(z) [A \cos(\omega t) + B \sin(\omega t)] \quad (2.32)$$

in the same way as Eq. (2.6), where  $\tilde{\Phi}(z)$  is the torsional shape function, and applying the method of separation of variables, Eq. (53) becomes

$$[J_z(z) \tilde{\Phi}'(z)]' + \frac{\rho \omega^2 I_z(z)}{G} \tilde{\Phi}(z) = 0 \quad (2.33)$$

This is the equation for the torsional shape function. As a special case, for the uniform beam where  $J_z(z) = J_z$  and  $I_z(z) = I_z$  are constants, Eq. (2.33) can be simplified as

$$\tilde{\Phi}''(z) + \frac{\rho \omega^2 I_z}{G J_z} \tilde{\Phi}(z) = 0 \quad (2.34)$$

To further investigate the solution of Eq. (2.33), the free-free boundary condition is applied for this case. It is worth noting that this is also a simplified condition as the

blade is attached to the transducer rather than free at both ends. The boundary condition is given as follows according to the theory of rotation [95, 96, 107, 116]

$$\tilde{\Phi}'(0) = 0 \quad (2.35)$$

$$\tilde{\Phi}'(L) = 0 \quad (2.36)$$

In order to satisfy Eq. (2.34)-(2.36),  $\omega$  must be certain values known as modal frequencies. The general solutions of  $\tilde{\Phi}(z)$  for a given modal frequency are the associated mode shape functions. Particularly, the solution obtained from a normalised input condition

$$\tilde{\Phi}'(0) = 1 \quad (2.37)$$

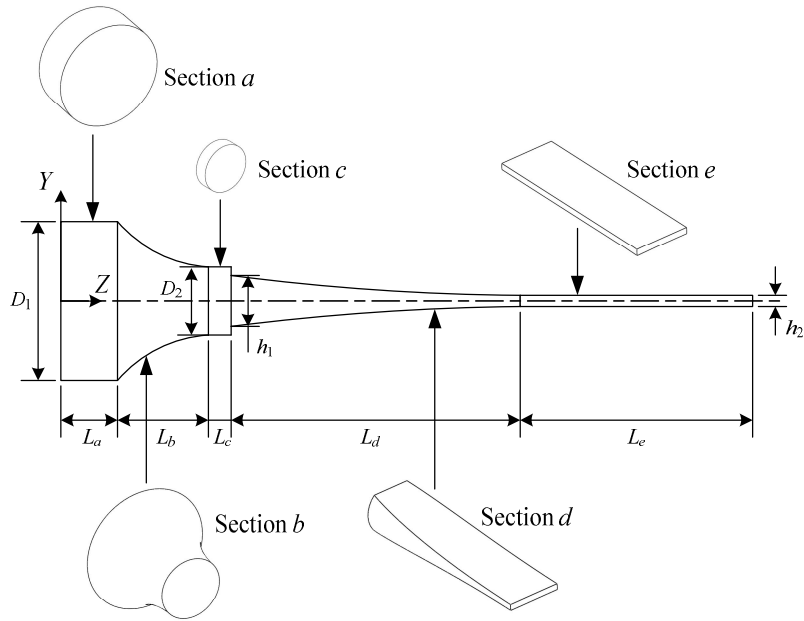
$$\tilde{\Phi}'(L) = 0 \quad (2.38)$$

is defined as the normalised mode shape under the relevant modal frequency. The modal frequencies and the normalised mode shape functions are used to characterise the torsional vibration of the ultrasonic blade.

## 2.3 Modelling of Ultrasonic Blades

### 2.3.1 Shape Parameters and Shape Functions

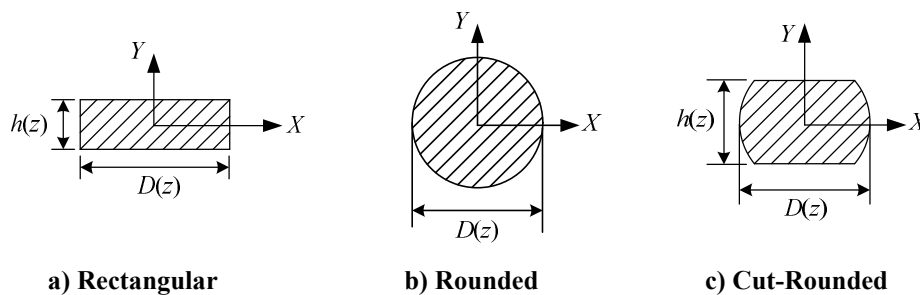
In real world applications, the shape of an ultrasonic blade is usually more complex than a uniform or tapered beam. To facilitate the analysis, a feasible solution is dividing the blade into sections of simple shape [93]. Figure 2.4 illustrates a typical case where a blade is represented as a sectional structure consisting of two cylinders (section *a* and *c*), a cone (section *b*), a tapered beam with cut-rounded cross-section (section *d*), and a uniform beam (section *e*). This type of profile is widely used in the design of ultrasonic cutting blades for both industry and surgical applications [14, 39, 53].



**Figure 2.4 Sectional Blade**

In terms of blade geometry, the solutions of the governing equations, Eq (2.5), (2.16) and (2.31), are determined by  $S(z)$ ,  $I_x(z)$ ,  $I_y(z)$ ,  $I_z(z)$  and  $J_z(z)$ . These functions are referred to as the shape functions of the blade. They are properties of the cross-section with respect to the axial coordinate  $z$ .

The shape functions can be computed based on the blade profile according to the shape of the cross-section. Three kinds of cross-sections exist in the sectional blade in Figure 2.4: rectangular, rounded and cut-rounded, which are associated with the uniform section, cylinder/cone, and tapered section, respectively. Figure 2.5 illustrates the shape of these cross-sections, where  $h(z)$  is the thickness of the blade at position  $z$  and  $D(z)$  is the width/diameter of the cross-section.



**Figure 2.5 Shape of Cross-section**

$S(z)$ ,  $I_x(z)$ ,  $I_y(z)$  and  $I_z(z)$  can be computed directly according to their definition. The following equations were presented without detailing the intermediate derivation.



For Rectangular Cross-Section:

$$S(z) = D(z)h(z) \quad (2.39)$$

$$I_x(z) = \iint_A y^2 dx dy = \frac{1}{12} D(z)h(z)^3 \quad (2.40)$$

$$I_y(z) = \iint_A x^2 dx dy = \frac{1}{12} D(z)^3 h(z) \quad (2.41)$$

$$I_z(z) = \iint_A x^2 + y^2 dx dy = \frac{1}{12} D(z)h(z)^3 + \frac{1}{12} D(z)^3 h(z) \quad (2.42)$$

For Rounded Cross-Section:

$$S(z) = \frac{1}{4} \pi D^2(z) \quad (2.43)$$

$$I_x(z) = \iint_A y^2 dx dy = \frac{\pi}{64} D(z)^4 \quad (2.44)$$

$$I_y(z) = \iint_A x^2 dx dy = \frac{\pi}{64} D(z)^4 \quad (2.45)$$

$$I_z(z) = \iint_A x^2 + y^2 dx dy = \frac{\pi}{32} D(z)^4 \quad (2.46)$$

For Cut-Rounded Cross-Section:

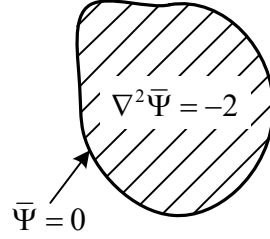
$$S(z) = \frac{1}{2} h(z) \sqrt{D(z)^2 - h(z)^2} + \frac{1}{2} D(z) \sin^{-1} \frac{h(z)}{D(z)} \quad (2.47)$$

$$I_x(z) = \frac{1}{16} h(z)^3 \sqrt{D(z)^2 - h(z)^2} + \frac{1}{32} [D(z)^4 \sin^{-1} \frac{h(z)}{D(z)} - D(z)^2 h(z) \sqrt{D(z)^2 - h(z)^2}] \quad (2.48)$$

$$I_y(z) = \frac{1}{48} h(z) [D(z)^2 - h(z)^2]^{3/2} + \frac{1}{32} [D(z)^4 \sin^{-1} \frac{h(z)}{D(z)} + D(z)^2 h(z) \sqrt{D(z)^2 - h(z)^2}] \quad (2.49)$$

$$I_z(z) = \frac{1}{16} h(z)^3 \sqrt{D(z)^2 - h(z)^2} + \frac{1}{48} h(z) [D(z)^2 - h(z)^2]^{3/2} + \frac{1}{16} D(z)^4 \sin^{-1} \frac{h(z)}{D(z)} \quad (2.50)$$

$J_z(z)$ , the effective polar area moment of cross-section, can be computed based on the Saint Venant's torsion theory using the method of Prandtl stress function [107, 123, 124].



**Figure 2.6 Prandtl Function**

As illustrated in Figure 2.6, the Prandtl stress function is defined as  $\Psi = G\phi'\bar{\Psi}$  where

$$\nabla^2 \bar{\Psi} = -2 \quad (\text{In the cross section area}) \quad (2.51)$$

$$\bar{\Psi} = 0 \quad (\text{On the boundary}) \quad (2.52)$$

and  $J_z(z)$  is obtained by

$$J_z = 2 \int_A \bar{\Psi} \, dx \, dy \quad (2.53)$$

As a special case, for rounded cross-sections, one obtains

$$J_z(z) = I_z(z) = \iint_A x^2 + y^2 \, dx \, dy = \frac{\pi}{32} D(z)^4 \quad (2.54)$$

For other types of cross-section,  $J_z(z)$  can be calculated by numerical integration of Eq. (2.53).

### 2.3.2 Finite Difference Method

For a multi-sectional ultrasonic blade as illustrated in Figure 2.4, the representation of its shape functions can be of considerable complexity. It is therefore usually impractical to find exact form solutions for the governing equations. Instead, solutions of numerical form would be a feasible option. In terms of the governing equation Eq. (2.7), (2.18) and (2.33), numerical methods are already available to solve such types of differential equations. They can be classified into two main categories which either attempts to obtain solution values at a finite number of nodes or to find

the coefficients of a number of basic functions that are the series expansions of the desired solution [132-134].

The finite difference method is a widely used numerical approach that belongs to the first category. It was applied in this study to derive the dynamic model of ultrasonic blades through the governing equations. The basic concept of this method is to approximate a differential equation by replacing the derivatives with difference operators which are represented as the sums and differences of a group of function values at discrete points (usually uniformly spaced). This will finally convert a differential problem into a set of algebraic equations that can be conveniently handled by a computer.

To find the appropriate difference approximations for Eq (2.7), (2.18) and (2.33), a function  $f(x)$  was expanded as a Taylor Series:

$$f(x+h) = f(x) + hf'(x) + \frac{h^2}{2} f''(x) + \frac{h^3}{6} f'''(x) + O(h^4) \quad (2.55)$$

$$f(x-h) = f(x) - hf'(x) + \frac{h^2}{2} f''(x) - \frac{h^3}{6} f'''(x) + O(h^4) \quad (2.56)$$

where  $h$  is a positive spatial step.

Therefore one obtains

$$f'(x) = \frac{1}{2h} [f(x+h) - f(x-h)] + O(h^2) \quad (2.57)$$

$$f''(x) = \frac{1}{h^2} [f(x+h) - 2f(x) + f(x-h)] + O(h^2) \quad (2.58)$$

Similarly, by further expanding the function into more terms, derivatives of higher order can be obtained as of the form

$$f'''(x) = \frac{1}{2h^3} [f(x+2h) - 2f(x+h) + 2f(x-h) - f(x-2h)] + O(h^2) \quad (2.59)$$

$$f''''(x) = \frac{1}{h^4} [f(x+2h) - 4f(x+h) + 6f(x) - 4f(x-h) + f(x-2h)] + O(h^2) \quad (2.60)$$

Eq. (2.57)-(2.60) can be denoted as follows

$$f'(x) \rightarrow D[f(x)] \equiv \frac{f(x+h) - f(x-h)}{2h} \quad (2.61)$$

$$f''(x) \rightarrow D^2[f(x)] \equiv \frac{f(x+h) - 2f(x) + f(x-h)}{h^2} \quad (2.62)$$

$$f'''(x) \rightarrow D^3[f(x)] \equiv \frac{f(x+2h) - 2f(x+h) + 2f(x-h) - f(x-2h)}{2h^3} \quad (2.63)$$

$$f''''(x) \rightarrow D^4[f(x)] \equiv \frac{f(x+2h) - 4f(x+h) + 6f(x) - 4f(x-h) + f(x-2h)}{h^4} \quad (2.64)$$

These are the difference operators that will be used in the following derivation. Due to their symmetric representation, they are referred to as the central difference approximations. It can be proved that the approximation is of second order accuracy [132-134].

### 2.3.3 Modelling of Longitudinal and Torsional Vibration

This sub-section will model the modal frequency and mode shape problem for longitudinal and torsional vibration of ultrasonic blades based on Eq. (2.7) and (2.33). By applying the finite difference method, the operators presented in Eq. (2.61) and (2.62), will be used to discretise the differential equations as well as compute the modal frequencies and mode shapes. As Eq. (2.7) and (2.33) are essentially second order differential equations of the same form, they can be processed using the same approach. Thus only the derivation of the longitudinal vibration will be detailed in this study.

#### 2.3.3.1 Finite Difference Equation

To obtain the finite difference approximation for the equation of the longitudinal mode shape function ( Eq. (2.7) ), one may define  $W_i$  as the discretised solution of  $\tilde{W}(z)$  at the point of  $z_i$

$$W_i = \tilde{W}(z_i) \quad (2.65)$$

and define  $S_i$  as

$$S_i = S(z_i) \quad (2.66)$$

where

$$z_i = ih \text{ for } i = 0, 1, \dots, m \quad (2.67)$$

$$h = L / m \quad (2.68)$$

$L$  is the total length of the beam,  $m$  is the number of intervals. This suggests that a total of  $m+1$  nodes uniformly distributed along the axis of the blade will be considered in the investigation.

Discretising  $S(z)\tilde{W}'(z)$  at the mid-point between  $z_{i+1}$  and  $z_i$  yields

$$S(z_{i+1/2})\tilde{W}'(z_{i+1/2}) = S_{i+1/2} \left( \frac{W_{i+1} - W_i}{h} \right) \quad (2.69)$$

and

$$S(z_{i-1/2})\tilde{W}'(z_{i-1/2}) = S_{i-1/2} \left( \frac{W_i - W_{i-1}}{h} \right) \quad (2.70)$$

Therefore

$$\begin{aligned} [S(z_i)\tilde{W}'(z_i)]' &\rightarrow \frac{1}{h} [S_{i+1/2} \left( \frac{W_{i+1} - W_i}{h} \right) - S_{i-1/2} \left( \frac{W_i - W_{i-1}}{h} \right)] \\ &= \frac{1}{h^2} [S_{i+1/2}W_{i+1} - (S_{i+1/2} + S_{i-1/2})W_i + S_{i-1/2}W_{i-1}] \end{aligned} \quad (2.71)$$

Applying Eq. (2.71) into Eq. (2.7), one may obtain the discretised form of the governing equation as

$$\frac{1}{h^2} [S_{i+1/2}W_{i+1} - (S_{i+1/2} + S_{i-1/2})W_i + S_{i-1/2}W_{i-1}] + \frac{\rho\omega^2 S_i}{E} W_i = 0 \quad (2.72)$$

or written as

$$K_{-1}^i W_{i-1} + K_0^i W_i + K_1^i W_{i+1} = 0 \quad (2.73)$$

where

$$K_{-1}^i = ES_{i-1/2} \quad (2.74)$$

$$K_0^i = \rho\omega^2 S_i h^2 - ES_{i+1/2} - ES_{i-1/2} \quad (2.75)$$

$$K_1^i = ES_{i+1/2} \quad (2.76)$$

By assigning  $i = 0, 1, \dots, m$  for Eq. (2.73), a set of algebraic equations for  $W_i$  can be obtained and written in matrix form as

$$\begin{bmatrix} K_{-1}^0 & K_0^0 & K_1^0 & & & \\ & K_{-1}^1 & K_0^1 & K_1^1 & & \\ & & \ddots & \ddots & \ddots & \\ & & & K_{-1}^m & K_0^m & K_1^m \end{bmatrix} \begin{bmatrix} W_{-1} \\ W_0 \\ W_1 \\ \vdots \\ W_m \\ W_{m+1} \end{bmatrix} = \hat{\mathbf{H}}_K \hat{\mathbf{W}} = 0 \quad (2.77)$$

This is the finite difference approximation of the longitudinal vibration problem, where  $W_0, W_1, \dots, W_m$  depict the shape of the longitudinal deformation. The terms such as  $K_{-1}^0, W_{-1}$  and  $W_{m+1}$  were introduced for the convenience of mathematical derivation. They are the properties of the virtual nodes extended outside the actual structure.

### 2.3.3.2 Modal Frequency Problem

In addition to Eq. (2.77), two more equations can be obtained from the boundary conditions. Based on Eq. (2.8) and (2.9), one can discretise the boundary conditions as

$$\frac{1}{2h}(W_1 - W_{-1}) = 0 \quad (2.78)$$

$$\frac{1}{2h}(W_{m+1} - W_{m-1}) = 0 \quad (2.79)$$

which can be written in matrix form as

$$\begin{bmatrix} 1 & 0 & 1 & 0 & \dots & \dots & 0 \\ 0 & \dots & \dots & 0 & 1 & 0 & 1 \end{bmatrix} \begin{bmatrix} W_{-1} \\ W_0 \\ W_1 \\ \vdots \\ W_m \\ W_{m+1} \end{bmatrix} = \hat{\mathbf{H}}_a \hat{\mathbf{W}} = 0 \quad (2.80)$$

Assembling Eq. (2.80) into (2.77) yields

$$\hat{\mathbf{H}}_L \hat{\mathbf{W}} = 0 \quad (2.81)$$

where

$$\hat{\mathbf{H}}_L = \begin{bmatrix} \hat{\mathbf{H}}_a \\ \hat{\mathbf{H}}_K \end{bmatrix} \quad (2.82)$$

is a  $m+3$  by  $m+3$  matrix. In fact, Eq. (2.81) is a collection of a set of homogeneous linear equations. For non-zero solutions, the determinant of  $\hat{\mathbf{H}}_L$  must be zero. Taking into account the fact that  $\hat{\mathbf{H}}_L$  is a function of  $\omega$ , this yields

$$\text{Det}[\hat{\mathbf{H}}_L(\omega)] = 0 \quad (2.83)$$

According to the vibration theory, the solutions of Eq. (2.83) are the modal frequencies of the longitudinal vibration [95, 96, 107, 116, 135]. Usually, it is not necessary to compute all the solutions for Eq. (2.83). Instead, one may apply a bisection method to search for the modal frequencies in the frequency range of interest.

### 2.3.3.3 Mode Shape Function Problem

On the basis of the solutions of Eq. (2.83), to calculate the associated mode shape function for a particular modal frequency, the normalised conditions of Eq. (2.10) and (2.11) were considered. Using a similar method, these equations can be discretised as

$$W_0 = 1 \quad (2.84)$$

$$\frac{1}{2h}(W_1 - W_{-1}) = 0 \quad (2.85)$$

or can be written in matrix form as

$$\underbrace{\begin{bmatrix} 1 & 0 & 1 & 0 & \dots & \dots & 0 \\ 0 & 1 & 0 & 0 & \dots & \dots & 0 \end{bmatrix}}_{m+3} \begin{bmatrix} W_{-1} \\ W_0 \\ W_1 \\ \vdots \\ W_m \\ W_{m+1} \end{bmatrix} = \begin{bmatrix} 1 \\ 0 \end{bmatrix} \quad (2.86)$$

Assembling Eq. (2.86) into (2.77) yields

$$\hat{H}_W \hat{W} = \hat{B} \quad (2.87)$$





Discretising  $EI_x(z)\tilde{U}''(z)$  at  $z_i$  yields

$$EI_x(z)\tilde{U}''(z) \rightarrow \frac{EI_{x_i}}{h^2}(U_{i-1} - 2U_i + U_{i+1}) \quad (2.95)$$

Discretising  $[EI_x(z)\tilde{U}''(z)]''$  at  $z_i$  yields

$$\begin{aligned} & [EI_x(z)\tilde{U}''(z)]'' \\ & \rightarrow \frac{1}{h^2} \left[ \frac{EI_{x_{i-1}}}{h^2}(U_{i-2} - 2U_{i-1} + U_i) - 2\frac{EI_{x_i}}{h^2}(U_{i-1} - 2U_i + U_{i+1}) + \frac{EI_{x_{i+1}}}{h^2}(U_i - 2U_{i+1} + U_{i+2}) \right] \\ & = \frac{E}{h^4} [I_{x_{i-1}}U_{i-2} - 2(I_{x_{i-1}} + I_{x_i})U_{i-1} + (I_{x_{i-1}} + 4I_{x_i} + I_{x_{i+1}})U_i - 2(I_{x_i} + I_{x_{i+1}})U_{i+1} + I_{x_{i+1}}U_{i+2}] \end{aligned} \quad (2.96)$$

Discretising  $[\rho\omega^2 I_x(z)\tilde{U}'(z)]'$  at  $z_i$  yields

$$[\rho\omega^2 I_x(z)\tilde{U}'(z)]' \rightarrow \frac{\rho\omega^2}{h^2} [I_{x_{i-1/2}}U_{i-1} - (I_{x_{i-1/2}} + I_{x_{i+1/2}})U_i + I_{x_{i+1/2}}U_{i+1}] \quad (2.97)$$

By applying Eq. (2.95)-(2.97) into Eq. (2.18), one obtains

$$\begin{aligned} & \frac{E}{h^4} [I_{x_{i-1}}U_{i-2} - 2(I_{x_{i-1}} + I_{x_i})U_{i-1} + (I_{x_{i-1}} + 4I_{x_i} + I_{x_{i+1}})U_i - 2(I_{x_i} + I_{x_{i+1}})U_{i+1} \\ & + I_{x_{i+1}}U_{i+2}] + \frac{\rho\omega^2}{h^2} [I_{x_{i-1/2}}U_{i-1} - (I_{x_{i-1/2}} + I_{x_{i+1/2}})U_i + I_{x_{i+1/2}}U_{i+1}] - \rho\omega^2 S_i U_i = 0 \end{aligned} \quad (2.98)$$

which can be simplified as

$$K_{-2}^i U_{i-2} + K_{-1}^i U_{i-1} + K_0^i U_i + K_1^i U_{i+1} + K_2^i U_{i+2} = 0 \quad (2.99)$$

where

$$K_{-2}^i = EI_{x_{i-1}} \quad (2.100)$$

$$\begin{aligned} K_{-1}^i &= K_{-1a}^i + \omega^2 K_{-1b}^i \\ &= (-2EI_{x_{i-1}} - 2EI_{x_i}) + \omega^2(\rho h^2 I_{x_{i-1/2}}) \end{aligned} \quad (2.101)$$

$$\begin{aligned} K_0^i &= K_{0a}^i + \omega^2 K_{0b}^i \\ &= (EI_{x_{i-1}} + 4EI_{x_i} + EI_{x_{i+1}}) + \omega^2(-\rho h^2 I_{x_{i-1/2}} - \rho h^2 I_{x_{i+1/2}} - \rho h^4 S_i) \end{aligned} \quad (2.102)$$

$$\begin{aligned} K_1^i &= K_{1a}^i + \omega^2 K_{1b}^i \\ &= (-2EI_{x_i} - 2EI_{x_{i+1}}) + \omega^2(\rho h^2 I_{x_{i+1/2}}) \end{aligned} \quad (2.103)$$



$$\underbrace{\begin{bmatrix} 0 & 1 & -2 & 1 \\ -1 & 2 & 0 & -2 & 1 \\ & & & 1 & -2 & 1 & 0 \\ & & & & -1 & 2 & 0 & -2 & 1 \end{bmatrix}}_{m+5} \begin{bmatrix} U_{-2} \\ U_{-1} \\ U_0 \\ \vdots \\ U_{m+1} \\ U_{m+2} \end{bmatrix} = \hat{\mathbf{H}}_a \hat{\mathbf{U}} = 0 \quad (2.110)$$

Assembling Eq. (2.110) into (2.105) yields

$$\hat{\mathbf{H}}_B \hat{\mathbf{U}} = 0 \quad (2.111)$$

where

$$\hat{\mathbf{H}}_B = \begin{bmatrix} \hat{\mathbf{H}}_a \\ \hat{\mathbf{H}}_K \end{bmatrix} \quad (2.112)$$

is a  $m+5$  by  $m+5$  matrix. It can be seen that Eq. (2.111) is a collection of a set of homogeneous linear equations, for non-zero solutions, the determinant of  $\hat{\mathbf{H}}_B$  must be zero. Taking into account the fact that  $\hat{\mathbf{H}}_B$  is a function of  $\omega$ , this yields

$$\text{Det}[\hat{\mathbf{H}}_B(\omega)] = 0 \quad (2.113)$$

Similar to the longitudinal vibration problem, the solutions of Eq. (2.113) are the modal frequencies of the bending vibration. The modal frequencies can be searched using a bisection method in the frequency range of interest.

### 2.3.4.3 Mode Shape Function Problem

On the basis of the solutions of Eq. (2.113), to calculate the associated mode shape function for a particular modal frequency, the normalised input condition given by Eq. (2.23)-(2.26) was considered. Similar to the problem of modal frequency, the discretised form of these equations was obtained as

$$U_0 = 1 \quad (2.114)$$

$$U_2 - 2U_1 + 2U_{-1} - U_{-2} = 0 \quad (2.115)$$

$$U_{m+1} - 2U_m + U_{m-1} = 0 \quad (2.116)$$

$$U_{m+2} - 2U_{m+1} + 2U_{m-1} - U_{m-2} = 0 \quad (2.117)$$



## 2.4 Case Study and Results

The preceding sections modelled the modal behaviour of ultrasonic blades using one dimensional theory and finite difference method. To investigate the application of the proposed model, two cases, a uniform beam and an ultrasonic cutting blade, will be studied in this section. The case study will concentrate on the computing of the modal frequencies and the associated mode shapes of the structure. Only the longitudinal vibration and the bending motion along the thickness of the beam/blade will be investigated in this study. However, similar processes can also be performed for the case of torsional vibration and bending motion along the breadth of the beam/blade.

### 2.4.1 Case Study of a Uniform Beam

The uniform beam investigated in this study is illustrated in Figure 2.7. This was a prismatic beam made of titanium alloy. The dimensions of the beam and the properties of the material are detailed in Table 2.1 and Table 2.2 respectively.

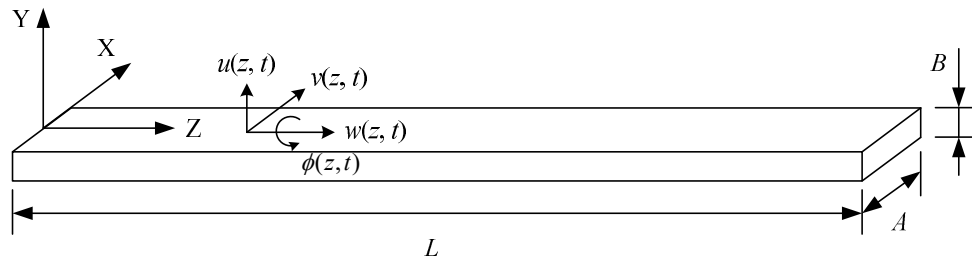


Figure 2.7 Profile of the Uniform Beam

Length ( $L$ / mm)	Width ( $A$ / mm)	Height ( $B$ / mm)
70.5	7.0	2.0

Table 2.1 Dimensions of the Uniform Beam

Material	Mass Density $\rho$ (kg/m <sup>3</sup> )	Young's Modulus $E$ (GPa)	Shear Modulus $G$ (GPa)	Poisson's Rate $\mu$
Ti90Al6V4	$4.42 \times 10^3$	110	41.4	0.33

Table 2.2 Material Properties

As the beam was of constant cross-section, the shape functions  $S(z)$  and  $I_x(z)$  were both constants, which can be calculated by Eq. (2.39) and (2.40). As a result, the

coefficients presented in Eq. (2.73)-(2.76) would all be constants. To ensure accurate solutions are obtained at acceptable computing cost, the step length of the difference operators (  $h$  in Eq. (2.61)-(2.63) ) was chosen to be 1/500 of the total length of the beam, which resulted in the following parameters:

$$K_{-1}^i = 7.7 \times 10^5 \quad (2.124)$$

$$K_0^i = 4.2078 \times 10^{-9} \times \omega^2 - 14 \quad (2.125)$$

$$K_1^i = 7.7 \times 10^5 \quad (\text{for } i=0, 1, \dots, m) \quad (2.126)$$

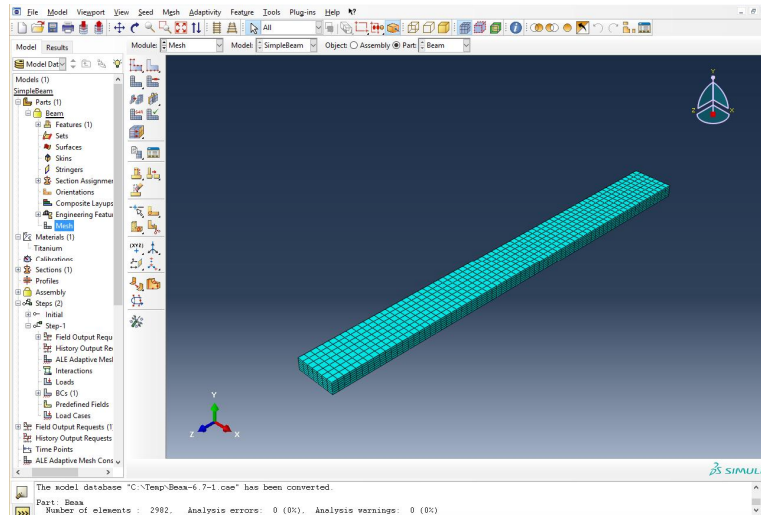
By substituting these parameters into Eq. (2.77), Eq. (2.82) and (2.88),  $\hat{H}_L$  and  $\hat{H}_W$ , the key matrices for computing modal frequencies and shape functions can be assembled. A similar process was implemented for the case of bending vibration to obtain  $\hat{H}_B$  and  $\hat{H}_U$  from Eq. (2.100)-(2.120).

On the basis of  $\hat{H}_L$  and  $\hat{H}_B$ , the modal frequencies of the uniform beam were computed by searching the roots of Eq. (2.83) and (2.113). This was conveniently done by performing a numerical bisectional search in the frequency range of 0.5-50kHz. Matlab 2008b was used to code the equations and carry out the calculation. The main Matlab script is showed in Appendix A.2.

To compare the results of the analytical modelling, finite element analysis of the uniform beam was also carried out. The FEA was conducted using the commercial package Abaqus 6.11 to calculate the modal frequencies and mode shapes for the same structure under the same conditions, as illustrated in Figure 2.8. The settings and relevant parameters of the FEA is showed in Table 2.3.

Item	Setting
Analysis Step	Natural Frequency Extraction
Frequency Range	0.5kHz-50kHz
Number of Elements	2982
Material	Ti90Al6V4, Isotropic

**Table 2.3 Setting of Finite Element Analysis**

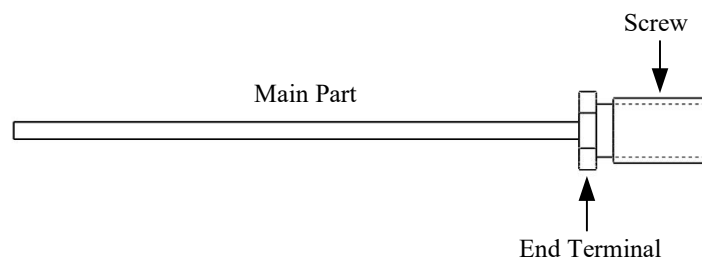


**Figure 2.8 Finite Element Analysis of Uniform Beam**

In addition, to verify these results experimentally, a beam was manufactured. As illustrated in Figure 2.9, the main part of this beam was designed to be the same size as detailed in Table 2.1. However, in order to attach the beam to the transducer, a small end terminal and a screw were introduced in the structure, which were carefully designed with an attempt to reduce their influence on the modal behaviour of the beam. This beam was excited by an ultrasonic transducer and subjected to experimental modal analysis (EMA) where its actual modal frequencies and mode shapes were extracted. The EMA results provided a reference for the solutions of the analytical model and the finite element method.



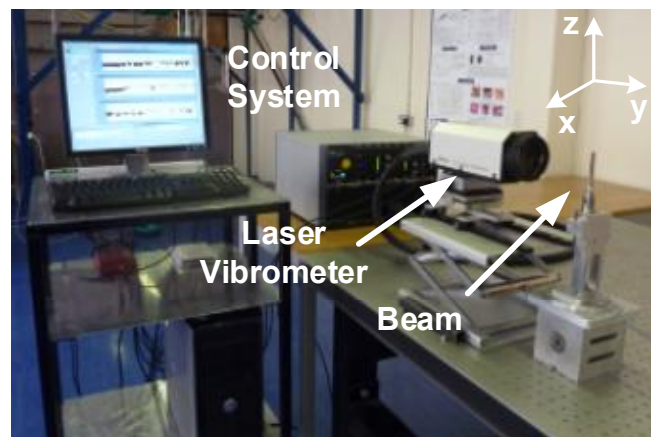
**a) Manufactured Uniform Beam**



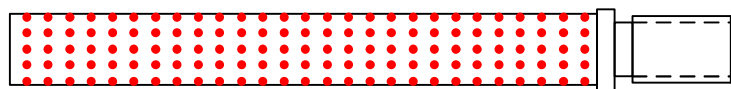
**b) Structure of the Uniform Beam**

**Figure 2.9 Manufactured Uniform Beam**

The experimental setup of EMA is illustrated in Figure 2.10. The beam was attached to a transducer clamped by a holder in front of a 3D laser vibrometer. The transducer was driven by the control system with amplified random white noise. To reduce non-linear dynamic behaviour of the beam in EMA, the output of the transducer was significantly lower than the normal level in ultrasonic cutting, only around  $0.5\mu\text{m}$  in amplitude. The vibration responses of the beam was measured using a 3D laser vibrometer by pointing the laser at specific grid locations on the beam surface ( Figure 2.10(b) ). Vibration displacement components on each grid point were measured simultaneously along three orthogonal directions: longitudinal (axis z), thickness (axis y) and width (axis x), and were used to calculate frequency response functions (FRFs). A total of 135 points were measured on the beam, generating 405 FRFs. These FRFs contained the necessary information for the reconstruction of the shape of vibration modes and extraction of the associated modal parameters.



a) Experimental Setup



b) Measure Points on the Beam

**Figure 2.10 Experimental Modal Analysis**

The modal frequencies and the associated mode shape functions obtained using the proposed analytical model are shown in Table 2.4 (labelled as "AM"), where  $L_n$  and  $B_n$  denote the  $n$ th order longitudinal and bending mode, respectively. The mode shape functions were computed using Eq. (2.87) and (2.119) by substituting  $\omega$  for particular modal frequencies. Table 2.4 also lists the solutions obtained by the finite element



analysis (labelled as FEA) and the experimental results obtained in EMA (labelled as EMA).

Table 2.4 shows that both the AM and FEA predicted the first longitudinal modal frequency accurately. The frequency difference of L1 mode was only 0.28% between the AM and EMA. For bending vibration, results of high accuracy were obtained in AM for low order modes such as B3 and B4, where the difference between the prediction and the experimental results was below 3.0%. However, larger differences, up to 6.2%, between AM and EMA was found in high order bending modes. Taking into account the fact that notably high differences up to 3.5% were also observed between FEA and EMA, this error may be partly ascribed to the introduction of the screw and end platform on the beam, which inevitably affects the dynamic behaviour of the beam. In addition, another important source of the error can be the method itself. As discussed in Section 4.2.2, Eq. (2.15) neglected the effect of shear deformation as a simplicity, which may cause increased computing errors for the cases of high order deformation [95, 96, 107, 116]. For all modes, the average difference was 3.6% in the case of AM and 2.4% in the case of FEA. Therefore, it is considered that AM predicted the modal frequencies of the beam with satisfactory accuracy, although its error was slightly larger than FEA.

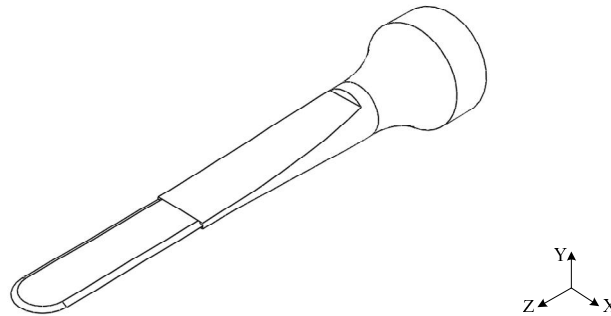
Mode		Mode Shape*	Frequency kHz	Difference AM(FEA)/EMA
L1	EMA		35.4	--
	AM		35.3	0.1kHz (0.28%)
	FEA		35.3	0.1kHz (0.28%)
B3	EMA		5.70	--
	AM		5.60	0.10kHz (1.8%)
	FEA		5.59	0.11kHz (1.9%)
B4	EMA		10.6	--
	AM		10.9	0.3kHz (2.8%)
	FEA		10.9	0.3kHz (2.8%)
B5	EMA		17.2	--
	AM		18.0	0.8kHz (4.7%)
	FEA		17.8	0.6kHz (3.5%)
B6	EMA		25.6	--
	AM		26.9	1.3kHz (5.1%)
	FEA		26.3	0.7kHz (2.7%)
B7	EMA		35.8	--
	AM		37.4	1.6kHz (4.5%)
	FEA		36.3	0.5kHz (1.4%)
B8	EMA		46.7	--
	AM		49.6	2.9kHz (6.2%)
	FEA		47.6	0.9kHz (1.9%)

\*AM for analytical model, FEA for finite element method and EMA for experimental model analysis results.

**Table 2.4 Modal Frequencies and Mode Shapes of Uniform Beams**

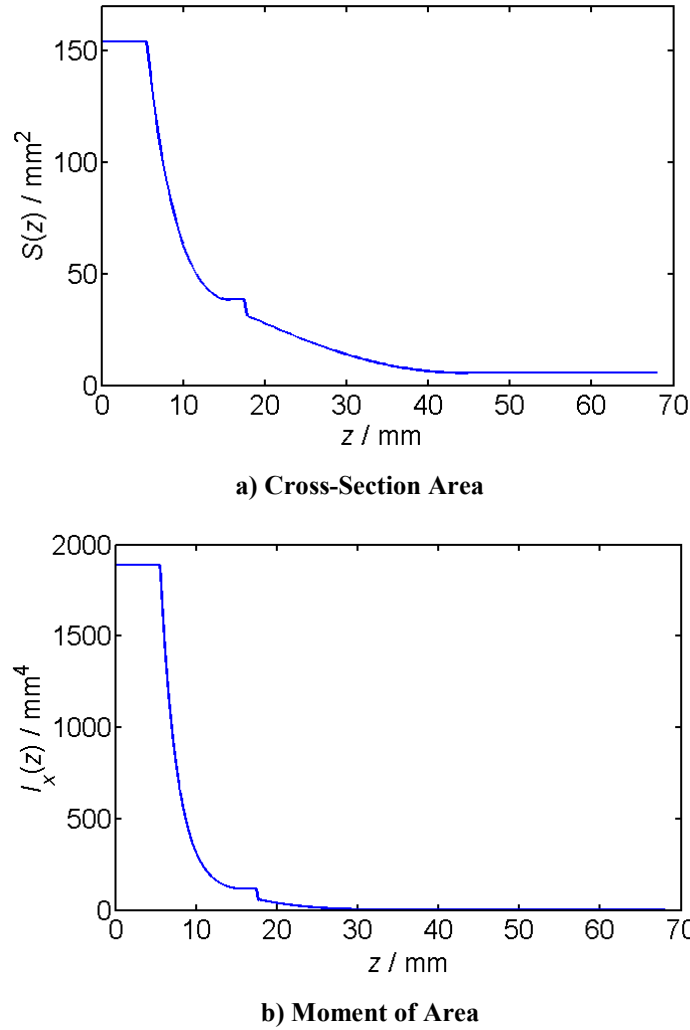
### 2.4.2 Case Study of an Ultrasonic Blade

A more complex case, an ultrasonic cutting blade, was considered in the second case study. This was a tool designed for bone cutting surgeries. As shown in Figure 2.11, it was a three-sectional structure as shown in Figure 2.4 except that the tip of the blade was rounded. Due to the insignificant change of the profile, the influence of the rounded tip was ignored in the analysis.



**Figure 2.11 Shape of the Blade**

The profile of the blade model was established using the sectional representation as detailed in section 2.3.1. The main job was to calculate the shape functions of the structure, including the area of cross-section  $S(z)$  and the moment of area  $I_x(z)$ . This was done in Matlab script according to Eq. (2.39)-(2.50). The code of the Matlab program is enclosed in Appendix A.2. Figure 2.12 plots the obtained shape functions. Due to the presence of steps in the blade profile, the shape functions and their derivatives are essentially discontinuous. To reduce the potential errors introduced by this feature, the shape functions were smoothed around the steps.



**Figure 2.12 Functions of Cross-section Area and Moment of Area**

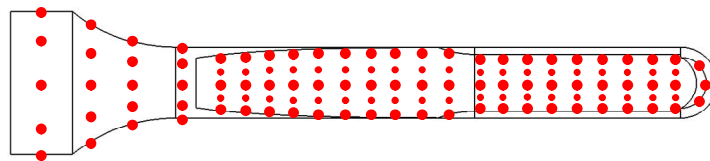
As the shape functions were not constants, the parameters in matrix  $\hat{H}_L$ ,  $\hat{H}_W$ ,  $\hat{H}_B$  and  $\hat{H}_U$  were also not constants. In spite of this, these matrices can be constructed in a similar way as shown in the case of uniform beam. The longitudinal and bending modes in the range 0.5-50kHz were calculated and the obtained results are illustrated in Table 2.5. As a comparison, Table 2.5 also shows the results of FEA for the same structure, which was obtained using similar settings as detailed in the case of the uniform beam.

In addition, to verify these results experimentally, a manufactured blade, which is illustrated in Figure 2.13, was tested. The blade was excited by an ultrasonic transducer and subjected to EMA using the same setup as in the case of the uniform beam. A total of 130 points were measured on the blade, as showed in Figure 2.14.

The actual modal frequencies and mode shapes of the blade were extracted, and the obtained results are shown in Table 2.5 as the comparison to AM and FEA.



**Figure 2.13 Manufactured Blade**



**Figure 2.14 Measured Points in EMA**

The blade was designed to be tuned at 35kHz. Table 2.5 shows that the actual frequency of the first longitudinal mode was 34.5kHz, which was within the tolerance of the frequency error. Therefore, although the AM prediction was closer to the experimental results than the FEA, the longitudinal frequency calculated by AM was slightly lower than expected. A possible source of error can be the complexity of the blade profile. According to the assumption of the theory, the stress is uniformly distributed along the cross-section and the vibration wave front lies in a plane along the whole structure. This assumption is a good approximation for slender beams with slightly tapered shapes [92, 93]. However, for an ultrasonic blade of complicated profile, the significant change of the blade outline and the appearance of steps can introduce excessive error and reduce the accuracy of prediction.

For bending modes, the differences between AM and EMA varied between 1.4% and 8%, and the differences between FEA and EMA varied between 1.6% and 7.9%. The average difference for all modes was 4.4% for AM and 4.2% for FEA, which was larger than the case of uniform beam but was considered to be satisfactory when taking account of the increased complexity of the blade profile. Therefore this case study showed that AM can be used as an alternative method to FEA in the calculation of modal frequencies for ultrasonic blades.

Mode		Mode Shape*	Frequency kHz	Difference AM/FEA AM(FEA)/EMA
L1	EMA		34.5	--
	AM		34.2	0.3kHz (0.87%)
	FEA		34.9	0.4kHz (1.2%)
B3	EMA		9.64	--
	AM		9.05	0.59kHz (6.1%)
	FEA		8.89	0.75kHz (7.9%)
B4	EMA		16.0	--
	AM		15.2	0.8kHz (5%)
	FEA		15.0	1.0kHz (6.3%)
B5	EMA		21.2	--
	AM		22.9	1.7kHz (8.0%)
	FEA		22.3	1.1kHz (5.2%)
7B	EMA		30.6	--
	AM		32.2	1.6kHz (5.2%)
	FEA		31.1	0.5kHz (1.6%)
8B	EMA		42.2	--
	AM		42.8	0.6kHz (1.4%)
	FEA		41.0	1.2kHz (2.8%)

\*AM for analytical model, FEA for finite element analysis and EMA for experimental model analysis results.

**Table 2.5 Modal Frequencies and Mode Shapes of the Ultrasonic Blade**

## 2.5 Summary

This chapter studied the analytical modelling of ultrasonic blades. Four modes of vibration, classified as longitudinal vibration, flexural bending, lateral bending, and torsional vibration, were considered in the modelling. It is assumed that a blade operates without the presence of coupling effects between different modes of vibration. Thus the motion of the structure can be studied with respect to the nature of vibration. In view of the slender profile of ultrasonic blades, the study applied one-dimensional vibration theories in the modelling. An advantage of this method is that it only requires shape functions of a single variable instead of 3D models to define the blade, enabling a straightforward and concise way of modelling.

In the presented model, the vibration of an ultrasonic blade was represented in the form of second and fourth order partial differential equations. This was later formulated into a natural modal frequency problem and a mode shape function problem using finite difference method. Both problems were arranged in matrix form where the modal frequencies can be obtained through a searching process and the mode shape problem can be dealt with using general linear equation solving techniques.

This analytical modelling method (referred to as AM) was further investigated through case studies of two structures, a uniform beam and an ultrasonic cutting blade. AM was used to calculate the longitudinal and bending modal frequencies and the associated mode shapes in both cases. To verify the results, prototypes of a beam and a blade were tested. Their modal parameters were extracted experimentally using EMA.

For the uniform beam, AM predicted the tuned frequency (first longitudinal modal frequency) accurately with a frequency difference of 0.28%. Larger frequency differences were observed in the prediction of bending vibration, especially for high order bending modes. This can be, to a certain extent, ascribed to the simplification of the theory that neglects the effects of the shear deformation in bending.

The second case concentrated on an ultrasonic blade, aiming to study the application of AM to a structure of complex profile. A slightly larger frequency difference was found in the prediction of the longitudinal mode, where the modal frequency was

lower than expected. The assumption of the uniformly distributed stress in the one-dimensional theory was regarded to be partly responsible for the error as it may not be a satisfactory approximation for the stress condition in a structure with steps and significant profile change.

The average frequency difference between AM and EMA was 3.6% in the case of uniform beam and 4.4% in the case of ultrasonic blade. This showed that AM is capable of predicting modal frequencies with satisfactory accuracy for both longitudinal and bending modes, even in the case where the structure is of complex profile. It is therefore considered that AM can be used as an alternative method to study the modal behaviour of ultrasonic blades. As AM does not require a 3D model to be constructed and meshed before the analysis, it can be used for quick performance estimation in the early stage of the design process, where a detailed design is not yet available. The calculation of a one-dimensional analytical model can be implemented faster than a 3D FE model. Thereby it can be more efficient to use AM instead of FEA for the characteristics evaluation when dealing with a large number of blade designs.



# **Chapter 3**

## **Analytical Modelling of Ultrasonic Blades Operating in Coupled Vibration**

### **3.1 Introduction**

Chapter 2 investigated the analytical modelling of ultrasonic blades, where it is assumed that vibrations of different modes are independent of each other and no interaction occurs between them during excitation. However, evidence shows that ultrasonic blades and other ultrasonic devices are often characterised by complicated dynamic phenomena including multiple responses of excitation and interaction between the vibration modes [14, 160]. For a longitudinally excited blade, this means bending or torsional vibration may also exhibit coupling with the working mode. This can bring about excessive vibration in the structure, causing energy to leak from the tuned mode to other modes [14]. The immediate consequences are increased stress in the material and reduced energy in the working mode. In view of this, it is worth studying this phenomenon by taking into account more than one mode of vibration in the modelling of ultrasonic blades. This chapter is therefore devoted to further extending the analytical models in Chapter 2 by introducing vibration interaction effects for ultrasonic blades in an appropriate way.

#### **3.1.1 Coupled Vibration in Ultrasonic System and Beam-Like Structures**

A study of coupled vibration in ultrasonic systems can be found in Cardoni et al [14, 161], where the combined resonances and modal coupling phenomena were investigated for single-blade and multi-blade cutting systems. The research was done using finite element analysis and experimental investigation. Based on the experimental results, a number of approaches, such as introducing slots in the horns and altering the location of the connecting studs, were suggested in order to reduce the negative effects of the modal interactions. In addition, it is reported that measurement of the responses and mathematical models of beam-like structures could be used to characterise the modal interactions of ultrasonic cutting systems.

Gallego-Juárez [162] investigated the nonlinearity and modal interaction phenomenon in high power ultrasonic transducers experimentally. The work focused on the ultrasonic stepped plate transducers that can be used for fluid processing. To enhance the performance, both longitudinal and flexural vibration was used in the transducers by incorporating a special plate in the structure. However, the complexity of this design makes it difficult to avoid interactions between the operation mode and untuned modes. Significant coupled vibration and exchange of energy between the modes were observed, which was unlikely to be predicted by linear analysis methods.

In addition to the ultrasonic systems, more general research objects are simple structures such as beams and rods. Nayfeh [163, 164] investigated the non-linear oscillation in a number of structures including beams and rods. It showed that under specific boundary condition and excitation, the steady state motion did not exist for certain values of the dynamic parameters. Instead, the phenomenon of continual energy exchange between the longitudinal and transverse vibration was expected for such a circumstance. This behaviour was reported again in Nayfeh [165] where the vibration energy was transferred from high frequency modes to low frequency modes in a flexural beam. The phenomenon was caused by motions modulated periodically and chaotically under certain conditions and was considered to have great potential danger in some structures as the response of the low frequency mode could be considerably larger than the directly excited high frequency mode.

Mukhopadhyay [166, 167] investigated a thin beam subjected to longitudinal excitation with an attempt to study its lateral and torsional vibration. The dynamics of the beam was represented by a set of coupled equations of Mathieu type. A key factor of the analysis was to take into account the initial built-in deflections in the structure. The initial deflection would introduce a forced term in the governing equation, resulting in effects of both parametric and forced excitation. This theory was in agreement with experimental results. However, significant non-linear phenomenon with high bending/torsional amplitude and limit cycle was reported in two instability regions, which could not be explained by the analysis based on linear theories.

### 3.1.2 Parametric and Auto-Parametric Vibration of Beam-Like Systems

Research has shown that complex multi-modal behaviour and coupling can be generated in relatively simple structures such as cantilever beams or rods by the phenomenon of parametric vibration. The terminology parametric vibration is used to describe cases where the excitation acts as a time varying modification of system parameters. This differs from forced vibration in that the alteration of the parameters can drive the system in addition to the excitation.

In the work of Cartmell [168], it is illustrated that more than one resonance could be excited simultaneously in a structure under an external excitation of a single frequency. It is also reported that a weaker type of coupling could impose considerable influence on a stronger type of coupling. The study was extended in later research [169], where a simple cantilever beam with a lumped end mass was excited in the stiff direction by a harmonic excitation at the base. The governing equations of this system were derived by applying the Lagrange's formulation on the system kinetic and potential energy functions. The work highlighted the conceptualisation of such problems by demonstrating the application of classical engineering theories in the modelling. Forehand [170] re-examined the work and confirmed that the key stages in the derivation of Cartmell's work were correct. The system investigated by Cartmell and Forehand is a typical case where both forced and parametric vibration occurs. Another feature of such structures is coupling of vibration between the longitudinal, lateral and torsion motion.

Cartmell's work was further extended by Ibrahim [171], where analytical, numerical and experimental investigation of the deterministic and stochastic response was conducted on an inextensible cantilever beam. The bending and torsional modes were cross-coupled through carefully applied excitation and inertia nonlinearities. It showed that nonlinear interaction occurred in the form of energy exchange. In certain conditions, the bending mode vibrated not merely at its own modal frequency but at frequency components close to the torsional modal frequency as well. In addition, a similar phenomenon was also found in the torsional vibration. It was reported that the level and bandwidth of the excitation was responsible for the generation of various types of responses.

Su [172] applied this theory for a flexible composite structure, which consists of a glass epoxy beam bonded with two pieces of pre-strained shape memory alloy (SMA). This structure was subjected to combined bending-torsional motions as well as the recovery force generated by the activation of the SMA. It showed that by investigating the natural frequencies and mode shapes of the beam, the theory can be used to study the influence that the SMA strip exerted on the structure.

A modified version of the lumped mass beam theory was presented by Oguamanam [173]. In his work, a mathematical model was proposed to investigate the modal behaviour and orthogonality condition of a cantilevered Euler-Bernoulli beam. The beam was characterised by an attached end mass with an offset between the gravity centre and the attachment. As a result of this special feature, the structure could experience both torsional vibration and planar bending. However, little attention was given to the effect of longitudinal deformation.

In addition, Bux [174, 175] studied a system with coupled beams and suggested that a considerable non-linear modal interaction effect may be introduced in such systems as a result of the so called autoparametric vibration. Under certain internal resonance conditions, the normal linear excited modes could be absorbed by the modes indirectly excited. A significant feature of these indirectly excited modes is that they may exhibit substantially large non-synchronous responses. The presence of high order non-linear coupling terms in the analytical model and the existence of internal resonance effects between the modes were regarded to be responsible for the occurrence of violent non-synchronous bending and torsional vibration. A later study by Warminski [176] investigated a similar system both theoretically and experimentally. It confirmed that the nonlinear terms caused by the coupled structure could result in a number of unexpected responses. However, as the theory involved two beams coupled at right angles, it is unlikely to be directly applied for the case of ultrasonic blades.

### **3.1.3 Other Research on the Coupled Vibration of Beam-Like Systems**

Silva [177, 178] formulated the nonlinear dynamics of inextensional beams that are experiencing torsional vibration and flexural oscillation along two principal directions. A set of governing differential equations were developed with an aim to retain the

contributions of the nonlinear curvature and nonlinear inertia. Nonlinearities of up to third order were included in the equations and the coupling effects of the flexural-torsional oscillations were incorporated by introducing three Euler angles. This was illustrated to be an effective model by a case study of forced vibration. However, as the theory was developed based on beams of inextension, the effects of longitudinal vibration is not possible to be incorporated.

A study on transverse and longitudinal vibration coupling was presented by Scurtu [179], where an automotive belt was modelled for the nonlinear coupling behaviour. The belt was excited longitudinally at one end and clamped at the other end, which allowed the coupled oscillation between the longitudinal and transverse modes to take place. The system was modelled based on a set of beam assumptions and solved by the Analog Equation Method whereby two coupled hyperbolic nonlinear differential equations were reduced to two linear uncoupled equations. A stable and predictable beating phenomenon was found in the transverse vibration, which was considered to be the result of an internal resonance caused by the periodic energy transfer between the transverse vibration and the longitudinal excitation. Jang [180] applied spectral element analysis to model the axial-bending-shear coupled vibration of composite laminated beams loaded axially. The study was conducted based on Timoshenko beams and the first order shear deformation theory. The model took into account the effect of axial-bending coupling and was claimed to be of high accuracy and computational efficiency.

In addition, Krawczuk [181] modelled the coupled bending and longitudinal forced vibration of a Timoshenko cantilever beam with a crack. The crack was introduced as a one-edge, non-propagating and closing transverse notch. The problem was modelled by the finite element method and formulated by the harmonic balance method. It showed that the response of the structure was predominantly decided by the location and depth of the crack as well as the frequency of the longitudinal excitation. Similar work was also done by Darpe [182] and Papadopoulos [183]. In their studies, the coupling between the longitudinal and bending vibration was introduced as a result of the presence of the crack. The relevant effects, however, would not occur in the case of non-cracked beams.

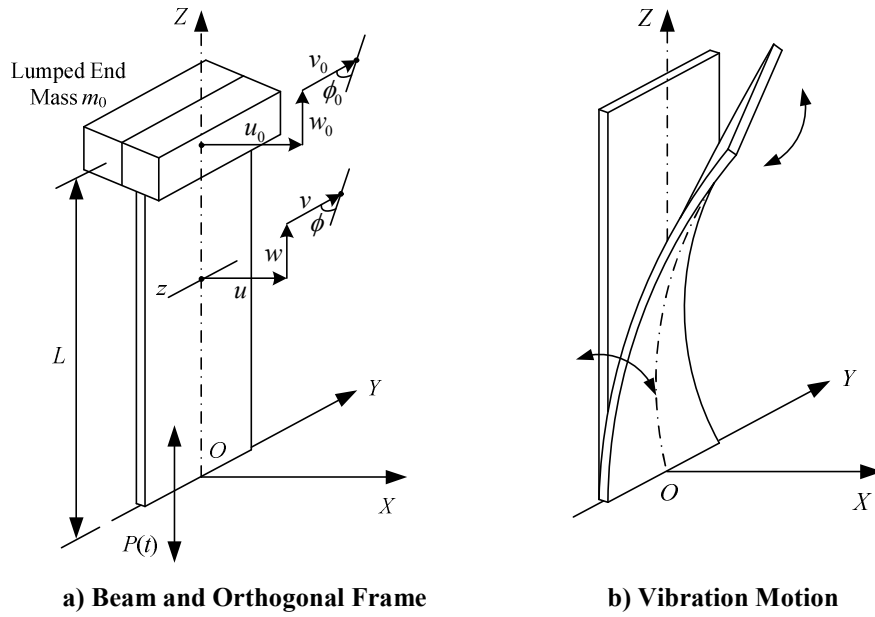
O'Reilly [184] applied a one-dimensional model to study the coupled lateral and longitudinal vibration of a rectangular parallelepiped. The method was developed based on Green and Naghdi's work [158, 159, 185-188] on rod theory. O'Reilly modelled the rod/beam using a directed curve, where a set of deformable vector fields were associated with the material points. An advantage of this method was its ability to model lateral contraction and expansion of the rod-like structure. Although the study concentrated on the relationship between the shape of the cross-section and the response of the structure, the presented method could be further extended to investigate the coupled behaviour between the longitudinal and the lateral vibration.

### **3.2 A Model for Parametric Excited Cantilever Beams**

As discussed in Chapter 2, taking into account the slender profile of ultrasonic blades, it is possible to approximate a blade using a one-dimensional beam. A uniform beam would be a relatively rough approximation for an ultrasonic blade. In spite of this, in view of its geometric simplicity, the investigation of such a structure is a good way to understand the coupled vibration of ultrasonic blades. Therefore this study will extend Cartmell's work [169] on the parametric vibration of beams with an attempt to apply this theory to ultrasonic systems.

#### **3.2.1 Assumptions and Representation of the Problem**

The representation of the problem is illustrated in Figure 3.1, where a beam with a lumped end mass  $m_0$  is used to represent the structure of an ultrasonic blade. As shown in Figure 3.1(a), an orthogonal frame  $X$ - $Y$ - $Z$  is established at the bottom of the beam with  $Z$  corresponding to the longitudinal direction. The bending, lateral, longitudinal displacement and the torsional angle of the beam on position  $z$  is denoted by  $u$ ,  $v$ ,  $w$  and  $\phi$ , respectively. The beam is subjected to a vertical periodic excitation  $P(t)$ , and exhibits combined bending and torsional motion under a slight initial bending displacement and twist angle, as illustrated in Figure 3.1(b).



**Figure 3.1 The Representation of the Problem**

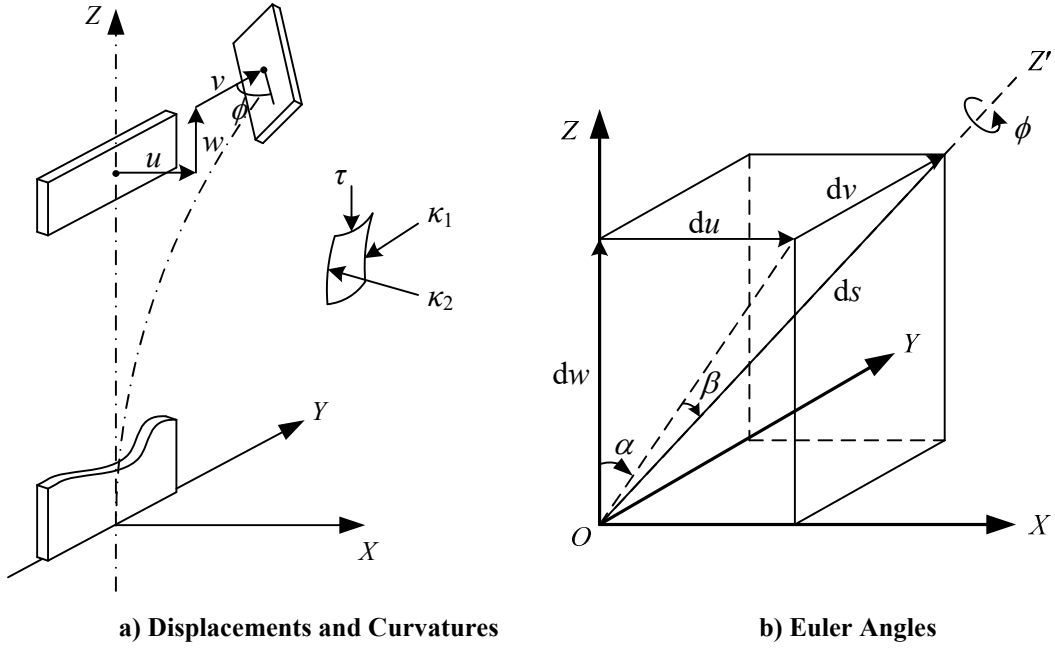
The coupling motion between the bending and torsional vibration was the main concern in several studies [169-172], where the longitudinal displacement  $w$  was regarded as the axial drop under the combined bending and torsional movement [171]. For this reason, these studies [169-172] represented  $u$  and  $\phi$  by the mode shapes and modal co-ordinates. However, in this chapter, the longitudinal displacement was considered to be of significant value due to the external excitation. Therefore instead of representing  $u$  and  $\phi$  directly,  $w$  and  $\phi$  were assumed to be of the form as

$$w(z,t) = f_1(z)w_{01}(t) \quad (3.1)$$

and

$$\phi(z,t) = g_1(z)\phi_{01}(t) \quad (3.2)$$

where  $f_1(z)$  and  $g_1(z)$  are the mode shape functions, and  $w_{01}(t)$  and  $\phi_{01}(t)$  are the modal co-ordinates. Only the first longitudinal and torsion modes were considered in this research, however, additional modes can be included if complicated modal behaviour is of interest.



**Figure 3.2 Component displacement and Euler angles**

On the basis of Eq. (3.1) and (3.2), the other two displacements,  $u$  and  $v$ , can be represented through  $w$  and  $\phi$  by taking into account the geometry restrictions. To do this, the curvatures were used to reveal the relationship between the displacements. Figure 3.2(a) shows an element taken from the beam, where the curvatures about the axis of  $X$ ,  $Y$  and  $Z$  are denoted as  $\kappa_1$ ,  $\kappa_2$  and  $\tau$ , respectively. According to the derivation in reference [169], the following equations were obtained

$$\kappa_1 = \alpha' \sin \phi \cos \beta - \beta' \cos \phi \quad (3.3)$$

$$\kappa_2 = \beta' \sin \phi + \alpha' \cos \phi \cos \beta \quad (3.4)$$

$$\tau = \alpha' \sin \beta + \phi' \quad (3.5)$$

where the prime denotes differentiation with respect to  $s$  the linear displacement along the deformed axis  $OZ'$ .

The link between the Euler angles and the elemental component displacements is illustrated in Figure 3.2(b), where angle  $\phi$  is the torsional co-ordinate.  $\alpha$  and  $\beta$  are expected to be expressed in terms of the component displacements. Assuming  $ds$  is sufficiently short, one may obtain

$$du = u' ds \quad (3.6)$$

$$dv = v' ds \quad (3.7)$$

$$dw = w' ds \quad (3.8)$$



By referring to the analysis in reference [169], the representation of the curvatures can be written as

$$\kappa_1 = u''\phi - v'' \quad (3.9)$$

$$\kappa_2 = v''\phi + u'' \quad (3.10)$$

$$\tau = v'u'' + \phi' \quad (3.11)$$

Since  $v$  is extremely small compared to the length of the beam, it is reasonable to state that

$$\kappa_1 \approx 0 \quad (3.12)$$

Therefore,

$$v'' = u''\phi \quad (3.13)$$

and

$$\kappa_2 = u''(1 + \phi^2) \quad (3.14)$$

By integrating Eq. (3.13) twice, the expression for the lateral displacement can be obtained as

$$v(\zeta, t) = \int_0^\zeta (\zeta - z)u''\phi dz \quad (3.15)$$

On the other hand, as shown in reference [169], the relationship between  $u$  and  $w$  can be written as

$$w(\zeta, t) = \frac{1}{2} \int_0^\zeta u'^2 dz \quad (3.16)$$

Substituting Eq. (3.1)-(3.2) into Eq. (3.15)-(3.16) yields,

$$u(\zeta, t) = \int_0^\zeta \sqrt{2w'} dz = \sqrt{w_{01}(t)} \int_0^\zeta \sqrt{2f_1'(z)} dz = B_1(\zeta) \sqrt{w_{01}(t)} \quad (3.17)$$

$$v(\zeta, t) = \phi_{01}(t) \sqrt{w_{01}(t)} \int_0^\zeta (z - \zeta) \frac{f_1''(z)g_1(z)}{\sqrt{2f_1'(z)}} dz = B_2(\zeta) \phi_{01}(t) \sqrt{w_{01}(t)} \quad (3.18)$$

$$u'' = -\frac{w''}{\sqrt{2w'}} = -f_1''(z) \sqrt{\frac{w_{01}(t)}{2f_1'(z)}} = B_3(z) \sqrt{w_{01}(t)} \quad (3.19)$$

where

$$B_1(\zeta) = \int_0^\zeta \sqrt{2f_1'(z)} dz \quad (3.20)$$

$$B_2(\zeta) = \int_0^\zeta (z - \zeta) \frac{f_1''(z)g_1(z)}{\sqrt{2f_1'(z)}} dz \quad (3.21)$$

$$B_3(z) = -\frac{f_1''(z)}{\sqrt{2f_1'(z)}} \quad (3.22)$$

### 3.2.2 System Energy and Equation of Motion

Based on the above analysis, the equations of motion can be derived by means of Lagrangian dynamics. By taking into account the motion along different axes [169], the total system kinetic energy can be obtained as

$$T = \frac{1}{2} m_0 [\dot{u}_0^2 + \dot{v}_0^2 + (\dot{P} - \dot{w}_{01})^2] + \frac{1}{2} I_0 \dot{\phi}_{01}^2 \quad (3.23)$$

where the dot denotes differentiation with respect to time. Substituting Eq. (3.17) and (3.18) into Eq. (3.23) yields,

$$\begin{aligned} T = & \frac{1}{4} B_{01} \frac{\dot{w}_{01}^2(t)}{w_{01}(t)} + B_{02} \dot{\phi}_{01}^2(t) w_{01}(t) + B_{02} \dot{\phi}_{01}(t) \phi_{01}(t) \dot{w}_{01}(t) \\ & + \frac{1}{4} B_{02} \phi_{01}^2(t) \frac{\dot{w}_{01}^2(t)}{w_{01}(t)} + \frac{1}{2} m_0 \dot{P}^2 - m_0 \dot{P} \dot{w}_{01} + \frac{1}{2} m_0 \dot{w}_{01}^2 + \frac{1}{2} I_0 \dot{\phi}_{01}^2 \end{aligned} \quad (3.24)$$

where

$$B_{01} = \frac{1}{2} m_0 B_1^2(L) \quad (3.25)$$

$$B_{02} = \frac{1}{2} m_0 B_2^2(L) \quad (3.26)$$

In addition, the total system potential energy can be obtained by adding together the potential energy induced in the bending, longitudinal and torsional deformation.

Therefore,

$$\begin{aligned}
U &= \int_0^L \frac{1}{2} EI_y u''^2 dz + \int_0^L \frac{1}{2} E w'^2 dz + \int_0^L c G J \phi'^2 dz \\
&= \int_0^L \frac{1}{2} EI_y B_3^2(z) w_{01}(t) dz + \int_0^L \frac{1}{2} E [f_1'(z) w_{01}(t)]^2 dz + \int_0^L c G J [g_{01}'(z) \phi_{01}(t)]^2 dz \\
&= B_{03} w_{01}^2(t) + B_{04} w_{01}^2(t) + B_{05} \phi_{01}^2(t)
\end{aligned} \tag{3.27}$$

where

$$B_{03} = \int_0^L \frac{1}{2} EI_y B_3^2(z) dz \tag{3.28}$$

$$B_{04} = \int_0^L \frac{1}{2} E f_1'^2(z) dz \tag{3.29}$$

$$B_{05} = \int_0^L c G J g_{01}'^2(z) dz \tag{3.30}$$

In Eq. (3.23)-(3.30),  $m_0$  is the mass of the lumped mass,  $P$  is the displacement of the excitation applied in the longitudinal direction,  $I_0$  is the moment of inertia of the beam about the  $Z$ -axis,  $E$  is the Young's modulus,  $EI_y$  is the flexural rigidity about the  $Y$ -axis,  $GJ$  is the torsional rigidity about the  $Z$ -axis,  $c$  is a non-circular section torsion constant and the dot denotes differentiation with respect to  $t$ .

According to the theory of Lagrangian dynamics, the governing equations of the system can be obtained by implementing Eq. (3.24) and (3.27) within Lagrange's equation which is of the form

$$\frac{d}{dt} \left( \frac{\partial T}{\partial \dot{q}_i} \right) - \frac{\partial T}{\partial q_i} + \frac{\partial U}{\partial q_i} = 0 \tag{3.31}$$

where  $q_i$  are generalised co-ordinates which are specified as  $w_{01}$  and  $\phi_{01}$  in this case.

This yields the following equations:

$$\begin{aligned}
&2B_{01} \ddot{w}_{01}(t) w_{01}(t) - B_{01} \dot{w}_{01}^2(t) + 4B_{02} \ddot{\phi}_{01}(t) \phi_{01}(t) w_{01}^2(t) \\
&+ 4B_{02} \dot{\phi}_{01}(t) \phi_{01}(t) w_{01}(t) \dot{w}_{01}(t) - B_{02} \phi_{01}^2(t) \dot{w}_{01}^2(t) + 2B_{02} \phi_{01}^2(t) \dot{w}_{01}(t) w_{01}(t) \\
&+ (4B_{03} - 4m_0 \ddot{P}) w_{01}^2(t) + 4m_0 \ddot{w}_{01} w_{01}^2(t) + 8B_{04} w_{01}^3(t) = 0
\end{aligned} \tag{3.32}$$

and

$$\begin{aligned}
& 4B_{02}\ddot{\phi}_{01}(t)w_{01}^2(t) + 4B_{02}\dot{\phi}_{01}(t)\dot{w}_{01}(t)w_{01}(t) + 2I_0\ddot{\phi}_{01}w_{01}(t) \\
& + 2B_{02}\phi_{01}(t)\ddot{w}_{01}(t)w_{01}(t) - B_{02}\phi_{01}(t)\dot{w}_{01}^2(t) + 4B_{05}\phi_{01}(t)w_{01}(t) = 0
\end{aligned}
\tag{3.33}$$

Eq. (3.32) and (3.33) are the equations of motion for the studied beam system, which are high order non-linear differential equations with respect to the modal displacement/angle  $w_{01}$  and  $\phi_{01}$ . These equations can be used with Eq. (3.1), (3.2), (3.17) and (3.18) to investigate the dynamic behaviour of the beam.

### 3.2.3 Discussion

A parametric excited beam was modelled in this section with an attempt to investigate the application of the theory to ultrasonic blades. This study extended the work in reference [169] by considering a clamped beam with a lumped mass. The motion of the beam was studied in a three-dimensional orthogonal frame plus a degree of torsion, which allows the coupled effect between vibrations of different axes to be considered.

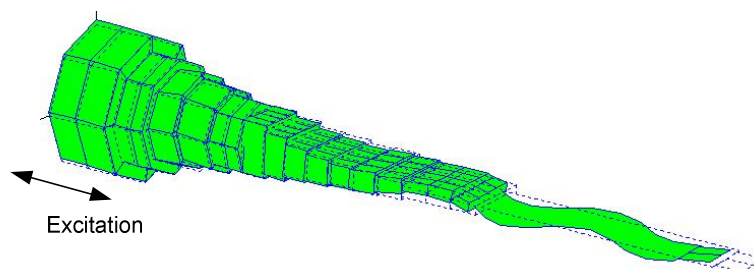
The beam was assumed to perform coupled bending and torsional vibration under the applied excitation as a result of its slender shape and the effect of the lumped end mass. This behaviour was modelled by taking into account the geometry restrictions of the structure, such as the relationship between the curvatures and displacements, as detailed in Eq. (3.3)-(3.22). The equations of motion were obtained by means of Lagrangian dynamics and presented as second order non-linear differential equations with respect to the generalised co-ordinates, as illustrated in Eq. (3.32) and (3.33). Together with the relationship defined by Eq. (3.1), (3.2), (3.17) and (3.18), these equations can provide insights into the dynamic behaviour of the system.

The study in this thesis extended the work of Cartmell [168-170] by reconsidering the motion of the lumped cantilever beam under a longitudinal excitation, which modelled the parametric vibration and modal coupling behaviour using a system of relatively simple structure. The original form of the parametric excited cantilever beam theory was theoretically and experimentally verified in Cartmell [168] and Ibrahim [171]. Cartmell [168] applied perturbation analyses on the analytical model, which showed the existence of steady state form responses of the combination

resonances. This was further confirmed by experimental verification. For excitation magnitude of medium level, in which case the modal responses of the structure are neither nonstationary nor non-stable, the theoretical predictions were in satisfactory agreement with the experimental results. Ibrahim [171] used Monte Carlo simulation to estimate response statistics of the cantilever beam. This technique successfully revealed that the type of response, deterministic or random, is primary determined by the level and bandwidth of the excitation. Together with the experimental measurement, Ibrahim's work showed that the parametric excited cantilever beam theory is effective and can be applied to the study of non-linear behaviour of such structure. Although further theoretical study on Eq. (3.32) and (3.33) were not carried out in this thesis, it is expected that similar techniques presented in Cartmell [168] and Ibrahim's [171] work can be applied in the proposed model to study the vibration of ultrasonic blades.

### 3.3 A Model for Longitudinal-Bending Coupled Vibration

For a longitudinally excited ultrasonic blade, due to the slender profile and non-linear behaviour, it is commonly observed that bending oscillation along the thickness of the blade exhibits simultaneously with the longitudinal vibration. Figure 3.3 shows a vibration model of a blade obtained from experimental modal analysis, where significant coupled longitudinal and bending vibration was found under a longitudinal excitation.

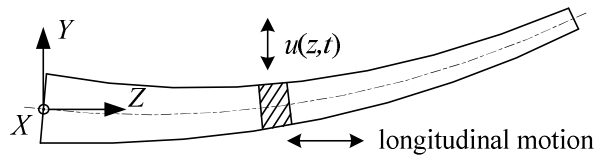


**Figure 3.3 Coupled Longitudinal and Bending Vibration**

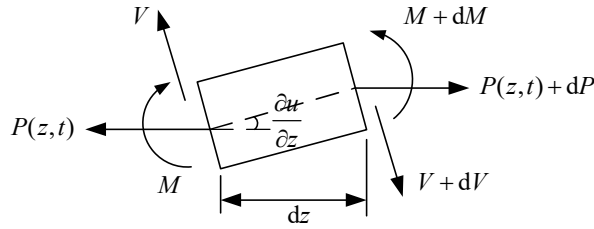
Such behaviour may cause negative effects on the blade as the bending vibration can increase the material stress and the possibility of structure failure. In view of this, this section will be devoted to the modelling of the coupling effects between the longitudinal and bending vibration in ultrasonic blades.

### 3.3.1 Basic Assumptions and Coupled Dynamic Equation

In this study, an ultrasonic blade is approximated using a beam subjected to longitudinal and bending oscillation simultaneously. This enables the vibration modelling based on the one-dimensional theories detailed in Chapter 2. The EMA data collected in this study suggested that, for the longitudinally excited blades, the motion along the length of the blade is normally notably stronger than the bending vibration. Therefore, the longitudinal vibration can be considered as independent by ignoring the influence of the bending vibration. Thus it is only necessary to model the behaviour of the bending motion, which simplifies the problem significantly.



a) Deformed Structure



b) Axial Force and Bending Moment

**Figure 3.4 Structure with Coupled Bending and Longitudinal Vibration**

A beam performing longitudinal and bending vibration simultaneously is shown in Figure 3.4(a). To investigate the bending motion under this condition, an element was taken from the structure. Load analysis of this element suggested that it suffers bending moment and axial forces at the same time, as illustrated in Figure 3.4(b), where  $M$  is the bending moment,  $V$  is the shear force on the cross section,  $P$  is the axial force resulting from longitudinal deformation. In this case, when the beam bends, due to the rotation of the element, an extra moment is introduced as a result of the axial force [95, 107], which is of the form

$$dM_c = P(z,t) \frac{\partial u}{\partial z} dz \quad (3.34)$$

Based on the analysis detailed in Section 3.2.2, the governing equation of the bending vibration was obtained by incorporating this extra moment into Eq. (3.16), which yields:

$$\frac{d^2}{dz^2} [EI_x(z) \frac{\partial^2 u(z,t)}{\partial z^2}] - \frac{d}{dz} [\rho I_x(z) \frac{\partial^3 u(z,t)}{\partial z \partial t^2}] + \rho S(z) \frac{\partial^2 u(z,t)}{\partial t^2} + P(z,t) \frac{\partial u(z,t)}{\partial z} = 0 \quad (3.35)$$

As it is assumed that the longitudinal vibration is independent, the axial force is regarded to be caused by the longitudinal deformation, therefore one obtains

$$P(z,t) = \sigma(z,t)S(z) = ES(z) \frac{\partial w(z,t)}{\partial z} \quad (3.36)$$

where the longitudinal displacement  $w(z,t)$  can be obtained by the method introduced in Section 2.3.3.

Eq. (3.35) is a fourth order partial differential equation. By comparing it to Eq. (3.16), it can be seen that the extra moment is introduced as a coupled term between the longitudinal and bending motion in the governing equation. Due to the presence of  $P(z,t)$ , Eq. (3.35) is in fact a parametric dynamic system, where the time-variable moment introduced in Eq. (3.34) acts as a parametric excitation.

### 3.3.2 Finite Difference Method and Solution

Eq. (3.35) can be solved numerically using the finite difference method. Taking into account the partial differential feature of this equation, a two-dimensional finite difference method was applied. This method used a similar concept as that introduced in Section 2.3.2 to discretise the derivatives. However, instead of involving only one spatial variable, the computing was conducted at instances of equal interval as well as at uniformly distributed nodes of the structure. To detail this, Eq. (3.35) was discretised at position  $z_i$  and time  $t_j$  by defining

$$u_{i,j} = u(z_i, t_j) \quad (3.37)$$

where

$$z_i = z_0 + ih \quad (i = 0, 1, \dots, m) \quad (3.38)$$

$$t_j = t_0 + jk \quad (j = 0, 1, 2, \dots) \quad (3.39)$$

$k$  is the time interval and,

$$h = L / m \quad (3.40)$$

is a positive step length. The length of the structure is  $L$  and the total number of the nodes is  $m+1$ .  $t_0$  and  $z_0$  are the initial time and the starting position, respectively, which are specified according to the application.

By performing similar operations as detailed in Section 2.3.2, Eq. (3.60) and Eq. (3.61) can be extended to approximate the partial derivatives:

$$\frac{\partial}{\partial z} f(z, t) \rightarrow D_z[f(z, t)] \equiv \frac{f(z+h, t) - f(z-h, t)}{2h} \quad (3.41)$$

$$\frac{\partial^2}{\partial z^2} f(z, t) \rightarrow D_z^2[f(z, t)] \equiv \frac{f(z+h, t) - 2f(z, t) + f(z-h, t)}{h^2} \quad (3.42)$$

$$\frac{\partial}{\partial t} f(z, t) \rightarrow D_t[f(z, t)] \equiv \frac{f(z, t+k) - f(z, t-k)}{2k} \quad (3.43)$$

$$\frac{\partial^2}{\partial t^2} f(z, t) \rightarrow D_t^2[f(z, t)] \equiv \frac{f(z, t+k) - 2f(z, t) + f(z, t-k)}{k^2} \quad (3.44)$$

These operators can be used to discretise Eq. (3.35) by replacing the derivatives with the respective difference representation:

$$\begin{aligned} & \frac{d^2}{dz^2} [EI_x(z) \frac{\partial^2 u(z, t)}{\partial z^2}] \rightarrow \\ & \frac{1}{h^2} \left[ \frac{EI_{x_{i-1}}}{h^2} (u_{i-2, j} - 2u_{i-1, j} + u_{i, j}) - 2 \frac{EI_{x_i}}{h^2} (u_{i-1, j} - 2u_{i, j} + u_{i+1, j}) + \frac{EI_{x_{i+1}}}{h^2} (u_{i, j} - 2u_{i+1, j} + u_{i+2, j}) \right] \\ & = \frac{E}{h^4} [I_{x_{i-1}} u_{i-2, j} - 2(I_{x_{i-1}} + I_{x_i}) u_{i-1, j} + (I_{x_{i-1}} + 4I_{x_i} + I_{x_{i+1}}) u_{i, j} - 2(I_{x_i} + I_{x_{i+1}}) u_{i+1, j} + I_{x_{i+1}} u_{i+2, j}] \end{aligned} \quad (3.45)$$



$$\begin{aligned}
\frac{d}{dz}[\rho I_x(z) \frac{\partial^3 u(z,t)}{\partial z \partial t^2}] &\rightarrow \frac{d}{dz} \left\{ \frac{\rho I_x(z)}{h} \frac{d^2}{dt^2} [(u_{i+1/2,j} - u_{i-1/2,j})] \right\} \\
&\rightarrow \frac{d}{dz} \left\{ \frac{\rho I_{x_i}}{hk^2} [(u_{i+1/2,j-1} - u_{i-1/2,j-1}) - 2(u_{i+1/2,j} - u_{i-1/2,j}) + (u_{i+1/2,j+1} - u_{i-1/2,j+1})] \right\} \\
&\rightarrow \frac{\rho}{h^2 k^2} \{ I_{x_{i+1/2}} [(u_{i+1,j-1} - u_{i,j-1}) - 2(u_{i+1,j} - u_{i,j}) + (u_{i+1,j+1} - u_{i,j+1})] \\
&\quad - I_{x_{i-1/2}} [(u_{i,j-1} - u_{i-1,j-1}) - 2(u_{i,j} - u_{i-1,j}) + (u_{i,j+1} - u_{i-1,j+1})] \} \\
&= \frac{\rho}{h^2 k^2} [I_{x_{i+1/2}} u_{i+1,j-1} - (I_{x_{i+1/2}} + I_{x_{i-1/2}}) u_{i,j-1} + I_{x_{i-1/2}} u_{i-1,j-1} \\
&\quad - 2I_{x_{i+1/2}} u_{i+1,j} + 2(I_{x_{i+1/2}} + I_{x_{i-1/2}}) u_{i,j} - 2I_{x_{i-1/2}} u_{i-1,j} \\
&\quad + I_{x_{i+1/2}} u_{i+1,j+1} - (I_{x_{i+1/2}} + I_{x_{i-1/2}}) u_{i,j+1} + I_{x_{i-1/2}} u_{i-1,j+1}]
\end{aligned} \tag{3.46}$$

$$\rho S(z) \frac{\partial^2 u(z,t)}{\partial t^2} \rightarrow \frac{\rho S_i}{k^2} (u_{i,j-1} - 2u_{i,j} + u_{i,j+1}) \tag{3.47}$$

$$P(z,t) \frac{\partial u(z,t)}{\partial z} \rightarrow \frac{P_i^j}{h^2} (u_{i+1,j} - 2u_{i,j} + u_{i-1,j}) \tag{3.48}$$

Therefore Eq. (3.35) can be discretised as

$$\begin{aligned}
C_{-1}^i u_{i-1,j+1} + C_0^i u_{i,j+1} + C_1^i u_{i+1,j+1} = \\
A_{-2}^i u_{i-2,j} + A_{-1}^i u_{i-1,j} + A_0^i u_{i,j} + A_1^i u_{i+1,j} + A_2^i u_{i+2,j} + B_{-1}^i u_{i-1,j-1} + B_0^i u_{i,j-1} + B_1^i u_{i+1,j-1}
\end{aligned} \tag{3.49}$$

Where

$$C_{-1}^i = \frac{\rho}{h^2 k^2} I_{x_{i-1/2}} \tag{3.50}$$

$$C_0^i = -\frac{\rho}{h^2 k^2} (I_{x_{i+1/2}} + I_{x_{i-1/2}}) + \frac{\rho S_i}{k^2} \tag{3.51}$$

$$C_1^i = \frac{\rho}{h^2 k^2} I_{x_{i+1/2}} \tag{3.52}$$

$$A_{-2}^i = \frac{E}{h^4} I_{x_{i-1}} \tag{3.53}$$

$$A_{-1}^i = -2 \frac{E}{h^4} (I_{x_{i-1}} + I_{x_i}) + 2 \frac{\rho}{h^2 k^2} I_{x_{i-1/2}} + \frac{P_i^j}{h^2} \tag{3.54}$$

$$A_0^i = \frac{E}{h^4} (I_{x_{i-1}} + 4I_{x_i} + I_{x_{i+1}}) - 2 \frac{\rho}{h^2 k^2} (I_{x_{i+1/2}} + I_{x_{i-1/2}}) - 2 \frac{\rho S_i}{k^2} - 2 \frac{P_i^j}{h^2} \quad (3.55)$$

$$A_1^i = -2 \frac{E}{h^4} (I_{x_i} + I_{x_{i+1}}) + 2 \frac{\rho}{h^2 k^2} I_{x_{i+1/2}} + \frac{P_i^j}{h^2} \quad (3.56)$$

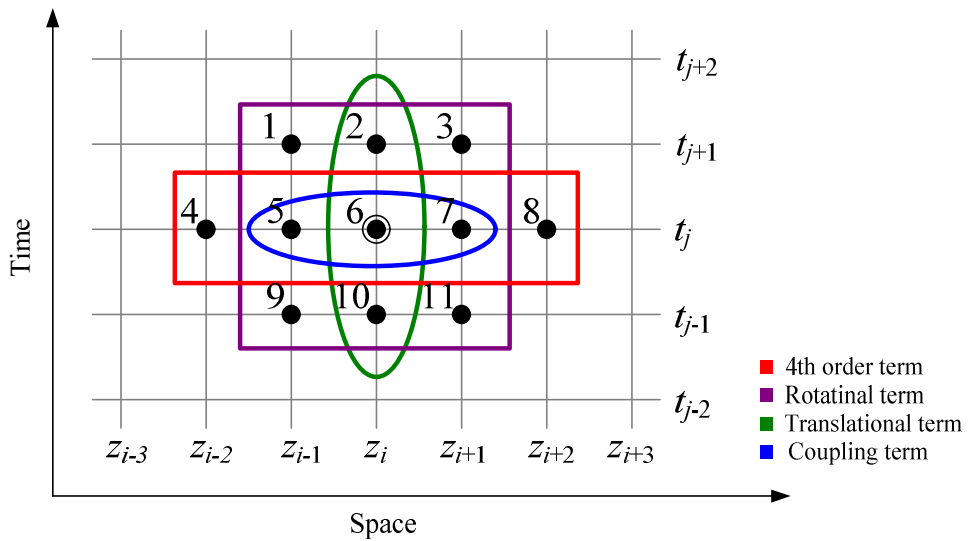
$$A_2^i = \frac{E}{h^4} I_{x_{i+1}} \quad (3.57)$$

$$B_{-1}^i = -\frac{\rho}{h^2 k^2} I_{x_{i-1/2}} \quad (3.58)$$

$$B_0^i = \frac{\rho}{h^2 k^2} (I_{x_{i+1/2}} + I_{x_{i-1/2}}) + \frac{\rho S_i}{k^2} \quad (3.59)$$

$$B_1^i = -\frac{\rho}{h^2 k^2} I_{x_{i+1/2}} \quad (3.60)$$

Eq. (3.49) is the difference equation that models the coupled longitudinal-bending vibration in an ultrasonic blade. For given indices  $i$  and  $j$ , Figure 3.5 illustrates how the adjacent points are involved in Eq. (3.49). The points are introduced into the equation due to the presence of the four terms in the left side of Eq. (3.35). To better demonstrate this, the terms on the left side of Eq. (3.35), from left to right, are named the 4th order term, the rotational term, the translational term and the coupled term, respectively, as labelled in Figure 3.5 by different colours. This form of figure is referred to as the stencil of the equation. It shows that a total of 11 points are involved in the differencing and the method is therefore named the 11-point stencil method.



**Figure 3.5 Stencil of Difference Equation**

To find out the solution of Eq. (3.49), one may define the bending state vector as of the form

$$\mathbf{U}_j = [u_{-2,j}, u_{-1,j}, u_{0,j}, u_{1,j}, \dots, u_{m,j}, u_{m+1,j}, u_{m+2,j}]^T \quad (3.61)$$

where  $u_{0,j}, u_{1,j}, \dots, u_{m,j}$  are the node displacements of the structure representing the bending shape of the beam at instant  $t_j$ . In addition,  $u_{-2,j}, u_{-1,j}, u_{m+1,j}$  and  $u_{m+2,j}$  are displacements of virtual nodes outside the structure, which are introduced to facilitate the mathematical derivation.

Applying  $i = 0, 1, 2, \dots, m$ , into Eq. (3.49) yields  $m+1$  equations, which can be written in matrix form as

$$\mathbf{H}_a \mathbf{U}_{j+1} = \mathbf{R}_a \begin{bmatrix} \mathbf{U}_j \\ \mathbf{U}_{j-1} \end{bmatrix} \quad (3.62)$$

where

$$\mathbf{R}_a = \begin{bmatrix} A_{-2}^0 & A_{-1}^0 & A_0^0 & A_1^0 & A_2^0 & & 0 & B_{-1}^0 & B_0^0 & B_1^0 \\ & A_{-2}^1 & A_{-1}^1 & A_0^1 & A_1^1 & A_2^1 & & & B_{-1}^1 & B_0^1 & B_1^1 \\ & & \ddots & \ddots & \ddots & \ddots & \ddots & & \ddots & \ddots & \ddots \\ & & & A_{-2}^m & A_{-1}^m & A_0^m & A_1^m & A_2^m & 0 & B_{-1}^m & B_0^m & B_1^m & 0 \end{bmatrix} \quad (3.63)$$

$$\mathbf{H}_a = \begin{bmatrix} 0 & C_{-1}^0 & C_0^0 & C_1^0 \\ & C_{-1}^1 & C_0^1 & C_1^1 \\ & & \ddots & \ddots & \ddots & \ddots \\ & & & C_{-1}^m & C_0^m & C_1^m & 0 \end{bmatrix} \quad (3.64)$$

$\mathbf{H}_a$  is a singular matrix of  $m+1$  by  $m+5$ .

In addition, four more equations were obtained by investigating the boundary conditions. Similar to the case in Chapter 2, taking into account the fact that the bending vibration is essentially of small amplitude, the “free-free” boundary condition was applied by rewriting Eq. (3.23)-(3.26) as

$$\left. \frac{\partial^2}{\partial z^2} u(z, t) \right|_{z=0} = 0 \quad (3.65)$$

$$\left. \frac{\partial^3}{\partial z^3} u(z, t) \right|_{z=0} = 0 \quad (3.66)$$

$$\left. \frac{\partial^2}{\partial z^2} u(z, t) \right|_{z=L} = 0 \quad (3.67)$$

$$\left. \frac{\partial^3}{\partial z^3} u(z, t) \right|_{z=L} = 0 \quad (3.68)$$

By applying Eq. (3.42)-(3.44) into Eq. (3.65)-(3.68) and let  $t = t_{j+1}$ , the finite difference form of boundary conditions can be obtained as follows,

$$\frac{1}{h^2}(u_{1,j+1} - 2u_{0,j+1} + u_{-1,j+1}) = 0 \quad (3.69)$$

$$\frac{1}{2h^3}(u_{2,j+1} - 2u_{1,j+1} + 2u_{-1,j+1} - u_{-2,j+1}) = 0 \quad (3.70)$$

$$\frac{1}{h^2}(u_{m+1,j+1} - 2u_{m,j+1} + u_{m-1,j+1}) = 0 \quad (3.71)$$

$$\frac{1}{2h^3}(u_{m+2,j+1} - 2u_{m+1,j+1} + 2u_{m-1,j+1} - u_{m-2,j+1}) = 0 \quad (3.72)$$

This can be written in matrix form as:

$$\underbrace{\begin{bmatrix} 0 & 1 & -2 & 1 & 0 & 0 & \cdots & 0 \\ -1 & 2 & 0 & -2 & 1 & 0 & \cdots & 0 \\ 0 & \cdots & 0 & 0 & 1 & -2 & 1 & 0 \\ 0 & \cdots & 0 & -1 & 2 & 0 & -2 & 1 \end{bmatrix}}_{m+5} \begin{bmatrix} u_{-2,j+1} \\ u_{-1,j+1} \\ u_{0,j+1} \\ \vdots \\ u_{m+2,j+1} \end{bmatrix} = \mathbf{H}_b \mathbf{U}_{j+1} = 0 \quad (3.73)$$

Assembling Eq. (3.73) into Eq. (3.62) yields

$$\mathbf{H} \mathbf{U}_{j+1} = \mathbf{R} \begin{bmatrix} \mathbf{U}_j \\ \mathbf{U}_{j-1} \end{bmatrix} \quad (3.74)$$

where

$$\mathbf{H} = \begin{bmatrix} \mathbf{P}_a \\ \mathbf{P}_b \end{bmatrix} \quad (3.75)$$

$$\mathbf{R} = \begin{bmatrix} \mathbf{R}_a \\ \mathbf{0} \end{bmatrix} \quad (3.76)$$

For the beam structure considered in this study, it is straightforward to prove that  $\mathbf{H}$  is a  $m + 5$  by  $m + 5$  non-singular matrix and  $\mathbf{R}$  is a  $m + 5$  by  $2(m + 5)$  matrix. Therefore the inverse matrix of  $\mathbf{H}$  exists and one obtains

$$\mathbf{U}_{j+1} = \mathbf{H}^{-1} \mathbf{R} \begin{bmatrix} \mathbf{U}_j \\ \mathbf{U}_{j-1} \end{bmatrix} = \mathbf{H}_R \begin{bmatrix} \mathbf{U}_j \\ \mathbf{U}_{j-1} \end{bmatrix} \quad (3.77)$$

where  $\mathbf{H}_R = \mathbf{H}^{-1} \mathbf{R}$  is called the iteration matrix. This means that by giving the bending state vectors of the current and previous moment, which is  $\mathbf{U}_j$  and  $\mathbf{U}_{j-1}$  respectively, the state of the next moment ( $\mathbf{U}_{j+1}$ ) can be iterated using Eq. (3.77). This process can be repeated to compute a series of state vectors until the desired instant is reached.

### 3.3.3 High Order Finite Difference Method (27-Point Stencil) and Solution

This section will present an alternative method to process Eq. (3.35). The main feature of the method is the application of higher order difference operators in the approximation of partial differential equations. It is expected to further improve Eq. (3.77) by reducing the truncation error and enhancing the accuracy of computing.

To illustrate the method, Eq. (3.35) was rewritten in terms of derivatives as the following form

$$\begin{aligned} K_{4,0}(z) \frac{\partial^4 u(z,t)}{\partial z^4} + K_{3,0}(z) \frac{\partial^3 u(z,t)}{\partial z^3} + [K_{2,0}(z) + P(z,t)] \frac{\partial^2 u(z,t)}{\partial z^2} + \\ K_{2,2} \frac{\partial^4 u(z,t)}{\partial z^2 \partial t^2} + K_{1,2}(z) \frac{\partial^3 u(z,t)}{\partial z \partial t^2} + K_{0,2}(z) \frac{\partial^2 u(z,t)}{\partial t^2} = 0 \end{aligned} \quad (3.78)$$

where

$$K_{4,0}(z) = EI_x(z) \quad (3.79)$$

$$K_{3,0}(z) = 2EI'_x(z) \quad (3.80)$$

$$K_{2,0}(z) = EI''_x(z) \quad (3.81)$$

$$K_{2,2}(z) = -\rho I_x(z) \quad (3.82)$$

$$K_{1,2}(z) = -\rho I'_x(z) \quad (3.83)$$

$$K_{0,2}(z) = \rho S(z) \quad (3.84)$$

Instead of replacing the derivatives using Eq. (3.41)-(3.44), this method approximated Eq. (3.78) using the following high order difference operators [135, 189]

$$D\left[\frac{\partial}{\partial z} f(z,t)\right] = \frac{1}{12h}[-f(z+2h,t) + 8f(z+h,t) - 8f(z-h,t) + f(z-2h,t)] \quad (3.85)$$

$$D\left[\frac{\partial^2}{\partial z^2} f(z,t)\right] = \frac{1}{12h^2}[-f(z+2h,t) + 16f(z+h,t) - 30f(z,t) + 16f(z-h,t) - f(z-2h,t)] \quad (3.86)$$

$$D\left[\frac{\partial^3}{\partial z^3} f(z,t)\right] = \frac{1}{8h^3}[-f(z+3h,t) + 8f(z+2h,t) - 13f(z+h,t) + 13f(z-h,t) - 8f(z-2h,t) + f(z-3h,t)] \quad (3.87)$$

$$D\left[\frac{\partial^4}{\partial z^4} f(z,t)\right] = \frac{1}{6h^4}[-f(z+3h,t) + 12f(z+2h,t) - 39f(z+h,t) + 56f(z,t) - 39f(z-h,t) + 12f(z-2h,t) - f(z-3h,t)] \quad (3.88)$$

$$D\left[\frac{\partial^2}{\partial t^2} f(z,t)\right] = \frac{1}{12k^2}[-f(z,t+2k) + 16f(z,t+k) - 30f(z,t) + 16f(z,t-k) - f(z,t-2k)] \quad (3.89)$$

These operators were obtained by means of undetermined coefficient and Taylor series expansion (see Appendix). With a computing stencil involving more points, they are expected to offer higher accuracy in the calculation [189]. On the basis of Eq. (3.85)-(3.89), the operators for the mixed partial derivatives can be obtained by applying the difference operation to each variable [189]. Therefore one obtains

$$\frac{\partial^4}{\partial z^2 \partial t^2} f(z,t) \rightarrow \frac{1}{12k^2}(-a_2 + 16a_1 - 30a_0 + 16a_{-1} - a_{-2}) \quad (3.90)$$

where

$$a_n = \frac{1}{12h^2}[-f(z+2h,t+n) + 16f(z+h,t+n) - 30f(z,t+n) + 16f(z-h,t+n) - f(z-2h,t+n)] \quad (3.91)$$

and

$$\frac{\partial^3}{\partial z \partial t^2} f(z, t) \rightarrow \frac{1}{12k^2} (-b_2 + 16b_1 - 30b_0 + 16b_{-1} - b_{-2}) \quad (3.92)$$

where

$$b_n = \frac{1}{12h} [-f(z + 2h, t + n) + 8f(z + h, t + n) - 8f(z - h, t + n) + f(z - 2h, t + n)] \quad (3.93)$$

To illustrate the representation of the derivation, the displacement of a node on the beam is denoted as

$$u_{i,j} = u(z_i, t_j) \quad (3.94)$$

where  $z_i$  and  $t_j$  have the same definition as detailed in Eq. (3.39)-(3.40). By applying Eq. (3.85)-(3.93) into Eq. (3.78), the difference representation of Eq. (3.35) can be obtained as of the form

$$F_{27} = \sum_{n=1}^{27} \alpha_n^{i,j} u_n^{i,j} = 0 \quad (3.95)$$

This yields a computational stencil of 27 points. Figure 3.6 illustrates the computing stencil of Eq. (3.95). To facilitate the discussion of the problem, the points in the stencil are labeled as 1 to 27.  $u_n^{i,j}$  is denoted as an alias of  $u(z, t)$  for the  $n$ -th point in this stencil, and  $\alpha_n^{i,j}$  is the associated coefficient of  $u_n^{i,j}$ . By referring to Figure 3.6, the relationships such as  $u_1^{i,j} = u_{i-2, j-2}$ ,  $u_{14}^{i,j} = u_{i,j}$ ,  $u_{15}^{i+1, j} = u_{i-1, j-2}$  and  $u_{14}^{i+1, j} = u_{i+1, j}$  can be obtained.

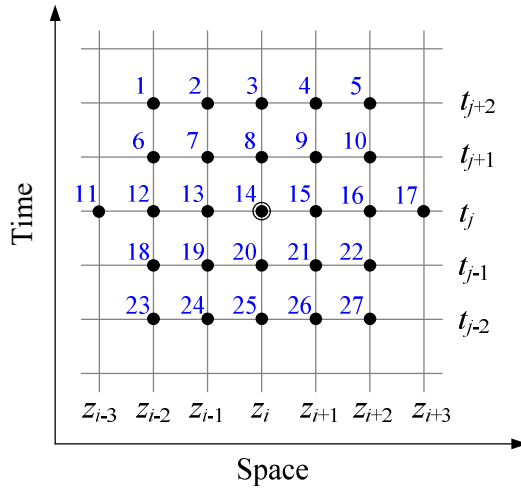


Figure 3.6 27-Points Stencil





Four additional equations can be found from the boundary conditions defined by Eq. (3.65)-(3.68). Using the method of undetermined coefficient (see Appendix), the difference representation of these boundary conditions can be obtained as

$$-u_{-2,j} + 16u_{-1,j} - 30u_{0,j} + 16u_{1,j} - u_{2,j} = 0 \quad (3.102)$$

$$-u_{-2,j} - 8u_{-1,j} + 35u_{0,j} - 48u_{1,j} + 29u_{2,j} - 8u_{3,j} + u_{4,j} = 0 \quad (3.103)$$

$$-u_{m-2,j} + 16u_{m-1,j} - 30u_{m,j} + 16u_{m+1,j} - u_{m+2,j} = 0 \quad (3.104)$$

$$-u_{m-4,j} + 8u_{m-3,j} - 29u_{m-2,j} + 48u_{m-1,j} - 35u_{m,j} + 8u_{m+1,j} + u_{m+2,j} = 0 \quad (3.105)$$

These equations were given in a form that avoids the presence of terms such as  $u_{-3,j}$  and  $u_{m+3,j}$ . By replacing  $j$  with  $j+2$ , Eq. (3.102)-(3.105) can be written as matrix form that can be conveniently incorporated into Eq. (3.96)

$$\begin{bmatrix} -1 & 16 & -30 & 16 & -1 & 0 & 0 & 0 & \dots & 0 \\ -1 & -8 & 35 & -48 & 29 & -8 & 1 & 0 & \dots & 0 \\ 0 & \dots & 0 & 0 & 0 & -1 & 16 & -30 & 16 & -1 \\ 0 & \dots & 0 & -1 & 8 & -29 & 48 & -35 & 8 & 1 \end{bmatrix} \mathbf{U}_{j+2} = \mathbf{Q}_b \mathbf{U}_{j+2} = 0 \quad (3.106)$$

$\underbrace{\hspace{15em}}_{m+5}$

In addition, two more equations can be obtained by considering the cases of  $i = 0$  and  $i = m$ . To avoid the appearance of  $u_{-3,j}$  and  $u_{m+3,j}$ , Eq. (3.35) was not discretised by Eq. (3.95). Instead, two modified operators, which use the computing stencil illustrated in Figure 3.7 and Figure 3.8 respectively, were applied.

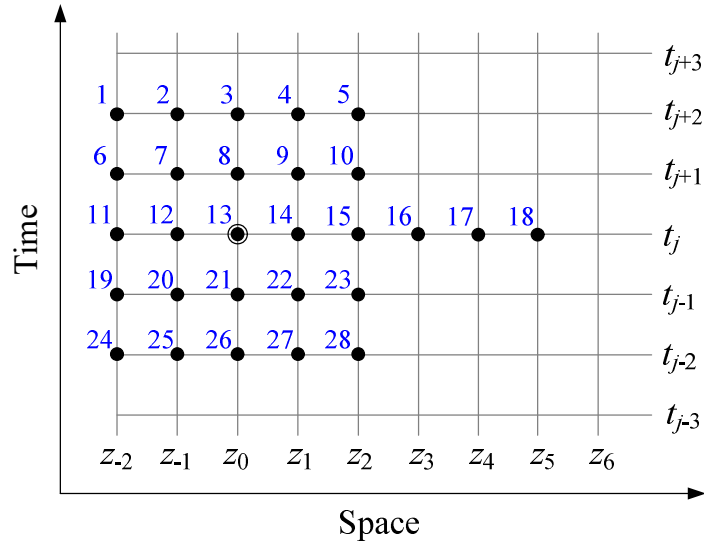


Figure 3.7 Stencil for Case of  $i=0$

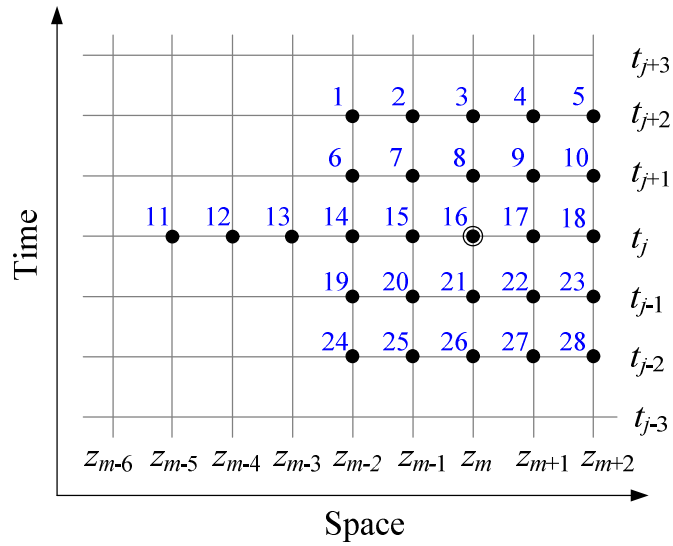


Figure 3.8 Stencil for Case of  $i=m$

By defining the notations in the same way as Eq. (3.95), the difference equations can be obtain as follows:

For  $i=0$

$$\sum_{n=1}^{28} \hat{\alpha}_n^{0,j} u_n^{0,j} = 0 \quad (3.107)$$

For  $i=m$

$$\sum_{n=1}^{28} \hat{\alpha}_n^{m,j} u_n^{m,j} = 0 \quad (3.108)$$

where  $\hat{\alpha}_n^{0,j}$  and  $\hat{\alpha}_n^{m,j}$  are the coefficients of the respective variables. Again, Eq. (3.107) and (3.108) can be placed together and be written in the matrix form as

$$\mathbf{Q}_c \mathbf{U}_{j+2} = [\mathbf{M}_{c1} \mid \mathbf{M}_{c2} \mid \mathbf{M}_{c3} \mid \mathbf{M}_{c4}] \begin{bmatrix} \mathbf{U}_{j+1} \\ \mathbf{U}_j \\ \mathbf{U}_{j-1} \\ \mathbf{U}_{j-2} \end{bmatrix} \quad (3.109)$$

where

$$\mathbf{Q}_c = \begin{bmatrix} \hat{\alpha}_1^{0,j} & \hat{\alpha}_2^{0,j} & \hat{\alpha}_3^{0,j} & \hat{\alpha}_4^{0,j} & \hat{\alpha}_5^{0,j} & & & & \\ & & & \alpha_1^{m,j} & \alpha_2^{m,j} & \alpha_3^{m,j} & \alpha_4^{m,j} & \alpha_5^{m,j} & \end{bmatrix} \quad (3.110)$$

$$\mathbf{M}_{c1} = \begin{bmatrix} \hat{\alpha}_6^{0,j} & \hat{\alpha}_7^{0,j} & \hat{\alpha}_8^{0,j} & \hat{\alpha}_9^{0,j} & \hat{\alpha}_{10}^{0,j} & & & & \\ & & & \alpha_6^{m,j} & \alpha_7^{m,j} & \alpha_8^{m,j} & \alpha_9^{m,j} & \alpha_{10}^{m,j} & \end{bmatrix} \quad (3.111)$$

$$\mathbf{M}_{c2} = \begin{bmatrix} \hat{\alpha}_{11}^{0,j} & \hat{\alpha}_{12}^{0,j} & \hat{\alpha}_{13}^{0,j} & \hat{\alpha}_{14}^{0,j} & \hat{\alpha}_{15}^{0,j} & \hat{\alpha}_{16}^{0,j} & \hat{\alpha}_{17}^{0,j} & \hat{\alpha}_{18}^{0,j} & & & & \\ & & & \alpha_{11}^{m,j} & \alpha_{12}^{m,j} & \alpha_{13}^{m,j} & \alpha_{14}^{m,j} & \alpha_{15}^{m,j} & \alpha_{16}^{m,j} & \alpha_{17}^{m,j} & \alpha_{18}^{m,j} & \end{bmatrix} \quad (3.112)$$

$$\mathbf{M}_{c3} = \begin{bmatrix} \hat{\alpha}_{19}^{0,j} & \hat{\alpha}_{20}^{0,j} & \hat{\alpha}_{21}^{0,j} & \hat{\alpha}_{22}^{0,j} & \hat{\alpha}_{23}^{0,j} & & & & \\ & & & \alpha_{19}^{m,j} & \alpha_{20}^{m,j} & \alpha_{21}^{m,j} & \alpha_{22}^{m,j} & \alpha_{23}^{m,j} & \end{bmatrix} \quad (3.113)$$

$$\mathbf{M}_{c4} = \begin{bmatrix} \hat{\alpha}_{24}^{0,j} & \hat{\alpha}_{25}^{0,j} & \hat{\alpha}_{26}^{0,j} & \hat{\alpha}_{27}^{0,j} & \hat{\alpha}_{28}^{0,j} & & & & \\ & & & \alpha_{24}^{m,j} & \alpha_{25}^{m,j} & \alpha_{26}^{m,j} & \alpha_{27}^{m,j} & \alpha_{28}^{m,j} & \end{bmatrix} \quad (3.114)$$

Combining Eq. (3.96), (3.106) and (3.109) yields

$$\mathbf{Q}\mathbf{U}_{j+2} = \mathbf{M} \begin{bmatrix} \mathbf{U}_{j+1} \\ \mathbf{U}_j \\ \mathbf{U}_{j-1} \\ \mathbf{U}_{j-2} \end{bmatrix} \quad (3.115)$$

where

$$\mathbf{Q} = \begin{bmatrix} \mathbf{Q}_a \\ \mathbf{Q}_c \\ \mathbf{Q}_b \end{bmatrix} \quad (3.116)$$

$$\mathbf{M} = \left[ \begin{array}{c|c|c|c} \mathbf{M}_1 & \mathbf{M}_2 & \mathbf{M}_3 & \mathbf{M}_4 \\ \mathbf{M}_{c1} & \mathbf{M}_{c2} & \mathbf{M}_{c3} & \mathbf{M}_{c4} \\ \mathbf{0} & \mathbf{0} & \mathbf{0} & \mathbf{0} \end{array} \right] \quad (3.117)$$

For the structure considered in this study, it is not difficult to prove that  $\mathbf{Q}$  is a  $m + 5$  by  $m + 5$  non-singular matrix and  $\mathbf{M}$  is a  $m+5$  by  $4m+20$  matrix. Therefore the inverse matrix of  $\mathbf{Q}$  exists and one obtains

$$\mathbf{U}_{j+2} = \mathbf{Q}^{-1} \mathbf{M} \begin{bmatrix} \mathbf{U}_{j+1} \\ \mathbf{U}_j \\ \mathbf{U}_{j-1} \\ \mathbf{U}_{j-2} \end{bmatrix} = \mathbf{Q}_R \begin{bmatrix} \mathbf{U}_{j+1} \\ \mathbf{U}_j \\ \mathbf{U}_{j-1} \\ \mathbf{U}_{j-2} \end{bmatrix} \quad (3.118)$$

where  $\mathbf{Q}_R = \mathbf{Q}^{-1} \mathbf{M}$  is a matrix of  $m+5$  by  $4m+20$  called the iteration matrix. Providing the bending state vectors of the earlier moments ( $\mathbf{U}_{j+1}$ ,  $\mathbf{U}_j$ ,  $\mathbf{U}_{j-1}$  and  $\mathbf{U}_{j-2}$ ) are known, the state of the next moment ( $\mathbf{U}_{j+2}$ ) can be iterated using Eq. (3.118). Therefore Eq.(3.118) provides a way to solve the governing equation and compute the coupled bending vibration of a blade from an initial state.

### 3.3.4 Error Analysis and Comparison of the Finite Difference Methods

In the finite difference method, truncation error is introduced when the difference operators are used to replace the derivatives. The error can propagate to other steps of the computing and accumulate as the calculation is carried on. This means for Eq. (3.77) and (3.118), the iteration may not converge to the desired results. To evaluate this issue, this sub-section will conduct the error analysis for the 11-point and 27-point stencil method presented in Section 3.3.2 and Section 3.3.3 respectively.

The basic concept of the error analysis is to expand the finite difference representation using Taylor series and compare it with the original differential expression [135]. To apply this, one may consider the following two-dimensional Taylor expansion:

$$\begin{aligned} f(x + \Delta x, y + \Delta y) = & \\ & f(x, y) + (\Delta x \frac{1}{\partial x} + \Delta y \frac{1}{\partial y}) f(x, y) + \frac{1}{2!} (\Delta x \frac{1}{\partial x} + \Delta y \frac{1}{\partial y})^2 f(x, y) + \dots \\ & + \frac{1}{(n-1)!} (\Delta x \frac{1}{\partial x} + \Delta y \frac{1}{\partial y})^n f(x, y) + \dots \end{aligned} \quad (3.119)$$

Let  $f(z, t) = u$  and expand it to the fourth order at the vicinity of  $(z_i, t_j)$ , this yields:

$$\begin{aligned}
& f(z_i + \Delta z, t_j + \Delta t) \\
& \approx f + \Delta z f^{(1,0)} + \Delta t f^{(0,1)} + \frac{1}{2} \Delta z^2 f^{(2,0)} + \Delta z \Delta t f^{(1,1)} + \frac{1}{2} \Delta t^2 f^{(0,2)} + \\
& \frac{1}{6} \Delta z^3 f^{(3,0)} + \frac{1}{2} \Delta z^2 \Delta t f^{(2,1)} + \frac{1}{2} \Delta z \Delta t^2 f^{(1,2)} + \frac{1}{6} \Delta t^3 f^{(0,3)} + \frac{1}{24} \Delta z^4 f^{(4,0)} + \\
& \frac{1}{6} \Delta z^3 \Delta t f^{(3,1)} + \frac{1}{4} \Delta z^2 \Delta t^2 f^{(2,2)} + \frac{1}{6} \Delta z \Delta t^3 f^{(1,3)} + \frac{1}{24} \Delta t^4 f^{(0,4)} \\
& = \sum_{k=1}^{15} \beta_k \hat{f}_k
\end{aligned} \tag{3.120}$$

where  $z_i$  and  $t_j$  have the same definition as detailed in Eq. (3.37)-(3.39).  $\hat{f}_k$  is the function of the  $k$ th term in the right side of Eq. (3.120) and  $\beta_k$  is the associated coefficient of  $\hat{f}_k$ .

To investigate the truncation error of the 11-point stencil method, rewriting Eq. (3.35) as

$$\begin{aligned}
F &= \frac{d^2}{dz^2} [EI_x(z) \frac{\partial^2 u(z, t)}{\partial z^2}] - \frac{d}{dz} [\rho I_x(z) \frac{\partial^3 u(z, t)}{\partial z \partial t^2}] \\
&+ \rho S(z) \frac{\partial^2 u(z, t)}{\partial t^2} + P(z, t) \frac{\partial u(z, t)}{\partial z^2} = 0
\end{aligned} \tag{3.121}$$

and Eq. (3.49) as

$$\begin{aligned}
F_{11} &= A_{-2}^i u_{i-2,j} + A_{-1}^i u_{i-1,j} + A_0^i u_{i,j} + A_1^i u_{i+1,j} + A_2^i u_{i+2,j} + B_{-1}^i u_{i-1,j-1} \\
&+ B_0^i u_{i,j-1} + B_1^i u_{i+1,j-1} - C_{-1}^i u_{i-1,j+1} - C_0^i u_{i,j+1} - C_1^i u_{i+1,j+1} \\
&= \sum_{n=1}^{11} a_n u_n = 0
\end{aligned} \tag{3.122}$$

where  $u_n$  is an alias of  $u(z, t)$  for the  $n$ -th point in the right side of (3.122) and  $a_n$  is the associated coefficient of  $u_n$ . Therefore  $u_n$  can be expressed in terms of  $z_i, t_j, h$  and  $k$  as follows

$$u_n = u(z_i + \Delta z, t_j + \Delta t) \tag{3.123}$$

where  $\Delta z = -2h, -h, 0, h, 2h$  and  $\Delta t = -k, 0, k$ . As an example, for point 10, one obtains

$$u_{10} = u(z_i - h, t_j + k) \quad (3.124)$$

By expanding Eq. (3.123) using Eq. (3.120) and substitute it into Eq. (3.122), one obtains

$$F_{11} \approx \sum_{n=1}^{11} a_n \sum_{k=1}^{15} \beta_k^n \hat{f}_k = \sum_{k=1}^{15} \left( \sum_{n=1}^{11} \beta_k^n \alpha_n \right) \hat{f}_k = \sum_{p=1}^{15} \kappa_p \hat{f}_k \quad (3.125)$$

where  $\kappa_p$  is the coefficient of  $\hat{f}_k$ .

The truncation error of the 11-point stencil method can be obtained by comparing the expanded difference equation with the original differential equation. Therefore

$$e_{11} = |F_{11} - F| = \frac{1}{12} \rho S k^2 \frac{\partial^4 u}{\partial t^4} + \frac{1}{12} h^2 (EI'' - P) \frac{\partial^4 u}{\partial z^4} + O(k^4 + h^4) \quad (3.126)$$

This means the truncation error is of  $O(k^2 + h^2)$ . Eq. (3.126) also suggests that the magnitude of the truncation error depends on a number of factors, especially  $h$  the spatial step and  $k$  the time interval. It is possible to reduce the truncation error to an acceptable degree by adopting sufficiently small  $h$  and  $k$  for the iteration. However, this is achieved at the cost of increased computing expense.

Using the same approach, one may obtain the truncation error for the 27-point stencil method as:

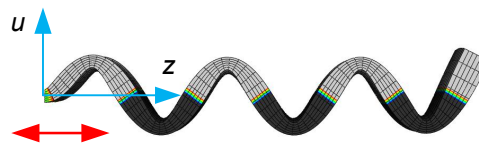
$$e_{27} = |F_{27} - F| = \frac{1}{12} \rho S k^2 \frac{\partial^4 u}{\partial t^4} + O(k^4 + h^4) \quad (3.127)$$

which suggests the truncation error is substantially reduced to be  $O(k^2 + h^4)$ .

Comparing this to the case of the 11-point stencil method, it suggests that higher accuracy can be achieved by the 27-point stencil method for the same value of  $k$  and  $h$ . This is in agreement with the purpose of the introduction of the high order difference method.

### 3.3.5 Case Study

To demonstrate the application of the proposed longitudinal-bending vibration model, a case study is presented in this section. The same uniform beam as detailed in Section 2.4.1 was used to study the interaction between longitudinal and bending vibration. In the analysis, the beam was subjected to forced vibration at its first longitudinal frequency (35.3kHz, Table 2.4) under a longitudinal excitation of  $40\mu\text{m}$  in amplitude, which is a typical level of excitation for ultrasonic cutting blades. Attention was placed at the B7 mode illustrated in Figure 2.4 as it is the bending mode closest to the excitation frequency. It is assumed that the beam undergoes an initial bending of  $2\mu\text{m}$  in amplitude, which is of low level comparing to the longitudinal excitation, as illustrated in Figure 3.9. The introduction of this initial bending allows the investigation of how the bending develops over time with the presence of longitudinal vibration. The conditions and settings of the analysis are summarised in Table 3.1.



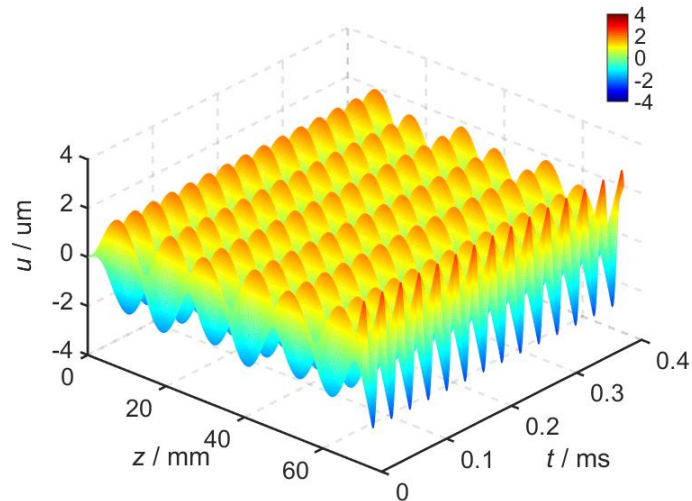
**Figure 3.9 Excitation and Initial Bending**

Setting	Value
Longitudinal Vibration Amplitude	$20\mu\text{m}$
Initial Bending Amplitude	$2\mu\text{m}$
Excitation Frequency	35.3kHz
Spatial Step ( $h$ )	0.34mm
Interactive Time Step ( $k$ )	$0.2\mu\text{s}$

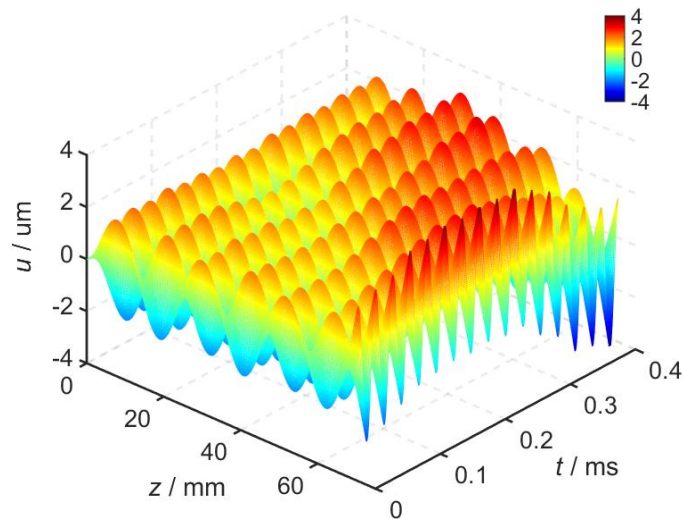
**Table 3.1 Conditions and Settings of Analysis**

The analysis was carried out using Matlab 2008b with the main script enclosed in Appendix A.3. The results of the calculation are illustrated in Figure 3.10-Figure 3.12. Figure 3.10(a) and Figure 3.10(b) plots the bending shape of the beam, obtained without and with the presence of longitudinal vibration respectively, against time. It shows that when longitudinal vibration is absent, the initial bending resulted in bending vibration of constant magnitude. However, when longitudinal excitation is applied, the magnitude of bending increases over time. Figure 3.11 illustrates the

displacement at the end point of the beam, and Figure 3.12 compares the bending shape of the beam at  $t=0\text{ms}$ ,  $t=0.187\text{ms}$  and  $t=0.374\text{ms}$ , at which moments the beam bends at the largest magnitude. It confirms that the beam is subjected to larger bending deformation with the presence of longitudinal motion. The maximum magnitude of the displacement of the end point reaches  $4.2\mu\text{m}$  comparing to just  $2.7\mu\text{m}$  at the initial moment. This implies the beam can suffer higher stress as a result of the coupled vibration.



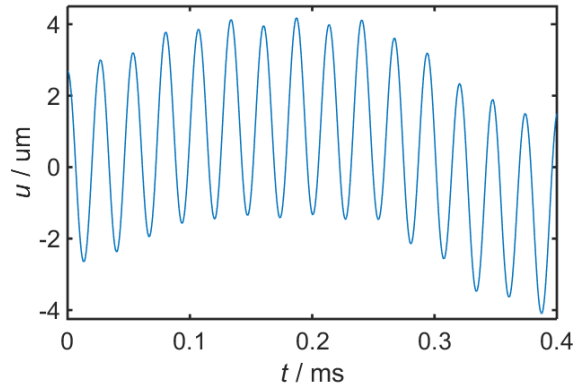
**a) Without Longitudinal Vibration**



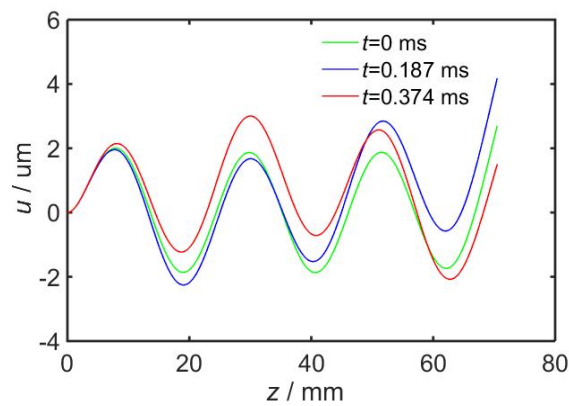
**b) With Longitudinal Vibration**

**Figure 3.10 Amplitude of Bending over Time**





**Figure 3.11 Displacement of End Point (with Longitudinal Vibration)**



**Figure 3.12 Overlay of Bending Shape**

### 3.3.6 Discussion

Longitudinal-bending coupled vibration of ultrasonic blades was studied in this section based on the one-dimensional beam theory. As the bending vibration was considered to be insignificant compared to the longitudinal motion, the influence of bending on the longitudinal vibration was ignored and coupled behaviour was only modelled for the bending vibration.

By taking into account the axial force associated with the longitudinal deformation and the deformed profile of the structure, the coupled effect was assumed to result from an extra rotation moment introduced by the axial force. This rotation moment can act as a parametric excitation for the bending vibration. However, the factor of damping was not taken into account in this model, which means there is no mechanism to damp the bending vibration and this may lead to improperly large oscillation in the computation. It should also be noted that the loading condition is not considered in the model either. The structure is free to vibrate without contacting

other object. Therefore, it is expected that the proposed method may not be applicable for modelling coupled vibration in cutting process.

Nevertheless, the model simplified the problem by concentrating only on the longitudinal and bending vibration and keeping the longitudinal vibration independent of the effects of coupling. This provided an insight into a most commonly observed coupling phenomenon in this type of blade while allowing the problem to be modelled in a relatively simple and solvable form. However, it is noteworthy that this simplicity may be inapplicable if the bending or torsional vibration becomes significant.

The generated governing equation for bending vibration was a fourth order non-linear partial differential equation. Two approaches, the 11-point and 27-point stencil method, were proposed based on the finite difference method to solve this equation using an iteration process. Both calculate the bending state vector of the next moment on the basis of the known vectors of the earlier moments. Error analysis of these methods suggested that the accuracy of the iteration depends on the value of the spatial step  $h$  and the time interval  $k$ , which must be sufficiently small in order to make sure the truncation error stays within an acceptable limit in the iteration. An improved accuracy was found in the 27-point stencil method in that it exhibits a truncation error of  $O(k^2 + h^4)$  instead of  $O(k^2 + h^2)$  in the 11-point stencil method. Therefore, the 27-point stencil method can be used in the case where faster convergence is required, or further reducing  $h$  and  $k$  to improve the accuracy is ineffective. However, comparison of Eq. (3.118) and Eq. (3.77) showed that this is achieved at the cost of increased computing complexity as the 27-point stencil requires substantially more state vectors (four vectors rather than two in the 11-point stencil) to be involved in the iteration.

The case study of a uniform beam showed that the proposed model can be used to study the interaction between the longitudinal and bending vibration. The computation suggested increased bending magnitude, which can result in higher stress in the structure, under the influence of longitudinal excitation. It is expected that similar approach can also be used in the study of coupled vibration for ultrasonic blades. However, this study did not take into account the issues such as damping, the stable region of vibration, and convergence of the calculation. Further research on these

issues would be essential in order to apply this model in the design and optimisation of ultrasonic blades.

In addition, although the results of the case study were not experimentally verified in this study, it is suggested that the coupled vibration may be further experimentally studied by investigating the actual amplitude change in terms of time using a similar setup as experimental modal analysis. With accurate laser vibrometer and high speed signal acquisition devices, real-time vibration velocity on the blade surface can be sampled and recorded. It is expected that extracting the change of vibration amplitude in time domain would enable the comparison of theoretical prediction and real-world phenomenon.

### **3.4 Summary**

This chapter presented two models for the coupled vibration of ultrasonic blades. The first model is a lumped mass beam system that exhibits parametric vibration. It models the motion of the beam in a four degree of freedom system using a one-dimensional structure. Due to its slender shape and the effect of the lumped end mass, the beam was able to perform coupled bending and torsional motion under a longitudinal excitation. The interaction of these motions was investigated by taking into account the geometry restrictions of the structure, including the relationship between the curvatures and displacements. This was further used to derive the governing equations of vibration by means of Lagrangian dynamics. The resulting equations were presented in the form of second order non-linear differential equations with respect to the generalised co-ordinates.

This model provides an approach to investigate the parametric vibration and modal coupling behaviour using a system of relatively simple structure. However, taking into account the complexity of the obtained governing equations, it is unlikely to find closed form solutions for the analysis. In addition, due to the geometry difference between a beam with lumped mass and a structure of tapered profile, difficulties may arise when determining the necessary parameters for the model. Therefore it is more appropriate to use this model for the purpose of theoretical study instead of performance prediction.

The second model concentrated on the longitudinal-bending coupled vibration. This provided an insight into the coupling phenomenon commonly observed in this type of blade while allowing the problem to be modelled in a relatively straightforward form. Taking into account the fact that the longitudinal motion is normally much stronger than the bending vibration, the problem can be further simplified by ignoring the effects that the bending motion exerts on the longitudinal vibration. Thus it is only necessary to model the motion of bending, as the longitudinal vibration would be free from coupling effects. Under this assumption, the governing equation of bending was obtained by introducing an extra rotation moment on the basis of the one dimensional beam theory.

This model resulted in a fourth order time dependent partial differential equation, which is essentially a parametric vibration system. Two approaches, referred to as the 11-point and 27-point stencil method, were proposed based on the finite difference method to solve this equation. These methods use an iteration process in the calculation to compute the future bending state based on the known vibration states. The error analysis confirmed that for both methods, it is possible to keep the truncation error within an acceptable limit by adopting sufficiently small value for  $h$ , the spatial step, and  $k$ , the computing time interval. However, the 27-point stencil has an improved accuracy over the 11-point stencil, though its iteration equation is of a more complicated form.

This method provides a way to investigate the bending motion of an ultrasonic blade under the presence of longitudinal vibration. Further work is recommended to study the issues such as damping, the stable region of vibration, and convergence of the calculation.

# Chapter 4

## Blade Performance Indicators and Optimal Design Method

### 4.1 Introduction

Chapter 2 and Chapter 3 discussed the modelling of vibration behaviour of ultrasonic blades. In addition to the understanding of blade dynamic characteristics, it is also important to adopt appropriate design process when designing high performance ultrasonic blades [14, 39, 53].

Conventionally, the design process starts with an initial design or a design concept. The design is analysed and adjusted repeatedly until a satisfactory solution is obtained. Since there are no general methods on how to make modifications or improvements to the design, it relies on the designer's experience, intuition and other information obtained from trial designs to complete the task. Therefore, a massive amount of work has been devoted to the investigation of design strategies, such as ways to decrease excessive vibration, reduce material stress and avoid high cutting temperature. These strategies can improve the design quality and enhance the performance of the blade. However, they do not guarantee a "best" design to be obtained. Better solutions may exist but are not explored in the design process. For these reasons, this chapter will be devoted to the proposal of an improved design method by adopting optimisation in the design process.

#### 4.1.1 The Conventional Method and Design Strategies

As introduced in Section 1.5.4, the conventional design process of ultrasonic blades includes initial design, modelling and analysis, and blade tests. To propose a new design method, the design strategies, which are used in the conventional design process to improve design quality, are reviewed. Cardoni et al. [1, 14, 212] discussed the design issues of ultrasonic blades, particularly for those with multiple components and complex geometries. Three strategies were proposed to reduce the stress level at the failure location of the blade, which include:

- (1) Proper design of blade profile;

- (2) Detuning of the block horn and blades to move the longitudinal node away from the highest stress section;
- (3) Redesign of the block horn to eliminate the effects of blade flexural vibrations in the longitudinal cutting mode.

These techniques were successfully applied in the design of multi-blade ultrasonic food cutting systems. McCulloch [53] designed different ultrasonic food cutting blades that had the same profile but were tuned at different frequencies. A large rate of change in the cross-section area was applied as a strategy to achieve an increased gain. This was done by adopting two symmetric circular curves in the blade geometry. MacBeath [39] demonstrated the application of a radial profile in the design of ultrasonic bone cutting blades, which has a gain exceeding ten. The stress limit of the material was considered as a factor that restricted the blade gain to be further increased. However, the blade profile introduced in the study was found to be unsuitable for deep cutting. An ultrasonic chisel for bone cutting was investigated by Khambay [87, 88]. The device was designed with a straight cutting tip shaped as a chisel, which resulted in a chiselling effect when excited longitudinally. This helps to remove bone debris in surgical applications. The unique design of the chisel shape was a key factor in achieving satisfactory cutting performance.

The design techniques developed in the study of other ultrasonic components such as cylindrical horns are also useful for ultrasonic blades as these components exhibit similar behaviour in terms of dynamic characteristics. Cardoni et al [213] studied the approaches to enhance the vibration performance of ultrasonic block horns. Slotting was incorporated in the horn design and was configured according to different applications to achieve good uniformity of vibration amplitude as well as avoid the modal participation of non-tuned modes. Rani [214] compared the dynamic performance of ultrasonic plastic welding horns of different profiles, including cylindrical, Gaussian, catenoidal, stepped and Bézier shape. The stepped and Bézier horns were found to have larger gain but suffered from higher material stress. The Bézier profile was considered to be a better solution as a result of its smooth shape.

Other design techniques developed for ultrasonic devices are not dealt with exhaustively here. In spite of this, the desire of improving the design method itself was raised as these strategies are only applicable for certain cases and rely heavily on

the designers' skills. There is a lack of a general method to produce better design solutions while reducing the need of designers' experience. In view of this, the concept of optimal design was introduced in the design of ultrasonic blades. Unlike the conventional approach, the design is updated by mathematical algorithms in the optimal design method. This bypasses the application of different empirical design techniques and offers a more robust way to complete the task.

#### **4.1.2 The Application of Optimisation in the Design of Ultrasonic Devices**

The basic procedures in general optimal design methods include formulation of the design problem, evaluation of the design, and updating the design using optimisation algorithms, as detailed in Section 1.5.5. Being powerful tools for research and product development, the concept of optimal design and the relevant algorithms have already been applied in the design of ultrasonic devices, including horns and transducers.

Derks [101] presented the optimisation of a rectangular ultrasonic horn using both experimental approaches and FEA. The study attempted to design a horn that achieves the best uniformity of vibration amplitude across its large output face. In the experimental approach, the size of the slots on the horn was adjusted in order to find the best performance for the whole system. However, the success of this method was strongly dependent on the first estimation of the overall size of the horn. The application of FEA improved the efficiency of optimisation by eliminating the need to alter and test the horn repeatedly. Nevertheless, no optimisation algorithm was applied to improve the design process. As this method considered a horn of specific shape, it was not applicable to other types of horns or ultrasonic blades. Wang [215, 216] developed a method to design ultrasonic horns using an optimisation scheme and FEA. The work was devoted to the design of a horn of Bézier profile that optimises two objects: first, minimising the difference between the horn's first longitudinal modal frequency and the transducer's working frequency; second, maximising the gain of the horn. This was done by a genetic algorithm that solves multi-objective problems in a single optimisation. An evolution process was incorporated in the algorithm which adjusted the parameters of the Bézier curve in each generation to obtain offspring of improved performance from the current population. FEA was used during the optimisation to compute the modal frequency and displacement distribution of the horn. It is reported that a horn obtained by this method was 71% higher in gain than

the traditional catenoidal horn of the same length and diameters of the end surfaces. However, other characteristics of the horn, such as the non-longitudinal modes and stress of material, were not taken into account in the optimisation process. Roşca [217] studied a mathematical optimisation procedure for ultrasonic horns based on the differential equation of wave propagation, which took into consideration the contact stiffness between the horn and the attached tool. The study presented a family of horn designs that have the maximum cross section at their nodal points. However, as the solution was obtained by an analytical method, this procedure was only applicable for horns with a specific profile. Amin [113] designed a double-conical shaped horn for ultrasonic machining by adapting an empirical optimisation procedure to maximise its gain. The procedure adjusted the end diameters and the length of different sections gradually in order to achieve an increased gain as well as low effective stress. The resultant horn was found to exhibit considerably higher gain than those designed using the conventional method. However, the method did not detail the variables and restrictions involved, and so the obtained design could be a solution optimised locally. Deibel [218] applied genetic algorithms and simplex method to optimise the shape of an ultrasonic horn used for ultrasonic assisted machining. Selected geometry parameters of the horn were altered during the optimisation in order to search for the desired shape. The global fitness function, or the optimising goal, was represented by the weighted sum of a number of sub-objective functions that evaluate different characteristics, including the vibration at the mounting point and target frequency of the horn. The proposed method applied both genetic algorithms and the simplex method in the optimal searching, where the former was used in the global searching and the latter in the local searching. As a result, a usable solution was found according to the application specifications. However, the way that the global fitness function was constructed raised the need to determine appropriate penalty factors for the relevant sub-fitness functions. These factors have a direct influence on the optimisation effect and the convergence of algorithm. They may introduce inconvenience as the proper weights could be difficult to determine in some applications.

The application of optimisation methods was also reported in the design of ultrasonic transducers. Fu [219] formulated the design of a Langevin transducer as a constrained multi-objective optimisation problem with the aim of maximising the output



amplitude while minimising the electric power consumption. This was achieved by applying the transfer matrix method to model the transducer structure. However, because of the involvement of conflicting objectives, it is impossible to optimise all objectives at the same time. To solve this problem, three Pareto-based multi-objective evolutionary algorithms, including the multi-objective genetic algorithm, elitist non-dominated sorting genetic algorithm and improved strength Pareto evolutionary algorithm, were introduced. The proposed procedure allowed the designer to obtain a preferred solution. However, additional information such as weight vectors must be considered when selecting the optimal result in the final stage. Although a design example was discussed in the study, the obtained solution was not verified by experiments. Heikkola [220] applied an interactive multi-objective optimisation method known as NIMBUS in the design of a high power ultrasonic transducer. This algorithm classified the objective functions in up to five classes:

- (1) To be improved;
- (2) To be improved until a certain aspiration level is reached;
- (3) Currently acceptable;
- (4) Allowed to be impaired until a certain upper bound is met;
- (5) Freely changeable.

This allowed a new optimal problem to be generated in each iteration during the optimisation [221, 222]. It is reported that the method was capable of solving non-differentiable, multi-objective, optimal problems and offered the ability to obtain a best compromise between several conflicting objectives. According to the design preference, three optimisation goals were raised with a decreasing importance: resonating at the correct frequency, minimising the acoustic pressure at transducer front and reducing the vibration at the casing attachment. The numerical simulation of a design problem demonstrated that this method improved the design process and resulted in a better solution than the conventional unoptimised approaches. Porto [223] adopted the genetic algorithm to optimise the shape of an ultrasonic transducer used for surgical applications. The presented work attempted to achieve the maximum transducer output by adjusting eleven geometric parameters. The genetic algorithm was used to conduct global and local searching in the optimisation process, which produced a solution in less than 5000 function evaluations. A similar study was conducted by Murphy [224] with a pseudo-gradient optimal method, based on an analytical transducer model. Almost the same results were reported but a lower

number of simulations was required by the genetic algorithm. However, neither of these studies included the consideration of stress in the optimisation, nor did they verify the resultant transducer designs experimentally.

The above research shows that it is a feasible approach to apply optimisation methods in the design of ultrasonic devices. This means it is possible to find an optimal design solution without manually applying specific design strategies. However, the optimisation of ultrasonic cutting blades was barely mentioned in the literature. As ultrasonic blades have their unique design requirements, especially in terms of geometry and dynamic performance, it is necessary to take their characteristics into account when investigating the application of optimal methods. In view of this, this study will be devoted to the proposal of an optimal design process for ultrasonic bone cutting blades. Instead of focusing on how to adjust the structure of an ultrasonic blade, this study will concentrate on the methods of evaluating and comparing the performance of different designs, which will enable the introduction of searching procedures and optimisation algorithms in the design process.

## **4.2 Blade Performance Indicators**

### **4.2.1 The Concept of Performance Indicators**

In order to apply the optimal design method in real world applications, the design problem must be formulated in a form that allows the optimisation algorithms to be incorporated. In the proposed method, it is done based on the introduction of performance indicators. The so called "performance indicator" is a value or a function that measures specific physical characteristics of a design in the form of mathematical representations. It serves as a bridge between the real world design problem and the mathematical algorithms.

How to select and construct the appropriate performance indicators is a major concern in this research as the indicators have a direct impact on the quality of optimisation. Two basic principles are followed in this study. The first one is that the indicators should be defined in a way that can be conveniently computed. This suggests that the calculation of an indicator must be both feasible and cost acceptable. As the indicators are usually computed frequently in the design process, those with ambiguous implementation definition or expensive computing costs would be either unrealizable

or impractical to use. The second principle is that the indicators should have clear physical meaning in order to reflect the performance of interest. This facilitates the formulation of the design problem by allowing the objective functions and constraints to be constructed in a straightforward way.

In fact, the concept of performance indicators shares similar ideas to the fitness/objective functions in that all of them attempt to quantify certain physical characteristics of a design using mathematical representations. Therefore, the relevant objective functions presented in the literature and their design targets will be reviewed before detailing the proposal of indicators.

One essential requirement of the design for most power ultrasonic components is to make sure the design is tuned at correct resonant frequency. To apply this condition in the optimisation, Fu [218] constructed the following function:

$$f = R_f \frac{|\omega_s - \omega_t|}{\omega_t} \quad (4.1)$$

where  $f$  is the fitness function,  $R_f$  is the weight factor that reflects the importance of this condition,  $\omega_s$  is the resonant frequency of the current design, and  $\omega_t$  is the desired resonant frequency. This function was summed up with other sub-objective functions in the global objective function. As a consequence, when the global objective function was minimised,  $f$  would be forced to be a sufficiently low value, making sure that  $\omega_s$  is close enough to  $\omega_t$ . On the other hand, this goal may also be achieved by treating the resonant frequency as an individual objective function and using multi-objective algorithms, such as a Pareto-based method, in the optimisation [219, 220].

The output amplitude is another design target of high priority as it is directly related to the work that can be delivered by an ultrasonic component. Sometimes this target is evaluated using the gain of the component, which is the vibration amplifying factor between the input and output interface of the component. Maximum output or gain was regarded in a number of studies as the main optimisation goal in order to obtain the highest performance [113, 215, 216, 220, 223]. This was usually handled directly as a separate fitness function by multi-objective algorithms. However, large output amplitude is often achieved at the price of high stress, which may lead to the failure of the ultrasonic component [14, 39].

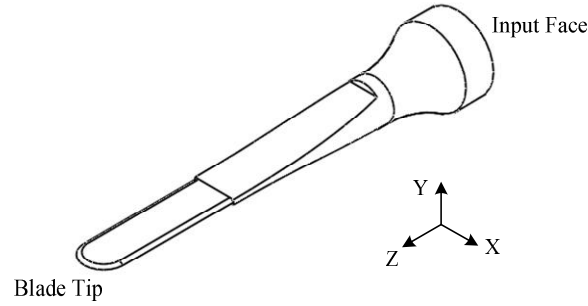
Low vibration amplitude or deformed displacement at certain positions of an ultrasonic component, such as the mounting point, can be a design objective as well. It is particularly important for transducers and horns of certain types as this allows them to be attached or mounted appropriately [218, 220]. This condition was represented by Deibel and Wegener [218] using the average displacement of the grid points at the specific location:

$$f = \frac{1}{N} \sum_i u_{zi} \quad (4.2)$$

where  $f$  is the fitness function,  $N$  is the number of grid points at the position,  $u_{zi}$  is the nodal displacement along the  $z$  direction (or another direction of interest). This target, however, was regarded as less important in some applications comparing to other conditions such as the resonant frequency [220].

Objectives such as material stress, power consumption and acoustic pressure, were taken into account in other studies [101, 219, 220]. By introducing the appropriate objectives in the design process, the designers will be able to control the optimisation so that design solutions with the desired performance can be generated by the optimisation algorithms.

Taking into account the features of ultrasonic cutting blades, this study puts forward four kinds of performance indicators: frequency based, gain based, displacement based and stress based indicators. They are classified according to their physical nature and are expected to provide the essential information on the vibration characteristics of an ultrasonic blade. To better illustrate the definition and the application of these indicators, an ultrasonic blade excited longitudinally will be used as the example for demonstration, as shown in Figure 4.1. Four kinds of vibration, the lateral bending (bending along the width/breadth of the blade, denoted as  $B_X$ ), flexural bending (bending along the thickness of the blade, denoted as  $B_Y$ ), longitudinal motion (denoted as  $L$ ) and torsional vibration (denoted as  $T$ ), will be considered as they are the most common motions presenting in an ultrasonic blade of this kind. Although the proposed indicators are initially constructed for ultrasonic blades, they are also applicable for other types of ultrasonic devices such as horns and transducers.



**Figure 4.1 Ultrasonic Blade**

### 4.2.2 Frequency Based Indicators

This kind of indicator is called modal distance. They are derived from the modal frequencies of an ultrasonic blade and are defined as the frequency difference between the working mode and the nearest undesired modes:

$$M = \min \{|f_t - f_0|\} \quad (4.3)$$

where  $M$  is the modal distance,  $f_t$  is the modal frequency of the undesired modes,  $f_0$  is the working mode.

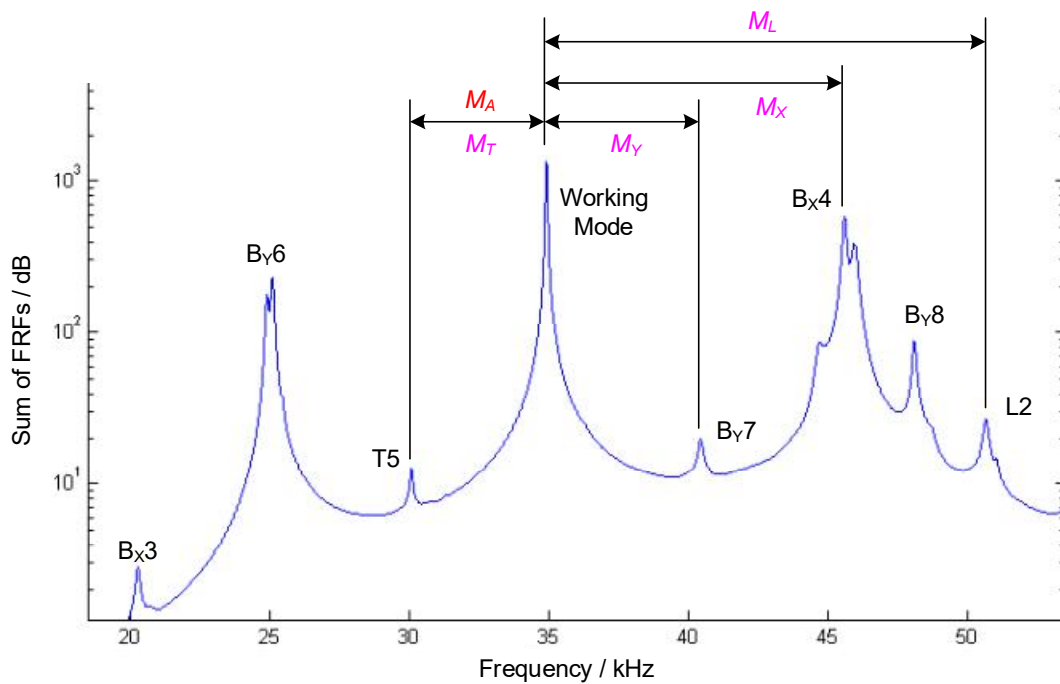
According to the nature of the undesired modes, there are five types of modal distance, as illustrated in Table 4.1.  $M_A$  is the general form of modal distance, which is defined as the minimum frequency difference between the working mode and the other modes. In addition, the indicator can be defined in terms of the distance between the working mode and a certain type of mode. As shown in Table 4.1,  $M_X$  is named  $B_X$  modal distance, which is the frequency difference between the working mode and the nearest  $B_X$  bending mode.  $M_Y$ ,  $M_L$  and  $M_T$  are defined in a similar way.

The example in Figure 4.2 demonstrates the physical meaning of the defined indicators. This figure is the sum of the amplitude of frequency response functions (FRFs) obtained in the experimental modal analysis of an ultrasonic blade. The vibration modes were found at the peaks of the curve and were named using letters which indicate their nature of vibration and a number of order. Different types of modal distance are illustrated in the figure, which clearly shows how far the relevant modes are separated from the working mode. It is an empirical experience that modal coupling behaviour is most likely to occur when two modal frequencies are too close to each other [14]. Thus these indicators suggest the possibility at which the working

mode might be affected by other modes. To avoid undesired modal coupling behaviour, constraints should be applied for these indicators to ensure the vibration modes are well separated in frequency.

Indicator	Name	Definition
$M_A$	Modal Distance	Frequency difference between the working mode and the nearest mode.
$M_X$	$B_X$ Modal Distance	Frequency difference between the working mode and the nearest $B_X$ bending mode.
$M_Y$	$B_Y$ Modal Distance	Frequency difference between the working mode and the nearest $B_Y$ bending mode.
$M_L$	Longitudinal Modal Distance	Frequency difference between the working mode and the nearest longitudinal mode.
$M_T$	Torsional Modal Distance	Frequency difference between the working mode and the nearest torsional mode.

**Table 4.1 Frequency Based Indicators**



**Figure 4.2 Modal Distance Indicators**

### 4.2.3 Gain Based Indicators

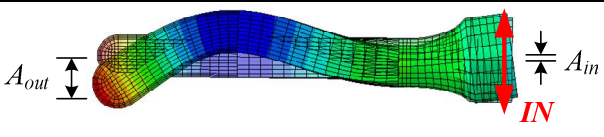
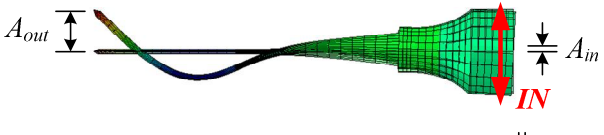
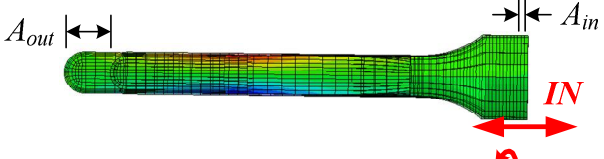
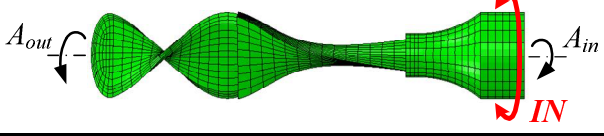
The gain is the amplifying factor of a blade with respect to its excitation. Normally, higher gain means larger vibration output can be obtained for the same input condition. Therefore the gain is one of the most commonly optimised goals in the design of ultrasonic devices for performance enhancement.

The concept of gain is extended in this study by defining the indicator under different excitation conditions. As illustrated in Table 4.2, four types of gains are defined, namely  $G_X$ ,  $G_Y$ ,  $G_L$  and  $G_T$ .  $G_X$  is defined as gain of  $B_X$  bending motion. This indicator is computed based on the FEA simulation where a normalised oscillating excitation is applied at the input face of the blade base. This input, as illustrated as  $IN$  in Table 4.2, vibrates along the width direction at the working frequency of the blade, which excites lateral ( $B_X$ ) bending in the blade. The value of  $G_X$  is obtained by dividing the displacement amplitude of the blade tip by the amplitude of the input, as shown in Eq. (4.4)

$$G = A_{out} / A_{in} \quad (4.4)$$

where  $G$  is the gain,  $A_{out}$  is the displacement amplitude at the blade tip and  $A_{in}$  is the amplitude of the input, as illustrated in Table 4.2.  $G_Y$ ,  $G_L$  and  $G_T$  are defined in a similar way.  $G_Y$  and  $G_L$  is computed by applying an input along the thickness and longitudinal direction respectively, and  $G_T$  is computed by applying a torsional input at the blade base. These gains are the vibration characteristics of an ultrasonic blade, which indicate how the blade responds to a specific type of excitation. If the blade is regarded as a structure where non-linear effects of vibration are ignored, the gains are independent of the input.

$G_L$  is the most important one among the proposed gains as it is closely related to the cutting performance of the blade. Under the same input condition,  $G_L$  determines how much longitudinal vibration can be delivered at the blade tip to perform ultrasonic cutting. The value range of this indicator should be determined according to the output amplitude of the transducer and the required vibration amplitude of cutting. Usually, higher  $G_L$ , which results in enhanced cutting by boosting the output of the transducer, is preferred. However, the maximum value of this indicator is restricted by the material strength as larger gain also brings about higher stress in material [14, 39].

Indicator	Name	Definition
$G_X$	Gain of $B_X$ bending.	
$G_Y$	Gain of $B_Y$ bending.	
$G_L$	Gain of longitudinal motion.	
$G_T$	Gain of torsional motion.	

**Table 4.2 Gain Based Indicators**

On the other hand, although a blade is expected to perform longitudinal vibration only, bending and torsional vibration may be excited as a result of non-linear effects, which is usually unwanted in ultrasonic cutting.  $G_X$ ,  $G_Y$ , and  $G_L$  suggest how the blade responds to these non-working motions in specific excitation conditions. A large value of the gain implies an increased possibility of the presence of the undesired motion. To reduce the potential negative influence,  $G_X$ ,  $G_Y$ , and  $G_L$  should be kept within an acceptable limit.

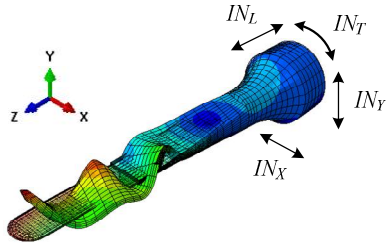
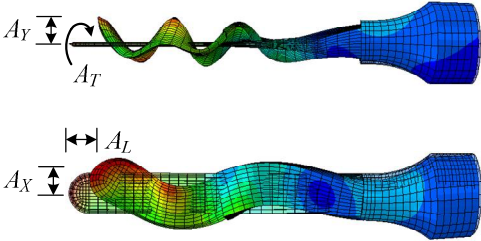
#### 4.2.4 Displacement Based Indicators

The gain based indicators deal with only one mode of vibration at a time. In the computing of a gain, the applied input is a single component excitation, which makes the blade perform forced bending, longitudinal or torsional vibration in the simulation without the involvement of coupling between different modes of vibration. This may be insufficient when it is desired to evaluate the performance of an ultrasonic blade in complex vibration condition where two or more vibration modes present simultaneously.

In ultrasonic cutting, a blade is usually excited longitudinally by a transducer. However, in real world applications, even though only longitudinal input is applied on the blade, other modes of vibration including bending and torsion may also present due to reasons such as vibration coupling and modal interaction [14]. Such



phenomenon can not be duplicated in the simulation if only longitudinal excitation is applied, as the input induces longitudinal response only. Instead, it can be simulated using a multi-component input. As illustrated in Table 4.3, an excitation with four components  $IN_X$ ,  $IN_Y$ ,  $IN_L$  and  $IN_T$ , can be applied at the base of the blade in the simulation. These input components are associated with the excitation of lateral bending, flexural bending, longitudinal and torsional vibration, respectively. The input forces the blade to vibrate in a way that involves four modes of vibration simultaneously. Four indicators, namely  $A_X$ ,  $A_Y$ ,  $A_L$  and  $A_T$ , are proposed by taking into account the responses of the blade in this condition, which are essentially the displacement/torsion amplitude of the blade tip, as illustrated in Table 4.3.

Input / Indicator	Definition	Illustration
$IN_X$ $IN_Y$ $IN_L$ $IN_T$	Input components that are associated with the excitation of lateral bending, flexural bending, longitudinal and torsional vibration respectively.	
$A_X$	Displacement amplitude of the blade tip along width direction.	
$A_Y$	Displacement amplitude of the blade tip along thickness direction.	
$A_L$	Displacement amplitude of the blade tip along longitudinal direction.	
$A_T$	Amplitude of the torsion angle of blade tip.	

**Table 4.3 Displacement Based Indicators**

It should be noted that the multi-component input applied in the computation is not the direct simulation of an actual excitation in real world cutting applications. Instead, it is applied in a way which introduces multiple modes of vibration in the analysis so that coupled vibration or other specific working condition can be simulated. The proposed indicators thereby provide an overview of how the blade behaves in the specified vibration condition. As the values of these indicators are dependent on the magnitude of the input, the input components  $IN_X$ ,  $IN_Y$ ,  $IN_L$  and  $IN_T$  should be

carefully selected so that the desired working condition is simulated in the computing. For a properly designed ultrasonic blade, it is desired that  $A_X$ ,  $A_Y$  and  $A_T$ , which are the responses of the unwanted modes, are minimised in order to reduce the negative effects of the unwanted vibration.

#### 4.2.5 Stress Based Indicators

Stress is another major concern in ultrasonic blade design. For cutting blades excited ultrasonically, the material stress caused by high frequency deformation can be significantly larger than that caused by the applied cutting force. To avoid blade failure, stress should be kept within the safe limit of material during operation. This can be evaluated using the von Mises criterion, which ascribes the occurrence of material failure to the distortion energy caused by deformation [225]. An equivalent stress called “von Mises stress” is derived and defined as the combination of the principle stresses:

$$\sigma_v = \sqrt{\frac{1}{2}(\sigma_1 - \sigma_2)^2 + (\sigma_2 - \sigma_3)^2 + (\sigma_3 - \sigma_1)^2} \quad (4.5)$$

where  $\sigma_v$  is the von Mises stress,  $\sigma_1$ ,  $\sigma_2$  and  $\sigma_3$  are the principle stresses. Failure is considered to take place when this stress exceeds the strength limit of the material. This criterion is widely used to investigate the strength safety of ductile materials such as metals.

To evaluate the strength of an ultrasonic blade, five indicators referred to as  $S_A$ ,  $S_X$ ,  $S_Y$ ,  $S_L$  and  $S_T$  are proposed based on the von Mises stress, as shown in Table 4.4.  $S_A$  is defined as the maximum von Mises stress found in the blade under a multi-component excitation. Similarl to the case in displacement based indicators, the multi-component input is applied for the purpose of inducing multiple modes of vibration in the computing rather than simulating the actual excitation in real-world applications. Thus  $S_A$  suggests how much stress the material suffers when the blade is performing coupled vibration.  $S_X$ ,  $S_Y$ ,  $S_L$  and  $S_T$  are defined as the maximum von Mises stress of the blade under an oscillating excitation, which is applied along the direction of width, thickness, longitude and torsion respectively. They indicate the stress condition of the blade vibrating in a single mode of vibration (lateral bending, flexural bending,

longitudinal or torsional vibration). Among the indicators,  $S_A$  and  $S_L$  are especially useful as an ultrasonic blade is normally excited longitudinally.  $S_L$  can be used to evaluate the blade stress according to the excitation output of the transducer. This can be further extended using  $S_A$ , which deals with not only longitudinal excitation but also the coupled vibration caused by non-linear dynamic behaviour of the blade, providing the multi-component input is applied in a way that induces the desired coupled vibration condition. For all stress based indicators, it is desired to minimise their values in the design process in order to avoid material failure and improve blade strength.

Indicator	Definition	Illustration
$S_A$	Maximum von Mises stress under an input with four components $IN_x$ , $IN_y$ , $IN_L$ and $IN_T$ .	
$S_X$	Maximum von Mises stress under an input along the width direction of the blade.	
$S_Y$	Maximum von Mises stress under an input along the thickness direction of the blade.	
$S_L$	Maximum von Mises stress under an input along the longitudinal direction of the blade.	
$S_T$	Maximum von Mises stress under a torsional input.	

**Table 4.4 Stress Based Indicators**

#### **4.2.6 Including Cutting Objects in the Analysis**

The above indicators consider only the behaviour of the ultrasonic blade, which allows their evaluation using relatively simple methods. However, due to the lack of information regarding the interaction between the blade and the cutting objects (bone or tissue), it would not be possible to evaluate the performance related to the cutting process or working conditions of the blade. To improve this and construct other types of performance indicators, the calculation can be extended to include the cutting objects in the modelling. It is expected that this can improve the quality of simulation, and enable the computation of frictional heat and temperature raise during cutting. Indicators, such as heat generation indicators and cutting efficiency indicators, can be constructed using similar concepts as proposed in this chapter.

#### **4.2.7 Summary**

The indicators introduced in Section 4.2.2 - 4.2.5 provide a means to characterise the performance of an ultrasonic blade. They can be used to construct the objective or fitness functions, whereby the design problem can be formulated. The main features of these indicators are summarised again in Table 4.5.

According to their nature, the indicators are classified as "large value preferred" and "low value preferred". All types of modal distance, gains (except gains of the working mode), and output displacement of the working mode are indicators belonging to the former class. The other indicators belong to the latter class. This feature should be included in the objective functions and constraints in order to make sure the optimisation is conducted properly.

The dependency of an indicator affects its computation. For those independent of the input, the indicators can be conveniently obtained by applying a normalised excitation (if required). However, for the indicators dependent on the input, the excitation should be applied in a way that induces the desired vibration condition.

These indicators evaluate the main dynamic characteristics of an ultrasonic blade. They enable the mathematical algorithms to compare and optimise the performance of ultrasonic blades in the design process. Although the characteristics such as heat generation or cutting efficiency, were not dealt with in this study, it is possible to

construct other types of performance indicators using similar principles to evaluate more features of ultrasonic blades.

Nature	Indicator	Definition	Value Preference and Constraints	Input of Computing
Modal Distance	$M_A$	Frequency distance between the working mode and other modes.	Large.	Independent of input.
	$M_X$			
	$M_Y$			
	$M_L$			
	$M_T$			
Gain	$G_X$	The factor of amplitude amplification for a specific mode of vibration.	Non-working modes: Low.	Independent of input.
	$G_Y$		Working mode: Large.	
	$G_L$			
	$G_T$			
Output Displacement	$A_X$	Displacement of the blade tip under a multi-component input.	Non-working modes: Low.	Multi-component input.
	$A_Y$		Working mode: Large.	
	$A_L$			
	$A_T$			
Stress	$S_A$	Maximum stress under a multi-component input.	Low. Must be within the material strength limit.	Multi-component input.
	$S_X$	Maximum stress under a single component input.		Single component input.
	$S_Y$			
	$S_L$			
	$S_T$			

**Table 4.5 Summary of Indicators**

### 4.3 Optimisation Algorithms

The introduced performance indicators work as a bridge between the real world problem and the optimisation, based on which an ultrasonic blade design problem can be formulated into a mathematical optimisation using a set of selected indicators. Thus the optimisation can be solved by algorithms that are already available for various optimisation problems. The optimisation algorithms widely used in engineering problems include the simplex method, genetic algorithm, simulated annealing algorithm and multi-objective optimisation.

### 4.3.1 Exhaustive Search and Graphic Method

Exhaustive search, sometimes known as brute-force enumeration, is one of the oldest approaches to solve optimisation problems. The concept of this method is simple: generate and test all possible configurations in the optimisation space where the desired solutions locate, and this will guarantee that the optimal solutions are found [226]. This concept is straightforward and results in very general algorithms that can be effectively applied to a large number of small scale optimisation problems. However, the amount of computing required by exhaustive search increases dramatically as the complexity of problem is increasing. It is usually not feasible to implement this algorithm for large scale optimisation as the calculation time would be unbearable.

If there are only two design variable to be optimised, it is possible to solve the optimisation graphically [110]. This method plots all the constraint functions in contour figures, which can be used to identify a set of feasible designs. Then the objective function is drawn based on these feasible designs and the optimal design can be obtained by inspecting the function values visually. One of the advantages of the graphic method is that the graphical representation of the constraints and objective function allows the designer to have an impression of the performance of different designs in the optimisation space. This may help the designers to improve the original design concepts.

### 4.3.2 Linear Programming Problem and Simplex Method

A linear programming problem (LP) is an optimisation problem with linear cost and constraint functions in its design parameters [110]. Some engineering design problems can be formulated as this kind, although most of the real world cases are in fact non-linear. Moreover, one of the most important approaches to solve a non-linear optimisation is to transfer it into one or more LP problems or apply LP algorithms in the local searching of solutions [218].

A standard LP problem can be represented as follows

$$f = c_1x_1 + c_2x_2 + \cdots + c_nx_n \quad (4.6)$$



A number of mature software packages or programs, such as the optimisation toolbox of Matlab, are already available to implement the simplex algorithm and solve LP problems. However, as this algorithm requires linear objective functions and constraints, for those applications with little preliminary information about the nature of their objective functions it is necessary to apply a more general approach to solve the optimisation.

### 4.3.3 Genetic Algorithm

A genetic algorithm is a kind of stochastic search optimisation method which comes from the idea of biological evolution that includes genetics and natural selection [110]. The basic techniques of this algorithm simulate the principle found in the evolution processes of natural systems known as "survival of the fittest".

The algorithm begins with a set of initial designs and then repeatedly produces generations randomly within the allowable region. Each generation contains a population of different solution which are assigned a fitness value or a penalty function as a criterion to compare their performance. During the evolution, fitter designs are selected and kept in the successive generation in order to bring the population evolving towards the maximum/minimum value. Eventually, the optimal solution is expected to be found after a sufficiently large number of iterations.

The algorithm duplicates a number of concepts in the natural system:

**Individual:** In the design problem, this refers to a specific design, which can be evaluated by the fitness function to examine its performance.

**Population and Generation:** The population is a group of potential design solutions in the current iteration process. At each iteration, the algorithm conducts a number of manipulations on the current population in order to generate a new population. The successive population is called a new generation.

**Diversity:** This is the measure of the average distance between the individuals of a population. Like biological diversity, a proper value of diversity is essential to the evolution process as it allows the algorithm to search a larger region of the solution space.

**Parents and Children:** The parents are certain individuals selected from the current population to create individuals for the next generation. The created individuals



are referred to as children. To push forward the evolution, parents with larger fitness value, which means they are designs with better performance, are more likely to be selected.

Based on the above concepts, the implementation of the genetic algorithm is very similar to the natural evolution process. The following procedures are the basic steps that should be included in a genetic algorithm applied for the design of ultrasonic blades.

- (1) Generation of Initial Population: As the first step of the algorithm, a certain number of potential designs are generated using a random algorithm as the initial population.
- (2) Determine the Fitness of the Population: This is to evaluate the performance of each individual/design in the population using the indicators proposed in Section 4.2.
- (3) Selection of Population: This operation resembles "survival of the fittest" in nature. It finds the individuals with the best performance in the current population and passes them to the next generation (survive).
- (4) Crossover: This operation allows a pair of individuals in the current population to combine their "genes" in order to create offspring for the next generation. The selection of parents for crossover and the combination of their genes are performed by a random operator carefully designed for the application.
- (5) Mutation: In order to maintain a good diversity of the population and avoid premature convergence, the mechanism of mutation is introduced, which allows a random change of the gene for a portion of new individuals. From the point of calculation, this results in random walking in the searching space which helps the algorithm to converge towards the optimal solution.
- (6) Stop Criterion: The algorithm stops when certain conditions are satisfied, such as the number of generations reaches a specific value, the computation time exceeds the limit, the fitness function finds a sufficiently small/large value.

One advantage of this algorithm is that it uses only objective function values in the optimisation and requires no detail of the nature of the function. This enables it to solve complex cases, such as discontinuous or non-differentiable, making it an extremely general method that can be applied to virtually all kinds of problems [110,

227]. In addition, the algorithm is robust, which offers excellent performance against the change of inputs and presence of noise.

However, there are inevitably limitations of the genetic algorithm. A major drawback is that the method requires a large amount of computation in order to obtain a satisfactory solution. This problem becomes even worse if it takes a considerable time to evaluate the performance of every single individual in the evolution process. In addition, the computational scale of the algorithm increases dramatically as the number of search variables is increased. This makes it unsuitable to be used for design problems of large scale.

#### **4.3.4 Simulated Annealing Algorithm**

Simulated annealing is another random search technique widely used in optimisation and artificial intelligence to find the global maxima/minima. This algorithm is motivated by the interesting physical phenomenon of annealing where a crystalline solid is able to achieve the most regular and defect free crystal status if it is carefully and slowly cooled. During this process, the solid is turned from a high energy state into a lowest energy configuration. By applying a set of "controlled cooling" operations, the simulated annealing algorithm simulates this phenomenon with an attempt to provide a general search method for optimisation.

Similar to the genetic algorithm, the simulated annealing requires no prior information about the objective function, which makes it extremely versatile, and it can be applied to almost any kind of problem including highly non-linear, discontinuous or non-differentiable ones. This is very important for the design of ultrasonic blades as the relationship between the blade performance and the design parameters is usually non-linear and difficult to know beforehand. One major advantage of this algorithm is its ability to avoid being trapped by local maxima/minima. Given sufficient computing time, the algorithm is able to find the global optimum with a carefully selected cooling rate.

In order to apply the simulated annealing algorithm to the design of ultrasonic blades, some basic elements must be included in the method:

- (1) The performance measure of different designs or representation of objective functions. This can be done based on the indicators introduced in Section 4.2.

- (2) An operator which changes a feasible solution randomly. This simulates the physical phenomenon of particle/atom movement in solids.
- (3) A cooling schedule that turns the concept of annealing into an application.
- (4) A temperature variable used as a parameter of the searching process.

Simulated annealing is in fact a concept of searching for the optimal solution. The implementation of the method is highly dependent on the application itself. For blade design applications, the following steps can be used to perform the algorithm :

- (1) Generate a random trial solution based on a distribution function  $F_d$  which depends on the current "temperature".
- (2) Check the performance (objective function) of the new solution. The new solution will replace the current one if it is found to be better. Otherwise, it can still be accepted with a probability given by an acceptance function  $F_c$ . As a general case, its probability of acceptance can be defined in the form of:

$$p = \frac{1}{1 + \exp\left(\frac{f_n - f_c}{\max(T)}\right)} \quad (4.10)$$

where  $p$  is the acceptance probability,  $f_n$  and  $f_c$  are the values of the objective function of the new and old solution respectively.  $\max(T)$  is the maximum temperature experienced so far.

- (3) Reduce the current temperature according to an annealing function  $F_a$  and keep a record of the best solution that has been obtained. The "cooling rate" must be selected properly as it is a parameter of great importance to the quality of the final solution.
- (4) Repeat the above procedures until the average change of objective functions is sufficiently small or the computing time reaches a predefined limit.

The main drawbacks of this method are the implementation and the computing costs. In order to achieve good performance, the procedure has to be tailored by defining appropriate  $F_d$ ,  $F_c$  and  $F_a$  for a specific application. This makes it difficult to use a general purpose program to solve all cases encountered. In addition, similar to the case in genetic algorithm, simulated annealing is also a stochastic searching algorithm. Thus it requires a large amount of calculations in order to obtain a solution of satisfactory precision. This may result in expensive computational costs when it takes

a considerable period of time to evaluate the performance of one design. In this case, a trade-off between the quality of the solution and the cost of computing must be made.

#### 4.3.5 Multi-objective Optimisation

The above algorithms take into account only one optimisation goal. However, in practical design applications, it is often desired to optimise two or more objectives simultaneously by considering multiple objective functions. Such cases are called multi-objective or vector optimisation problems.

A major challenge of such type of problem is that some objectives may be conflicting due to the physical constraints or limitations of the design problem. For example, increasing the gain of the blade often results in higher material stress as a result of the increased deformation. This means that maximising the gain and minimising the stress are conflicting objectives. It is therefore unlikely to find a single solution that optimises all the objective functions simultaneously in such cases. Compromises between different goals must be made in order to obtain a feasible solution.

One method to solve the multi-objective problem is to convert it into a single objective optimisation by combining different goals into one global objective function using a weighted sum:

$$U = \sum_i w_i f_i \quad (4.11)$$

where  $U$  is the global objective function,  $f_i$  is a single sub-objective function and  $w_i$  is the weight that reflects the importance of the associated objective in the global goal. The new optimisation problem can subsequently be solved using the well developed single objective algorithms. However, there are a number of significant disadvantages with this solution:

- (1) The sub-objective functions are often constructed to reflect different aspects of the nature of the design. As a result, it can be ambiguous to compare their values or sum them.
- (2) The determination of the weight of the sub-objective functions relies heavily on the designer's experience and preference.
- (3) It is difficult to control the optimisation process of an individual goal as the computing is performed on the global objective function.

- (4) There is often a lack of a clear mechanism to make a trade-off between conflicting goals.

Therefore optimisation methods dealing with multiple objectives directly are developed. The predominant theory is the Pareto optimality [110], which introduces the concept of optimal solution set, namely the Pareto optimal set. The solutions in this set are considered to be optimal in the sense that no other feasible designs exist that improves at least one objective function without deteriorating the others. This means instead of a single solution, the optimisation produces a number of designs that are equally optimal.

As a general and versatile method, the genetic algorithm introduced in Section 4.3.3 can be extended to a new algorithm called a multi-objective genetic algorithm, which provides an effective approach to solve the multi-objective optimisation as it does not require any preliminary information about the nature of the problem. This algorithm has been reported to be applied in the design of ultrasonic horns and transducers successfully [215, 216, 219, 223]. Similar to the single objective genetic algorithm, the multi-objective genetic algorithm shares concepts in solution searching. The main operations that are included in the algorithm are: initialisation of population, reproduction of offspring and replacing the individual. However, due to the multi-objective nature of this algorithm, the definition of its fitness function and the genetic operations, including the selection, crossover and mutation, must be adapted in a way that incorporates the concept of the Pareto optimality and handles objective vectors.

#### **4.4 Proposal of an Optimal Design Method**

Based on the performance indicators and the optimisation algorithms, an optimal design method is proposed for ultrasonic bone cutting blades. This method aims to improve the conventional design process by reducing the need for designers' experience and enabling the "best" solution to be obtained. As illustrated in Figure 4.3, the proposed design process is divided into three major stages: formulation, optimisation and verification. This is significantly different from the conventional design method in that the stages of formulation and optimisation are introduced.

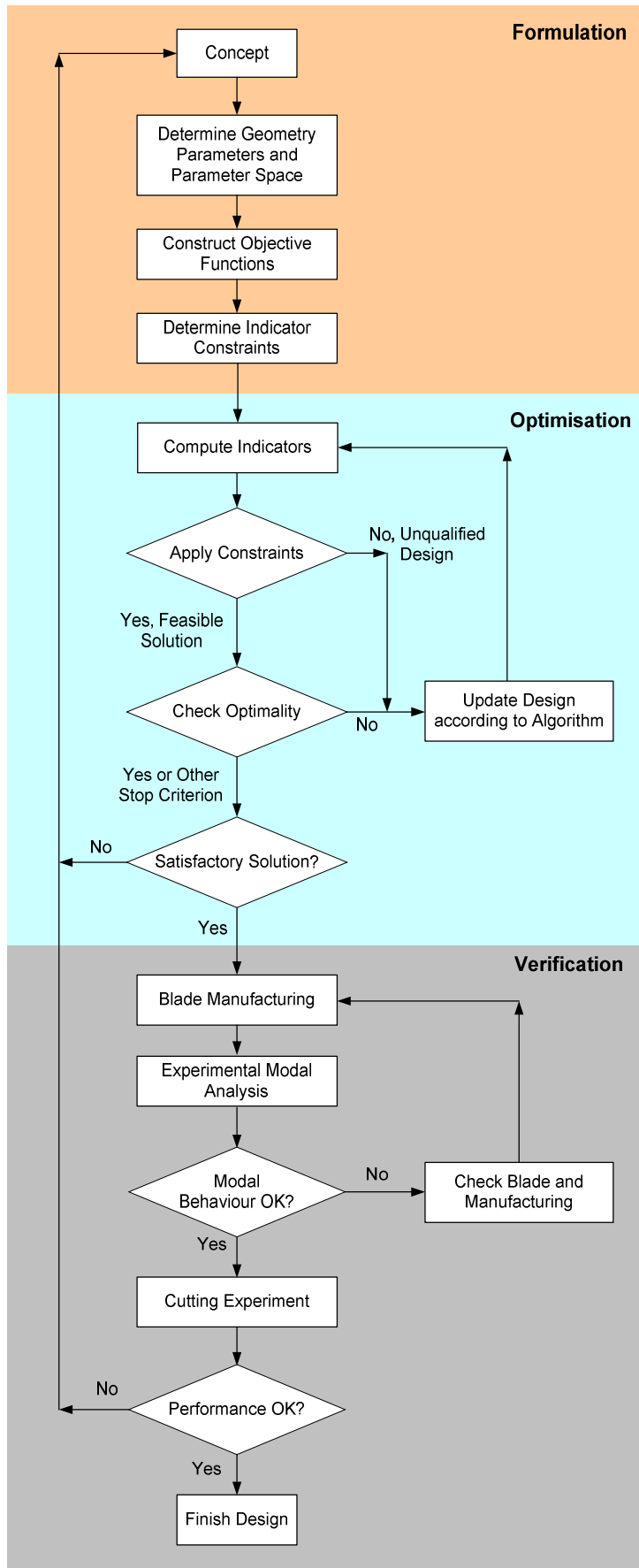
#### **4.4.1 Formulation of the Problem**

The first stage is the formulation of the design problem. As the optimal method uses algorithms to update the design, the blade design problem must be represented as an optimisation problem in order to solve it using mathematical approaches. This is done based on the design concept through three procedures: representing the blade geometry in terms of parameters, constructing the objective functions, and determining the constraints of indicators, as illustrated in Figure 4.3.

##### **4.4.1.1 Geometry Parameters and Parameter Space**

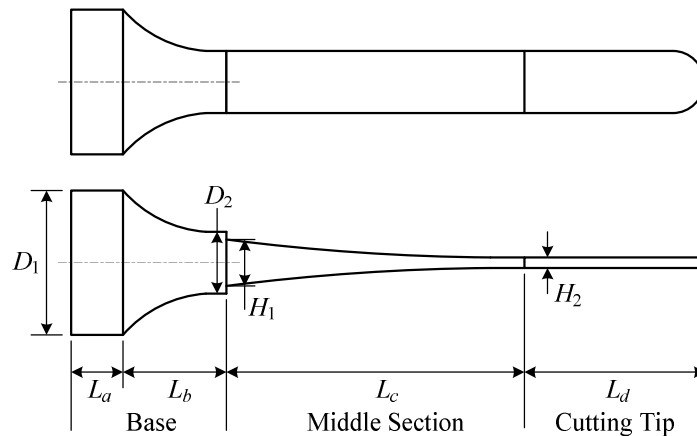
The design process begins with the design concept. The general and essential information about the blade, such as the requirements of the performance, the overall size, shape of the blade, and the selection of material, is proposed in this step. This sets the basis for the formulation of the problem.

According to such information, the geometry parameters are selected for the blade. They are a group of arguments that shape the profile of the design. Representing the blade in terms of parameters allows the algorithm to update the design by varying the value of these parameters. This means that the mechanical problem of blade design can be treated as a mathematical process that determines the value of a set of geometry parameters so that the performance of the blade is optimised in terms of the indicators. However, it may not be necessary to involve all the geometry parameters in the optimisation process. Those parameters that are required to be determined by the optimisation algorithm are referred to as adjustable parameters. They determine how the algorithm interacts with the design process. The multi-dimensional space formed by all the adjustable parameters is called the parameter space. Usually it is a space with boundaries set by the scope of the parameters. This defines a zone where the optimisation searching will be conducted.

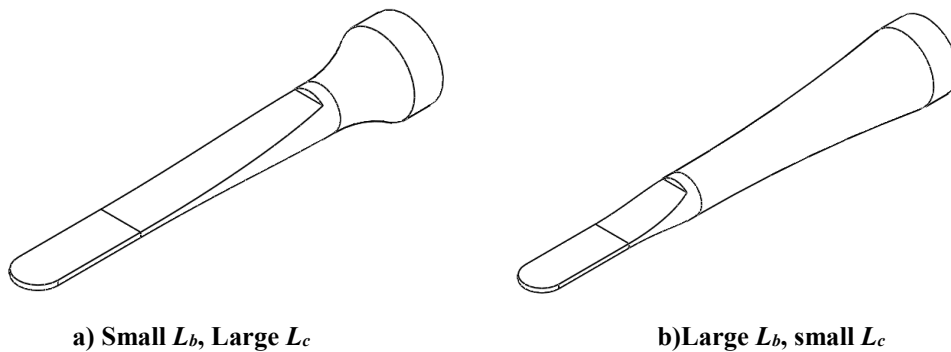


**Figure 4.3 The Optimal Design Method**

To illustrate this, the example of a three section blade mentioned in Chapter 2 is shown again in Figure 4.4. This blade is defined by 8 geometry parameters:  $H_1$ ,  $H_2$ ,  $D_1$ ,  $D_2$ ,  $L_a$ ,  $L_b$ ,  $L_c$  and  $L_d$ . By assigning different values for these parameters, various designs can be obtained. Figure 4.5 shows two examples which are significantly different designs at a glance. They, however, are produced by assigning different values for the same set of geometry parameters.



**Figure 4.4 Geometry Parameters**



**Figure 4.5 Blade Shape and Parameters**

If all parameters in Figure 4.4 are treated as adjustable parameters, the searching will be carried out in a parameter space of eight dimensions, which can introduce considerable computing costs for the optimisation. In fact, it may not be necessary to deal with such a complex space as some parameters can be determined prior to the optimisation by other means, which reduces the number of adjustable variables and simplifies the problem.



#### 4.4.1.2 Objectives and Constraints

Based on the parameterisation of the blade profile, the goal of the design can be represented by objective functions which take into account the performance preference of the blade. This can be done using the performance indicators proposed in Section 4.2.

By treating the adjustable geometry parameters as the arguments, an indicator can be used directly as an objective function, as shown in Eq. (4.12)

$$f_k = g_k(x_{a1}, x_{a2}, \dots, x_{aN}) \quad (4.12)$$

where  $f_k$  is the objective function,  $g_k$  is an indicator,  $x_{a1}, x_{a2}, \dots, x_{aN}$  are the adjustable geometry parameters. The target of the optimisation is to minimise/maximise the value of the objective function by varying the adjustable parameters. More than one indicator can be used to construct multiple objective functions for different design goals. These objective functions can be dealt with using the method of weighted sum global function and single objective optimisation algorithms, as introduced in Section 4.3.5. Alternatively, it is possible to process the objectives simultaneously using multiple objective optimisation algorithms.

In addition to the goal of design, the other design requirements, such as the strength and the tuned frequency of the blade, are formulated as the constraints. The introduction of constraints imposes physical restrictions on the blade design. This filters out the incompetent designs and makes sure all the generated solutions exhibit the desired characteristics.

Generally, a constraint is represented as an allowable range of an indicator, as illustrated in Eq. (4.13)

$$a_{\min} \leq g_k(x_{a1}, x_{a2}, \dots, x_{aN}) \leq a_{\max} \quad (4.13)$$

where  $a_{\min}$  and  $a_{\max}$  are the lower and upper limits respectively. This introduces boundaries in the searching space to avoid unfeasible solutions. As a special case, when  $a_{\min}=a_{\max}$ , the constraint becomes an equal condition:

$$g_k(x_{a1}, x_{a2}, \dots, x_{aN}) = a_{\text{fix}} \quad (4.14)$$

which forces the optimisation to be conducted on a multi-dimensional surface.

#### 4.4.2 Optimisation

Optimisation is the main part of the design process, which applies an optimisation algorithm to modify and update the blade profile until a satisfactory solution is obtained. As illustrated in Figure 4.3, whichever algorithm is used in the optimisation, the process consists of the following four basic steps:

- (1) **Compute the indicators:** This step computes the performance indicators for the current design. It is usually the most time consuming procedure in the optimisation as most of the calculation is conducted based on finite element analysis which may take a considerable period of time to complete.
- (2) **Apply the constraints:** This operation is sometimes integrated into the optimisation algorithm. Thorough checking of the performance of the design is conducted according to the constraint inequations/equations introduced in the formulation stage. A design will be discarded if it fails to comply with any constraint, making sure only the qualified ones are considered in the optimisation.
- (3) **Check the stop criteria:** The optimisation terminates when the stop criteria is met. This is usually triggered when an optimal design/design set is obtained. However, the process can also be terminated when there is a timeout in the calculation or searching. Inappropriate formulation of the problem or the application of unsuitable algorithms may result in the optimisation to be terminated before satisfactory solutions are obtained.
- (4) **Update the current design:** This is the core step of the design process where the optimisation algorithm is introduced. The current design will be submitted for the optimisation algorithm to be updated if it satisfies the constraints and triggers no stop criteria. The newly generated design will be subjected to the above process again until the optimisation is terminated.

#### 4.4.3 Blade Verification

If one or more satisfactory blade designs are obtained by the optimisation process, the prototypes can be manufactured and tested. The verification stage in the optimal method is similar to that in the conventional design method. Experimental modal analysis or other tests will be conducted to examine the working frequency and the relevant modal behaviour of the blade. The actual value of the performance indicators

will be measured and compared with their predictions to make sure the expected characteristics are obtained.

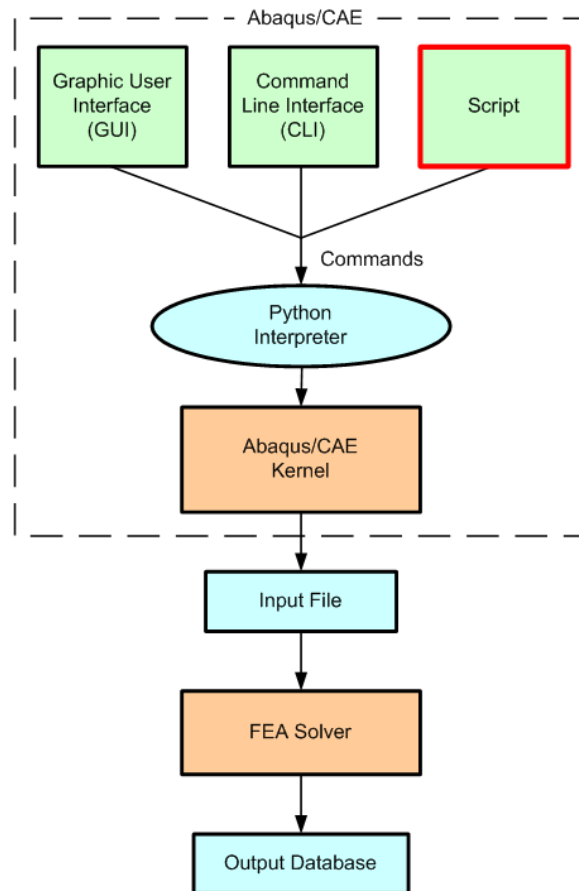
The overall performance of the blade will be examined in cutting tests, where a prototype is excited at full power and used in the cutting of bone samples or other test materials. Its performance can be investigated by measuring the cutting parameters such as cutting speed and temperature under various working conditions. The whole design process is completed if satisfactory results are obtained. Otherwise either the manufacturing, optimisation algorithm or the blade concept has to be reviewed and the design process will be restarted again.

#### **4.4.4 Implementation and Programming**

##### **4.4.4.1 Software and Programming Environment**

To implement the proposed optimal design method, a software toolkit was developed in this research based on Abaqus and Python language. Abaqus (version 6.11) is a commercial general purpose FEA package, which provides a scripting interface to access its functions and data. The scripting interface uses an extension of Python language to act as an application programming interface (API) , as illustrated in Figure 4.6. It allows the user to use a command script to communicate with the software kernel and perform complex tasks such as creating models, conducting calculations and processing results. This enables the designer to automate repetitive jobs, perform a parametric study or interact with the output in a convenient way.

The script is one or more plain ASCII files containing a sequence of Python commands to perform certain tasks. In the application, it is submitted to a Python interpreter embedded in Abaqus to invoke the internal functions. This facilitates the programming and extends the scripting function by adopting the features provided by Python language. Being an object-oriented programming language created in the late 1980s, Python is now widely used in a number of fields such as web and internet development, scientific and numerical computing, and education. Its characteristics such as its high level programming ability, dynamic characteristic, automatic memory management and tidy syntax enable the user to make the most of the Abaqus scripting interface.



**Figure 4.6 Abaqus Scripting Interface**

#### 4.4.4.2 Software Development and Modules

The optimal design toolkit was developed using an IDE (Integrated Development Environment) provided within Abaqus/CAE, referred to as Abaqus PDE. This IDE provides the necessary functions, such as text editing and keyword highlighting, for script development. A screenshot of the working development environment is illustrated in Figure 4.8. When debugging the code, the built-in Python interpreter of Abaqus was invoked to execute the program from within Abaqus/CAE.

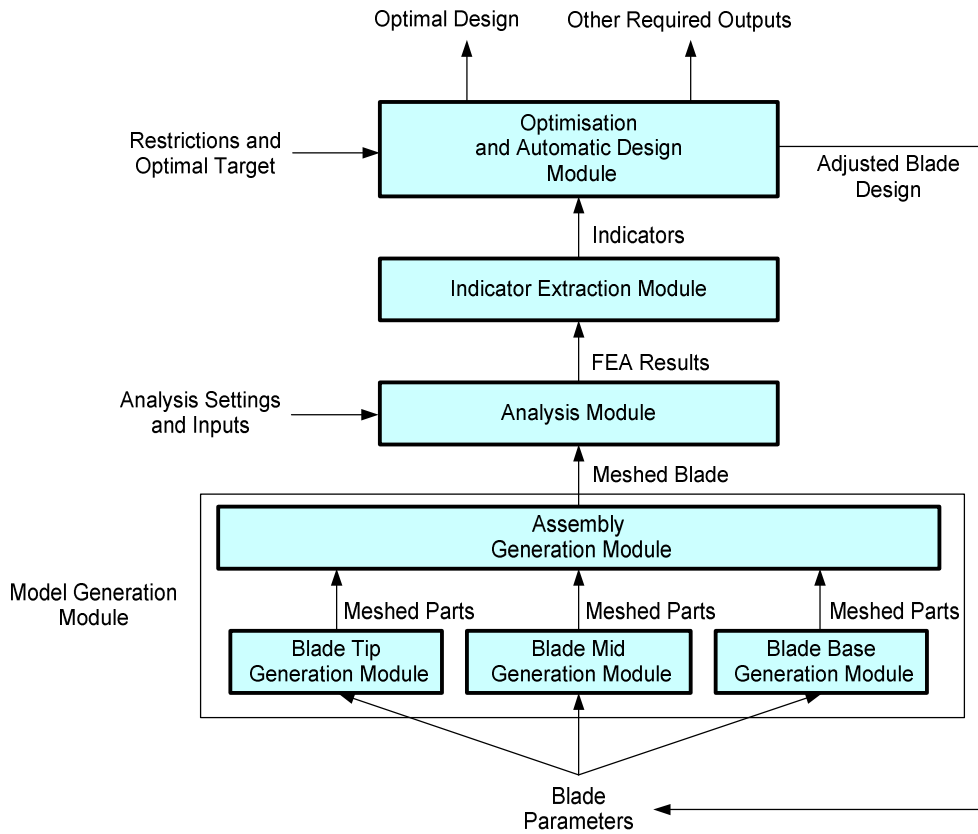
```

1 import imp
2 from abaqusConstants import *
3
4 def _tieParts(model, assembly, p0, p1, aflip, fflip):
5     #Add Position Relation
6     a0=p0.part.features['VerticalAxis']
7     a1=p1.part.features['VerticalAxis']
8     assembly.ParallelEdge(fixedAxis=p0.datums[a0.id], movableAxis=p1.datums[a1.id], flip=aflip)
9
10    a0=p0.part.features['FrontPlane']
11    a1=p1.part.features['BasePlane']
12    assembly.ParallelFace(fixedPlane=p0.datums[a0.id], movablePlane=p1.datums[a1.id], flip=fflip)
13
14    a0=p0.part.features['FrontCentralPoint']
15    a1=p1.part.features['BaseCentralPoint']
16    assembly.CoincidentPoint(fixedPoint=p0.datums[a0.id], movablePoint=p1.datums[a1.id])
17
18    #Tie Parts together
19    a0=p0.surfaces['FrontFaces']
20    a1=p1.surfaces['BaseFaces']
21    model.Tie(name=p0.name+'*p1.name, master=a0, slave=a1,
22             positionToleranceMethod=COMPUTED, adjust=ON, tieRotations=ON, thickness=ON)
23
24
25 def CreateAssembly(model, *parts, **flip):
26     if not parts: return ()
27     nua=len(parts)
28
29     axis_flip=flip.get('axis_flip', [OFF]*nua)
30     face_flip=flip.get('face_flip', [OFF]*nua)
31     base_align=flip.get('base_align', None) #Determine whether the first part put lastly so that the second will start at z=
32
33     assembly=model.rootAssembly
34     instance=[]
35
36     n=1 #Order of Name
37     i=1 #Index of part
38     if i>nua:
39         p0=assembly.Instance(name='Part-'+str(n), part=parts[i], dependent=ON)
40         instance.append(p0)
41     for p in parts[i+1:]:
42         n+=1
43         i+=1
44

```

**Figure 4.7 Screenshot of the Development Environment**

The optimal design toolkit was structured in an object-oriented way that consists of several modules of different functions. It is a script library serving as an add-on function for Abaqus, which offers the necessary functions for the process of the optimal design. The toolkit includes four top level modules: model generation modules, analysis module, indicator extraction module and optimisation/automatic design module, as illustrated in Figure 4.8. These modules are implemented using 7 main files and a number of sub-files, as shown in Table 4.6. The model generation modules are mainly implemented in 4 files: BladeBase.py, BladeMid.py, BladeTip.py and BladeDesign.py. The analysis and indicator extraction module is mainly implemented in BladeAnalysis.py. The optimisation module is implemented in UtilityModule.py. Each module contains the essential functions that interact with Abaqus and perform the relevant calculation. Figure 4.9 shows the interaction between the modules and Abaqus. Selected codes of the modules are showed in Appendix A.4.



**Figure 4.8 Modules of the Optimal Design Package**

File	Description
BladeBase.py	Provide functions to create and mesh the base section of a blade.
BladeMid.py	Provide functions to create and mesh the middle section of a blade.
BladeTip.py	Provide functions to create and mesh the tip section of a blade.
BladeDesign.py	Implement functions including defining blade geometry, assembling, and creating datum set for post-analysis processing.
BladeAnalysis.py	Provide functions to perform FEA, process output file and implement post-analysis calculation.
FileProcess.py	Provides functions relevant to the processing of input and output files.
UtilityModule.py	Implement the functions of optimal design.

**Table 4.6 Main Files of the Optimal Design Library**

As illustrated in Figure 4.8, the model generation module includes four sub-modules: blade tip, mid and base generation modules, and assembly generation module. The modules accept the inputs and settings given by the user and interact with

Abaqus/CAE to generate the finite element model of the blade. The blade tip/mid/base generation modules are capable of creating and meshing the relevant parts of the blade automatically. These parts are then used by the assembly generation module to produce a full analysis model. To facilitate the application of these modules, an Abaqus plug-in is developed, providing a GUI to invoke the relevant functions. The interface of the plug-in is illustrated in Figure 4.10. This plug-in allows the user to define parameters for the blade and analysis. The model and codes generated by the plug-in can be directed used for the following optimisation process.

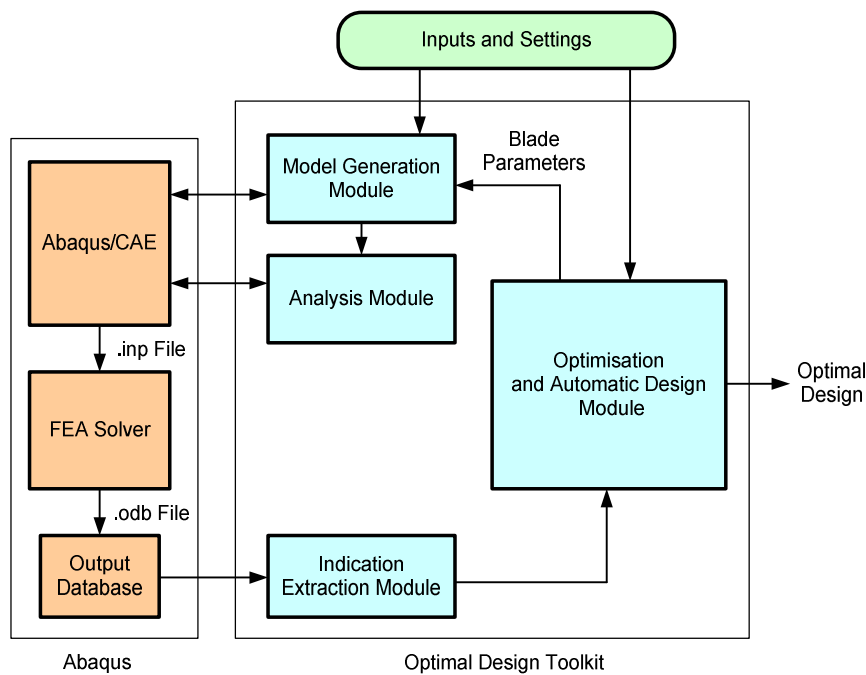


Figure 4.9 Interaction between Modules and Abaqus

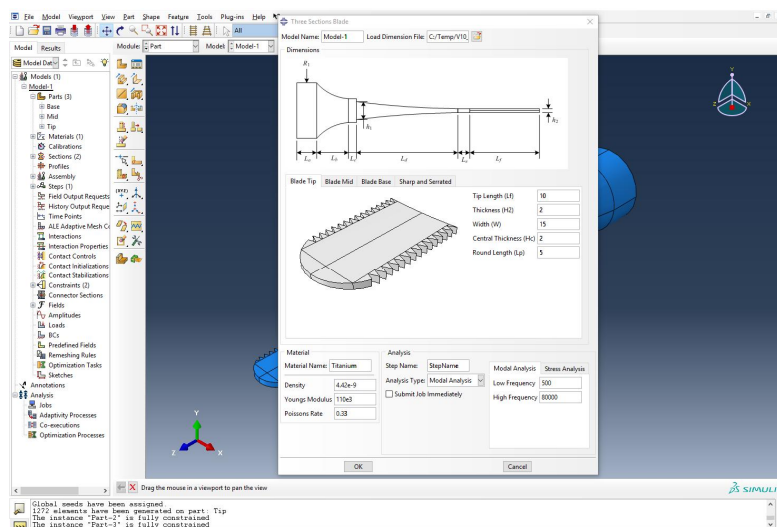


Figure 4.10 GUI of Abaqus Plug-in

The analysis module is used to perform the required finite element analysis based on the FE model generated by the model generation module. It provides functions to define the input and load conditions of the simulation. It also offers commands to invoke the appropriate Abaqus functions to carry out the calculation. The obtained FEA results would be stored in a *.odb* file (output database) and processed by the indicator extraction module which unfolds the useful information, such as the displacement of the nodes, the frequency of the modes, from the database. Such information will be used to compute the required indicators using methods introduced in Section 4.2.

After the indicators are obtained, the optimisation and automatic design module can be applied to perform the optimisation. The module plays a vital role in the design as it controls and directs the calculation process by adjusting the geometry parameters and initiating the finite element analysis. This allows the optimal design to be performed in an automatic way. To improve the flexibility of the program and allow different algorithms to be applied conveniently, this module does not include the implementation of a specific optimisation algorithm. Instead, it offers an interface to embed the algorithm into the application. This strategy improves the extensibility and enables a wider range of application of the toolkit.

## **4.5 Summary**

This chapter presented an optimal design method for ultrasonic cutting blades, which applies optimisation algorithms instead of designer's experience or intuition to update the blade design during design process.

The method is proposed based on the introduction of performance indicators. By representing the physical characteristics of an ultrasonic blade as values or mathematical functions, the indicators act as a bridge between the real world problem and the mathematical algorithms. Four kinds of indicators: the frequency based, gain based, displacement based and stress based indicators, are proposed and classified according to their nature. These indicators reflect the dynamic performance of an ultrasonic blade from various aspects. Although they do not cover characteristics such as heat generation and cutting efficiency, other types of indicators can be constructed using similar concepts as introduced in this chapter.



The target of the optimal design process is to maximise the blade performance represented in the form of indicators. There are already a number of optimisation algorithms available for different kinds of problems, such as the simplex algorithm, genetic and simulated annealing algorithm. Regardless of the algorithm applied, the process of the optimisation consists of three major stages: formulation, optimisation and verification.

In the formulation stage, a blade design is represented by a group of geometry parameters that define the profile of the blade, which enables the algorithm to evaluate the blade performance and update the design conveniently. The design requirements are formulated as optimisation objectives and constraints. This can be done using a group of carefully selected indicators to construct the appropriate objective functions and constraint inequations/equations.

In the optimisation stage, the algorithm evaluates and checks the performance of the designs, discarding those failing to comply with the problem constraints. New designs are generated and the optimal searching is conducted using optimisation algorithms. The procedure is repeated until the stop criteria are met.

Verification of the design is carried out if a satisfactory design is obtained. The blade will be manufactured and subjected to tests to verify its dynamic characteristics and cutting performance. The whole design process is finished if satisfactory performance is obtained. Otherwise either the manufacturing of the blade, optimisation method or the design concept has to be reviewed.

A software toolkit was developed in order to implement the proposed method and apply it in real design cases. The toolkit was developed based on the Abaqus script interface using Python language. It consists of a number of software modules that are capable of generating the blade model, extracting the performance indicators and conducting the optimisation searching. However, to improve the flexibility of the program and allow different algorithms to be applied conveniently, the toolkit did not implement specific optimisation algorithms. Instead, it offers an interface to embed the algorithm in a later stage of the application.

The proposed method and the developed toolkit introduce a new approach to design ultrasonic cutting blades. Although they were initially proposed for ultrasonic blades,

they can be further extended for the design of other ultrasonic devices. In the next chapter, the application of the optimal method will be demonstrated by design cases.

# Chapter 5

## Design of Ultrasonic Cutting Blades and Experiments

### 5.1 Introduction

The design methods for ultrasonic cutting blades were detailed in Chapter 1 and Chapter 4. The conventional method is an iterative design process terminated explicitly with one useable solution. On the other hand, the optimal method finds the design that offers the most desired performance. To demonstrate the application of both methods and highlight the advantages of the optimal method, design examples of ultrasonic bone cutting blades and the experimental tests of these blades are presented in this chapter.

As this research focused on the design of ultrasonic blades, the optimality of the blade excitation parameters for specific cutting applications would not be discussed. Instead, the excitation requirements of the blades were determined based on previous research and the specification of the ultrasonic generators used in the tests.

In terms of tuned frequency, all blades designed in this study are required to work with an existing ultrasonic generator, which is designed to drive ultrasonic cutting blades at 35kHz. Previous work by Cardoni [14] and MacBeath [39] has shown that under this operation frequency, good cutting performance can be obtained for a relatively small cutting device. As the ultrasonic generator allows a frequency tolerance of  $\pm 1.0\text{kHz}$ , the blades should be resonant at their first longitudinal mode at  $35.0\pm 1.0\text{kHz}$  to ensure proper excitation in cutting process. The blades are expected capable of delivering vibration amplitude of 15-60 $\mu\text{m}$  at the blade tip, a typical level of vibration for ultrasonic cutting devices [15].

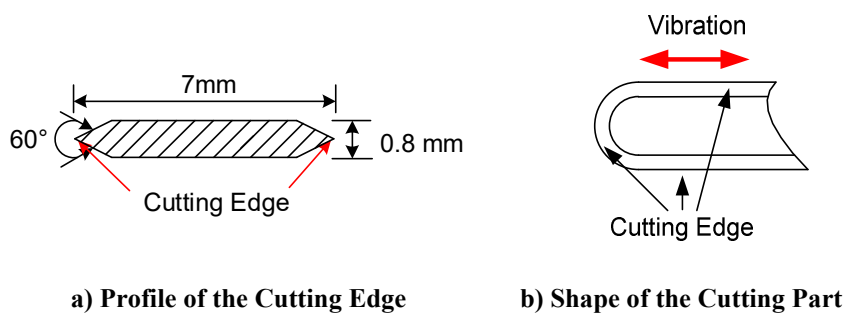
In terms of general cutting performance, the blades are designed as surgical bone cutting tools that are capable of make incisions of at least 5mm deep in human bones such as femur. This would allow the blades to cut through the cortical bone in a typical human femur [247]. To facilitate the cutting operation, the blades should be capable of penetrating into a bone axially or cutting laterally. Hence they should be

designed with appropriate cutting edges with adequate mechanical strength to withstand the stress caused by material deformation. Although the blades presented in this study are not intended to be applied in practical surgeries at this stage, the techniques developed will be of great use in the design of ultrasonic surgical cutting tools.

## 5.2 Blade Designed Using Conventional Method

### 5.2.1 Blade I: Blade with Sharp Cutting Edge

Blade I was designed to perform ultrasonic cutting on large bones, with the intention of testing on ovine femur bone. The cutting edge, which refers to the cutting surface of the blade that contacts the bone directly, was considered to be of great importance in the blade design due to its significant influence on ultrasonic cutting performance. Like non-ultrasonic blades, as sharpening the cut edge reduces the contact area between the blade and bone, sharp cutting edge is expected to enhance cutting by increasing the contact stress. Blade I adopted a sharp cutting profile which is similar to the design of ultrasonic bone cutting and food cutting blades in previous research [14, 39, 53]. As illustrated in Figure 5.1, the thickness of the blade is 0.8mm, and the angle of the cutting edge is 60°. The blade was sharpened on the sides and front of the tip, aiming to enable the application of the blade in a flexible way where either the edges or the tip could be involved in the cutting.



**Figure 5.1 Profile and Shape of the Sharp Cutting Edge**

### 5.2.1.1 Blade Design and Analysis

#### (1) Geometry and Shape

Blade I was designed by following the conventional design process detailed in Section 1.5.4. In the initial design, the length and size of the blade was estimated using Eq. 1.1, and then a more detailed shape was derived from previous ultrasonic blades that were designed for food processing or bone cutting [14, 39]. Although the blade was a single component machined from one block of metal, in order to facilitate the discussion, the profile of the blade is divided into three sections: the cutting tip, middle section and the base, as illustrated in Figure 5.2(a). The cutting tip was the thin part with constant thickness and sharp cutting edge, which was over 10mm in length. According to previous research [39], this was expected to be capable of achieving the required cutting effect. The middle section was the tapered part of the blade between the cutting tip and the base. Its length was adjusted during the design to tune the blade at the correct frequency. The base section included a cone and a cylinder. A threaded hole was drilled in the end of the cylinder in order to screw the blade onto a transducer, as shown in Figure 5.2(b). As a result of the tapered shape, this section functioned as a horn, which amplifies the excitation inputted from the end of the blade. The profile of the blade and the main dimensions are illustrated in Figure 5.2(c).

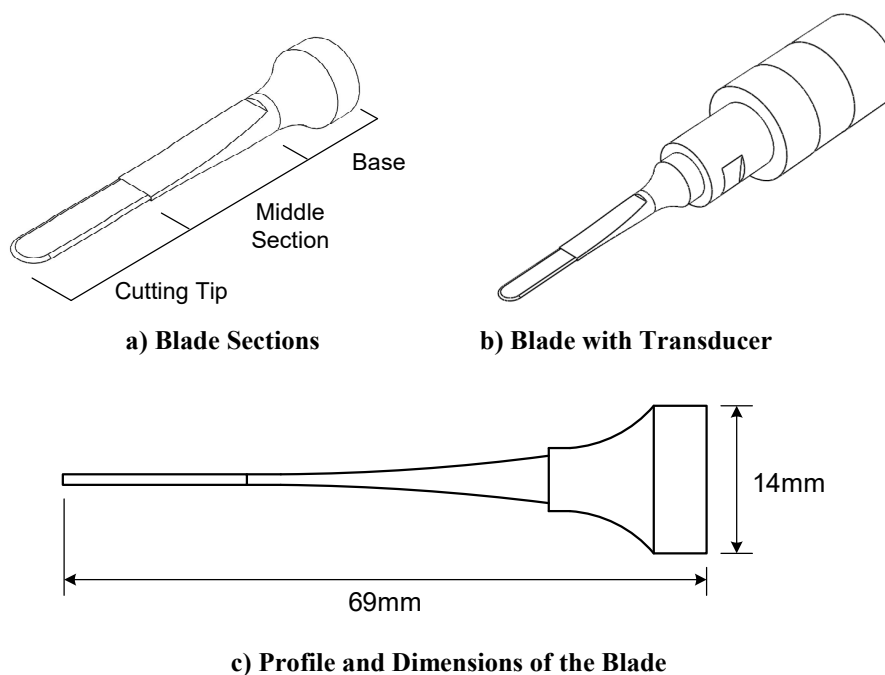


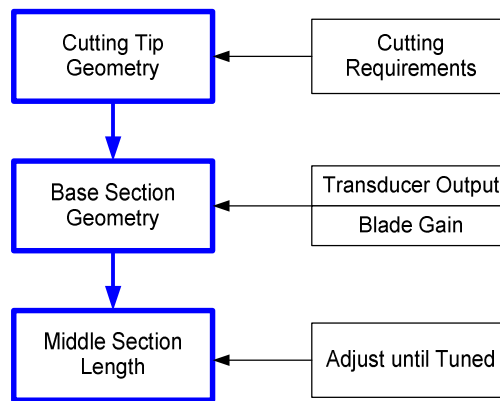
Figure 5.2 Shape of the Blade

Titanium alloy Ti90Al6V4 was used as the blade material. It is one of the most commonly used titanium alloys, which has a mechanical composition of 90% titanium, 6% aluminium and 4% vanadium. Its mechanical properties are shown in Table 5.1. This alloy has good corrosion resistance and excellent biocompatibility [248], enabling it to be safely used for surgical tools. In addition, its hardness and low density allows relatively light tools to be made with adequate strength. Another significant advantage of titanium alloy is its low internal mechanical losses under ultrasonic vibration [249, 250]. This means that ultrasonic tools can work more efficiently and are less likely to heat up. All these characteristics make titanium alloy an excellent material for ultrasonic cutting tools.

Property	Value	Property	Value
Density	$4.42 \times 10^3 \text{ kg/m}^3$	Izod Impact Strength	20 J/m
Young's Modulus	110 GPa	Thermal Conductivity	5.8 W/m·K (@ 23 °C )
Poisson's Rate	0.33	Tensile Strength	895 MPa
Fatigue Limit	448MPa ( $10^7$ Cycle)	Coefficient of Thermal Expansion	$8.0 \times 10^{-6} \text{ K}^{-1}$ (@20-100 °C )

**Table 5.1 Properties of Ti90Al6V4**

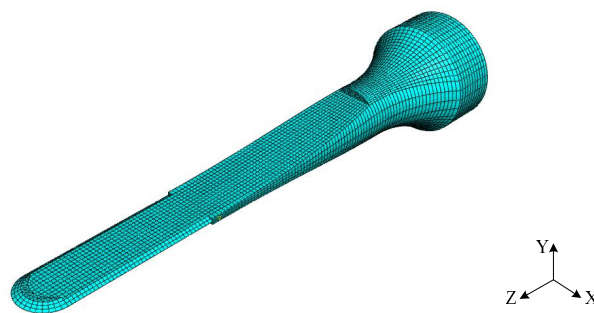
The final geometry of the blade was designed by taking into account the cutting requirements. As illustrated in Figure 5.3, the size of the cutting tip was decided according to the required depth of incision and the overall size of blade. For the base section, mechanical assembly and blade gain were the main concern. Sufficient space must be allowed in order to incorporate a threaded stud for transducer attachment. In addition, to achieve adequate blade gain and deliver sufficient displacement amplitude at the cutting tip, the diameter of the cylinder and the length of the cone were adjusted. Once the geometry of the base section and the cutting tip had been determined, the length of the middle section was adjusted to tune the blade at the correct frequency. These procedures were repeated to modify the profile of the blade until a satisfactory design was obtained.



**Figure 5.3 Design Procedure**

## (2) Modal Analysis

FEA was conducted during the design phase to characterise the modal frequencies and mode shapes of the blade. This was carried out using commercial software Abaqus version 6.11. As an essential part of the analysis, a finite element model was created for the blade. Generally, the accuracy of FEA is improved by refining the mesh. A meshing study was carried out to ensure all predicted modes and modal frequencies in the frequency range of interest were converged. This led to a model with around 20000 elements, as illustrated in Figure 5.4. This mesh also offered a good balance between analysis accuracy and computing time.










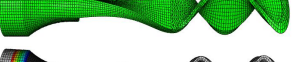




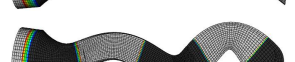

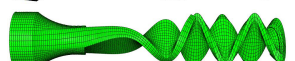
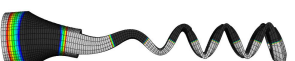
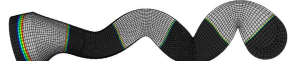
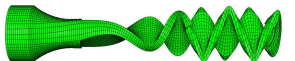


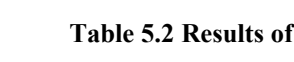
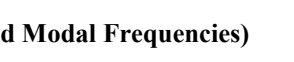


**Figure 5.4 Finite Element Model of the Blade**

The analysis characterised the blade by extracting the modal frequencies and mode shapes. The function of natural frequency extraction in Abaqus was applied to compute the vibration modes between 0.5-80 kHz. As only the blade was considered in FEA, free-free end condition was applied, which simplified the analysis by avoiding the need of additional boundary conditions. The first longitudinal mode, which is the working mode that is excited during ultrasonic cutting, was the main

concern in the analysis. In addition, those modes with close modal frequencies to the working mode were also given special attention.

Table 5.2 shows the mode shapes and modal frequencies obtained by FEA. Four types of modes were identified in the results. The modes were named using characters and numbers, where the characters indicate the type of mode: L for longitudinal, T for torsional, B<sub>Y</sub> for flexural bending in the thickness direction and B<sub>X</sub> for lateral bending in the width direction. The number indicates the order in which a mode appears in a specific type of vibration.

Mode	Mode Shape	$f / \text{kHz}$	Mode	Mode Shape	$f / \text{kHz}$
B <sub>Y</sub> 1		1.02	B <sub>Y</sub> 2		4.12
B <sub>X</sub> 1		5.81	T1		6.68
B <sub>Y</sub> 3		8.98	B <sub>Y</sub> 4		15.0
B <sub>X</sub> 2		16.3	T2		18.3
B <sub>Y</sub> 5		22.3	T3		27.8
B <sub>X</sub> 3		30.6	B <sub>Y</sub> 6		31.1
L1		34.9	T4		37.8
B <sub>Y</sub> 7		41.0	T5		47.6
B <sub>X</sub> 4		49.3	B <sub>Y</sub> 8		52.0
T6		58.8	B <sub>Y</sub> 9		63.9
B <sub>X</sub> 5		69.1	T7		70.2
L2		70.2	B <sub>Y</sub> 10		76.8

**Table 5.2 Results of FEA (Mode Shapes and Modal Frequencies)**

By investigating the shapes of the modes in Table 5.2, it is found that notably larger deformation appeared in the section of cutting tip where the blade was significantly thinner. L1 mode, the working mode, was predicted at 34.9kHz, which was within an

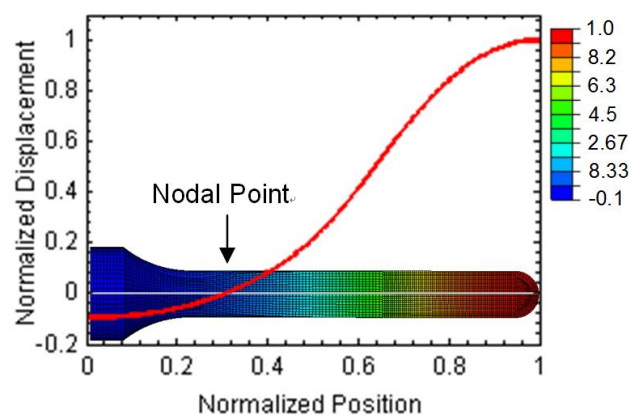


acceptable range of the tuning requirements. In addition to the longitudinal vibration, bending and torsional modes were identified. The frequency differences between these modes and the L1 mode were no less than 3.1kHz. According to the experience of previous studies, it is considered that the working mode was appropriately frequency-separated from other undesired modes.

It is noteworthy that the results shown in Table 5.2 are for the blade only. The effects of the attached transducer were not included in the analysis. However, as the blade and the transducer are in fact working together as an assembly in ultrasonic cutting, the actual vibration characteristics of the system are determined by both the blade and the transducer. In this design stage, the analysis was simplified by considering the blade only and ignoring the transducer involved modes in FEA.

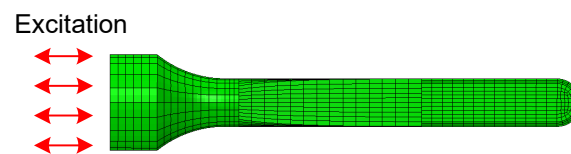
### (3) Displacement and Stress Analysis

To study the behaviour of the blade subjected to ultrasonic excitation, the deformed displacement and the material stress of the L1 mode was investigated. Figure 5.5 plots the amplitude of the deformed longitudinal displacement along the blade central line, which was obtained from the FE modal analysis. This normalised displacement distribution shows how the blade deforms in the working mode. The maximum displacement is observed on the tip of the blade and one nodal point was found at the illustrated position. By dividing the displacement at position 1 (blade tip) to that at position 0 (blade base), the gain of the blade was obtained to be 11, a sufficiently large value that would enable adequate amplitude to be achieved on the cutting edge.



**Figure 5.5 Amplitude of Longitudinal Displacement**

The material stress was another major concern in the blade design. When subjected to ultrasonic excitation, the internal stress caused by the high frequency vibration is significantly larger than that introduced by the external applied force. In view of this, the applied force was ignored in the stress analysis. As illustrated in Figure 5.6, a blade under excitation was simulated by introducing a periodic displacement at the base of the blade model, which resulted in forced vibration at the working frequency. Taking into account the fact that the vibration outputted by an ultrasonic transducer is typically 5-10 $\mu$ m (amplitude) in cutting applications, an excitation of 10 $\mu$ m, which is the largest value expected, was applied in the analysis to simulate the vibration input of the blade.

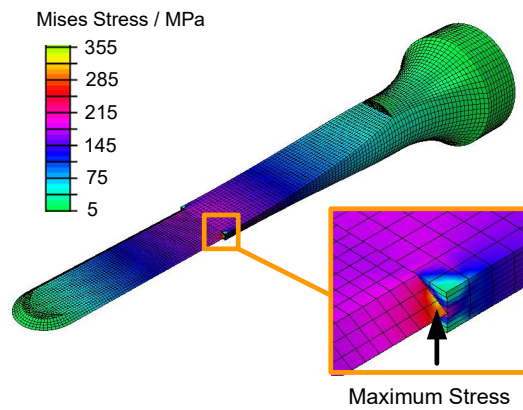


**Figure 5.6 Model for Stress Analysis**

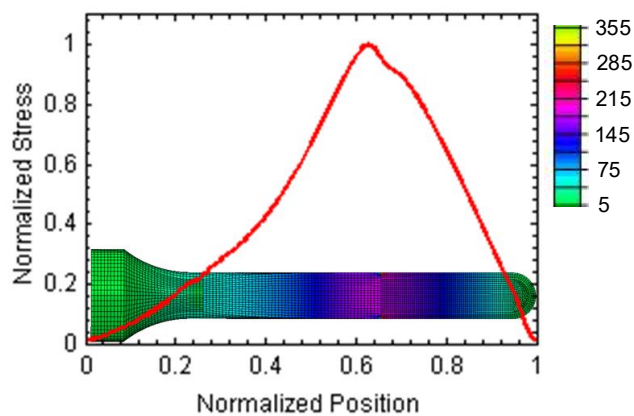
The Mises stress was used to evaluate the strength of the blade. This is an equivalent tensile stress derived from the Von Mises yielding criterion. The Von Mises criterion is a widely used method for estimating the yielding of isotropic ductile material, such as metal, subjected to loading conditions. According to this theory, failure occurs when the distortion energy in the material exceeds a certain value [225]. This means that in order to prevent blade failure, the associate Mises stress should stay below the material tensile strength.

Figure 5.7 shows the Mises stress obtained by FEA. To better illustrate the stress distribution, Figure 5.8 plots the normalised stress distribution along the blade centre line. The results suggest that high stress presents around the region which connects the cutting tip and the middle section. As a consequence this area was considered to be a weak part of the blade. The maximum stress was found on the cutting edge with a value of 352MPa, lower than the material tensile strength (895MPa, Table 5.1). This implies that the blade may have adequate strength according to the Von Mises criterion. However, in view of the high frequency periodic deformation experienced in the blade, there is a potential risk of metal fatigue failure. Therefore, fatigue limit, which is the highest stress a material can withstand for a given number of cycles

without failure, is used instead of tensile strength to evaluate the blade strength. Usually, fatigue limit is applied in low frequency working condition. However, taking into account the fact that ultrasonic fatigue testing, which applies ultrasonic vibration to reduce test time in the experiment, is also a means of obtaining fatigue limit [251, 252], the application of fatigue limit in ultrasonic vibration was considered to be acceptable in this study. Therefore an improved criterion was applied to evaluate the strength of ultrasonic blades, which uses the fatigue limit of  $10^7$  cycles as the material strength limit. In this case, Blade I has a safety factor of 1.3 under this criterion. As the stress analysis was carried out under an input of the largest expected value, the blade was considered to be safe in strength but would be safer used under a lower excitation level.



**Figure 5.7 Mises Stress in Blade**



**Figure 5.8 Normalised Stress Distribution, Mises Stress**

### 5.2.1.2 Tests and Experiments

Based on the design and the preceding analysis, Blade I was manufactured, as shown in Figure 5.9. It was fabricated from a block of titanium alloy using a CNC machine. Due to the hardness of the material, a slow machine speed and extra cooling was applied to avoid the presence of high machining temperature which could alter the material property and result in changes of dynamic characteristics of the blade. To study the actual performance of the blade, Blade I was subjected to three tests: impedance analysis, experimental modal analysis and ultrasonic cutting tests.



**Figure 5.9 Manufactured Blade**

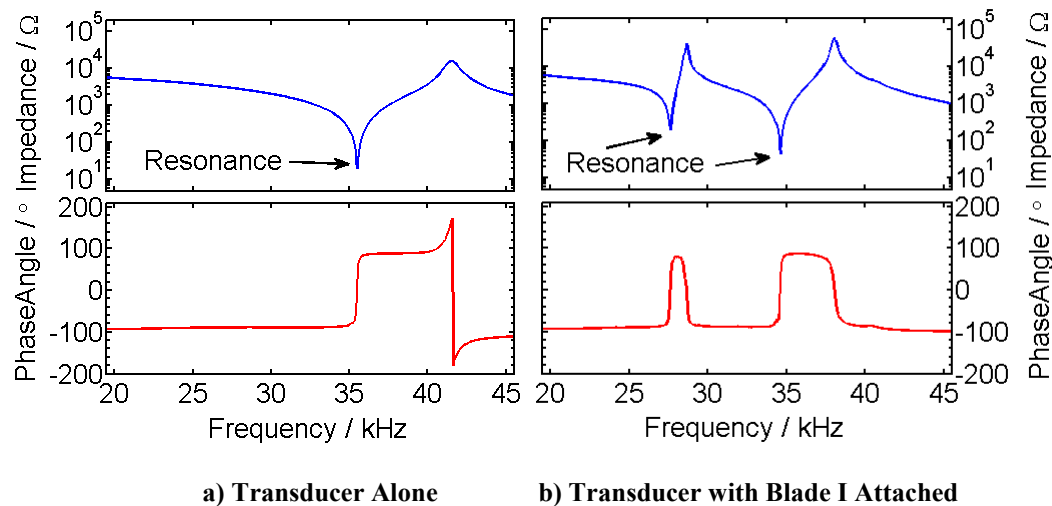
#### **(1) Impedance Analysis**

An ultrasonic blade relies on the output of a piezoelectric transducer, which converts sinusoidal electrical excitation into mechanical vibration, to perform ultrasonic cutting. To do this efficiently, the transducer is driven at its resonant frequency (where the lowest impedance presents) by an ultrasonic generator. This frequency, on the other hand, can be shifted according to the load of the transducer. For the case where an ultrasonic blade is attached, the resonant frequency of the transducer becomes very close to the tuned frequency of the blade. Therefore it is possible to verify whether an ultrasonic blade is tuned properly by measuring the resonance of the transducer. This can be done through impedance analysis that measures the electrical impedance of a piezoelectric transducer which is attached to the ultrasonic blade.

In the test, Blade I was attached to an ultrasonic transducer connecting to an impedance analyser (Agilent 4294A) which is capable of performing precise impedance analysis in a broad frequency range (40Hz-110MHz). The analyser drove the transducer with a small test signal (50mV amplitude) and calculated the

impedance through the applied voltage and the consumed current. An impedance curve was obtained by sweeping the test signal from 20kHz to 45kHz with a step of 50Hz. For comparison, an additional test was performed for the same transducer without Blade I attached.

Figure 5.10(a) plots the impedance obtained from the transducer alone (without Blade I), showing a resonance at 35.2kHz where the lowest impedance and a zero phase angle exhibited. It implies that the transducer is a pure resistance at this frequency. Figure 5.10(b) illustrates the case where the blade is attached. An additional resonance presents at 27.5kHz as a result of the involvement of the blade in the dynamic system. This resonance was not studied as the ultrasonic generator is not expected to drive around its frequency. Instead, attention was placed at the main resonance around the working frequency. It shows that the blade is tuned at 34.5kHz, 0.5kHz away from the expected excitation frequency (35kHz). This is acceptable as the ultrasonic generator allows a frequency tolerance of  $\pm 1$ kHz. Therefore the impedance analysis concluded that Blade I was properly tuned and ready for further tests.

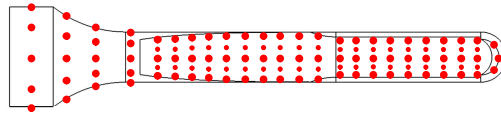


**Figure 5.10 Result of Impedance Analysis**

## (2) Experiment Modal Analysis

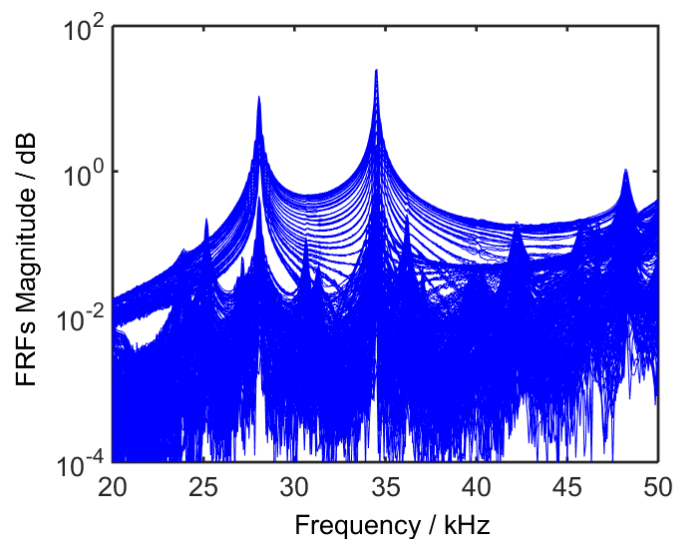
Experimental modal analysis (EMA) was conducted to further characterise the dynamic behaviour of Blade I. The experimental setup was the same as detailed in Section 2.4.1. A total of 130 points were measured on the blade, as shown in Figure 5.11, which resulted in 390 FRFs. These FRFs contained the necessary information

for the reconstruction of the shape of vibration modes and extraction of the associated modal parameters.



**Figure 5.11 Measure Points on Blade**

Figure 5.12 plots the overlaid magnitude of all FRFs obtained in the EMA test. According to the theory of experimental modal analysis [254], the peaks of the curves are the modal responses. Comparing Figure 5.10 with Figure 5.12 shows that, due to the increased number of measurement and higher frequency resolution (1Hz in EMA), more information on the blade responses can be obtained in EMA. The modal frequencies and mode shapes were extracted from the FRFs using a commercial software, ME'Scope. Table 5.3 shows the obtained modal frequencies and the associated mode shapes. For comparison, the relevant results computed by FEA are also presented in the same table, where the predicted modal frequencies are the FEA results obtained independently of EMA and the adjusted values are calculated by an FE model improved according to the EMA results. For each mode, the difference of modal frequency was calculated by comparing the FEA result to the EMA result.



**Figure 5.12 Overlay of FRFs**

As shown in Table 5.3, seven modes were found in the 20-45kHz frequency range by EMA. The working mode L1 was observed at 34.5kHz, the same frequency as the

resonance found by impedance analysis. Although the EMA aimed to investigate the modes of the ultrasonic blade, as the transducer was also involved in the vibration, the EMA results were in fact the modes of the blade-transducer system. Therefore, it is expected that there is some degree of discrepancy between the results of EMA and FEA which considered only the blade in the analysis.

Mode	Mode Shape (EMA/FEA)	Frequency / kHz		Difference (FEA vs EMA)*
		Predicted	Adjusted	
B <sub>γ</sub> 5		EMA: 21.2		P: 1.1kHz (5.2%) A: 0.7kHz (3.3%)
		22.3	21.9	
T3		EMA: 27.1		P: 0.7kHz (2.6%) A: 0.4kHz (1.5%)
		27.8	27.5	
B <sub>γ</sub> 6		EMA: 30.6		P: 0.5kHz (1.6%) A: 0.1kHz (0.33%)
		31.1	30.7	
L1		EMA: 34.5		P: 0.4kHz (1.2%) A: Adjusted Value
		34.9	34.5	
T4		EMA: 37.1		P: 0.7kHz (1.9%) A: 0.3kHz (0.8%)
		37.8	37.4	
B <sub>γ</sub> 7		EMA: 42.2		P: 1.2kHz (2.8%) A: 1.6kHz (3.8%)
		41.0	40.6	

**Table 5.3 Results of EMA and Comparison with FEA**

Overall, the FEA results were in good agreement with EMA. For all modes, the average difference of modal frequencies between the predicted FEA and EMA was 2.2%. The working mode L1 was predicted with a difference of 1.2% (0.4kHz). As the ultrasonic generator, which provides high power periodic driving current for vibration excitation, can accommodate a frequency shift of  $\pm 1.0$ kHz around the nominate excitation frequency (35.0kHz), it is considered that the difference between

FEA and EMA was acceptable. The actual tuned frequency of the blade (34.5kHz) is within the frequency tolerance ( $35.0 \pm 1.0$ kHz), suggesting that the blade can be excited for cutting properly. A higher difference, 5.2% was seen for B<sub>γ</sub>5 mode, which may be partly ascribed to the ignorance of transducer in the analysis. Also, the difference between the analysis and experimental results could be caused by other factors such as alteration of material properties and imperfection of manufacturing. By adjusting the FE model using the EMA data (mainly adjusting the Young's Modulus of the material), the FEA results were improved, where the average difference of modal frequencies reduced to 1.6%. Nevertheless, not all the modes predicted in Table 5.2 were found in this test. As the blade was excited by the transducer longitudinally at low power level, the responses of some modes could be buried in signal noise, preventing the modes from being extracted in EMA.

In conclusion, the EMA revealed the modal behaviour of Blade I and provided information for FEA improvement. Taking into account the fact that good agreement was obtained between the FEA, especially the adjusted FEA, and EMA, Blade I was considered to be properly designed and manufactured with the expected dynamic characteristics.

### **(3) Ultrasonic Cutting Tests**

To test the cutting performance of Blade I, ultrasonic cutting was carried out using the fabricated blade. The tests were conducted on two kinds of material: a biomechanical test sample and ovine femur.

#### **Cutting of Biomechanical Test Sample**

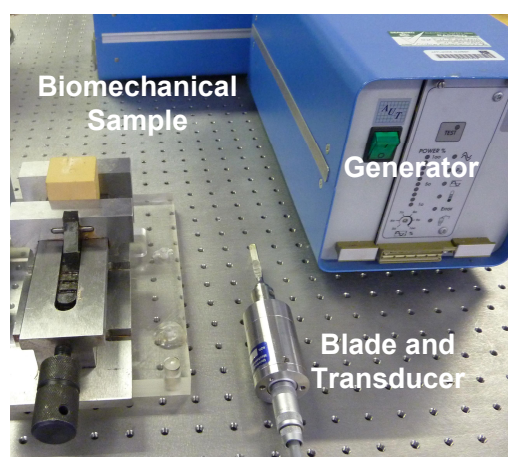
In this test, a biomechanical test sample made of polyurethane foam was cut. This material was a commercial product of Sawbones<sup>®</sup> Pacific Research Laboratories, Inc. It is often used as an alternative test medium for human cortical bones due to its consistency and similarity in mechanical properties. Table 5.4 shows the main material properties of the biomechanical material, and selected properties of bones from ovine, rat and human. It should be noted that as bones are complex anisotropic material, the value of the listed properties may differ from case to case depending on the testing model and conditions of the tissue [256-259].



Properties	Material			
	Biomechanical Material [255] (Solid Rigid Foam)	Ovine Femur (Cortical Bone)	Rat Bone	Human Bone [256] (Cortical Bone)
Density (g/cm <sup>3</sup> )	0.64	2.15-2.26 (Tissue Density [257])	1.36 - 2.44 (Tissue Density [258])	1.9 (Typical Tissue Density)
Compressive Strength (MPa)	31	-	139.50 ± 19.14 [258]	133-295
Compressive Modulus (MPa)	759	-	-	-
Tensile Strength (MPa)	19	13-147 (Ultimate [259])	-	92-188 (Ultimate)
Tensile Modulus (MPa)	1000	-	-	-
Ultimate Tensile Load (N)	-	-	30±15 [259]	-

**Table 5.4 Material Properties of Biomechanical Material and Bones**

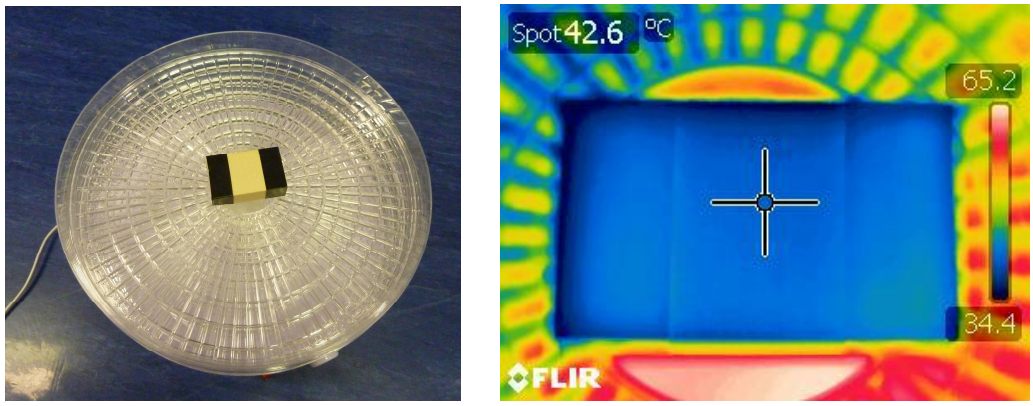
Figure 5.13 illustrates the test sample and the devices used in the experiment, including a transducer and a high power ultrasonic generator that drives the transducer. Blade I was screwed on the transducer and excited to produce vibration of around 55µm amplitude at the blade tip. This enabled the delivery of sufficient power for cutting while keeping the material stress in a safe level. The ultrasonic cutting was operated by holding the transducer by hand, performing incisions using both the sharp blade tip and the sharp cutting edge.



**Figure 5.13 Ultrasonic Devices and Cutting Sample**

A thermal camera was used to measure the temperature on the sample during the cutting process. To conduct calibrated measurements, the emissivity of the

biomechanical material was determined. This is a parameter ranging from 0 to 1, which indicates the ability of a material surface to emit energy through radiation. It was obtained by comparing the biomechanical sample to a black electrical tape with known emissivity of 0.99. As illustrated in Figure 5.14(a), the tape was attached to a sample block and heated evenly to a stable temperature (around 50 °C as recommended). The emissivity of the sample was obtained to be 0.98 by comparing the thermal reading between the tape and the sample surface, as shown in Figure 5.14(b).

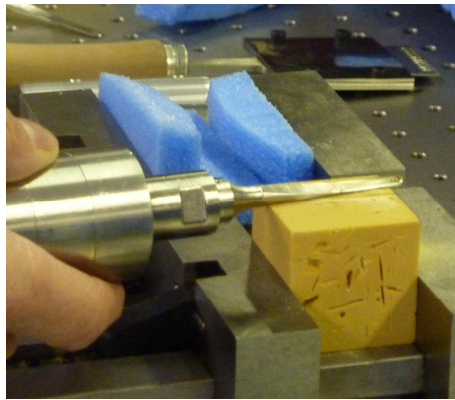


a) Heater and Calibration Sample

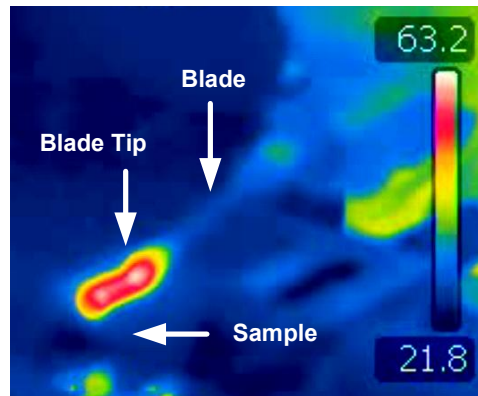
b) Thermal Image

**Figure 5.14 Calibration of Material Emissivity**

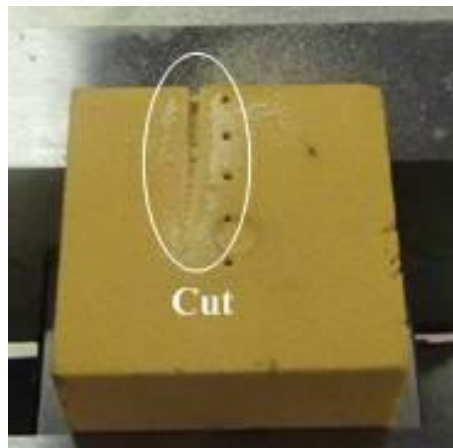
Figure 5.15(a) illustrates the cutting test and Figure 5.15(b) shows a thermal picture taken during the test. The measurement provided an insight into the temperature on the sample, although the cutting site inside the sample could not be observed directly. As shown in Figure 5.15(b), generation of heat was observed around the blade tip. A temperature of over 60 °C was measured around this area most of the time during cutting. The maximum temperature reached as high as 108 °C, which would be unacceptable in bone cutting. The sample was inspected after cutting, showing an incision with no signs of burning, as illustrated in Figure 5.15(c). Benefiting from the ultrasonic vibration, a smooth cut was achieved with low cutting force.



a) Cutting of Biomechanical Material



b) Measurement of Surface Temperature



b) Cut on Sample

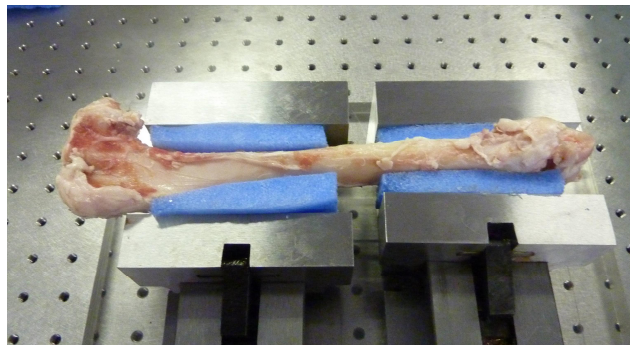
**Figure 5.15 Cutting Test, Biomechanical Material**

### **Cutting of Ovine Femur**

An ovine femur was cut in the second test. As shown in Figure 5.16, the bone measures around 15cm in length and 5cm in width in the femur body. The bone was preserved in freezing conditions and was defrosted before cutting. To compare different cutting techniques, ultrasonic cutting was first carried out manually and then performed using a test rig. In both tests, the blade was excited using the same power configuration as that in the cutting of the biomechanical sample.

In the first test, the bone was cut in a natural way by holding the transducer and cutting smoothly by hand. Using this technique, mainly the sharp cutting edge was involved in the cutting. The ultrasonic cutting was performed with an applied force and a gentle slicing motion that removed away the cutting debris. The blade was kept contacting with the bone until an incision of around 3mm deep was achieved. No extra cooling approach was applied for the cutting. As it may take over 20 seconds to

make an incision on the bone, the heat generated in the cutting could be sufficient to cause burning of the bone. This was confirmed by investigating the bone after cutting. Figure 5.17(a) shows the cuts made on the bone. The notable signs of bone burning around the incisions suggested the presence of high temperature in the cutting. In spite of this, Blade I worked stably in the cutting test. The blade was capable of achieving incisions deeper than 5mm on the bone, which means the ovine femur could be truncated using this blade.



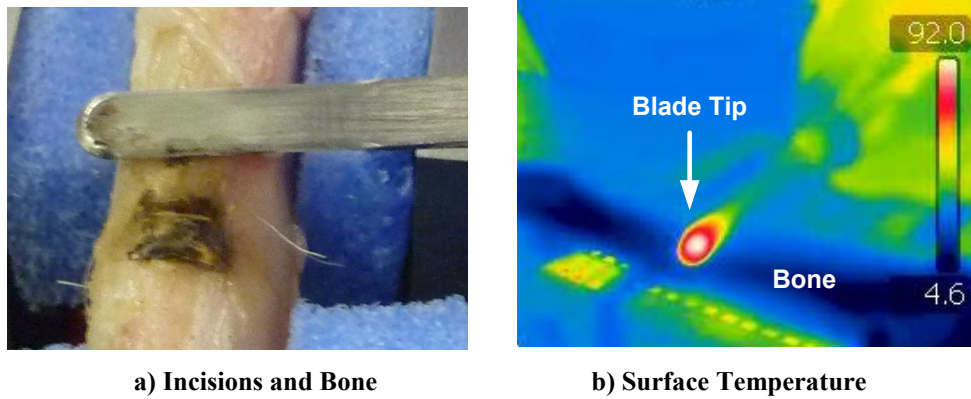
**Figure 5.16 Sheep Femur**

More information on the cutting temperature was revealed by the thermal pictures taken during cutting. It can be seen from Figure 5.17(b) that heat accumulated at the cutting site and the surface temperatures reached over 90 °C. The heat continued to build up as the ultrasonic cutting was carried on, causing the bone exposing to elevated temperatures for a long period of time, which would be undesired in bone cutting surgery as it can cause irreparable thermal damage or necrosis [11, 72, 260, 261]. It is therefore necessary to applying appropriate cooling for this blade in surgical applications. It is also noted that the way of performing the cut substantially accounts for the occurrence of excessive cutting temperature. The temperature was found to decrease as cutting was slowed down or a lower force was applied. Such actions could reduce friction and allow more time for heat dissipation.

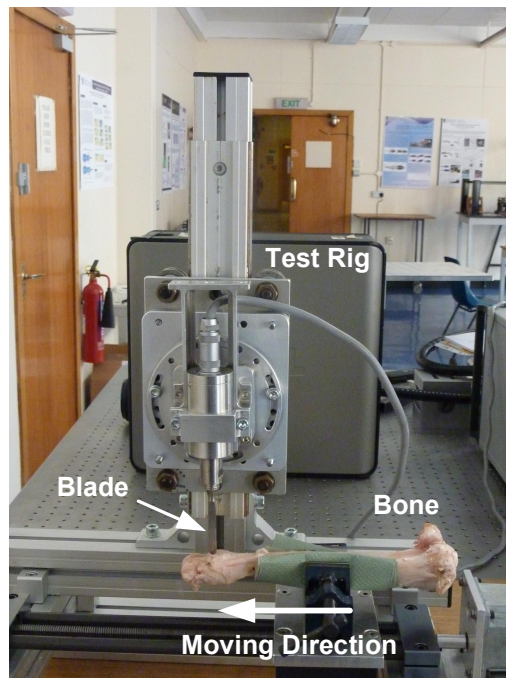
The experiment was also conducted on a test rig to study the ultrasonic cutting under a slicing motion of constant speed. Figure 5.18 illustrates the test rig, where the blade was attached on a transducer fixed vertically. The bone to be cut was clamped firmly on a holder driven by a motor. When the test began, it was moved towards the ultrasonically excited blade, causing an incision be made on the surface. In this case, the cutting was performed by the blade tip under a slicing motion perpendicular to the longitudinal excitation. To make sure the cutting force was within an acceptable limit,



the moving speed of bone was set at 0.2m/s and the cutting depth was restricted to 2mm by carefully adjusting the vertical position of the blade.



**Figure 5.17 Ultrasonic Bone Cutting, Manually Performed**



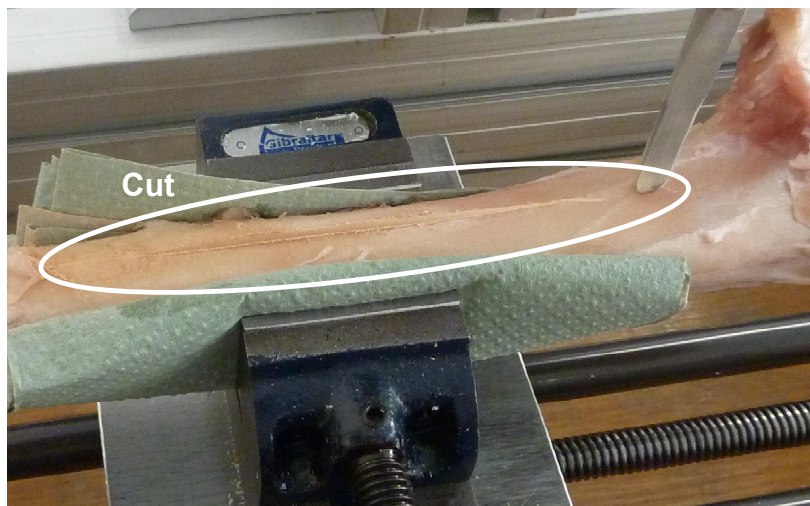
**Figure 5.18 Test Rig and Bone Sample**

The thermal image illustrates that the temperature around the blade tip reached over 100°C during cutting, as shown in Figure 5.19(a). However this area quickly cooled down to well below 50°C as the blade moved away from the cutting site. The femur was examined after cutting. As shown in Figure 5.19(b), the cut can be clearly seen and there was no accumulating debris around the incision. Some slight discolouration rather than signs of burning were noted, suggesting that heat damage was more limited in this case. By comparing the thermal images of this test to those of the manual cutting test, it is showed that the slicing motion avoided heat accumulation as

the cutting site was moving on the bone. Thereby the bone was allowed to cool down before burning occurs.



a) Surface Temperature



b) Cut on Sample

**Figure 5.19 Ultrasonic Bone Cutting, Test Rig**

As a conclusion, the ultrasonic cutting tests showed that Blade I was designed with the required cutting performance. The blade worked stably under high power ultrasonic excitation and performed ultrasonic cutting on the biomechanical test sample and ovine femur. Incisions can be achieved either using the sharp cutting edge or the sharp cutting tip. This confirmed that the blade was properly tuned and had adequate strength to withstand the stress in cutting, as predicted in the modal analysis and stress analysis. By taking into account the results of the impedance analysis, EMA and cutting tests, it is showed that using the conventional design process, a proper design of ultrasonic blade can be obtained by analysing the modal behaviour and stress of the blade.

Although the heat generation of ultrasonic cutting was not considered in the blade design, the cutting temperature was investigated in the ultrasonic cutting tests, which showed that the temperature in the material was affected by how the cutting was performed. The manual cutting test of ovine femur illustrated that the accumulated heat at the cutting site could lead to high temperature and bone burning. However, by introducing slicing motion in the cutting carried out on the test rig, bone burning was avoided as the cutting site was allowed to cool down. Nevertheless, taking into account the occurrence of high cutting temperature and the potential danger of heat damage, Blade I was considered not suitable for surgical applications without the application of cooling.

### 5.2.2 Blade II: Blade with Serrated Cutting Edge

Section 5.2.1 showed that Blade I was properly designed and performed ultrasonic cutting effectively. However, there was a need to further improve the cutting performance by altering the shape of the cutting edge. As a feasible solution, serrated cutting profile have been widely used in orthopaedic cutting [23, 24, 39]. Figure 5.20 illustrates a simplified version of the interaction between the serrations and the material during ultrasonic cutting. When ultrasonic vibration is applied, all serrations move at small amplitude but high velocity, causing large impact on their tips when they contact with the workpiece. This enhances cutting by increasing friction and facilitating debris removal.

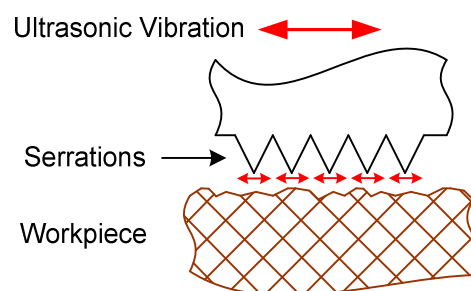


Figure 5.20 Serrated Cutting Edge

### 5.2.2.1 Blade Design and Analysis

#### (1) Geometry and Shape

Blade II was designed with serrated cutting edges by following the same design process as Blade I. The main dimensions of the blade and the shape of the serrations are shown in Figure 5.21. The new blade resembled Blade I in terms of profile but was fabricated with a larger width in order to incorporate the serrations on both sides. With a cutting edge measuring up to 20mm in length, the blade was designed mainly to perform lateral cutting using the serrated edges.

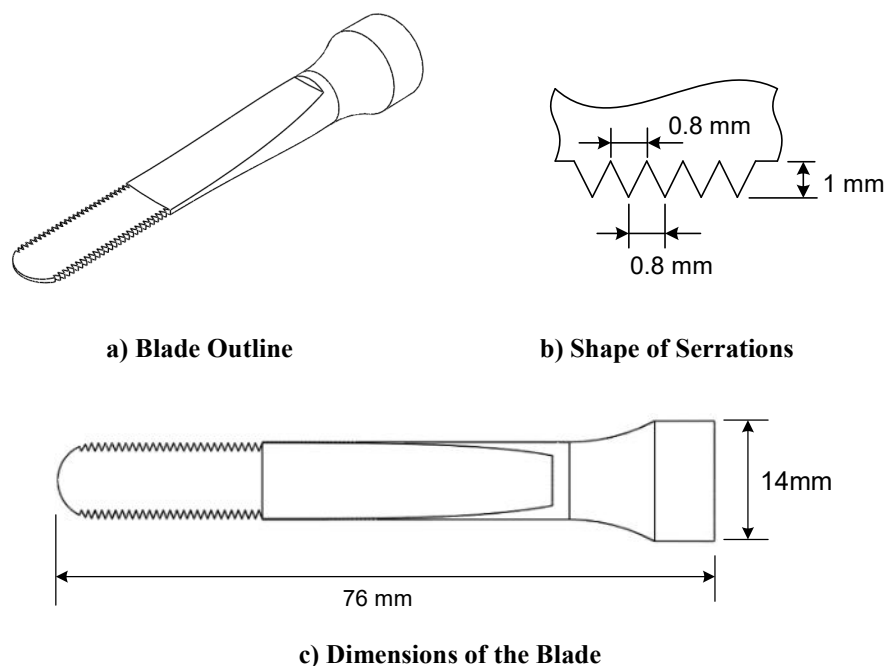


Figure 5.21 Blade II with Serrated Cutting Edges

#### (2) Modal Analysis

Modal analysis was conducted to study the blade modes between 0.5-50kHz using the same method as that in Blade I. Similarly, bending, torsional and longitudinal modes were found and were named using the same way as detailed in Section 5.2.1.1, as illustrated in Table 5.5 (modes with modal frequencies lower than 10kHz are not listed in the table). The non-working modes were well separated from the working mode L1 with a frequency separation of 3.4kHz. In addition, apart from the bending modes identified previously, more complex bending mode shapes were observed above 40kHz. They were named  $B_{Cn}$ , where  $n$  is a number indicating the appearance order of the mode. As bending occurs along both thickness and width direction, which



causes more complex distortion of material, these modes were identified as the combinations of lateral (bending along the width direction) and flexural (bending along the thickness direction) bending modes. Nevertheless, as they were far from the tuned frequency, these modes were considered having little influence on the working mode.

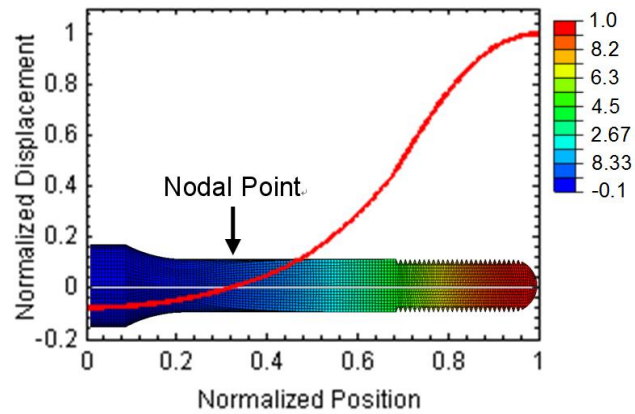
Mode	Modal Shape	$f$ / kHz	Mode	Modal Shape	$f$ / kHz
T2		10.7	By5		11.6
T3		16.9	By6		17.1
Bx3		17.8	By7		23.7
T4		24.4	T5		30.8
By8		30.9	Bx4		31.5
L1		35.0	T6		38.4
By9		38.9	*Bc1		41.9
*Bc2		45.5	T7		46.3
*Bc3		48.7	Bx5		49.2

\*Complex bending mode.

**Table 5.5 Results of FEA (Mode Shapes and Modal Frequencies)**

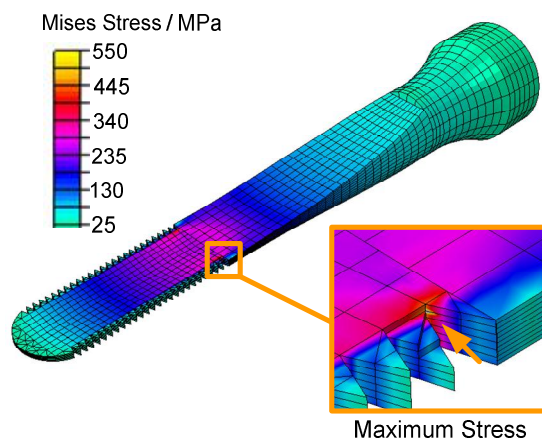
### (3) Displacement and Stress Analysis

Based on the modal analysis, the normalised deformed displacement of the L1 mode and the stress distribution under excitation was computed. Figure 5.22 plots the deformed displacement along the central line of the blade. For Blade II, the gain was obtained to be 12.

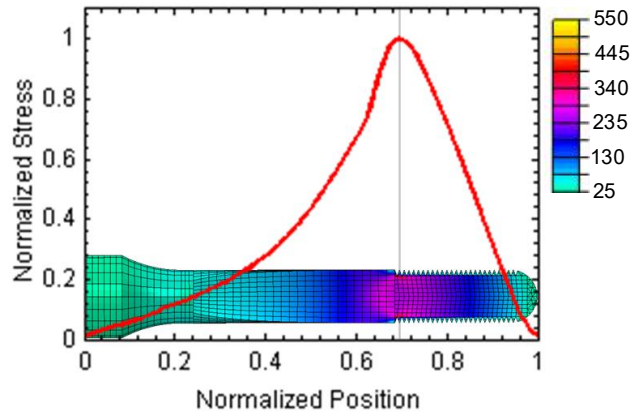


**Figure 5.22 Normalised Displacement**

Using the same analysis technique as that in the design of Blade I, the strength of Blade II was evaluated by applying a  $10\mu\text{m}$  (amplitude) periodic displacement at the blade base. The resultant Mises stress was computed and illustrated in Figure 5.23. Its normalised stress distribution along the blade central line is shown in Figure 5.24. One peak was identified in the stress curve. Detailed investigation showed that the maximum Mises stress was as high as 514MPa, locating at the first serration next to the middle section. Though the maximum stress was lower than the material tensile limit (Table 5.1, 895MPa), it exceeded the fatigue strength (Table 5.1, 448MPa). According to the criterion introduced in Section 5.2.1.1, this suggested that the blade could be at risk of material fatigue. It may not have adequate strength to withstand the stress under high power ultrasonic excitation.



**Figure 5.23 Stress in Blade II**



**Figure 5.24 Normalised Stress Distribution**

### 5.2.2.2 Tests and Experiments

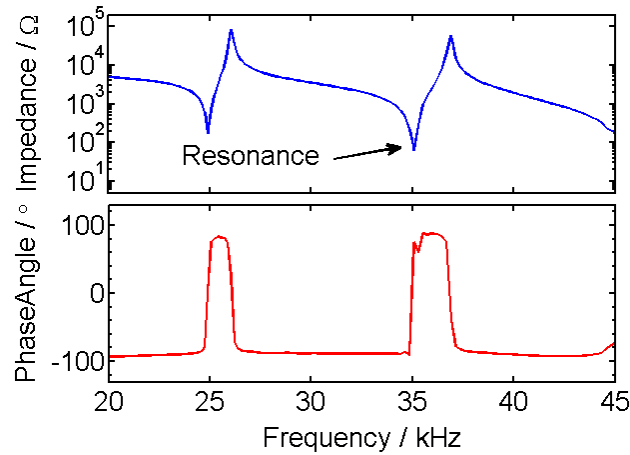
Although the serrated blade was considered to be an unsafe design, it was manufactured to verify the preceding analysis experimentally. The fabricated blade is shown in Figure 5.25. Similarly, impedance analysis and EMA were conducted to test the blade using the same experimental setup as Blade I.



**Figure 5.25 Manufactured Blade**

#### (1) Impedance Analysis

Figure 5.26 illustrates the result of the impedance analysis. Similar to the case of Blade I, two resonances were observed in the impedance curve. The main resonance associated with the working mode was found at 35.1kHz.



**Figure 5.26 Result of Impedance Analysis**

## **(2) Experiment Modal Analysis**

EMA was carried out to characterise the modal behaviour of Blade II. A total of 130 points were measured on the blade, generating 390 FRFs. Figure 5.27 plots the overlaid FRFs, which shows a least 7 peaks in these curves. Further investigation extracted 5 clear modes from these FRFs. Table 5.6 illustrates the comparison of the EMA and FEA results, where the latter were the predicted results obtained using an FE model that was not adjusted according to EMA. Overall, the average frequency difference between FEA and EMA was 3.6%, which was slightly higher than the case of Blade I but was still satisfactory. The working mode L1 was predicted precisely with a difference of 0.1kHz(0.28%). For other modes, the differences were slightly larger. Mode B<sub>Y</sub>7 was predicted with the largest frequency difference, 1.3kHz(5.2%). Mode T4, B<sub>X</sub>4 and B<sub>Y</sub>9 were predicted with differences of 1.1kHz(4.3%), 1.4kHz(4.7%) and 1.5kHz(3.7%), respectively. The increased difference in this case may be partly ascribed to by the introduction of serrations, which resulted in higher complexity of blade geometry. Thereby it can be more difficult to predict high order vibration modes accurately. Nevertheless, as the working mode was precisely predicted and the average difference was satisfactory, it is considered that the FEA results were in good agreement with EMA and Blade II was properly manufactured.

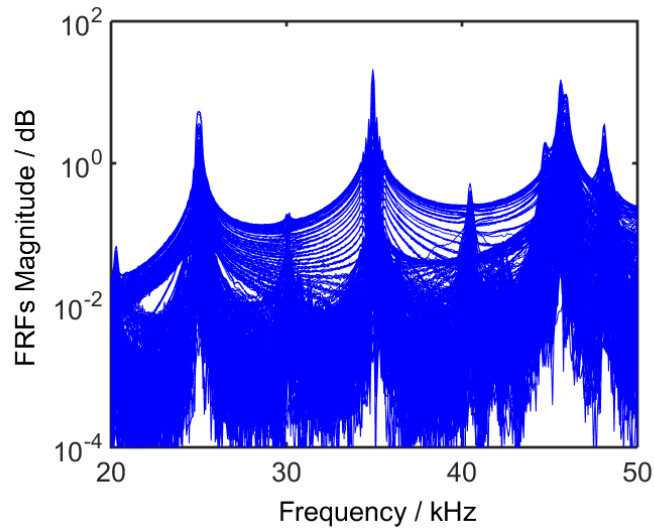


Figure 5.27 Overlay of Transfer Functions, Magnitude

Mode	Mode Shape (EMA/FEA)	Frequency kHz	Difference (FEA vs EMA)
B <sub>Y</sub> 7		EMA: 25.0	1.3kHz (5.2%)
		FEA: 23.7	
T4		EMA: 25.5	1.1kHz (4.3%)
		FEA: 24.4	
B <sub>X</sub> 4		EMA: 30.1	1.4kHz (4.7%)
		FEA: 31.5	
L1		EMA: 35.1	0.1kHz (0.28%)
		FEA: 35.0	
B <sub>Y</sub> 9		EMA: 40.4	1.5kHz (3.7%)
		FEA: 38.9	

Table 5.6 Results of EMA and Comparison with FEA

### (3) Blade Failure

As discussed in the stress analysis, it was concluded that Blade II was designed with inadequate strength to withstand the stress in ultrasonic cutting. However, this

problem could not be revealed by impedance analysis or EMA where the blade was excited using significantly lower power than normal cutting applications in order to reduce the influence of non-linear effects and avoid material heating up. The material stress in such conditions was well below the safe limit.

However, when the blade was used in ultrasonic cutting, where the excitation can be 10 times larger than that in EMA, the stress reached a significantly higher level. As expected, a crack was observed when the blade was subjected to excitation for a short period of time. It propagated quickly under ultrasonic vibration and led to the entire cutting tip breaking off, as illustrated in Figure 5.28. Careful inspection of the blade condition revealed a clear broken edge, suggesting the occurrence of metal fatigue failure [262, 263]. The initial crack occurred very close to where the maximum stress was predicted in Figure 5.23. This test confirmed that the FEA was correct and the applied stress criterion was effective. An ultrasonic blade designed with insufficient strength could be vulnerable to fatigue failure as a result of the high frequency periodic deformation. The study suggested that to make sure an ultrasonic blade works safely during cutting, the maximum stress should be kept below the fatigue limit.



**Figure 5.28 Broken Blade**

### **5.2.3 Summary**

The design and test of two ultrasonic blades were presented in Section 5.2. Blade I and Blade II were designed with sharp and serrated cutting edges respectively. They were both designed using the conventional method introduced in Section 1.5.4. EMA verified FEA was applied in the study to make sure the blades were designed with the expected vibration characteristics.

Modal behaviour was a major concern in the design. Both blades were expected to be tuned at the correct frequency with adequate frequency separation from non-working modes. This was achieved by analysing the modal parameters and adjusting the blade geometry in the design process. It was confirmed by experiments that both blades were tuned correctly and exhibited satisfactory modal behaviour. Good agreement between FEA and EMA suggested that the blades were properly fabricated.

Material stress was also taken into account in the design. To avoid material failure under ultrasonic vibration, von Mises stress was computed and fatigue strength was applied as a safety criterion. Comparison of the case of Blade I and Blade II highlighted the failure by material fatigue and demonstrated the application of the criterion. The maximum stress in both blades was within the material yield strength. However, it was below the fatigue strength limit in Blade I whereas above the limit in Blade II. As a result, Blade I worked properly in ultrasonic cutting tests while Blade II failed as predicted. This suggested that instead of using the tensile strength as the material limit, a more conservative criterion taking into account the fatigue strength should be applied to evaluate the safety of ultrasonic blades.

Blade I performed ultrasonic cutting on biomechanical material and ovine femur. The blade worked stably and incisions were made effectively in the tests, confirming that the blade was properly designed with the required cutting performance. Temperature of the biomechanical sample around the cutting site was measured by a thermal camera, showing high temperature during the cutting process. When cutting the ovine femur manually, the heat accumulated during ultrasonic cutting caused notable burning of the bone. This should be prevented in surgical applications as it could cause necrosis or other injury in bone. However, in the cutting carried out on the test rig, bone burning was avoided as the heat accumulation was significantly reduced by the slicing motion. As a conclusion, the blade was considered not suitable to be used in surgical applications without the application of cooling.

It is demonstrated in the design of both blades that on the basis of the FEA and experimental verification, ultrasonic blades with satisfactory performance can be obtained by following the conventional design process. However, the design process can not guarantee that the resultant blades are the best optimised. Other better

solutions may exist but are not examined in the design. It is expected that the optimal design method proposed in this study offers a way to overcome this drawback.

### **5.3 Blade Designed Using Optimal Method**

In this section, an ultrasonic blade will be designed using the optimal method detailed in Chapter 4, which applies mathematical algorithms to update the blade design and find the most desired design. This will be done on the basis of the proposed blade performance indicators, which enable the algorithm to measure and compare the performance of a design during the design process. This section will also investigate the influence of the shape of the cutting edges on ultrasonic cutting based on the obtained blades.

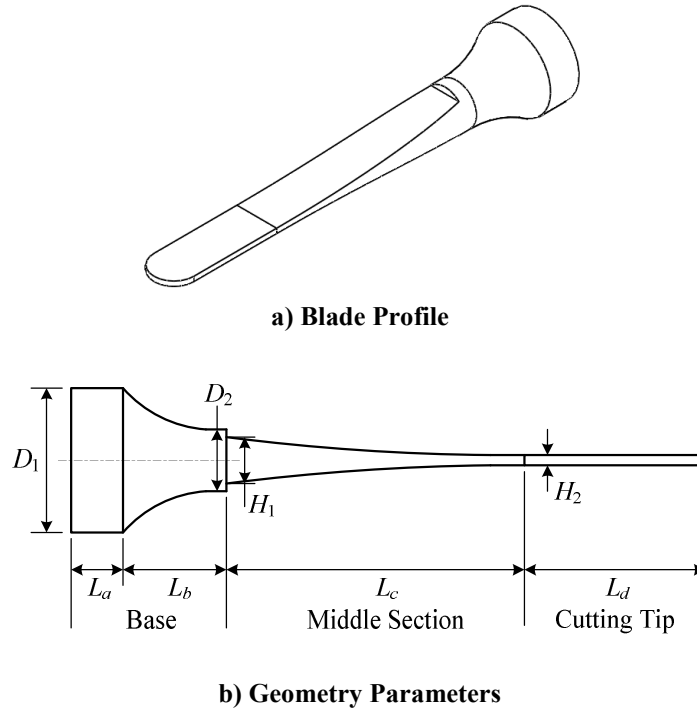
#### **5.3.1 Blade III: Blade Shape and Geometry Parameters**

Blade III was designed using the optimal method. The profile of the blade was defined by geometry parameters as discussed in Section 4.4.1.1. Figure 5.29 and Table 5.7 illustrate the profile of the blade and the geometry parameters used in this case. This three-sectional style profile provided a flexible and effective solution for the design of ultrasonic blades. The main features of the blade geometry were determined by eight geometry parameters, which also determined the main dynamic characteristics of the blade, such as the gain and tuned frequency. Additional parameters were defined to incorporate more details, such as the serrated cutting edge, in the geometry. They were of less importance to the blade performance and are therefore not shown in Figure 5.29 and Table 5.7.

It is not necessary to adjust all the geometry parameters in the design of Blade III. As discussed in Section 4.4.1, more adjustable parameters means higher dimensions of optimisation space and considerably increased computing time. In fact, most of the parameters in this case can be determined by other means to simplify the problem. Among them, the width of the blade ( $D_2$ ), the thickness of the middle section ( $H_1$ ), the thickness and the length of the cutting tip ( $H_2$  and  $L_d$ ) can be determined based on the application requirements and previous design experience, as detailed in Table 5.7.  $L_a$  was regarded as a parameter with less influence on the critical dynamic characteristics of the blade. To further simplify the problem without compromising the flexibility of design, a pre-defined value was assigned to  $L_a$ . As a consequence, it was only



necessary to adjust three parameters  $D_1$ ,  $L_b$  and  $L_c$  in the optimisation. This would not change the nature of the optimal design but could reduce the complexity of the problem significantly.



**Figure 5.29 Blade Profile and Geometry Parameters**

Symbol	Parameter	Value
$*D_1$	Large diameter of the blade base.	Adjustable variable. Ranging between $D_2$ and the diameter of the transducer output terminal.
$D_2$	Small diameter of the blade base, equal to the width of the blade.	Determined by the requirements of the application.
$H_1$	Large thickness of the middle section.	Determined according to $D_2$ .
$H_2$	Thickness of the cutting tip, equal to the small thickness of the middle section.	Determined by the requirements of the application.
$L_a$	Length of the cylinder part in the blade base.	Pre-defined.
$*L_b$	Length of the cone part in the blade base.	Adjustable variable.
$*L_c$	Length of the middle section.	Adjustable variable.
$L_d$	Length of the cutting tip, including the rounded tip.	Determined by the requirements of the application.

\*Adjustable variable

**Table 5.7 Blade Geometry Parameters**

In addition, the value scope of the adjustable parameters was determined by estimating the geometry limit of the blade. As Blade III was designed to be a half wavelength blade, the approximate overall length of the blade, estimated using Eq 1.1, was used as the upper limit of  $L_b$  and  $L_c$ . The value scope of  $D_1$  was determined by considering the attachment of the blade.  $D_1$  is expected to be larger than the blade width and smaller than the diameter of the output face of the transducer. Thus, a bounded three-dimensional optimisation space can be fully defined for this design problem.

### 5.3.2 Blade Performance Indicators

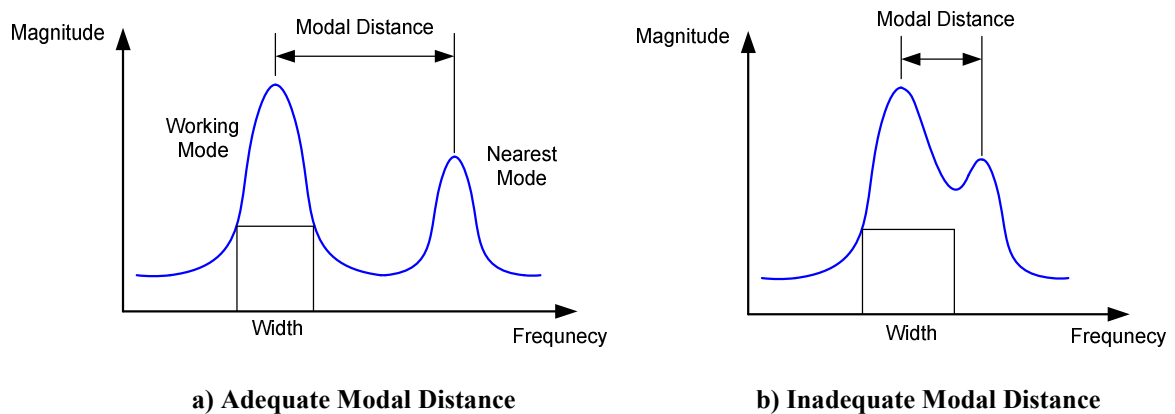
As presented in Chapter 5, the optimal design method relies on indicators to evaluate the performance of a design. Six indicators selected from Table 4.5 were used in this case, including the modal distance ( $M_A$ ), maximum stress ( $S_A$ ), and the gains of the blade ( $G_A, G_X, G_Y, G_T$ ), as illustrated in Table 5.8. These indicators provided insights into the main characteristics affecting the dynamic performance of the blade.

#### (1) Modal Distance

As illustrated in Table 5.8 and explained in Chapter 4, the modal distance ( $M_A$ ) is a measure indicating how the working mode is frequency separated from the other modes. It provides information on the possibility of the occurrence of modal coupling. A preferred design should have adequate modal distance so that the blade can work stably at the working mode with limited influence from other non-working modes. This idea is illustrated in Figure 5.30, where two examples of FRFs are shown. The peaks of the FRFs are associated with the presence of vibration modes. It is assumed that the peaks may overlap when the modal distance is smaller than the peak width, in which case modal coupling could occur. Figure 5.30(a) shows a case where the working mode is well separated from an adjacent mode. As a contrast, Figure 5.30(b) illustrates a case where the working mode may be influenced as the modes are overlapping their peaks. Thus based on this principle, the modal distance should be at least greater than the peak width of the working mode.

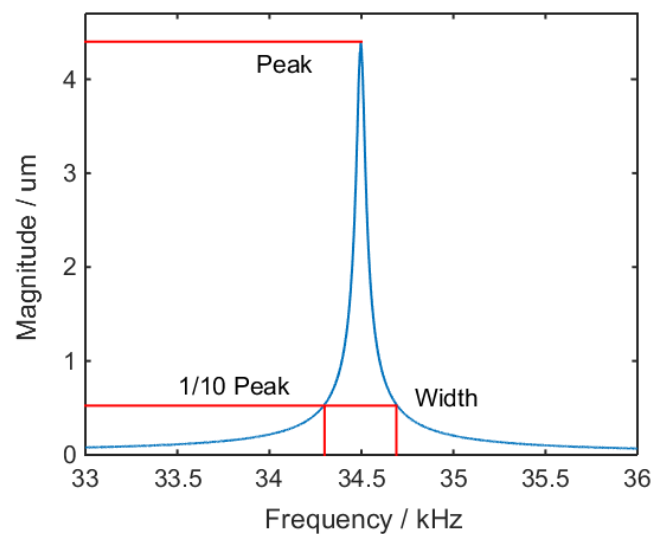
Indicator	Name	Definition and Value	Preference
$M_A$	Modal Distance	The lowest frequency difference between the working mode (L1) and non-working modes.  Indication for the possibility of the occurrence of modal coupling.	High
$S_A$	Maximum Stress	The maximum Mises stress in the blade under a multi-component excitation.  Indication for blade strength.	Low  Must be lower than the material fatigue limit.
$G_A (G_L)$	Gain of Blade	The factor by which the amplitude of the longitudinal excitation is increased at the tip of the blade.  Indication for excitation amplification.	High  Adequate value to achieve efficient cutting.
$G_X$	Gain of Lateral Bending	The factor by which the amplitude of the lateral bending (bending along the width of the blade) at blade base is increased at the tip of the blade.  Indication for amplification of undesired vibration.	Low
$G_Y$	Gain of Flexural Bending	The factor by which the amplitude of the flexural bending (bending along the thickness of the blade) at blade base is increased at the tip of the blade.  Indication for amplification of undesired vibration.	Low
$G_T$	Gain of Torsion	The factor by which the amplitude of torsion at blade base is increased at the tip of the blade.  Indication for amplification of undesired vibration.	Low

**Table 5.8 Performance Indicators**



**Figure 5.30 Modal Distance and Mode Coupling**

To determine the lower limit of modal distance for this study, the case of Blade I was reviewed. The amplitude of a FRF obtained in the EMA of Blade I is illustrated in Figure 5.31. It shows the response of the blade tip in the longitudinal direction around the tuned frequency. The peak of the FRF was associated with the working mode of the blade (first longitudinal mode). The width was measured around the peak base at 1/10 of the height, which was 405Hz, as shown in Figure 5.31. This is a convenient way to appropriately evaluate the peak width for a sharp peak [8]. It is necessary to apply allowance when using the width as the limit of the modal distance as peak width varies between different designs. Also, giving consideration to the existence of difference between the computing and actual modal frequencies, extra allowance was applied and 2kHz was used as the minimum modal distance. Although, this restriction may not guarantee the avoidance of coupling behaviour in all cases, it provided a simple and feasible solution to quickly filter out unqualified designs in optimisation.

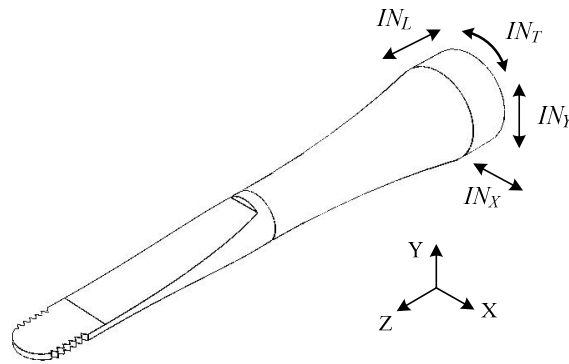


**Figure 5.31 FRF and Width of the Peak  
(Blade I, Tip, Longitudinal Direction)**

## (2) Maximum Stress

The maximum stress ( $S_A$ ) was used as the indication of blade strength. It was calculated by applying a multi-component input and using the method detailed in Section 4.2.5. Four vibration components were included in the input:  $IN_L$  for the longitudinal input,  $IN_X$  for the input in the width direction,  $IN_Y$  for the input in the thickness direction, and  $IN_T$  for the torsional input. The values of these components are shown in Table 5.9.  $IN_L$  was applied with the largest transducer output that was

allowed for this type of blade, which in this case was  $10\mu\text{m}$ .  $IN_X$ ,  $IN_Y$ , and  $IN_T$  were  $0.5\mu\text{m}$ ,  $0.5\mu\text{m}$  and  $10^{-4}\text{rad}$ , respectively, which were not intended to simulate the actual transducer output and their values were not associated with physical excitations. Instead, they were applied in a way just to introduce significant non-longitudinal vibration in the analysis. This simulated an extreme working condition where the blade was subjected to large excitation and coupled vibration. The obtained  $S_A$  is therefore the largest stress the blade may suffer. It is expected that a blade will have adequate strength to withstand the ultrasonic excitation in normal operating conditions if it stands the stress in such extreme conditions. To determine the lower limit of  $S_A$ , the stress criterion proposed in Section 5.2.1.1 was applied with a safety factor of 1.3. The successful design of Blade I showed that a blade with adequate strength can be achieved under this criterion. Thereby, by reviewing the case of Blade I, 350MPa was used as the lower limit of  $S_A$ .



**Figure 5.32 Input for Stress Analysis**

Input	Amplitude
$IN_X$	$0.5\ \mu\text{m}$
$IN_Y$	$0.5\ \mu\text{m}$
$IN_Z$	$10\ \mu\text{m}$
$IN_T$	$10^{-4}\ \text{rad}$

**Table 5.9 Input for Stress Analysis**

### (3) Gains of Blade

The gains indicate the responses of the blade subjected to different excitations. As illustrated in Table 5.8, four types of gains were considered in this study.  $G_A$  ( $G_L$ ) was

the gain of the blade, which was defined as the factor by which the amplitude of the longitudinal excitation at the base is increased at the tip of the blade. It was calculated through the displacement of the blade under a normalised longitudinal excitation using the method detailed in Section 4.2.3. As ultrasonic cutting normally requires vibration amplitude of minimum  $30\mu\text{m}$  and the vibration output of a transducer is typically  $5\text{-}10\mu\text{m}$ , the gain of an ultrasonic blade should be at least 3 in order to achieve sufficient output at the cutting tip. In this study, it is expected that the blade has a gain greater than 5. Larger gain is preferred but it may be achieved at the price of higher material stress.

The gains of non-working motions,  $G_X$ ,  $G_Y$  and  $G_T$ , were also considered in the optimisation. They indicate how the blade responds to unwanted vibrations, which may be caused by coupled vibration or non-linear behaviour. The definition and computing method of these indicators were detailed in Table 5.8 and Section 4.2.3. To reduce the presence of undesired motions, such gains should be controlled below an acceptable level. A study of the ultrasonic blades designed in previous research [14, 39, 53] showed that their  $G_X$  is 5-13,  $G_Y$  is 9-21, and  $G_T$  is 11-30. Therefore middle values 10, 15 and 25 were used as the limits for  $G_X$ ,  $G_Y$  and  $G_T$ , respectively. It is expected that this can impose restrictions on undesired vibration while allowing the comparison of adequate number of designs in the optimisation.

#### **(4) Constraints and Optimal Target**

Unlike the conventional design method, the optimal design was conducted in terms of constraints and an optimisation target (objective function) based on the selected indicators. A qualified design was expected to meet all the design requirements formulated as indicator constraints. This took into account the desired blade performance and was determined according to the goal of the design.

Table 5.10 illustrates the constraints and the optimisation target applied in this study, which include:

- the modal frequency of the first longitudinal mode ( $f$ ) that must be at the correct frequency to make sure the blade could be properly excited;
- the modal distance that should be larger than 2kHz to avoid modal coupling behaviour;

- the maximum stress ( $S_A$ ) that must be less than a fatigue limit of 350MPa to achieve sufficient strength;
- the gain of the blade ( $G_A$ ) which should be greater than 5 to ensure delivering adequate vibration amplitude for cutting;
- the non-longitudinal gains of the blade ( $G_X, G_Y, G_T$ ) that should be lower than their upper limits to reduce the presence of undesired vibration.

These constraints would filter out those unqualified designs, ensuring the optimisation process to be conducted correctly.

Moreover, to obtain a final design from the qualified candidates, a single optimisation target was applied with an aim to minimise the maximum stress ( $S_A$ ). This attempted to generate a blade with the highest strength, which would enable the blade to not only withstand high power ultrasonic excitation and cutting forces, but also work reliably in surgical applications.

Indicator/ Parameter	Constraints	Remark
$f$	$= 35 \pm 0.5\text{kHz}$	Ensure proper excitation.
$M_A$	$> 2\text{kHz}$	Avoid modal coupling.
* $S_A$	$< 350\text{MPa}$	Ensure adequate blade strength.
$G_A (G_L)$	$\geq 5$	Enable adequate cutting amplitude.
$G_X$	$< 10$	Reduce undesired vibration.
$G_Y$	$< 15$	Reduce undesired vibration.
$G_T$	$< 25$	Reduce undesired vibration.

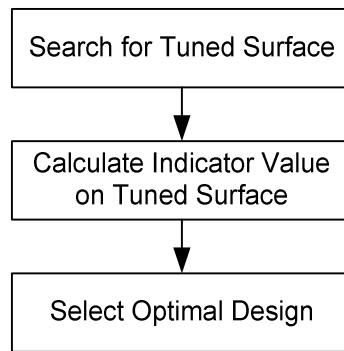
\*Optimisation target (objective function).

**Table 5.10 Constraints of Indicators/Parameters**

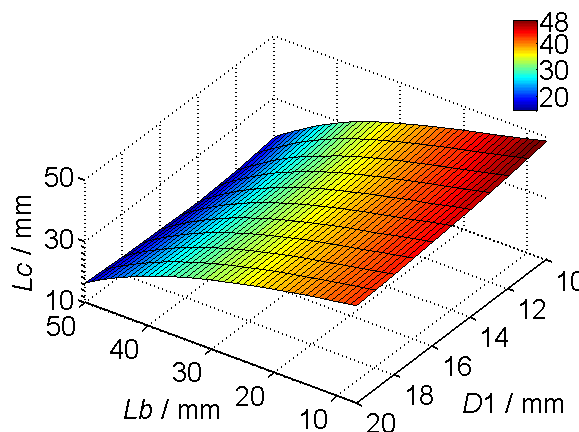
### 5.3.3 Calculation and Result Discussion

With the constraints and optimisation target defined, the optimal design was ready to be conducted using the method introduced in Chapter 6. In order to illustrate the intermediate results between the steps and better demonstrate the concept of optimal design, this case study applied a procedure slightly different from Figure 4.3. Instead of processing one design at a time and discarding the unqualified designs, the procedure used an exhaustive algorithm to evaluate all the designs in the optimisation space, keeping and plotting the obtained results. However, the two procedures are completely equivalent in terms of their functions.

As illustrated in Figure 5.33, the first step of the optimisation was to obtain the tuned surface in the optimisation space formed by the adjustable parameters ( $D_1$ ,  $L_b$  and  $L_c$ ). The optimisation space was a three dimensional space representing all the possible designs, where each point was mapped to a specified blade. However, not all the points in this space result in blades tuned at the correct working frequency. In fact, there were only two independent parameters when the tuned frequency was applied as a constraint. Consequently, the correctly tuned blades were located only on a specific surface called the "Tuned Surface" which could be found through a bisection searching. Figure 5.34 illustrates the obtained tuned surface, on which are the designs with a working frequency of 35kHz. These designs were referred to as the tuned designs. This simplified the calculation of the following steps as it is only necessary to compute the indicators for the tuned designs.



**Figure 5.33 Calculation Procedure**



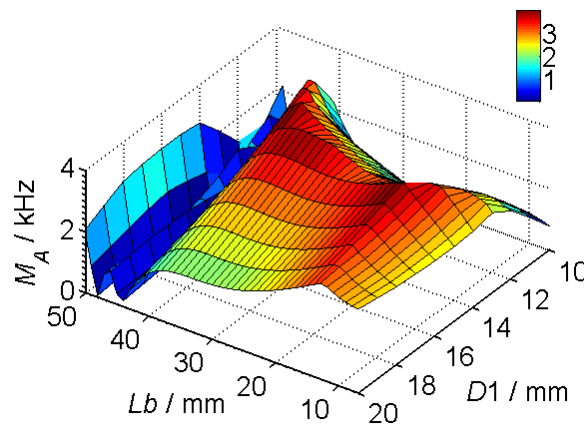
**Figure 5.34 Optimisation Space and Tuned Surface**

Based on the tuned surface, the value of the indicators was computed. To facilitate the process,  $L_b$  and  $D_1$  were chosen as independent parameters, which would vary with a



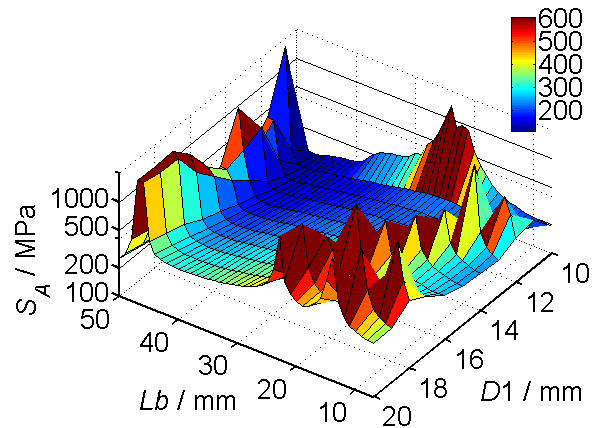
step increment of 1mm. As the optimisation was carried out using an exhaustive and graphic approach, the step size did not affect the convergence of computing. Further reducing the step increment could improve the resolution of optimisation. However, this would be achieved at the price of dramatically increased amount of computing. The step size used in this study provided a good balance between the optimisation resolution and computing expense.

Figure 5.35 illustrates the modal distance ( $M_A$ ) obtained over the tuned surface, which was plotted with respect to  $L_b$  and  $D_1$ .  $M_A$  was found to vary between 30Hz to 3.91kHz. According to the constraints of the indicator, a qualified design should have a modal distance greater than 2kHz. This filtered out 37.2% of the tuned designs with inadequate frequency separation between the working and non-working modes. The qualified designs were located in the regions with red and yellow colour.



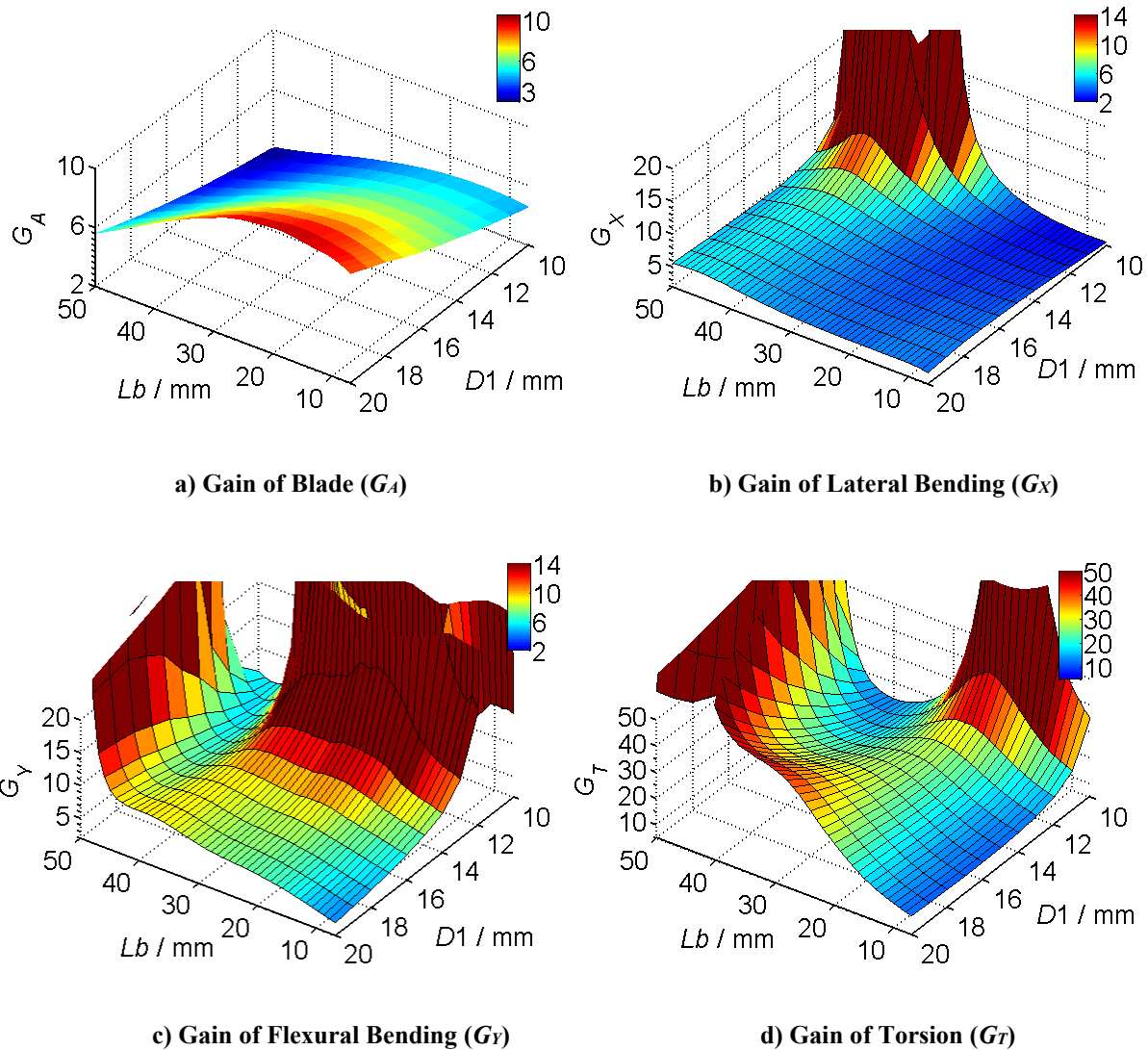
**Figure 5.35 Modal Distance ( $M_A$ )**

The maximum Mises stress ( $S_A$ ) is illustrated in Figure 5.36 in a similar way. Peaks were observed in this figure, suggesting that significantly high stress values were predicted. As the maximum  $S_A$  allowed in the optimisation was 350MPa, 31.4% of the tuned designs were disqualified due to their stress exceeding the material fatigue limit. The designs with low stress level were located in the regions in light and dark blue. Most of them were in the large flat area in the centre and a narrow region near the edge of  $L_b=10$ .



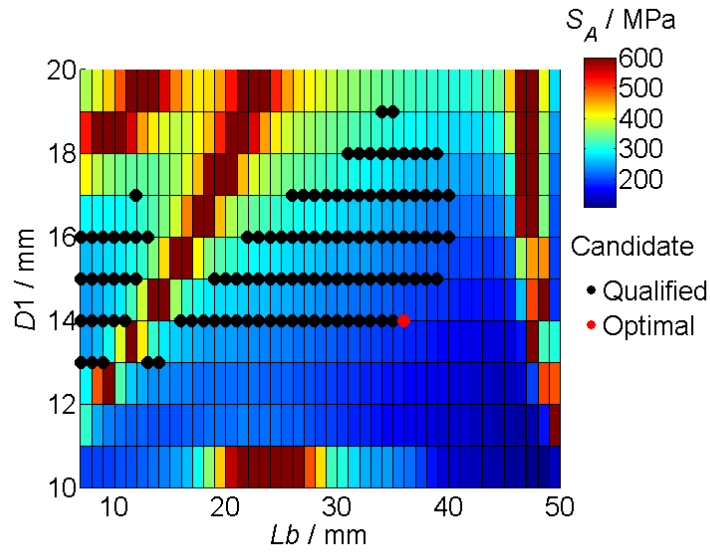
**Figure 5.36 Maximum (Mises) Stress ( $S_A$ )**

In addition, the gains of the blade ( $G_A$ ,  $G_X$ ,  $G_Y$ ,  $G_T$ ) are shown in Figure 5.37(a)-(d). Figure 5.37(a) illustrates the obtained  $G_A$ . The minimum gain of the tuned designs was 2 and the maximum was 10.5. There were 32.4% designs with a longitudinal gain lower than 5, which were located in the dark blue region in Figure 5.37(a). These designs were undesired as they could not deliver sufficient vibration output at the cutting tip. Figure 5.37(b) illustrates the gain in the lateral bending direction ( $G_X$ ), which was a gain of non-working vibration. To reduce unwanted vibration, the maximum  $G_X$  allowed for a blade was 10. This restriction filtered out 9.1% tuned designs in the optimisation, which were located around the red region in Figure 5.37(b). The gain in the flexural bending direction ( $G_Y$ ) and torsion ( $G_T$ ) were plotted in a similar way, as shown in Figure 5.37(c) and Figure 5.37(d) respectively. The constraints of  $G_Y$  and  $G_T$  filtered out 24% and 42.3% of the tuned designs, respectively.



**Figure 5.37 Gains of Blade**

Based on the indicators, the qualified candidate designs were obtained by applying all the constraints summarised in Table 5.10. Figure 5.38 plots these designs by marking the designs with dots and superimposing them on the value of the maximum stress ( $S_A$ ). By comparing Figure 5.38 with Figure 5.35-Figure 5.37, it can be seen that the qualified candidates avoided the regions that are of high stress and high non-longitudinal gains. On this basis, the optimal design was obtained by applying the optimisation target: the lowest  $S_A$ . It was found at  $D_1=14$ ,  $L_b=36$ , as illustrated by the red dot in Figure 5.38. The details of its indicators are shown in Table 5.11. By comparing to Table 5.10, it is confirmed that this design met all the constraints and had a stress value of only 201MPa.



**Figure 5.38 Qualified and Optimal Design (Superimposing on Values of  $S_A$ )**

Parameter / Indicator	Value	Parameter / Indicator	Value
$L_c$	30mm	$G_A$	5.1
$L_b$	36mm	$G_X$	5.5
$D_1$	14mm	$G_Y$	11
$M_A$	3.6kHz	$G_T$	21
$S_A$	201MPa	$f$	35kHz

**Table 5.11 Parameters and Indicators of the Optimal Design**

The geometry of the optimal design is shown in Figure 5.39. Further analysis was conducted to verify the performance of this solution. Similarly to Blade I and Blade II, modal analysis and stress analysis was carried out using the FE method. Table 5.12 illustrates the result of the modal analysis. It confirmed that the first longitudinal mode was correctly tuned at 35kHz with a distance of 3.6kHz to the adjacent mode. The normalised displacement of the working mode obtained along the central line of the blade is illustrated in Figure 5.40. The gain of the blade was found to be 5.1, the same value of  $G_A$ , as presented in Table 5.11.

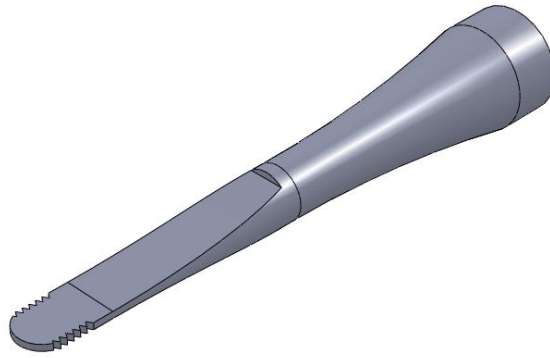


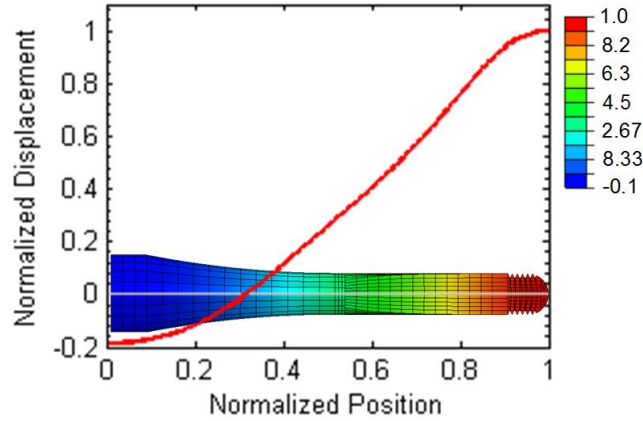
Figure 5.39 Model of the Optimal Design

Mode	Mode Shape	$f$ / kHz	Mode	Mode Shape	$f$ / kHz
T1		11.4	BY4		12.4
BX3		14.6	BY5		20.2
T2		24.4	BX4		26.7
BY6		29.8	T3		31.4
L1		35.0	BY7		40.0
T4		44.1	BX5		41.5

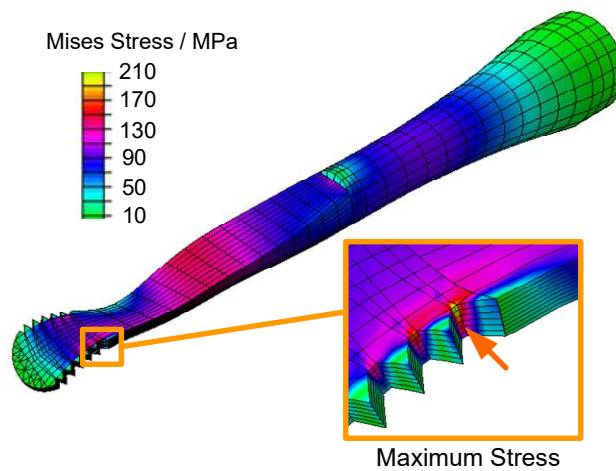
Table 5.12 Results of Modal Analysis

The stress analysis was conducted using the same multi-component excitation as discussed in Section 5.3.2. In addition to longitudinal vibration, bending and torsional vibration was deliberately introduced in the analysis to simulate an extreme working condition, where multiple modes of vibration presence in the blade simultaneously. The result of the stress analysis is shown in Figure 5.41 and the normalised stress distribution along the blade central line is illustrated in Figure 5.42. As a result of the coupled vibration, more than one peaks were observed in the stress curve, as illustrated in Figure 5.42. The maximum Mises stress was found to be 204MPa, locating at a serration of the cutting edge. This value was in agreement with indicator  $S_A$  obtained in the optimisation. Further investigation of the stress distribution showed that the maximum stress was significantly larger than the stress in other regions of the blade due to the stress concentration effect. However, the blade was considered to be of sufficient strength as the maximum stress was well within the allowable limit

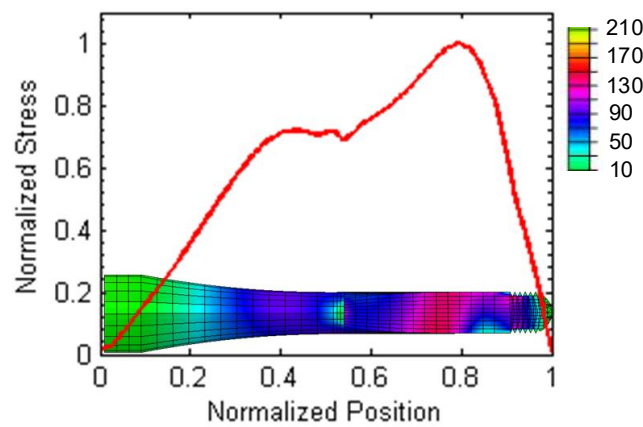
(350MPa, Table 5.10). As the results of both modal and stress analysis were in agreement with the outcome of the optimal method, it is confirmed that the proposed design process evaluated the characteristics of the blade appropriately.



**Figure 5.40 Normalised Displacement**



**Figure 5.41 Stress Distribution (Under Multi-Component Excitation)**



**Figure 5.42 Normalised Stress Distribution (Under Multi-Component Excitation)**

## 5.3.4 Experimental Verification

### 5.3.4.1 Impedance Analysis

To experimentally verify and test the performance of the optimal solution, the obtained design (Blade III) was manufactured using a CNC machine and is shown in Figure 5.43. Blade III was subjected to impedance analysis using the same experimental setup as that in the case of Blade I. Figure 5.44 plots the results of the impedance analysis, showing that the main resonance frequency was 34.5kHz. This suggests that the blade was tuned correctly. The slight difference (0.5kHz) between the experiment and the FEA was acceptable in this study.



Figure 5.43 Manufactured Blade

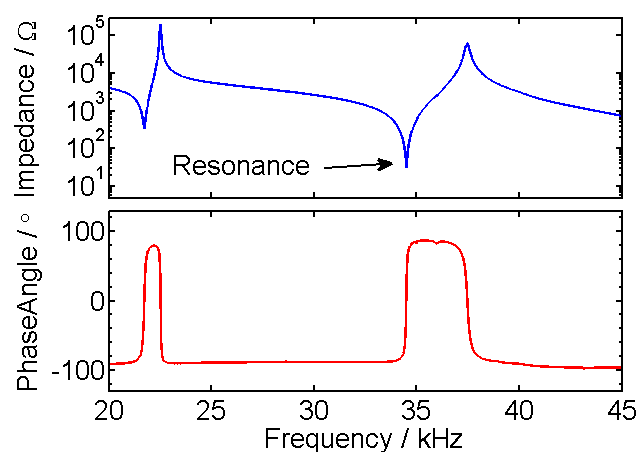


Figure 5.44 Result of Impedance Analysis

### 5.3.4.2 Experimental Modal Analysis

EMA was carried out to characterise the modal behaviour of Blade III using the same approach as detailed in Section 5.2.1.2. A total of 150 grid points were located on the blade, as illustrated in Figure 5.45. 450 FRFs were obtained, which are overlaid and plotted in Figure 5.46. The main peak indicates the presence of the first longitudinal mode around 35kHz. Further analysis extracted the modal frequencies and mode shapes, which are detailed in Table 5.13.

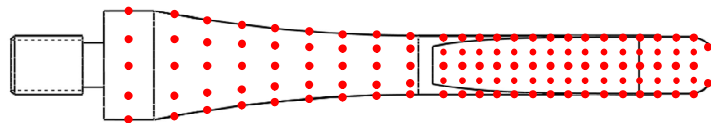


Figure 5.45 EMA Grid Points on Blade III (Serrations not Shown)

Longitudinal, bending and torsional modes were measured. They were named using the same way as presented for Blade I. A coupled mode, named T4B $\gamma$ 7, was observed. Carefully investigation showed that this was a combined mode involving two modes, T4 and B $\gamma$ 7.

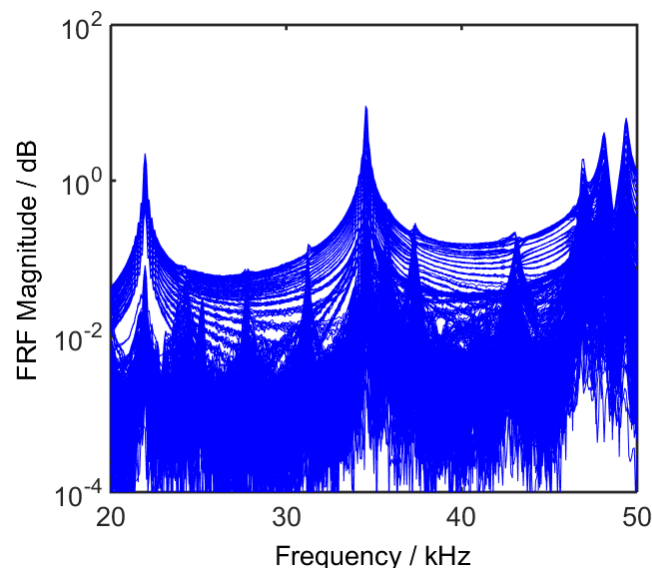


Figure 5.46 Result of Impedance Analysis

The results of EMA were compared to the predictions of FEA (without correction using EMA). As illustrated in Table 5.13, good agreement was found between FEA and EMA. The difference of modal frequency between the FEA and EMA were lower than 5% in all cases except for B $\gamma$ 7. The average difference for all modes was 2.8%, which suggested that the blade exhibited the expected characteristics. The combined



mode T4B<sub>Y</sub>7 could not be predicted by FEA as the analysis did not take into account the non-linear behaviour of the blade. However, comparing its modal frequency to T4 mode showed that, due to the coupled vibration, a frequency difference of 3.0kHz(6.4%) was observed. As this mode was far away from L1, its influence on the working mode could be ignored. For the working mode L1, the difference between EMA and FEA was 0.5kHz(1.4%), which confirmed that the blade was properly tuned at the correct frequency.

Mode	Modal Shape (EMA/FEA)	Frequency / kHz	Difference (FEA vs EMA)
B <sub>Y</sub> 5		EMA: 19.9	0.3kHz (1.5%)
		FEA: 20.2	
T2		EMA: 25.2	0.8 kHz (3.2%)
		FEA: 24.4	
B <sub>X</sub> 4		EMA: 27.7	1.0 kHz (3.6%)
		FEA: 26.7	
B <sub>Y</sub> 6		EMA: 31.2	1.4 kHz (4.5%)
		FEA: 29.8	
L1*		EMA: 34.5	0.5 kHz (1.4%)
		FEA: 35.0	
B <sub>Y</sub> 7		EMA: 37.8	2.2 kHz (5.8%)
		FEA: 40.0	
T4B <sub>Y</sub> 7 (Coupled mode)		EMA: 47.1	3.0 kHz ** (6.4%)**
		T4 FEA: 44.1	
B <sub>X</sub> 5		EMA: 42.5	1.0 kHz (2.3%)
		FEA: 41.5	

\*Working mode.

\*\*Difference between T4 FEA and EMA.

**Table 5.13 Results of EMA and Comparison with FEA**

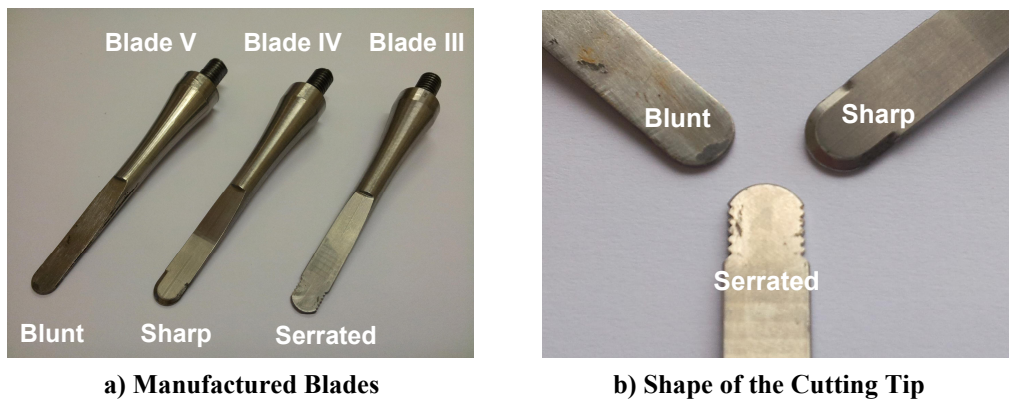
It is obtained from Table 5.13 that the actual modal distance ( $M_A$ ) is 3.3kHz, which is closed to the theoretical value (3.6kHz in Table 5.11) and is greater than the restricted limit (2kHz as discussed in Section 5.3.2). The true value of the blade gain ( $G_A$ ) was obtained by dividing the measured vibration amplitude at the blade tip to that at the base, which was found to be 5.2, a value sufficiently closed to the expected gain (5.1 in Table 5.11). This shows that the blade performance was appropriately evaluated by the optimal method. However, due to the difficulty of measurement and the input, the actual value of the other gain indicators, including  $G_X$ ,  $G_Y$  and  $G_T$ , were not obtained in this study. Moreover, as there was no easy way to measure the maximum stress in the blade, it was not possible to verify the optimality of this design. Nevertheless, taking into account the good agreement between the analysis prediction and experimental results, it is considered that the proposed optimal method produced the required design effectively.

### 5.3.5 Ultrasonic Cutting Test

The optimal method used in the design of Blade III focused on the dynamic behaviour of ultrasonic blades. The cutting performance, however, was not directly optimised in the design process. Taking into account the features of an ultrasonic bone cutting blade, it is considered that, under the same condition, the cutting performance of a blade is closely related to the design of the blade tip, including the shape of the cutting edge. To study this issue, two more ultrasonic blades were derived from Blade III and tested.

These new blades, Blade IV and Blade V, were fabricated using the same design as Blade III except that different types of cutting edges were incorporated. As illustrated in Figure 5.47, Blade IV was manufactured with a sharp cutting edge and Blade V was fabricated with a blunt cutting edge. Similar to the case of Blade I, the sharp edge is inspired by non-ultrasonic cutting tools, which take advantage of the reduced contact area and increased contact stress to improve cutting. The blunt edge, however, is easier to manufacture than the sharp and serrated edges. It requires less maintenance as the wearing has less influence on the shape of the edge. Also, comparing to serrated edges, the simplicity of the blunt edge can simplify the sterilisation procedures. Therefore, it is worth to investigate the cutting performance of this type of cutting edge.

As only insignificant changes were made on the blade profile, Blade IV and Blade V exhibited similar dynamic characteristics as Blade III, except an even lower maximum stress ( $S_A$ ), 184MPa for Blade IV (sharp) and 177MPa for Blade V (blunt), was found by FEA. Therefore, as long as the same excitation configuration is applied, the cutting tests of these blades can be regarded as carried out under same vibration conditions. Thus the difference of cutting performance between the blades can be ascribed to the different design of their cutting edges.

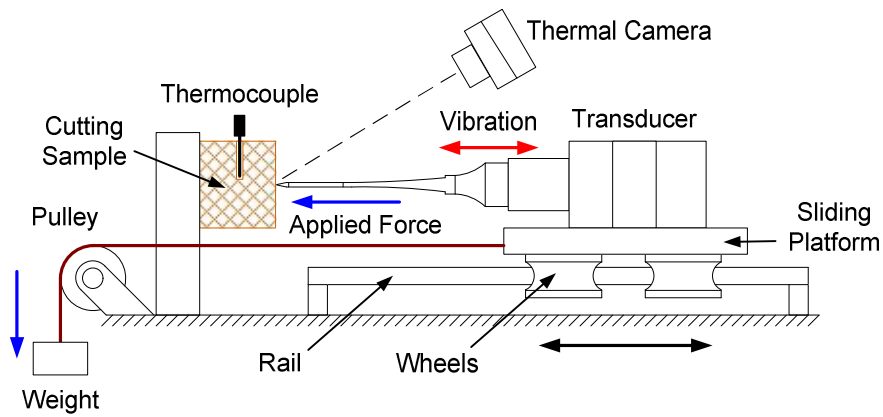


**Figure 5.47 Manufactured blades**

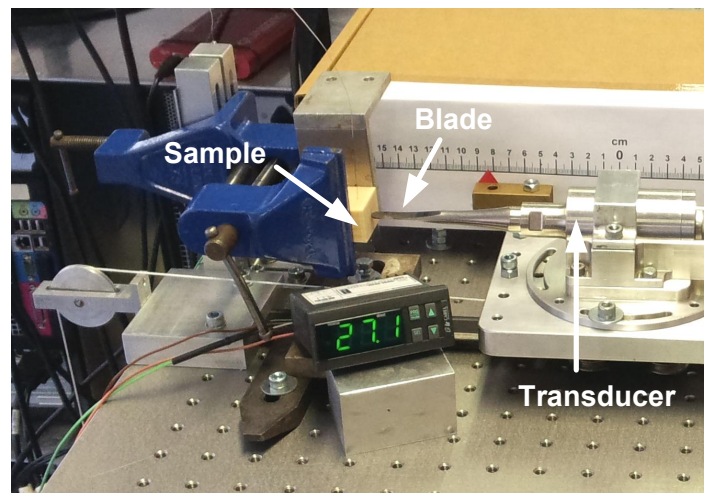
### 5.3.5.1 Test I: Ultrasonic Cutting of Biomechanical Samples under Static Load

Cutting temperature is the main concern in bone cutting. To reduce the possibility of necrosis in surgery, the temperature on the bone should be kept within a safe level during cutting. There are various factors influencing cutting temperature, such as the shape of the cutting edge, contact force and angle of cutting. To study this issue, Test I was conducted on a test rig to perform ultrasonic cutting on biomechanical samples under static loading.

Figure 5.48 and Figure 5.49 illustrate the test rig, where the ultrasonic blade was attached to a transducer fixed on a platform sliding freely on a rail. The platform was pulled by a weight through a string and a pulley to bring the blade in contact with the cutting sample. Providing the friction of the rail and the pulley was carefully balanced by a pre-load weight, the force applied on the blade can be controlled accurately by loading the correct amount of weight, allowing ultrasonic cutting to be performed under a specific constant load.



**Figure 5.48 Experimental Setup**



**Figure 5.49 Test Rig**

In addition, to conduct the ultrasonic cutting using different cutting angles, the transducer could be adjusted to form a certain angle between the blade and the direction of the applied force. As shown in Figure 5.50, three angle settings were applied in this study. Figure 5.50(a) illustrates the axial cut setting, where the blade was placed with its longitudinal axis parallel to the direction of the applied force. In this case, cutting would be performed by the blade tip, enabling the blade to penetrate into the sample. The second setting was the angle cut, as illustrated in Figure 5.50(b), where the blade was placed at an angle of  $45^\circ$  to the applied force. This allowed both the tip and the cutting edge to be involved in cutting. The third setting was the side cut as illustrated in Figure 5.50(c), where the blade was placed perpendicular to the applied force. This allowed the cutting edge to contact with the sample and perform cutting. These settings simulated typical ways in which the blade would be used in cutting applications.

To obtain the cutting temperature on the sample, a thermocouple and a thermal camera were used in the experiment. The thermocouple was applied to measure the temperature inside the sample. As illustrated in Figure 5.51, the thermocouple was placed inside a small hole drilled in the sample, measuring temperature inside the sample. In the testing, the blade cut into the sample and passed just below the thermocouple, which enabled the measurement of temperature around the cutting site. Taking into account factors such as heat conduction in the material and friction between the thermocouple and the sample, the temperature obtained in this way was subject to errors. Nevertheless, it did provide an insight into heat generation in ultrasonic bone cutting. The maximum temperature measured by the thermocouple during cutting was recorded and referred to as the internal temperature.

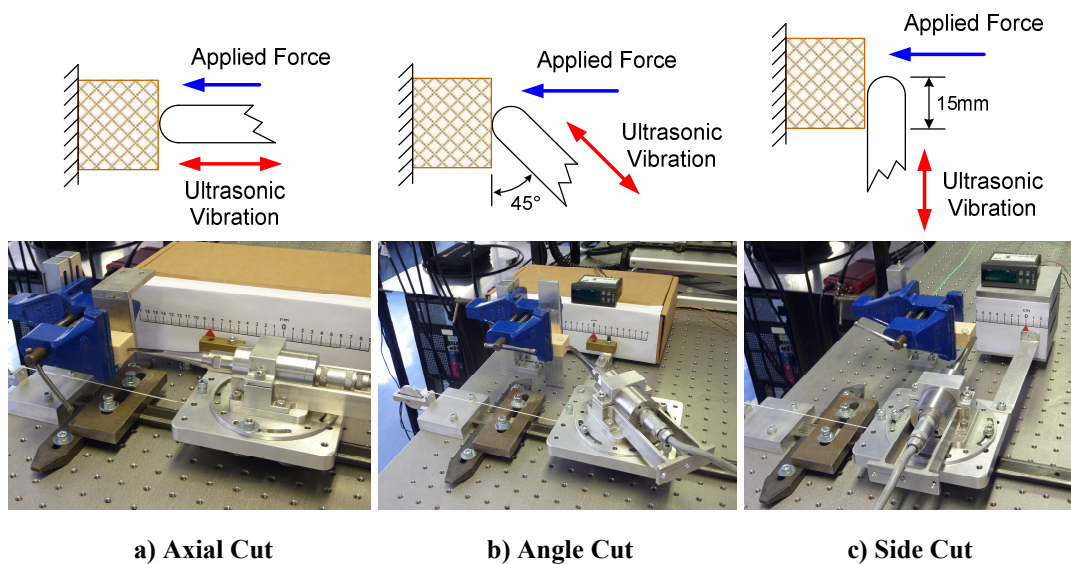


Figure 5.50 Cutting Angles

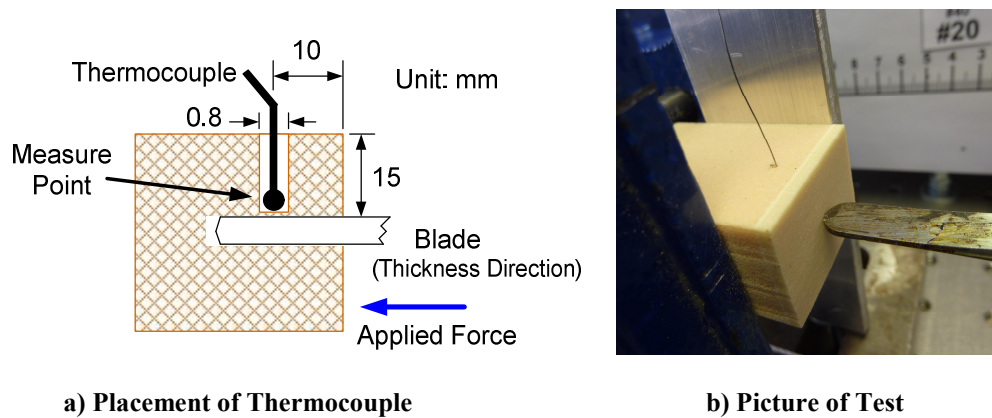
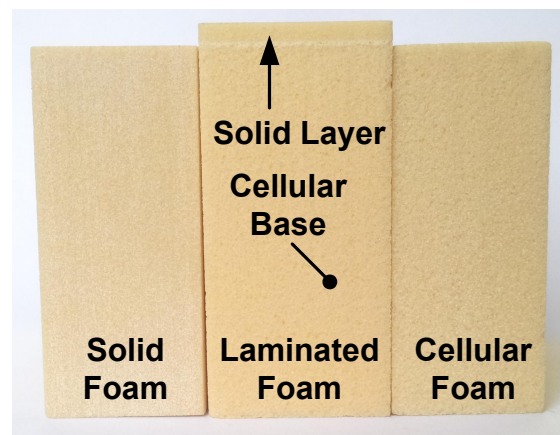


Figure 5.51 Measurement of Temperature Inside the Sample

In addition to the thermocouple, a thermal camera was used to measure the temperature on the sample surface around the cutting site, as illustrated in Figure 5.48. As the surface is not the location where cutting took place, this temperature was not the real cutting temperature either. It simply provided another way to investigate the temperature of the sample. The maximum temperature observed by the thermal camera during cutting was recorded and referred to as the surface temperature.



**Figure 5.52 Biomechanical Test Sample**

To ensure the material properties were consistent in the tests, biomechanical materials were used instead of real bones as the test samples. They are products of Pacific Research Laboratories, Inc. (Sawbones<sup>®</sup>). Three types of biomechanical materials, solid foam, cellular foam and laminated foam, were used to simulate different types of bones encountered in surgical cutting. These materials are illustrated in Figure 5.52 and their mechanical properties are listed in Table 5.14. The solid foam material is made of rigid polyurethane foam. It has physical strength properties similar to human cortical (compact) bones. The cellular foam is an inner cancellous material, which has lower density and strength than the solid foam material, and resembles trabecular (spongy) bones. The laminated foam material consists of two layers. It is made by laminating a thin solid foam layer (2mm) on the cellular foam base. This simulates the outer cortical layer and inner trabecular bone. It should be noted that although the biomechanical materials resemble bones in strength properties, they can not offer exactly the same features as real bones. For example, it melts and burns easily at high cutting temperatures in a different way to bones.



Material	Density (g/cm <sup>3</sup> )	Compressive		Tensile		Shear	
		Strength (MPa)	Modulus (MPa)	Strength (MPa)	Modulus (MPa)	Strength (MPa)	Modulus (MPa)
Cellular Foam	0.32	8.4	210	5.6	284	4.3	49
Solid Foam	0.64	31	759	19	1000	11	130
Laminated Foam	2mm Solid Foam Layer + 48mm Cellular Foam Base						

**Table 5.14 Mechanical Properties of Biomechanical Material [255]**

Blade V (blunt) was used to perform ultrasonic cutting on the solid, cellular and laminated foam. For each kind of sample, the cutting was conducted in three ways, axial cut, angle cut and side cut, where the samples were cut with varying applied force ( 1N(excluding solid foam and side cut of cellular foam), 2N, 4N, 6N, 8N and 10N ). In each test, an incision to a depth of 15mm was made. Both the surface and internal temperature were measured and the total cutting time was recorded. The cutting speed was calculated based on the depth of incision and the total cutting time. Each type of test was repeated three times using the same cutting settings with the average and error recorded in the plotted data. The results of the tests are illustrated in Figure 5.53, Figure 5.54 and Figure 5.55, which plot the cutting speed, surface temperature and internal temperature against the applied force, respectively.

The errors of the data were evaluated using standard deviation and relative error. The standard deviation of the data was computed using the following equation

$$\sigma = \sqrt{\frac{1}{m-1} \sum_{i=1}^m (x_i - \bar{x})^2} \quad (5.1)$$

where  $\sigma$  is the standard deviation,  $x_i$  is the data obtained under the same cutting force and cutting material,  $m$  is the number of tests for the specific force and material,  $\bar{x}$  is the mean of data, which

$$\bar{x} = \frac{1}{m} \sum_{i=1}^m x_i \quad (5.2)$$

The average standard deviation was calculated by averaging the standard deviation of different cutting settings, as shown in Eq. (5.3)

$$\bar{\sigma} = \frac{1}{n} \sum_{k=1}^n \sigma_k \quad (5.3)$$

where  $\sigma_k$  is the standard deviation for a specific cutting setting and  $n$  is the number of tests. The maximum standard deviation  $\sigma_{\max}$  is the largest value of these standard deviations. Both  $\bar{\sigma}$  and  $\sigma_{\max}$  were used to evaluate the overall error of the tests. Based on the standard deviation, the relative error was obtained by

$$e_r = \frac{\sigma}{\bar{x}} \times 100\% \quad (5.4)$$

The average relative error was calculated using a similar way to  $\bar{\sigma}$

$$\bar{e}_r = \frac{1}{n} \sum_{k=1}^n e_{rk} \quad (5.5)$$

and the maximum relative error  $e_{r \max}$  is the largest value of the relative errors.  $\bar{e}_r$  and  $e_{r \max}$  were also used to evaluate the overall error of the tests.

The cutting speed was illustrated in Figure 5.53 and the standard deviation and relative error of the speed data were shown in Table 5.15. The cutting speed can be influenced by factors including friction between the sample and blade, and debris accumulation around the cutting site. Such influence may introduce higher error in the measurement when the cutting speed is low, especially when the applied force is also low. The average standard deviation in this test was 0.047mm/s, and the maximum relative error was 31.6%, observed in the case of axial cut, laminated foam, 1N applied force. This was also the case where the lowest cutting speed, 0.28mm/s, was seen. Nevertheless, for the tests with cutting speed greater than 1mm/s the error was lower than 8%, and the average error of all tests was 7.0%. This suggests that the data was appropriately measured and the errors were within acceptable limit.

It is observed in Figure 5.53 that for the same test sample and cutting angle, the cutting speed increased as the applied force was increasing. The correlation coefficient, which evaluates the degree of linear relationship between two variables using a value ranging from -1 to 1, was computed for the cutting speed and the applied force. As illustrated in Table 5.16, the correlation coefficients were greater than 0.9 in all cases, suggesting that there is a significant linear correlation between the applied force and the speed of cutting. Therefore, a linear model

$$v = aF + b \quad (5.6)$$



was used to characterise the relationship between these two variables, where  $v$  is the cutting speed (mm/s),  $F$  is the applied force (N),  $a$  and  $b$  are the parameters of the model. Taking account of the fact that the influence of measurement errors became significant when the applied force was low, this model was not intended to be applied for the case where  $F$  is relatively closed to zero.

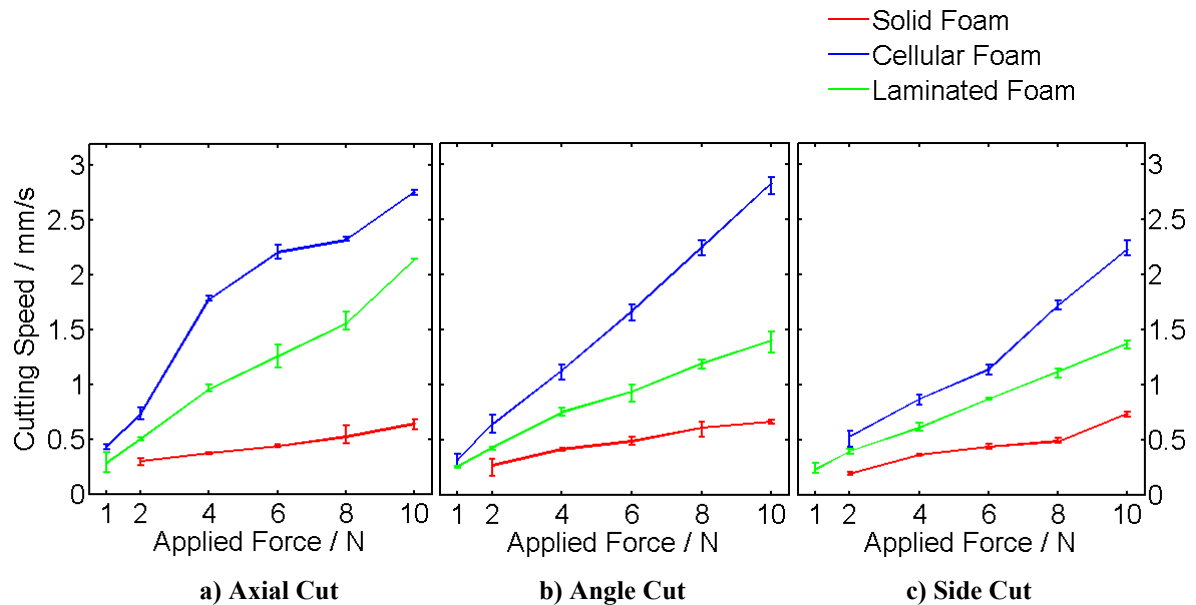


Figure 5.53 Cutting Speed

	Standard Deviation		Relative Error	
	Average	Maximum	Average	Maximum
Cutting Speed	0.047mm/s	0.11mm/s	7.0%	31.6%
Surface Temperature	9.5°C	41.6°C	7.7%	17.8%
Internal Temperature	16.1°C	35.5°C	9.2%	23.8%

Table 5.15 Standard Deviation and Relative Error

The parameters of the model were estimated using the method of least squares and their values are shown in Table 5.16. Parameter  $a$ , which is the increase rate of the cutting speed and is associated with the slope of the plot, was of interest. As the material strength is the highest in solid foam and the lowest in cellular foam, for the same cutting angle and applied force, the largest cutting speed was seen in the cellular foam and the lowest speed was seen in the solid foam. The influence of the material strength on the cutting speed can also be observed from parameter  $a$ , whose value, for the same cutting angle, was the largest in the cellular foam and the smallest in the

solid foam. The influence of the cutting angle on the cutting speed, however, was not identified from the data. For solid foam, parameter  $a$  was the largest in the case of side cut. However, for cellular foam, the largest value was found in angle cut, and for laminated foam, this was in axial cut. Therefore, no conclusion was drawn for the relationship between the cutting angle and the cutting speed.

Cutting Setting		Correlation Coefficient	Model Parameter	
Angle	Material		$a$	$b$
Axial Cut	Solid	0.939	0.0415	0.205
	Cellular	0.959	0.256	0.381
	Laminated	0.990	0.196	0.102
Angle Cut	Solid	0.945	0.049	0.190
	Cellular	0.997	0.276	0.0436
	Laminated	0.989	0.126	0.176
Side Cut	Solid	0.963	0.0608	0.0760
	Cellular	0.986	0.212	0.0245
	Laminated	0.997	0.125	0.122

**Table 5.16 Correlation Coefficients and Model Parameters**

Figure 5.54 and Figure 5.55 plot the surface and internal temperature against the applied force, respectively. The factors affecting the measurement of temperature include the position of the thermocouple, heat conduction in the material and the condition of heat dissipation. As the internal temperature was measured by a thermocouple placing closed to the cutting site, it can be subjected to higher error than the surface temperature. As shown in Table 5.15, the average standard deviation of the surface and internal temperature data was  $9.5^{\circ}\text{C}$  and  $16.1^{\circ}\text{C}$ , respectively, and the average relative error of the surface and internal temperature was 7.7% and 9.2%, respectively. To further illustrate the change of temperature in the material, Figure 5.56 plots the internal temperature, measured in axial cut, solid foam under 6N applied force, with respect to the cutting time and cutting depth. It shows that the temperature remained almost unchanged at the first 18 seconds before rising rapidly. The temperature continued to increase after the cutting stopped at 15mm cutting depth, and its maximum value was seen at around 40 seconds. The lag between cutting and temperature measurement is considered to be mainly caused by the time required in heat conduction in the material.

The correlation coefficients between the temperature and the applied force were computed and illustrated in Table 5.17. Both positive and negative coefficients were seen, of which the absolute value varies between 0.0285 to 0.913. This suggested that a linear relationship was not identified between the temperature and the applied force. For each cutting setting, the temperatures obtained under different applied force were averaged with an attempt to compare the overall surface and internal temperature between different cutting angles and cutting samples. As shown in Table 5.17, the lowest and highest average temperature was 97°C and 288°C respectively, which was observed in the cases of angle cut cellular foam, and side cut solid foam, respectively. For either type of material, the average temperature in the case of side cut was higher than axial cut and angle cut. It implied that the side cut may be a less favourable option when attempting to minimise the cutting temperature. This may be partly ascribed to the non-uniformly distributed vibration amplitude along the cutting edge. As illustrated in Figure 5.40, according to the longitudinal deformed mode shape of the blade, the maximum vibration amplitude appears at the tip of the blade. The amplitude decreases quickly along the cutting edge. In the side cut setting, the difference in vibration amplitude may result in difference in cutting effect and increased heat accumulation at the cutting site. Nevertheless, taking into account the fact that the average temperatures were above 100°C in most cases, the blade was considered not suitable for bone cutting without the application of cooling.

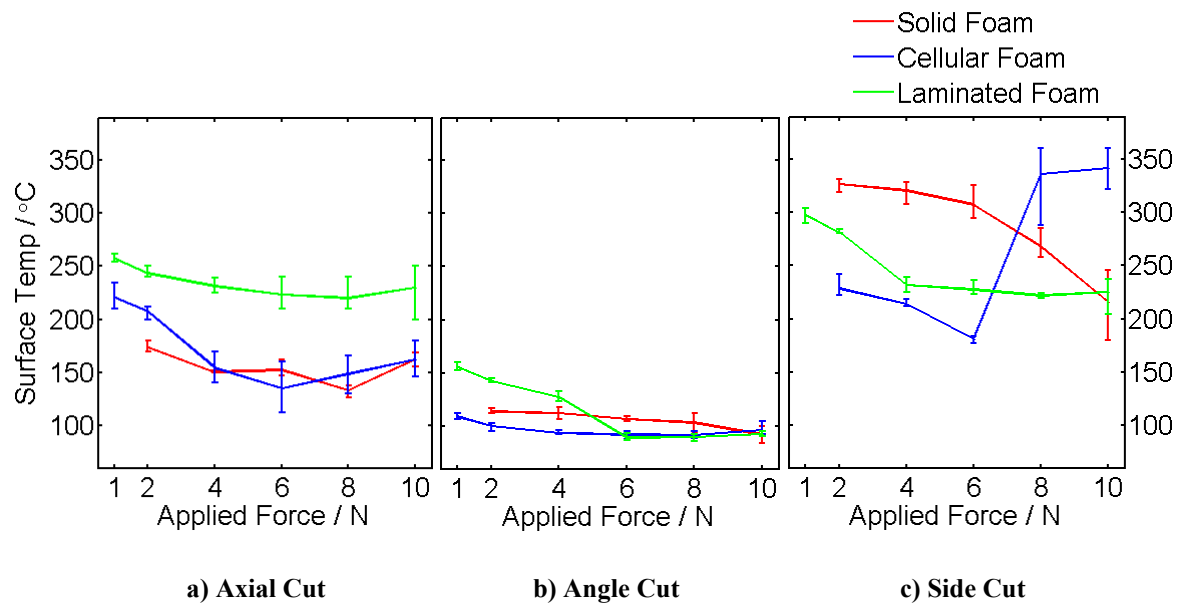
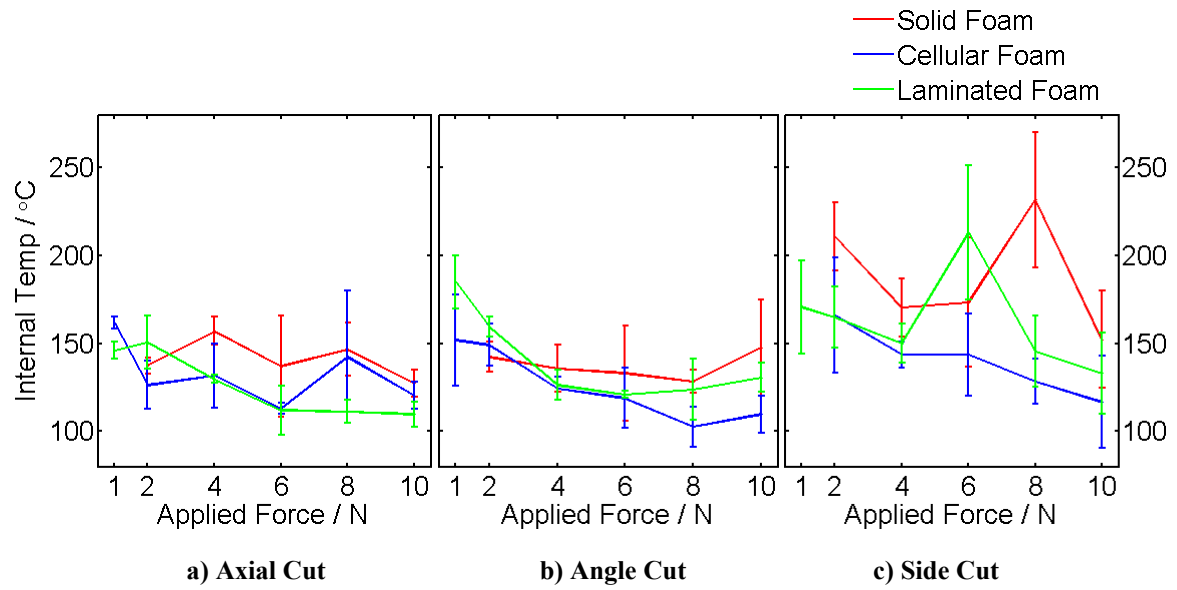


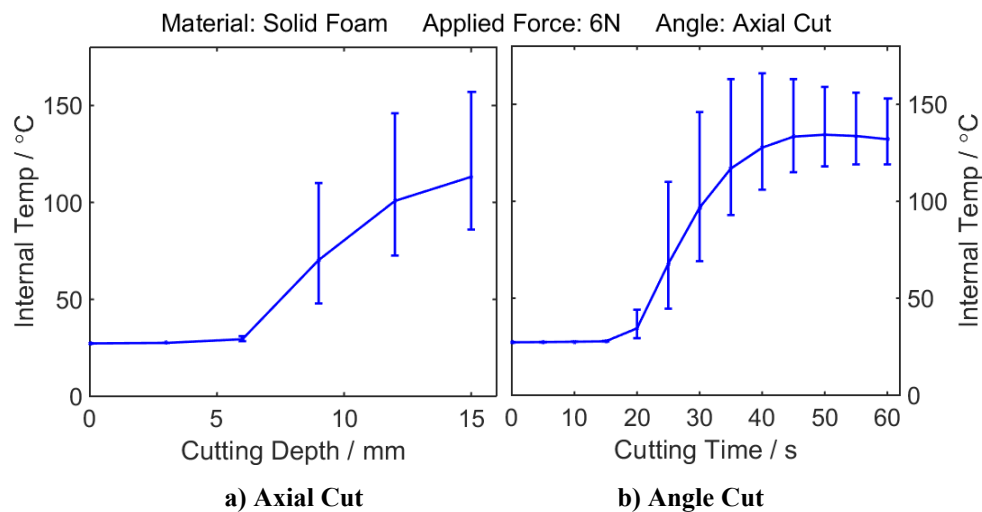
Figure 5.54 Surface Temperature



**Figure 5.55 Internal Temperature**

Cutting Setting		Correlation Coefficient		Average Temperature (°C)	
Angle	Material	Surface	Internal	Surface	Internal
Axial Cut	Solid	-0.392	-0.274	154	141
	Cellular	-0.672	-0.367	171	133
	Laminated	-0.575	-0.851	234	127
Angle Cut	Solid	-0.795	0.0284	106	137
	Cellular	-0.581	-0.768	97	126
	Laminated	-0.913	-0.701	116	141
Side Cut	Solid	-0.880	-0.213	288	188
	Cellular	0.722	-0.661	260	140
	Laminated	-0.832	-0.288	248	163

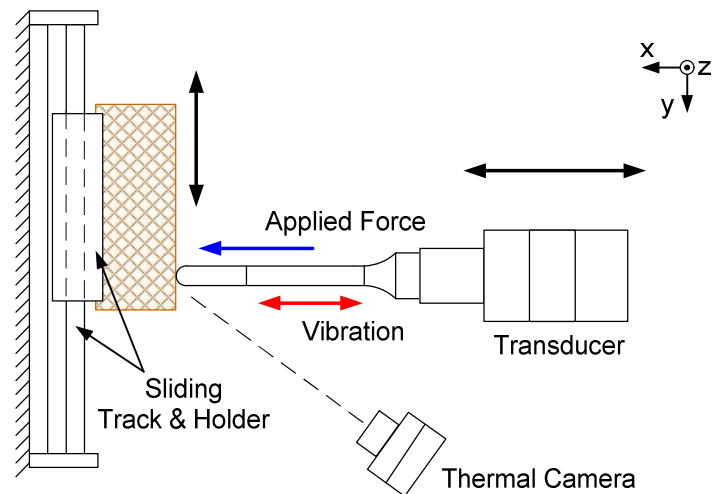
**Table 5.17 Correlation Coefficients and Average Temperature**



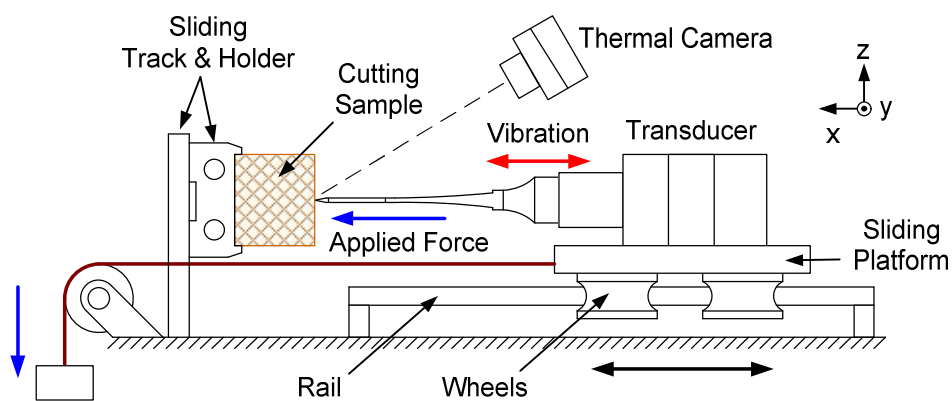
**Figure 5.56 Internal Temperature vs. Cutting Depth & Time**

### 5.3.5.2 Test II: Ultrasonic Cutting of Biomechanical Samples under Slide Motion

A sliding motion was introduced in Test II. The test used a rig which resembled the one in Test I except that it was assembled with a sliding holder driven by an electrical motor, as illustrated in Figure 5.57 and Figure 5.58. In this test, the cutting sample was fixed on the sliding holder with a load applied on the blade in the same way as Test I. During ultrasonic cutting, instead of allowing the blade to cut into the sample freely, the sample was moved at a constant speed, resulting in an incision on its surface. This was a movement more similar to the motion repeated in normal cutting. Benefiting from sliding, Test II avoided the problems of debris accumulating at the cut site.

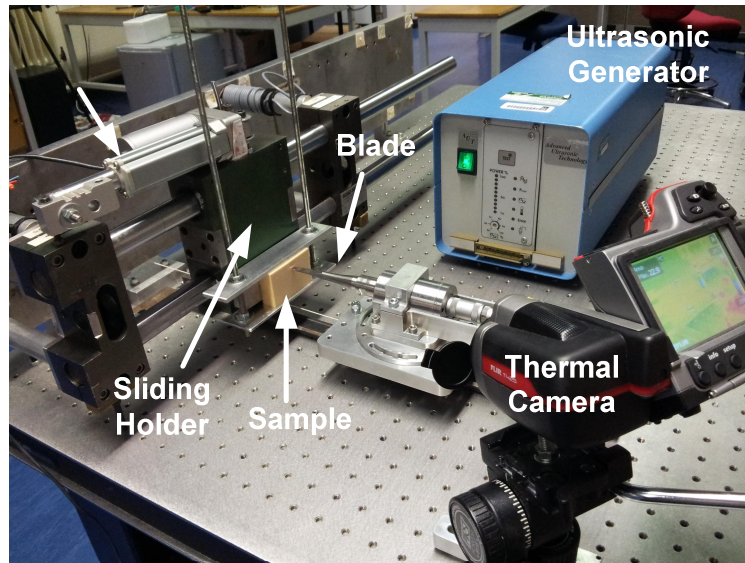


(a) Top View



(b) Side View

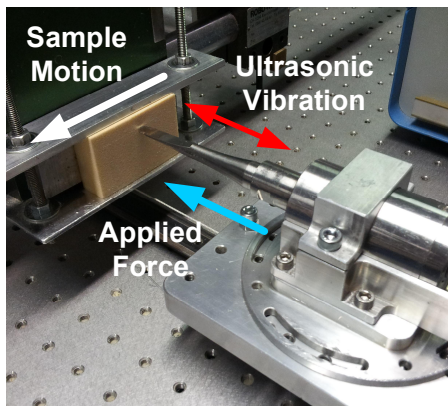
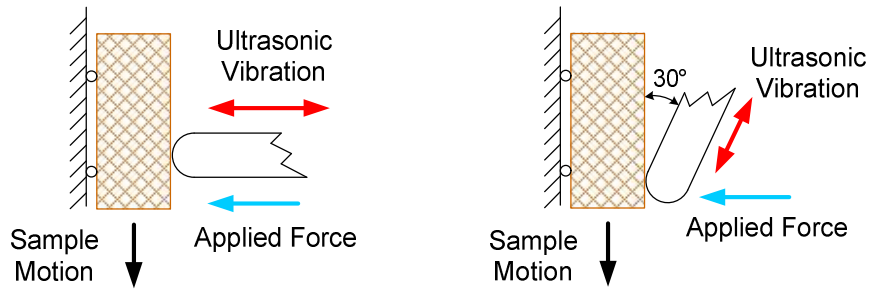
Figure 5.57 Test Rig



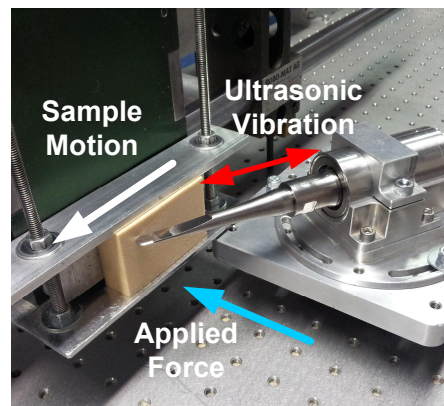
**Figure 5.58 Experimental Setup**

Ultrasonic cutting was performed in two ways, perpendicular cut and angle cut, as illustrated in Figure 5.59. Figure 5.59(a) shows the setting for perpendicular cut, where the blade was placed perpendicular to the sliding direction, allowing only the blade tip to be involved in cutting. Figure 5.59(b) illustrates the setting for angle cut, where the blade was placed at an angle of  $30^\circ$  to the sample surface, enabling the involvement of the cutting edge in ultrasonic cutting. Particularly, for the serrated blade, this means the serrations could be used in the tests. In either way, the force was applied perpendicular to the sample surface.

All three blades, blunt, sharp and serrated, were used to cut the solid and cellular foam biomechanical materials in the test. The blades were excited by the same transducer at the same power setting which resulted in a vibration amplitude of  $40\mu\text{m}$  at the blade tip. Ultrasonic cutting was performed under a constant applied force and a sliding motion of  $0.9\text{mm/s}$ , which simulated the condition of a typical cutting action in surgical operations. Details of the cutting settings are shown in Table 5.18.



a) Perpendicular Cut



b) Angle Cut

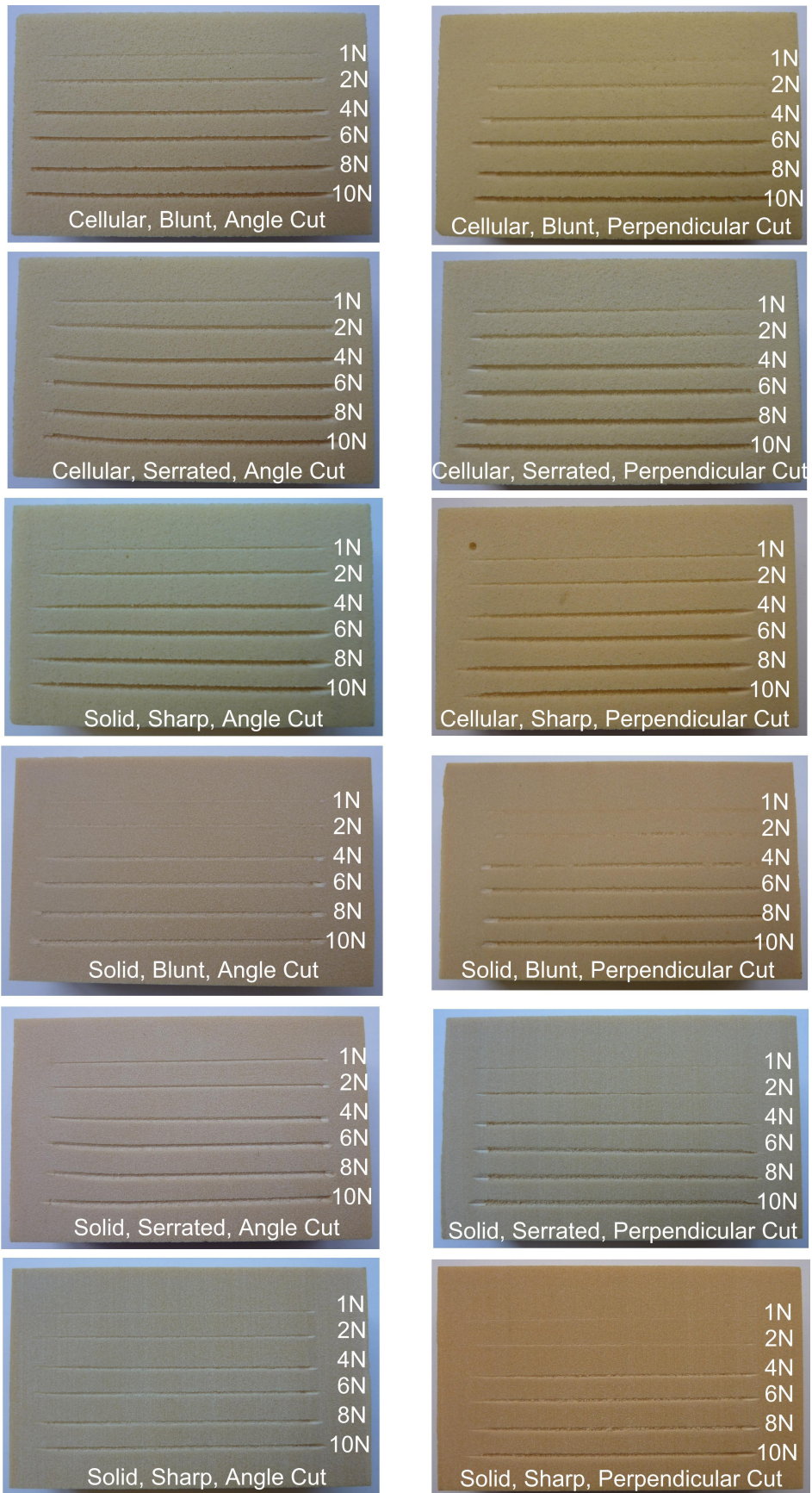
Figure 5.59 Cutting Setting

Item	Value / Remark
Cutting Sample	Biomechanical Material, Solid Foam and Cellular Foam
Cutting Blade	Blade III (serrated), Blade IV (sharp) and Blade V (blunt)
Cutting Style	Perpendicular Cutting, 30° Angle Cutting
Applied Force	1N, 2N, 4N, 6N, 8N, 10N
Sliding Speed	0.9mm/s
Sliding Distance	65mm

Table 5.18 Cutting Settings

The incisions made by different blades under different cutting settings are illustrated in Figure 5.60. The depth of the incisions varied between 0.3mm-2.5mm. The depth achieved in cellular foam was significantly higher than their counterparts in solid foam, and for both materials, cutting depth increased with force. In the cases of angle cuts, where serrations could be involved in the cutting, incisions were notably deeper than those cut by the other blades, suggesting that improved cutting performance was achieved by the serrated blade. This was also confirmed by repeating the ultrasonic cutting manually, which again saw enhanced cutting effects using the serrated blade.

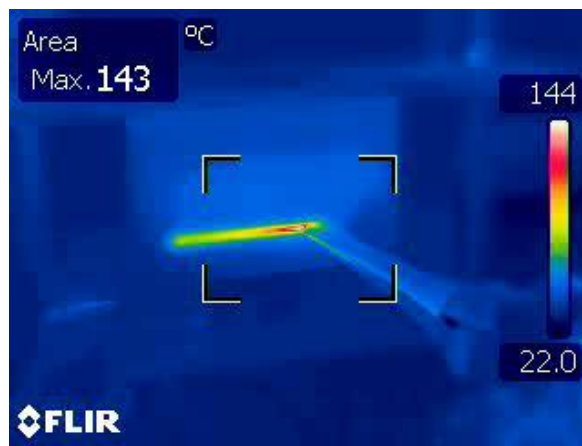




**Figure 5.60 Incisions under Different Cutting Settings**



Similar to Test I, the temperature around the cutting site was measured by a thermal camera focusing on the cutting spot, as shown in Figure 5.57 and Figure 5.61. As the cutting depth was low comparing to the size of the blade, the blade tip, which contacted with the sample in cutting, was visible to the thermal camera. Also as the sliding motion avoided debris accumulation in cutting, there was less chance that the view of the cutting site was blocked by the debris. Therefore it is expected that Test II allowed an improved temperature measurement for ultrasonic cutting. The maximum temperature measured around the cutting site was recorded for each test and was referred to as the surface temperature.



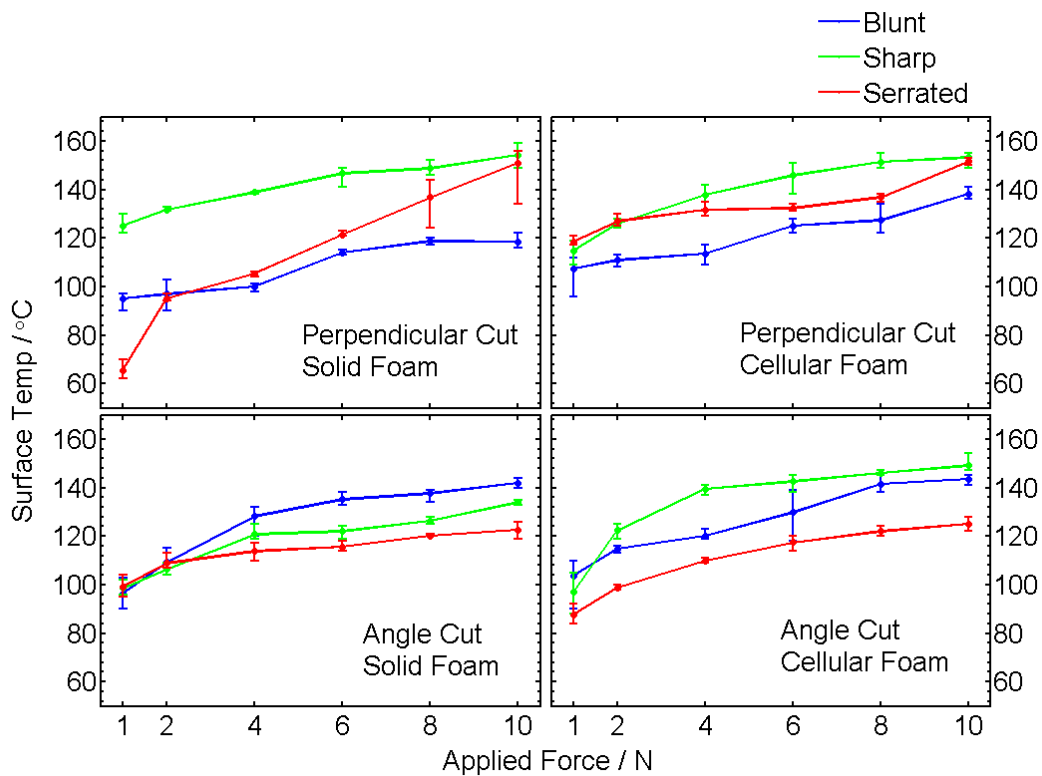
**Figure 5.61 Cutting Temperature Measurement**

The surface temperatures obtained for different cutting settings are illustrated in Figure 5.62. Each cutting test was repeated five times with the same settings. The maximum and average standard deviation of the temperature data for all tests was  $9.5^{\circ}\text{C}$  and  $2.8^{\circ}\text{C}$ , respectively, and the relative error was 1.2%-3.8%, which showed that the measurement errors were lower than the case of Test I.

The highest surface temperature observed in the cutting was  $159^{\circ}\text{C}$ , and the lowest was  $62^{\circ}\text{C}$ . Figure 5.62 illustrates that under the same cutting setting, the temperature increased as the applied force was increasing. The correlation coefficient between the temperature and the applied force was calculated and shown in Table 5.19. The coefficients were greater than 0.9 in all tests, except for the case of angle cut performed by sharp blade on cellular foam, where the coefficient was 0.871. This suggested a significant positive linear correlation between the applied force and the surface temperature. Therefore, a linear model

$$T=aF+b \quad (5.7)$$

was used to characterise the relationship between these two variables, where  $T$  is the surface temperature ( $^{\circ}\text{C}$ ),  $F$  is the applied force (N),  $a$  and  $b$  are parameters of the model. Parameter  $a$  and  $b$  were estimated using the method of least squares and their values are shown in Table 5.19. Parameter  $a$  is associated with the increase rate of temperature. Among the tests, both the largest increase rate and the lowest increase rate were achieved by the serrated blade. The former was  $9.00^{\circ}\text{C}/\text{N}$ , which was seen in the case of perpendicular cut on solid foam, and the latter was just  $2.11^{\circ}\text{C}/\text{N}$ , which was seen in the case of angle cut on solid foam. For all cutting settings, the temperature exceeded  $80^{\circ}\text{C}$  when the applied force was greater than 2N. This is a high temperature that could cause thermal damage in bone. For this reason, it is considered that all of the blades require the application of cooling in surgical bone cutting.



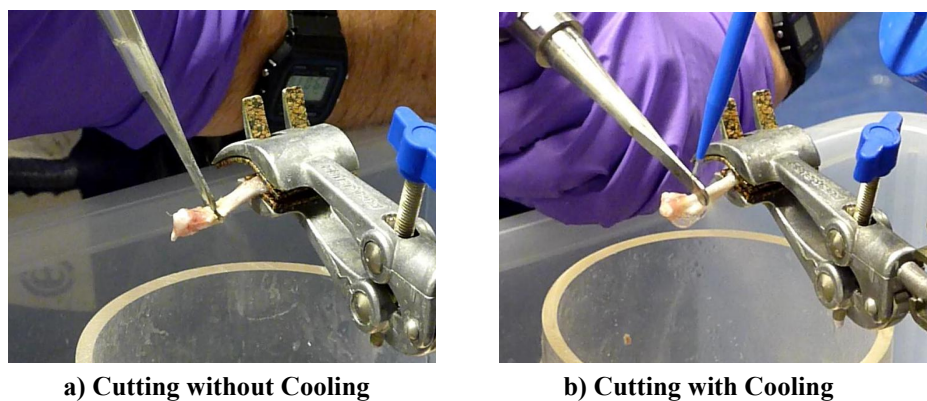
**Figure 5.62 Cutting Temperature**

Cutting Setting		Correlation Coefficient	Model Parameter	
Angle/Material	Blade		<i>a</i>	<i>b</i>
Perpendicular Solid Foam	Blunt	0.909	2.76	93.0
	Sharp	0.949	2.77	126.1
	Serrated	0.980	9.00	67.8
Perpendicular Cellular Foam	Blunt	0.928	3.36	102.1
	Sharp	0.925	4.17	115.6
	Serrated	0.934	2.85	118.3
Angle Cut Solid Foam	Blunt	0.919	5.00	99.2
	Sharp	0.955	3.69	98.8
	Serrated	0.913	2.11	103.3
Angle Cut Cellular Foam	Blunt	0.922	4.23	102.3
	Sharp	0.871	5.02	106.6
	Serrated	0.930	3.96	88.7

**Table 5.19 Correlation Coefficients and Model Parameters**

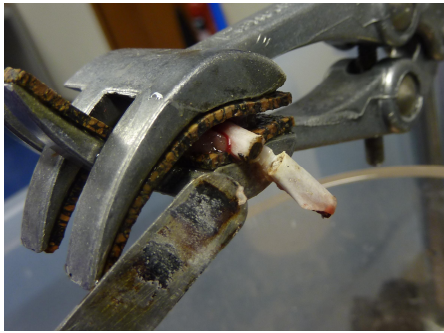
### 5.3.5.3 Test III: Ultrasonic Bone Cutting Test

Test I and Test II investigated the blade performance using biomechanical samples. Due to the nature of the material, the samples could not fully replicate the properties and reveal the behaviour of real bones in cutting tests. In view of this, Test III was conducted on fresh animal bones. For the reason of sample availability, cutting was performed on bones taken from rat legs, which were freshly prepared a few hours before the experiment. All three blades shown in Figure 5.47 were used in the cutting tests.



**Figure 5.63 Ultrasonic Cutting of Rat Bones**

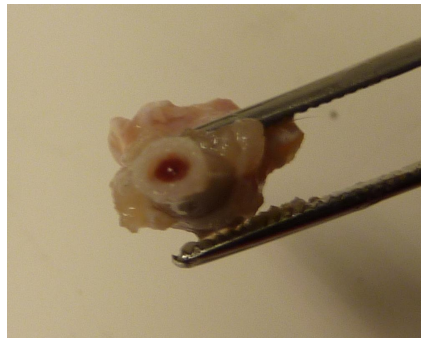
As illustrated in Figure 5.63, a rat bone was clamped in a holder and ultrasonic cutting was performed manually. All the blades were excited using the same power setting as in Test II. To compare the cutting effects, tests were carried out in two ways: without cooling and with cooling. Figure 5.63(b) illustrates applying cooling during cutting. Water at room temperature was guided by a pipe and ejected directly at the cutting site. This also helped to wash away the debris generated at the cutting site.



**a) Without Cooling**



**b) With Cooling**



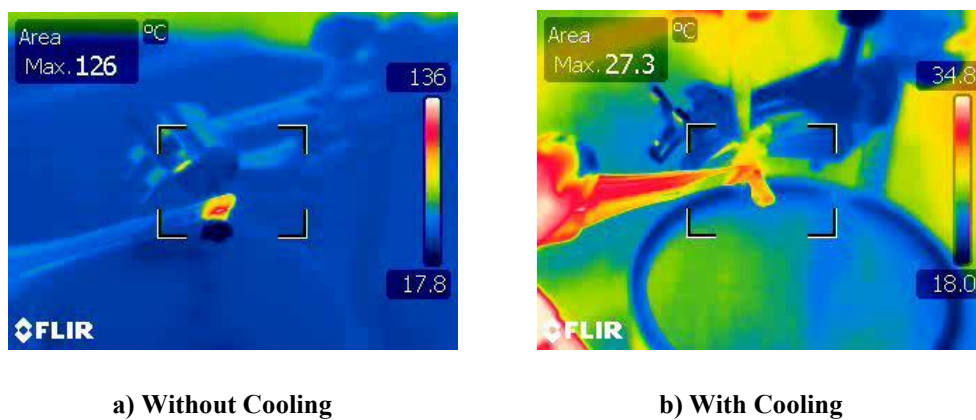
**c) Cross Profile of Sample Cut with Cooling**

**Figure 5.64 Bone Samples after Cutting**

All of the blades performed ultrasonic cutting smoothly and effectively with very low force required. Enhanced cutting performance was found in the serrated blade. The cutting was faster yet as smooth as other blades. For all blades, some smoke was emitted when no cooling was applied during cutting, indicating high cutting temperatures. The bones were inspected after cutting, which showed notable burning around the incision. Figure 5.64(a) illustrates the condition of the bone cut by the blunt blade. It clearly shows the occurrence of heat damage on the bone that should be avoided in surgical applications.

This problem was improved significantly when cooling was applied. The coolant eliminated the smoke, resulting in a clean and smooth cut with no sign of burning, as

shown in Figure 5.64(b) and Figure 5.64(c). This was observed in the case of all blades. The temperature of the bone was measured by a thermal camera during the cutting. Figure 5.65 shows thermal image from a test using the serrated blade. When no cooling was applied, the cutting temperature reached over 100°C, as illustrated in Figure 5.65(a). However, when cooling was applied, as shown in Figure 5.65(b), the temperature at the cutting site was kept around room temperature. Similar results were observed in the case of the blunt and sharp blades. This test confirmed that the fabricated blades were able to deliver satisfactory cutting performance as long as cooling was applied.



**Figure 5.65 Temperature Measurement (Serrated Blade)**

### 5.3.6 Summary

Section 5.3 presented the application of the optimal design method and the tests of three ultrasonic blades. The optimal method was applied to design a serrated blade with an attempt to deliver a solution aimed at low material stress, adequate modal distance and blade gain. Based on the performance indicators introduced in Chapter 5, the optimisation was carried out using an exhaustive algorithm and a graphic method. The designs in the optimisation space were evaluated, and the disqualified designs were filtered out. The optimal design, Blade III, was obtained by applying the optimal target, which selected the design with the lowest stress.

The obtained solution was considered to be the optimal result in terms of the defined performance. However, the optimal target and constraints concerned in this study only focused on the dynamic characteristics of a blade. Other performance indicators such

as heat generation and cutting efficiency were not taken into account in the optimisation.

Blade III was manufactured and tested. Although it was not possible to verify all the indicators and the optimality of the design, due to the limitation of measurement, impedance analysis and EMA confirmed that the blade exhibited the expected modal behaviour. The blade was tuned correctly with sufficient gain and the working mode was appropriately frequency separated from other undesired modes. It worked stably and performed ultrasonic cutting effectively. This showed that the blade was successfully designed using the optimal design method.

Two more blades (Blade IV and Blade V) were fabricated by replacing the serrations of Blade III with sharp and blunt edges respectively, aiming to compare the influence of the cutting edges. The tests conducted using these blades are summarised in Table 5.20.

	<b>Cutting Blades</b>	<b>Remark</b>
Test I	Blade V	Ultrasonic cutting of biomechanical samples under static load.
Test II	Blade III, IV and V	Ultrasonic cutting of biomechanical samples under sliding motion.
Test III	Blade III, IV and V	Ultrasonic cutting of rat leg bones.

**Table 5.20 Ultrasonic Cutting Tests**

Test I showed that there is a positive linear correlation between the applied force and the cutting speed under the same cutting angle and on the same cutting sample. A linear model was applied to characterise this relationship and the model parameters were evaluated using the test data. The test confirmed that under the same cutting angle and applied force, the highest cutting speed was achieved in cellular foam, where the material strength is low, and the lowest speed was seen in solid foam, where the material strength is high. However, no conclusion was drawn for the relationship between the cutting angle and the cutting speed. Test I also measured the temperature around the cutting site using a thermocouple and a thermal camera.

Average temperatures of over 100°C were seen in most tests, which suggested that the blade is not suitable for bone cutting without the application of cooling.

Test II introduced sliding motion in ultrasonic cutting. Notably deeper incisions were made by the serrated blade under the same cutting setting, which showed that the serrations enhanced the cutting performance. Measurement of the temperature around the cutting site identified a positive linear correlation between the applied force and the surface temperature under the same cutting settings, which was characterised using a linear model. For all blades, temperatures over 80°C were observed when the applied force was larger than 2N. This suggested that all three blades require the application of cooling in ultrasonic bone cutting.

The cutting performance of the blades was further tested in Test III using fresh rat bones. All blades achieved effective cutting in the tests without the requirement of large applied force. The tests confirmed again that the serrations enhanced the cutting. For all blades, although high temperature and notable burning were seen on the bone when no cooling was applied, the cutting was satisfactory when cooling was applied. This showed that the blades were designed with the desired performance.

## 5.4 Discussion

This chapter presented the design and tests of five ultrasonic bone cutting blades, among which Blade I and Blade II were designed using the conventional method, Blade III was designed using the proposed optimal method, and Blade IV and Blade V were fabricated based on the design of Blade III by incorporating cutting edges of different shapes. Table 5.21 summarised the basic information of these blades.

	<b>Cutting Edge</b>	<b>Design Method</b>
Blade I	Sharp	Conventional
Blade II	Serrated	Conventional
Blade III	Serrated	Optimal
Blade IV	Sharp	Same profile as Blade III
Blade V	Blunt	Same profile as Blade III.

**Table 5.21 Ultrasonic Blades**

The design of Blade I and Blade II showed that evaluating the dynamic and vibration characteristics of an ultrasonic blade is of great importance in the design process. The characteristics concerned in this study include vibration modes, gain and stress, which were also the basis of the concept of performance indicators in the optimal design method. The vibration modes, especially the working mode, determine whether a blade can be excited properly for ultrasonic cutting, and were investigated in the design using EMA verified FEA. As both Blade I and Blade II were designed using the conventional method, it relied on the designer to adjust the working mode to the correct frequency by modifying the blade profile repeatedly. The frequency separation between the working mode and non-working modes was given consideration in the design. It is expected that the influence of the non-working modes on the working mode can be minimised by allowing sufficient frequency separation between the working and non-working modes. The EMA and cutting tests of Blade I showed that this strategy was effective. No modal interaction was observed for the working mode in EMA and the blade worked stably in ultrasonic cutting.

Stress analysis was another important part of the design, whose aim was to ensure the blade has adequate strength to work reliably in ultrasonic cutting. As an ultrasonic blade is subjected to high frequency periodic deformation in cutting, material fatigue was considered more likely to cause blade failure. For this reason, this study proposed a strength criterion based on the material fatigue limit. Although it is more conservative than the criterion using the tensile strength, the successful cutting tests of Blade I and the failure of Blade II suggested that it is an effective criterion.

As Blade I and Blade II were designed using the conventional design process, the main job of the design was to adjust the characteristics of the blade by modifying its geometry, especially the lengths of the blade sections, until a satisfactory design is obtained. This is a procedure heavily relying on the designer's experience and intuition. Also it was a challenge to optimise the modal frequencies and minimise the blade stress at the same time. This demonstrated that there is a need to further improve the conventional design method.

Blade III was designed using the proposed optimal design method. The introduction of blade performance indicators and the implementation of the optimal design method are major contributions of this study. The performance indicators are the basis of the



optimal design method as they serve as the bridge between the real world problem and the mathematical algorithm. Three types of performance indicators, the modal distance, maximum stress and gains, were used. They were considered to be capable of evaluating the main vibration characteristics of Blade III as their basic principles are similar to the analysis method applied in the design of Blade I and Blade II. The optimisation constraints and the objective function represented using the performance indicators are in fact a mathematical abstraction of a blade design concept. This study demonstrated that formulating the design problem of an ultrasonic blade using this abstraction allows the optimisation algorithms to implement the design process in a way that reflects the designer's expectations and requirements.

The basic principle of the design of Blade III was to maximise the overall performance of the blade through the optimisation of vibration characteristics measured in terms of performance indicators. This was implemented using a process including evaluating indicators, filtering out disqualified designs and selecting the optimal candidate. The optimisation was carried out on the basis of three adjustable geometry parameters using an exhaustive algorithm. However, it is possible to extend this by including more adjustable geometry parameters to improve the flexibility of design, and applying other optimisation algorithms to increase computing efficiency.

The calculation of indicators is the most time consuming procedure in the optimal design process. As a large number of designs are examined in the optimisation, performing thorough analysis on every single design can require a considerable amount of time. Although in the case of Blade III all performance indicators were calculated using FEA, it is also possible to compute the tuned frequency, modal distance and gains, using the analytical model introduced in Chapter 3, which is faster than FEA as its calculation is based on a one-dimension model instead of a 3D meshed FE model. Using the analytical model to quickly filter out disqualified designs before performing detailed FEA can be a feasible solution to reduce the total computing time without compromising the accuracy of analysis, especially when the searching space of optimisation is large.

Although the cutting performance of Blade III was not directly optimised in the design process, it was studied by comparing the cutting effects between different cutting edges. Three types of cutting edges, blunt, sharp and serrated, were studied.

The tests of Blade IV and Blade V showed that altering the cutting edges did not result in significant changes in the blade vibration characteristics. This suggested that, on the basis of the optimised design, the optimisation of the cutting performance can be further carried out by selecting the cutting edges that fit the most for a specific application. Cutting tests using biomechanical samples and fresh rat bones showed that enhanced cutting was achieved by the serrated blade. However, as cutting debris can adhere to the serrations, the serrated cutting edge may bring about difficulties for post-surgery sterilisation. This disadvantage is less significant in blunt and sharp blades. The blunt blades can further benefit from low maintenance requirements as the wearing has less influence on the shape of its cutting edges.

This study showed that the proposed optimal design method is an effective approach to design ultrasonic bone cutting blades. Comparing with the conventional design method, this method can improve the quality of design as it applies performance indicators and optimisation algorithms rather than the designer's experience and intuition in the design process, which makes it possible to find the solution with the most desired performance from a large number of candidate designs. Defining the right performance indicators and applying appropriate constraints according to the design requirements are crucial to the optimisation. The performance indicators proposed in this study were demonstrated to be effective, although they focused only on the dynamic characteristics of an ultrasonic blade. However, using similar principles, other types of performance indicators can be constructed to evaluate other characteristics of interest. Moreover, although the optimal design method is proposed for ultrasonic blades, it is also applicable for other ultrasonic devices, such as horns and dies, as long as appropriate performance indicators are applied.

# Chapter 6

## Conclusions and Further Work

The research carried out within this thesis focused on the modelling and design of ultrasonic bone cutting blades. The aim of the modelling was to better understand the dynamic characteristics of ultrasonic blades and provide useful information for the design and application of ultrasonic bone cutting devices. The thesis proposed a non-coupled analytical model, two coupled analytical models and an optimal design method. Five ultrasonic blades were designed, manufactured and tested. The advances and innovations made during the research are summarised in the following sections.

### 6.1 Conclusions

#### 6.1.1 Analytical Modelling of Ultrasonic Blades

##### (1) Modelling of Non-coupled Vibration

Four modes of vibration in ultrasonic blades, including longitudinal oscillation, flexural bending, lateral bending, and torsional vibration, were modelled based on non-coupled one-dimensional theories. It is assumed that these modes of vibration are independent of each other and no interaction occurs between them, which enabled vibration modelling with respect to each mode of vibration. Based on the one-dimensional theories, the profile of the ultrasonic blade was represented using shape functions with a single variable, allowing a straightforward and concise way of vibration study. The obtained models were second order partial differential equations for longitudinal and torsional vibration, and fourth order partial differential equations for flexural and lateral bending vibration. They were further formulated into a natural modal frequency problem and a mode shape function problem using finite difference method, which can be used to characterise the modal behaviour of an ultrasonic blade.

Through the case study of a uniform beam and an ultrasonic cutting blade, it is showed that this analytical modelling method (referred to as AM) was able to predict the longitudinal and bending modal frequencies with satisfactory accuracy. The average difference of modal frequencies between AM and EMA was 3.6% in the case of uniform beam and 4.4% in the case of ultrasonic blade, which suggested that AM

can be used as an alternative method to FEA to compute the modal frequencies of ultrasonic blades. As AM applies a one-dimensional model in the calculation, AM can be used for quick performance estimation in the early stage of the design process without constructing and meshing a 3D FE model. It can also be used to reduce the computing time for applications dealing with a large number of designs.

## **(2) Modelling of Coupled Vibration**

Two models, a parametric vibration model and a longitudinal-bending coupled vibration model, were proposed to investigate the coupled vibration of ultrasonic blades. The parametric vibration model formulated the motion of a lumped mass beam in a four degree of freedom space using a one-dimensional structure. Such a system was able to exhibit coupled bending and torsional motion under a longitudinal excitation as a result of its slender shape and the effect of the lumped end mass. The interaction mechanism between these motions was obtained through the geometry restrictions of the structure, such as the relationship between the curvatures and displacements, whereby the governing equations of vibration were derived by means of Lagrangian dynamics. Although the parametric vibration and modal coupling behaviour was formulated using a system of relatively simple structure, this model resulted in governing equations of considerable complexity for which closed form solutions are unlikely to be obtained. Apart from that, due to the geometry difference between a beam with lumped mass and a structure of tapered profile, difficulties may arise when determining the necessary parameters for the model. For this reason, it is more appropriate to use this model for the purposes of theoretical study instead of performance prediction.

In addition, the longitudinal-bending coupled model was proposed with an attempt to understand a type of coupled vibration that is commonly observed in ultrasonic blades of beam-like profile. Similar to the non-coupled vibration models, the application of one-dimensional theories allowed a relatively straightforward form of modelling. Based on the assumption that the longitudinal motion is normally much stronger than the bending vibration, the coupled vibration problem was simplified by ignoring the effects that bending exerts on the longitudinal motion. As a result, the longitudinal motion was free from coupling and the bending vibration was modelled by

introducing an extra rotation moment. This resulted in a fourth order time-dependent partial differential equation, which is in effect a parametric vibration system.

The model can be solved using two numerical iteration approaches, namely the 11-point and 27-point stencil method respectively. The error analysis confirmed that for both methods, it is possible to keep the truncation error within an acceptable range by applying proper calculation parameters, including the spatial step and the computing time interval. The 27-point stencil has an improved accuracy over the 11-point stencil, though its iteration equation is of more complicated form. The case study of a uniform beam showed that the proposed model provides an approach to study the interaction between the longitudinal and bending vibration in ultrasonic blades.

### **6.1.2 Proposal of the Optimal Design Method**

An optimal design method was proposed to improve the conventional design process of ultrasonic blades. The basic concept of this method was to use mathematical algorithms instead of designers' experience and intuition to update and optimise blade designs during the design process. This can improve the design quality by making sure the most desired characteristics are achieved. The main innovation of this method is the introduction of blade performance indicators, which bridges the real world design problem and the mathematical algorithms. Four kinds of indicators were defined in this study: the frequency based, gain based, displacement based and stress based indicators, which were classified according to their nature. They characterise the typical dynamic features that are of interest in the design of ultrasonic blades. Apart from them, it is possible to define other types of performance indicators using the concepts proposed in this study.

The process of the optimal design method is to maximise the blade performance through the optimisation of the performance indicators. This can be done in three major stages: formulation, optimisation and verification. The implementation of the method was detailed based on the proposed indicators. A software toolkit which enabled the application of the method in design applications was developed using Abaqus script interface and Python language, which offers functions including blade model generating, indicator computing and extracting, and optimisation control. Specific optimisation algorithms were not implemented in this toolkit. Instead, an

interface was provided to allow algorithm embedding in a later stage of the application.

### **6.1.3 Design of Ultrasonic Bone Cutting Blades**

Five ultrasonic bone cutting blades were designed in this thesis. Blade I and Blade II were designed using the conventional method, Blade III was designed using the optimal design method, Blade IV and Blade V were made based on the same design of Blade III by incorporating different cutting edges.

The modal behaviour and material stress were major concerns in the designing of Blade I and Blade II, which were investigated using EMA verified FEA. The impedance analysis and EMA showed that both blades were designed with the expected vibration characteristics. Blade I worked stably and Blade II failed in the cutting test as predicted due to insufficient strength. Cutting tests of Blade I confirmed that the blade was capable of performing ultrasonic cutting on biomechanical material and ovine femur. Clear incisions were made on both materials. However, high temperature was measured at the cutting site and burning was observed in the incision of ovine femur, which implied that Blade I was not suitable for use in surgical applications without the application of cooling. This study suggested that the modal analysis and the stress criterion applied in the design were effective, and a satisfactory blade design can be achieved by making sure the desired dynamic characteristics are obtained.

The optimal design method proposed in this research was applied to design Blade III with an attempt to deliver a solution aimed at low material stress, adequate modal distance and blade gain. Six performance indicators were used to evaluate the dynamic characteristics of the blade, and the optimisation was carried out using an exhaustive algorithm and a graphic method. The impedance analysis and EMA showed that the blade exhibited the expected modal behaviour. The blade was tuned correctly with sufficient gain and modal distance. It worked stably and performed ultrasonic cutting effectively. Although it was not possible to verify all indicators and the optimality of the design, due to the limitation of measurement, the case of Blade III confirmed that ultrasonic blades with satisfactory performance can be designed effectively using the proposed optimal design method.

Blade IV and Blade V were fabricated based on the same design of Blade III by replacing the serrations with sharp and blunt edges respectively, which enabled the comparison of cutting performance between different cutting edges. The tests of Blade IV and Blade V showed only insignificant changes in the vibration characteristics of the blades, suggesting that the optimisation of cutting performance can be further carried out on the basis of an optimised design by selecting the cutting edges that fit the most for a specific application.

Blade III, Blade IV and Blade V were subjected to ultrasonic cutting tests. The tests performed under static load showed that there is a positive linear correlation between the applied force and the cutting speed under the same cutting angle and cutting sample, which was characterised using a linear model. Although no conclusion was drawn for the relationship between the cutting angle and the cutting speed, the tests confirmed that under the same cutting settings higher cutting speed can be achieved in lower strength material. In terms of cutting temperature, average internal and surface temperatures over 100°C were measured in most tests.

The depths of incisions made by different cutting edges under the same cutting settings were compared in the ultrasonic cutting tests performed under sliding motion, which showed that enhanced cutting performance was achieved by the serrated blade. A positive linear correlation between the applied force and the surface temperature around the cutting site was identified and characterised using a linear model. For all blades, temperatures over 80°C were observed when the applied force was larger than 2N, which suggested that these blades require the application of cooling in ultrasonic bone cutting.

Ultrasonic cutting tests performed on fresh rat bones confirmed again that the serrations enhanced the cutting effects. However, as cutting debris can adhere to the serrations, the serrated edges may bring about difficulties for post-surgical sterilisation. For all three blades, although high temperature and notable burning were seen on the bone when no cooling was applied, the incisions were clear and satisfactory cutting was achieved when cooling was applied. As a conclusion, the tests showed that these blades were successfully designed with the expected performance.

## **6.2 Further Work**

The following recommendations are suggested to further expand the work of this thesis.

### **(1) Application of the Non-coupled Analytical Model**

Although the non-coupled analytical model was proposed and studied using the case of a uniform beam and an ultrasonic blade, the model was not applied in the design process of ultrasonic blades. However, it is possible to use this model as a fast predictor in either the conventional or the optimal design method. In addition, more works are needed to further study the accuracy of this model, especially when modelling ultrasonic devices with complex profile.

### **(2) Improving the Longitudinal-Bending Coupled Analytical Model**

The longitudinal-bending coupled analytical model ignored the coupling effects of the longitudinal vibration by assuming that the longitudinal vibration is significantly stronger than the bending motion. Although this simplified the derivation, it may not be a satisfactory approximation in certain cases. An option to improve this is to take into account the coupling effects in both longitudinal and bending vibration. In addition, to apply this model for design applications, more research is needed to address the problems such as determination of the initial bending state, incorporation of damping, and convergence of the calculation.

### **(3) Research of Performance Indicators**

The performance indicators proposed in this thesis focused only on the main dynamic characteristics of ultrasonic blades. However, it is usually of great interest to understand and optimise other performance in the design process of a blade, such as heat generation and cutting efficiency. Therefore, more research can be addressed on constructing other types of performance indicators to enable more control over the blade performance in the design.

### **(4) Optimisation of Ultrasonic Blades**

This study demonstrated the effectiveness of the optimal design method through the design and tests of an ultrasonic blade. The design was a simplified case where only



three free geometry parameters were considered, which allowed the application of an exhaustive algorithm and a graphic method to demonstrate the optimisation. For more complicated design problem, it is recommended to increase the number of free geometry parameters to allow more flexibility of design and apply appropriate optimisation algorithms to improve the efficiency of computing. In addition, although the method was proposed for ultrasonic cutting blades, the optimal design method can be further extended for the design of other ultrasonic devices, such as horns and transducers, by formulating the design concept properly and applying the appropriate performance indicators.

### **(5) Incorporating Bone in Modelling**

This research focused on the behaviour of ultrasonic blade only. However, as ultrasonic bone cutting is a complex process involving both the blade and bone, modelling the blade only would not provide sufficient information for the optimisation of the entire cutting process and cutting effects. Therefore it is suggested that the bone can be incorporated in the analysis in future research. This would enable the calculation of heat generation and cutting efficiency through simulation, and also allow the optimisation of the blade design with respect to the whole cutting system and specific surgical application.

### **(6) Cooling and Irrigation**

As suggested in the cutting experiments, for practical surgical applications, the ultrasonic blades should be working with the application of appropriate cooling. One possible solution would be integrating irrigation system in the blade design, for example adopting a design with built-in irrigation guide and nozzle. Further research can be devoted to the design of such irrigation facility inside the blade, and study the influence of the introduced structure on the blade vibration.

# Appendix

## A.1 Undetermined Coefficient Method

The method of undetermined coefficient can be used to derive the finite difference approximation for a differential expression based on a set of given points [135]. The basic idea of this method is to assign an undetermined coefficient for each term of the difference approximation. Using Taylor series to expand these terms, these coefficients can be determined by comparing the similar items to the original differential expression.

Suppose  $f(x)$  is approximated based on  $f(x+2h)$ ,  $f(x+h)$ ,  $f(x)$ ,  $f(x-h)$ , and  $f(x-2h)$ , of the form

$$D(f) = a_1 f(x+2h) + a_2 f(x+h) + a_3 f(x) + a_4 f(x-h) + a_5 f(x-2h) \quad (7.1)$$

Expanding each term in the right side of Eq. (7.1) using Taylor series yields

$$f(x+h) = f(x) + hf'(x) + \frac{1}{2}h^2 f''(x) + \frac{1}{6}h^3 f'''(x) + \frac{1}{24}h^4 f''''(x) + O(h^5) \quad (7.2)$$

$$f(x-h) = f(x) - hf'(x) + \frac{1}{2}h^2 f''(x) - \frac{1}{6}h^3 f'''(x) + \frac{1}{24}h^4 f''''(x) + O(h^5) \quad (7.3)$$

$$f(x+2h) = f(x) + 2hf'(x) + 4h^2 f''(x) + \frac{4}{3}h^3 f'''(x) + \frac{2}{3}h^4 f''''(x) + O(h^5) \quad (7.4)$$

$$f(x-2h) = f(x) - 2hf'(x) + 4h^2 f''(x) - \frac{4}{3}h^3 f'''(x) + \frac{2}{3}h^4 f''''(x) + O(h^5) \quad (7.5)$$

By applying Eq. (7.2)-(7.5) into Eq. (7.1) one obtains

$$\begin{aligned} D(f) &= (a_1 + a_2 + a_3 + a_4 + a_5)f(x) + (2a_1 + a_2 + a_3 - a_4 - 2a_5)hf'(x) \\ &+ (4a_1 + \frac{1}{2}a_2 + a_3 + \frac{1}{2}a_4 + 4a_5)h^2 f''(x) + (\frac{4}{3}a_1 + \frac{1}{6}a_2 + a_3 - \frac{1}{6}a_4 - \frac{4}{3}a_5)h^3 f'''(x) \\ &+ (\frac{2}{3}a_1 + \frac{1}{24}a_2 + a_3 + \frac{1}{24}a_4 + \frac{2}{3}a_5)h^4 f''''(x) + O(h^5) \end{aligned} \quad (7.6)$$

To use Eq. (7.6) as an approximate of  $f(x)$ , the following equations should be satisfied

$$a_1 + a_2 + a_3 + a_4 + a_5 = 0 \quad (7.7)$$

$$(2a_1 + a_2 + a_3 - a_4 - 2a_5)h = 1 \quad (7.8)$$

$$(4a_1 + \frac{1}{2}a_2 + a_3 + \frac{1}{2}a_4 + 4a_5)h^2 = 0 \quad (7.9)$$

$$(\frac{4}{3}a_1 + \frac{1}{6}a_2 + a_3 - \frac{1}{6}a_4 - \frac{4}{3}a_5)h^3 = 0 \quad (7.10)$$

$$(\frac{2}{3}a_1 + \frac{1}{24}a_2 + a_3 + \frac{1}{24}a_4 + \frac{2}{3}a_5)h^4 = 0 \quad (7.11)$$

This yields

$$a_1 = -\frac{1}{12h}, a_2 = \frac{2}{3h}, a_3 = 0, a_4 = -\frac{2}{3h}, a_5 = \frac{1}{12h} \quad (7.12)$$

Therefore Eq. (7.1) can be written as

$$D(f') = \frac{1}{12h}[-f(x+2h) + 8f(x+h) - 8f(x-h) + f(x-2h)] \quad (7.13)$$

From Eq. (7.6) it can be seen that the truncation error of this approximation is of  $O(h^5)$ . Similarly, it is also possible to use other sets of points to approximate other derivatives or differential expressions.

## A.2 Selected Matlab Script for One Dimensional Analytical Modelling

```

% This function calculates the moment inertia vector of
the structure
function Ia=XMomentInertia(x)
    h=Thickness(x);
    Ia=x;
    [a,b]=size(x);

    pi=3.1415926545;
    % Geometric parameters La, Lb, Lc, Ld, Le, h1, h2, D1,
    D2 defined

    for j=1:a
        for i=1:b
            if x(j,i)>C
                Ia(j,i)=h(j,i)^3*sqrt(D2^2-
                h(j,i)^2)/16+(D2^4*asin(h(j,i)/D2)-
                D2^2*h(j,i)*sqrt(D2^2-h(j,i)^2))/32;
            else
                Ia(j,i)=pi*h(j,i)^4/64;
            end
        end
    end
end

```

```

% This function calculates the cross section area vector
of the structure
function S=CrossSecArea(x)
    h=Thickness(x);
    S=x;
    [a,b]=size(x);

    pi=3.1415926545;
    % Geometric parameters La, Lb, Lc, Ld, Le, h1, h2, D1,
    D2 defined

    for j=1:a
        for i=1:b
            if x(j,i)>C
                S(j,i)=abs((h(j,i)*sqrt(D2*D2-
                h(j,i)*h(j,i))+D2*D2*asin(h(j,i)/D2)))/2;
            else
                S(j,i)=pi*h(j,i)*h(j,i)/4;
            end
        end
    end
end

```

```

% This function is used to search for the modal frequency
of the bending modes
function F=FindBModalFreq(Ix, Sa, Ea, den, L, fmin, fmax,
fstep, N, lBC, rBC)

```

```

    if N<1
        return
    end

```

```

    MSize=N+5;
    A=sparse(MSize,MSize);
    B=sparse(MSize,MSize);

```

```

    h=L/N;
    h2=L*L/(N*N);
    pi2=3.1415926545*2;
    Ia=@(k) Ix((k)*h);
    S=@(k) Sa((k)*h);

```

```

    Kn2a=@(k) Ea*Ia(k-1);
    Kn1a=@(k) -2*Ea*(Ia(k-1)+Ia(k));
    Kn1b=@(k) den*h2*Ia(k-0.5);
    Koa=@(k) Ea*(Ia(k-1)+4*Ia(k)+Ia(k+1));
    Kob=@(k) -den*h2*(Ia(k-0.5)+Ia(k+0.5)+h2*S(k));
    Kp1a=@(k) -2*Ea*(Ia(k)+Ia(k+1));
    Kp1b=@(k) den*h2*Ia(k+0.5);
    Kp2a=@(k) Ea*Ia(k+1);

```

```

    if strcmp(lBC,'Free')
        A(1,2)=1;
        A(1,3)=-2;
        A(1,4)=1;
        A(2,1)=-1;
        A(2,2)=2;
        A(2,4)=-2;
        A(2,5)=1;
    elseif strcmp(lBC,'Hinged')
        A(1,3)=1;
        A(2,2)=1;
        A(2,3)=-2;
        A(2,4)=1;
    elseif strcmp(lBC,'Float')
        A(1,2)=-1;
        A(1,4)=1;
        A(2,2)=1;
        A(2,3)=-2;
        A(2,4)=1;
    elseif strcmp(lBC,'Clamped')
        A(1,3)=1;
        A(2,2)=-1;
        A(2,4)=1;
    end

```

```

else
    disp('Left Boundary Condition Error!');
    return;
end

if strcmp(rBC, 'Free')
    A(MSize, MSize)=1;
    A(MSize, MSize-1)=-2;
    A(MSize, MSize-3)=2;
    A(MSize, MSize-4)=-1;
    A(MSize-1, MSize-1)=1;
    A(MSize-1, MSize-2)=-2;
    A(MSize-1, MSize-3)=1;
elseif strcmp(rBC, 'Hinged')
    A(MSize, MSize-1)=1;
    A(MSize, MSize-2)=-2;
    A(MSize, MSize-3)=1;
    A(MSize-1, MSize-2)=1;
elseif strcmp(rBC, 'Float')
    A(MSize, MSize-1)=1;
    A(MSize, MSize-2)=-2;
    A(MSize, MSize-3)=1;
    A(MSize-1, MSize-1)=1;
    A(MSize-1, MSize-3)=-1;
elseif strcmp(rBC, 'Clamped')
    A(MSize, MSize-1)=1;
    A(MSize, MSize-3)=-1;
    A(MSize-1, MSize-2)=1;
else
    disp('Right Boundary Condition Error!');
    return;
end

for i=0:N
    j=i+3;
    A(j, j-2)=Kn2a(i);
    A(j, j-1)=Kn1a(i);
    A(j, j)=Koa(i);
    A(j, j+1)=Kp1a(i);
    A(j, j+2)=Kp2a(i);

    B(j, j-1)=Kn1b(i);
    B(j, j)=Kob(i);
    B(j, j+1)=Kp1b(i);
end

w1=(fmin*pi2)^2;      %start frequency
w2=(fmax*pi2)^2;     %end frequency
ws=(fstep*pi2)^2;    %frequency step

H=@(x)Msign(A+x*B);

```

```

F=[];
k=0;
for w=w1:ws:w2-ws
    disp(['-->Searching at
',num2str(sqrt(w)/pi2,'%d')]);
    if (H(w)*H(w+ws)>0)           %No root here
        continue;
    end
    f=fzero(H,[w,w+ws]);
    k=k+1;
    F(k,1)=sqrt(f)/pi2;
end

```

% This function is used to search for the modal frequency of the longitudinal modes

```

function F=FindLModalFreq(Sa, Ea, den, L, fmin, fmax,
fstep, N)

```

```

F=[];

```

```

if N<1
    return
end

```

```

A=sparse(N+1,N+1);
B=sparse(N+1,N+1);
h=L/N;
pi2=3.1415926545*2;
k=0;

```

```

A(1,1)=-2*Ea;
A(1,2)=2*Ea;
A(N+1,N+1)=-2*Ea;
A(N+1,N)=2*Ea;
B(1,1)=den*h*h;
B(N+1,N+1)=den*h*h;

```

```

for i=1:N-1    %index of W
    j=i+1;    %index of matrix position
    A(j,j-1)=Ea*Sa((i-0.5)*h);
    A(j,j)=-Ea*Sa((i+0.5)*h)-Ea*Sa((i-0.5)*h);
    A(j,j+1)=Ea*Sa((i+0.5)*h);
end

```

```

for i=1:N-1    %index of W
    j=i+1;    %index of matrix position
    B(j,j)=den*Sa(i*h)*((L^2)/(N^2));
end

```

```

w1=(fmin*pi2)^2;      %start frequency
w2=(fmax*pi2)^2;      %end frequency
ws=(fstep*pi2)^2;      %frequency step

H=@(x)Msign(A+x*B);

F=[];
k=0;
for w=w1:ws:w2-ws
    disp(['-->Searching at
',num2str(sqrt(w)/pi2,'%d')]);
    if (H(w)*H(w+ws)>0)      %No root here
        continue;
    end
    f=fzero(H,[w,w+ws]);
    k=k+1;
    F(k,1)=sqrt(f)/pi2;
end

function [Y,lBy,rBy]=GetBModeShape(freq, Ix, Sa, Ea, den,
L, N, lBC, rBC)
    %Returns the modal displacements of the given
frequencies
    %Y is the displacement within the body, each row
represent a shape to the
    %frequencies in freq.
    %lBy is the left boundary displacement
    %rBy is the left boundary displacement
    %[lBy,Y,rBy] gives the displacement of the whole
structure

    if N<1
        return
    end

    h=L/N;
    h2=L*L/(N*N);
    pi2=3.1415926545*2;
    Ia=@(k)Ix((k)*h);
    S=@(k)Sa((k)*h);

    w2=(freq.*pi2).^2;
    l=length(w2);      %Number of frequencies
    MSize=N+5;
    A=sparse(MSize,MSize);
    B=sparse(MSize,MSize);
    Y=zeros(l,N+1);
    lBy=zeros(l,2);

```



```

rBy=lBy;

Kn2a=@(k) Ea*Ia(k-1);
Kn1a=@(k) -2*Ea*(Ia(k-1)+Ia(k));
Kn1b=@(k) den*h2*Ia(k-0.5);
Koa=@(k) Ea*(Ia(k-1)+4*Ia(k)+Ia(k+1));
Kob=@(k) -den*h2*(Ia(k-0.5)+Ia(k+0.5)+h2*S(k));
Kp1a=@(k) -2*Ea*(Ia(k)+Ia(k+1));
Kp1b=@(k) den*h2*Ia(k+0.5);
Kp2a=@(k) Ea*Ia(k+1);

if strcmp(lBC,'Free')
    A(1,3)=1;
    A(2,2)=1;
    A(2,3)=-2;
    A(2,4)=1;
elseif strcmp(lBC,'Hinged')
    A(1,2)=-1;
    A(1,4)=1;
    A(2,3)=1;
elseif strcmp(lBC,'Float')
    A(1,3)=1;
    A(2,2)=-1;
    A(2,4)=1;
elseif strcmp(lBC,'Clamped')
    A(1,2)=1;
    A(1,3)=-2;
    A(1,4)=1;
    A(2,3)=1;
else
    disp('Left Boundary Condition Error!');
    return;
end

if strcmp(rBC,'Free')
    A(MSize,MSize)=1;
    A(MSize,MSize-1)=-2;
    A(MSize,MSize-3)=2;
    A(MSize,MSize-4)=-1;
    A(MSize-1,MSize-1)=1;
    A(MSize-1,MSize-2)=-2;
    A(MSize-1,MSize-3)=1;
elseif strcmp(rBC,'Hinged')
    A(MSize,MSize-1)=1;
    A(MSize,MSize-2)=-2;
    A(MSize,MSize-3)=1;
    A(MSize-1,MSize-2)=1;
elseif strcmp(rBC,'Float')
    A(MSize,MSize-1)=1;
    A(MSize,MSize-2)=-2;
    A(MSize,MSize-3)=1;

```

```

        A(MSize-1,MSize-1)=1;
        A(MSize-1,MSize-3)=-1;
    elseif strcmp(rBC,'Clamped')
        A(MSize,MSize-1)=1;
        A(MSize,MSize-3)=-1;
        A(MSize-1,MSize-2)=1;
    else
        disp('Right Boundary Condition Error!');
        return;
    end

    for i=0:N
        j=i+3;
        A(j,j-2)=Kn2a(i);
        A(j,j-1)=Kn1a(i);
        A(j,j)=Koa(i);
        A(j,j+1)=Kp1a(i);
        A(j,j+2)=Kp2a(i);

        B(j,j-1)=Kn1b(i);
        B(j,j)=Kob(i);
        B(j,j+1)=Kp1b(i);
    end

    J=zeros(MSize,1);
    J(1,1)=1;
    for k=1:l
        H=A+w2(k)*B;
        [l,u,p]=lu(H);
        H=SolveLU(l,u,p,J);
        Y(k,:)=H(3:MSize-2,1)';
        lBy(k,:)=H(1:2,1)';
        rBy(k,:)=H(MSize-1:MSize,1)';
    end
end

```

*% This function calculates the mode shape for a given longitudinal modal frequency*

*function Y=GetLModeShape(freq,Sa, Ea, den, L, N)*

```

h=L/N;
p=den*L^2/N^2;
pi2=3.1415926545*2;
f=(freq.*pi2).^2;
l=length(f);
Y=zeros(l,N+1);
for k=1:l
    Y(k,1)=1;
    Y(k,2)=1-p*f(k)/2/Ea;
    for i=3:N+1

```

```

        Y(k,i)=-Sa((i-1.5)*h)/Sa((i-0.5)*h)*Y(k,i-2)...
            -(p*f(k)*Sa((i-1)*h)/Sa((i-0.5)*h)/Ea-1-
Sa((i-1.5)*h)/Sa((i-0.5)*h))*Y(k,i-1);
    end
end
end

```

### A.3 Selected Matlab Script for Longitudinal-Bending Coupled Analytical Modelling

```

function [Y,time_vec]=CoupledBending(y_n1, y_0, Ix, Sa,
Ea, den, L, Pa, t0, expand, dt, lBC, rBC, msg)
%When msg='y' or 'Y', show the calculation process.
%Y will retain maximum Maximum_Num time frames, other
frames will be discarded.
Maximum_Num=3000;           %maximum time frames

N=length(y_0)-5;
MSize=N+5;
Ha=sparse(N+5,2*MSize);
Hb=Ha;
Ca=sparse(N+5,N+5);

h=L/N;
h2=L*L/(N*N);
h4=h2*h2;
dt2=dt*dt;
pi2=3.1415926545*2;
Ia=@(k) Ix((k)*h);
S=@(k) Sa((k)*h);

Cn1=@(k) den/(h2*dt2)*Ia(k-0.5);
Co=@(k) -den/(h2*dt2)*(Ia(k+0.5)+Ia(k-0.5))-den*S(k)/dt2;
Cp1=@(k) den/(h2*dt2)*Ia(k+0.5);

An2=@(k) Ea/h4*Ia(k-1);
An1=@(k) -2*Ea/h4*(Ia(k-1)+Ia(k))+2*den/(h2*dt2)*Ia(k-0.5);
Ao=@(k) Ea/h4*(Ia(k-1)+4*Ia(k)+Ia(k+1))-
2*den/(h2*dt2)*(Ia(k+0.5)+Ia(k-0.5))-2*den*Sa(k)/dt2;
Ap1=@(k) -2*Ea/h4*(Ia(k)+Ia(k+1))+2*den/(h2*dt2)*Ia(k+0.5);
Ap2=@(k) Ea/h4*Ia(k+1);

Bn1=@(k) -den/(h2*dt2)*Ia(k-0.5);
Bo=@(k) den/(h2*dt2)*(Ia(k+0.5)+Ia(k-0.5))+den*S(k)/dt2;
Bp1=@(k) -den/(h2*dt2)*Ia(k+0.5);

%Main Matrix
for i=1:N+1
    Ha(i,i)=An2(i-1);
    Ha(i,i+1)=An1(i-1);
    Ha(i,i+2)=Ao(i-1);
    Ha(i,i+3)=Ap1(i-1);
    Ha(i,i+4)=Ap2(i-1);

    Ha(i,i+N+6)=Bn1(i-1);
    Ha(i,i+N+7)=Bo(i-1);
    Ha(i,i+N+8)=Bp1(i-1);

```

```

    Hb(i,i+1)=1/h2;
    Hb(i,i+2)=-2/h2;
    Hb(i,i+3)=1/h2;

    Ca(i,i+1)=Cn1(i-1);
    Ca(i,i+2)=Co(i-1);
    Ca(i,i+3)=Cp1(i-1);
end

pBC=Cn1(0);           %This is a factor to scale the
                      %boundary condition in order to
                      %facilitate the computing
                      %Theoratically the value of this
                      %factor will not change the result.

%Boundary Conditions
if strcmp(lBC,'Clamped')
    i=N+2;           %Zero order partial derivative equals
                    %zero [0 0 1 0 0]

    Ca(i,3)=pBC;
    i=N+3;           %First order partial derivative
                    %equals zero [-1 8 0 -8 1]

    Ca(i,2)=pBC;
    Ca(i,4)=-pBC;
else
    %Default free boundary condition
    %Second order partial derivative
    %equals zero [0 1 -2 1 0]
    i=N+2;

    Ca(i,2)=pBC;
    Ca(i,3)=-2*pBC;
    Ca(i,4)=pBC;
    i=N+3;           %Third order partial derivative
                    %equals zero [-1 2 0 -2 1]

    Ca(i,1)=-pBC;
    Ca(i,2)=2*pBC;
    Ca(i,4)=-2*pBC;
    Ca(i,5)=pBC;
end

if strcmp(rBC,'Clamped')
    i=N+2;           %Zero order partial derivative equals
                    %zero [0 0 1 0 0]

    Ca(i,MSize-2)=pBC;
    i=N+3;           %First order partial derivative
                    %equals zero [-1 8 0 -8 1]

    Ca(i,MSize-3)=pBC;
    Ca(i,MSize-1)=-pBC;
else
    %Default free boundary condition
    %Second order partial derivative
    %equals zero [0 1 -2 1 0]
    i=N+4;

    Ca(i,MSize-1)=pBC;
    Ca(i,MSize-2)=-2*pBC;

```

```

Ca(i,MSize-3)=pBC;
i=N+5;           %Third order partial derivative
                 equals zero [-1 2 0 -2 1]
Ca(i,MSize)=pBC;
Ca(i,MSize-1)=-2*pBC;
Ca(i,MSize-3)=2*pBC;
Ca(i,MSize-4)=-pBC;
end

step_num=expand/dt;
if step_num>Maximum_Num
    rec_dt=expand/Maximum_Num;
else
    rec_dt=dt;
end

yp=y_n1;
yc=y_0;
rec_t=t0+rec_dt;
Y=[];
time_vec=[];
a=0;
for t=t0:dt:t0+expand
    H_Pa=diag(sparse(Pa(t)));
    H_q=Ha+H_Pa*Hb;
    if strcmp(lBC,'Clamped')
        Hk=Ca(2:MSize,2:MSize)\H_q(2:MSize,:);
        Ya=[yc;yp];
        Yb=[0;Hk*Ya];
        yp=yc;
        yc=Yb;
    else
        Hk=Ca\H_q;
        Ya=[yc;yp];
        Yb=Hk*Ya;
        yp=yc;
        yc=Yb;
    end

    if t>=rec_t
        rec_t=rec_t+rec_dt;
        a=a+1;
        Y=[Y,Yb];
        time_vec=[time_vec,t];
        if msg=='Y' || msg=='y'

disp([num2str(t),'/',num2str(t0+expand),' : ',num2str(a)]);
        end
    end
end
end

```

## A.4 Selected Python Script of Optimal Design Toolkit

```
def CreatAssembly(model, *parts, **flip):
    if not parts: return ()
    num=len(parts)

    axis_flip=flip.get('axis_flip', [OFF]*num)
    face_flip=flip.get('face_flip', [OFF]*num)
    base_align=flip.get('base_align', None)
    #Determine whether the first part put lastly so that the
    second will start at z=0, useful when tran is included

    assembly=model.rootAssembly
    instance=[]

    n=1 #Order of Name
    i=1 if base_align else 0 #Index of part
    if i<num:
        p0=assembly.Instance(name='Part-'+str(n),
part=parts[i], dependent=ON)
        instance.append(p0)

    for p in parts[i+1:]:
        n=n+1
        i=i+1
        p1=assembly.Instance(name='Part-'+str(n), part=p,
dependent=ON)
        instance.append(p1)

        aflip=axis_flip[i]
        fflip=face_flip[i]
        _tieParts(model, assembly, p0, p1, aflip, fflip)

        p0=p1

    if base_align:
        p0=assembly.Instance(name='Part-0', part=parts[0],
dependent=ON)
        if not instance: return [p0]
        #Move current instance to the back of the assm
        p1=instance[0]
        f=p0.part.features['FrontCentralPoint']
        a0=p0.datums[f.id].pointOn
        f=p1.part.features['BaseCentralPoint']
        a1=p1.datums[f.id].pointOn
        vec=[b1-b0 for b0, b1 in zip(a0, a1)]
        assembly.translate(instanceList=('Part-0', ),
vector=vec)
        _tieParts(model, assembly, p0, p1, axis_flip[1],
face_flip[1])
        instance=[p0]+instance
```

```

    return instance

def CreatBlade(model, blade_section, blade_para,
with_tran=None, tran_section=''):

    global Transducer
    global TranDimension

    if not tran_section:
        tran_section=blade_section

    size=blade_para['_Dimension_'](blade_para)
    Lx=size[0]
    Ly=size[1]
    Lz=size[2]

    W=max(with_tran.Dimension[0], Lx) if with_tran else
Lx
    H=max(with_tran.Dimension[1], Ly) if with_tran else
Ly
    L=with_tran.Dimension[2]+Lz if with_tran else Lz

    #Generate Parts
    map=blade_para['_ParaMapping_']
    para=[m(blade_para) for m in map]
    parts=blade_para['_Parts_']
    components=[p(model=model, section=blade_section, **a)
for p, a in zip(parts, para)]

    if with_tran:
        tran=with_tran.CreatPart(model=model,
section=tran_section, name='Transducer')
        allcomponents=[tran]+components
    else:
        allcomponents=components

    instances=CreatAssembly(model, *allcomponents,
base_align='Y') if with_tran else CreatAssembly(model,
*allcomponents)
    myAssembly=model.rootAssembly
    tolerance=1e-5

##Define Node Sets
#Central Nodes
nodes=[]
for ins in instances:
    n=ins.nodes
    n=n.getByBoundingBox(xMin=-tolerance, yMin=-
tolerance, zMin=-L-tolerance,

```



```

xMax=tolerance, yMax=tolerance, zMax=L+tolerance)
    nodes=nodes+n if nodes else n
    if nodes: myAssembly.Set(nodes=nodes,
name='CentralLine')

    #Nodes on Central Plane
    nodes=[]
    for ins in instances:
        n=ins.nodes
        n=n.getByBoundingBox(xMin=-W-tolerance, yMin=-
tolerance, zMin=-L-tolerance,

xMax=W+tolerance, yMax=tolerance, zMax=L+tolerance)
    nodes=nodes+n if nodes else n
    if nodes: myAssembly.Set(nodes=nodes,
name='CentralPlane')

    #Nodes on Vertical Central Plane
    nodes=[]
    for ins in instances:
        n=ins.nodes
        n=n.getByBoundingBox(xMin=-tolerance, yMin=-H-
tolerance, zMin=-L-tolerance,

xMax=tolerance, yMax=H+tolerance, zMax=L+tolerance)
    nodes=nodes+n if nodes else n
    if nodes: myAssembly.Set(nodes=nodes,
name='VCentralPlane')

    #Nodes on Base
    nodes=[]
    p=instances[1:] if with_tran else instances
    for ins in p:
        n=ins.nodes
        n=n.getByBoundingBox(xMin=-W-tolerance, yMin=-H-
tolerance, zMin=-tolerance,

xMax=W+tolerance, yMax=H+tolerance, zMax=tolerance)
    nodes=nodes+n if nodes else n
    if nodes: myAssembly.Set(nodes=nodes,
name='BaseTerminal')

    #Nodes of all parts, not include transducer
    nodes=[]
    p=instances[1:] if with_tran else instances
    for ins in p:
        n=ins.nodes
        nodes=nodes+n if nodes else n
    if nodes: myAssembly.Set(nodes=nodes, name='Parts')

```

```

#Nodes on transducer output surface
if with_tran:
    n=instances[0].nodes
    nodes=n.getByBoundingBox(xMin=-
with_tran.Dimension[0]-tolerance, yMin=-
with_tran.Dimension[1]-tolerance, zMin=-tolerance,

xMax=with_tran.Dimension[0]+tolerance,
yMax=with_tran.Dimension[1]+tolerance, zMax=tolerance)
    if nodes: myAssembly.Set(nodes=nodes,
name='TranOutput')

    num=len(parts)
    extension=blade_para.get('_PartsExtension_', None)
#Run Extension Program (for each parts), if provided
    if extension:
        for i, ext in enumerate(extension):
            if i>=num: break
            if ext:
                s='Part-'+str(i+1)
                ext(model=model, section=blade_section,
part=components[i], instance=myAssembly.instances[s],
assembly=myAssembly,
part_para=para[i], blade_para=blade_para)

    extension=blade_para.get('_AssmExtension_', None)
#Run Extension Program (for assembly), if provided
    if extension:
        extension(model=model, assembly=myAssembly,
blade_para=blade_para)

    return myAssembly

def StressAnalysis(blade_para, input, frequency,
tran_material=None, with_tran=None,
submit='Y', wait='Y',
model_name='Blade', job_name='StressAnalysis',
step_name='StressAnalysis'):

    if isinstance(frequency, dict):
        min_freq=frequency['Low']
        max_freq=frequency['High']
        nPoints=frequency['nPoints']
    else:
        min_freq=frequency
        max_freq=frequency
        nPoints=2

```

```

if max_freq<min_freq:
    a=max_freq
    max_freq=min_freq
    min_freq=a

    Prototype (blade_para=blade_para,
tran_material=tran_material, with_tran=with_tran,
model_name=model_name)

    myModel = mdb.models[model_name]
    myAssembly=myModel.rootAssembly
    #Step and boundary conditions
    myModel.SteadyStateDirectStep(name=step_name,
previous='Initial',

frequencyRange=((min_freq, max_freq, nPoints , 1.0), ))

    #Boundary Condition (Input)

    if 'T' in input or 'XT' in input or 'YT' in input:
#Torsion

points=myModel.rootAssembly.sets['BaseTerminal'].nodes
    n=0
    for p in points:
        n=n+1
        x, y, z=p.coordinates
        R=sqrt(x*x+y*y)

        At=2*R*sin(input.get('T', 0)/2)    #Torsion
angle
        Ay=2*y*sin(input.get('YT', 0)/2)    #Flip
angle on Y
        Ax=2*x*sin(input.get('XT', 0)/2)    #Flip
angle on X

        u1t=y*At/R if R else 0
        u2t=-x*At/R if R else 0
        u3y=y*Ay/y if y else 0
        u2y=-z*Ay/y if y else 0
        u1x=z*Ax/x if x else 0
        u3x=-x*Ax/x if x else 0

        u1d=input.get('X', 0)
        u2d=input.get('Y', 0)
        u3d=input.get('Z', 0)

        u1=u1t+u1x+u1d if 'T' in input or 'XT' in
input or 'X' in input else UNSET

```

```

        u2=u2t+u2y+u2d if 'T' in input or 'YT' in
input or 'Y' in input else UNSET
        u3=u3x+u3y+u3d if 'XT' in input or 'YT' in
input or 'Z' in input else UNSET

        a=mesh.MeshNodeArray((p, ))
        region=regionToolset.Region(nodes=a)

myModel.DisplacementBC(name='InputDisplacement'+str(n),
createStepName=step_name,
                        region=region, u1=u1, u2=u2,
u3=u3, url1=UNSET, ur2=UNSET,
                        ur3=UNSET, amplitude=UNSET,
fixed=OFF, distributionType=UNIFORM,
                        fieldName='', localCsys=None)

    else:
        region=myAssembly.sets['BaseTerminal']
        u1=input.get('X', UNSET)
        u2=input.get('Y', UNSET)
        u3=input.get('Z', UNSET)
        myModel.DisplacementBC(name='InputDisplacement',
createStepName=step_name,
                        region=region, u1=u1, u2=u2,
u3=u3, url1=UNSET, ur2=UNSET,
                        ur3=UNSET, amplitude=UNSET,
fixed=OFF, distributionType=UNIFORM,
                        fieldName='', localCsys=None)

    #Job
    myJob=mdb.Job(name=job_name, model=model_name,
description='', type=ANALYSIS,
                atTime=None, waitMinutes=0, waitHours=0,
queue=None, memory=40,
                memoryUnits=PERCENTAGE,
getMemoryFromAnalysis=True,
                explicitPrecision=SINGLE,
nodalOutputPrecision=SINGLE, echoPrint=OFF,
                modelPrint=OFF, contactPrint=OFF,
historyPrint=OFF, userSubroutine='',
                scratch='', multiprocessingMode=DEFAULT,
numCpus=1, numGPUs=0)

    #Submit and Analysis
    if submit:
        myJob.submit(consistencyChecking=OFF)
        print (job_name+' has been submitted.')
        if wait:
            print ('Waiting for job to be completed...')
            myJob.waitForCompletion()
    else:

```

```

        myJob.writeInput(consistencyChecking=OFF)
        print (job_name+'.inp has been created but not
submitted.')
```

```

    res=dict(Job=myJob, Inp=job_name+'.inp',
Step=step_name, Name=job_name)
    if submit and wait:      #If result is obtained, the
return value contains job path
        res['Path']=job_name+'.odb'

    return res              #Return the name of the job, which
can be used to open the database
```

```

def GetModalDistance(target_mode, odb_path=None,
step_name='ModalAnalysis', mode=[], type=''):
    if not mode:
        if isinstance(odb_path, dict): #Unpack
            odb=session.openOdb(name='myOdb',
path=odb_path['Path'], readOnly=True)
            step_name=odb_path['Step']
        elif isinstance(odb_path, str): #Use file
path
            odb=session.openOdb(name='myOdb',
path=odb_path, readOnly=True)
        else: #Object itself
            odb=odb_path
            mode=TraitModes(odb_path, step_name)

    mode.sort()
    for m in mode:
        if m[1]==target_mode:
            f=m[0]
            break
    else:
        return None

    fm=None
    for m in mode:
        if m[1]==target_mode: continue
        if (not type or type==m[1][-1]) and m[1]!='Base':
            a=m[0]-f
            fm=a if fm==None else a if abs(a)<abs(fm)
    else fm

    return fm
```

```

def PerformanceIndicators(indicators, blade_para,
input={}, para_comb=[], frequency=-1, data_path='',
msg_path='',
                                para_info=None, file_info=None,
print_head='Y', transducer=None, tran_material={},
job_name='Indicators',
                                MD_target='', MDT_target='',
min_freq=500, max_freq=80000):
    if isinstance(para_comb, str): #Read from file
        para=ReadSection(path=para_comb,
name='Parameters')
        blade_para.update(para)
        para_comb=ReadSection(path=para_comb,
name='DataBlock')

    all_ind=('MD', 'XMD', 'YMD', 'ZMD', 'TMD', 'MD-T',
'XMD-T', 'YMD-T', 'ZMD-T', 'TMD-T', 'XMPS', 'Lx', 'YMPS',
'Ly', 'ZMPS', 'Lz',
            'TMPS', 'Lt', 'MPS', 'Lm', 'Gx', 'Gy', 'Gz',
'Gt', 'Ax', 'Ay', 'Az', 'At', 'Mode', 'Mode-T') #All
possible indicators

    ind_names=[a for a in all_ind if a in indicators]
#The indicator to be abstracted
    ind_set=set(ind_names)

    if msg_path: open(msg_path, 'w').close()
    if data_path: open(data_path, 'w').close()

    if msg_path: #Message file showing the
progress
        MsgPrintL('Get Performance Indicators Start\n',
path=msg_path)

    if data_path:
        if print_head: #Write into data file
            WriteSection('Start', path=data_path)
            WriteSection('Information', file_info,
path=data_path)
            WriteSection('Parameters', blade_para,
para_info, path=data_path) #File head, blade
parameters
            WriteSection('Input', input, path=data_path)
            WriteSection('DataBlock', path=data_path)
            p=para_comb[0]+ind_names if para_comb else
ind_names
            DataPrintL(*p, sep='\t', prefix='# ',
path=data_path)

    work_dir=os.getcwd()
    N=len(para_comb)-1 if para_comb else 1

```

```

    Na=len(para_comb[0]) if para_comb else 0    #Number of
changeable parameters
    n=0
    while n<N:
        n=n+1

        para=blade_para.copy()
        if para_comb and msg_path:
            t=time.localtime()
            a='-->'+time.strftime('%Y.%m.%d %H:%M:%S', t)
            MsgPrintL(a, path=msg_path)
            MsgPrintL('Calculating ', str(n)+' / '+str(N),
' ... ', path=msg_path)
            for k, a in enumerate(para_comb[0]):
#Pack and change variables
                para[a]=para_comb[n][k]

                jobs=_submitJobs(work_dir=work_dir,
ind_set=ind_set, para=para, frequency=frequency,
msg_path=msg_path,
                                input=input,
tran=transducer, tran_material=tran_material,
job_name=job_name, min_freq=min_freq, max_freq=max_freq)

                _waitForJobs(work_dir=work_dir, jobs=jobs)

                ind_val=_abstIndicators(work_dir=work_dir,
job_name=job_name, indicators=ind_set,
MD_target=MD_target, MDT_target=MDT_target)

                #Print result to file
                if para_comb and data_path:
                    p=para_comb[n][0:Na]+[ind_val[a] for a in
ind_names]
                    DataPrintL(*p, sep='\t', path=data_path)

                if para_comb and msg_path:
                    MsgPrintL('Calculation ', str(n)+' / '+str(N),
' completed.\n', path=msg_path)

                if para_comb and msg_path:
                    MsgPrintL('All Calculation Completed
Sucessfully!\n', path=msg_path)

                if para_comb and data_path and print_head:
                    DataPrintL('##End', path=data_path)

                if not para_comb:
                    return ind_val

    return

```

## **Publications**

- [1] Ganilova O.A., Lucas M., Pan Z., Muir A.Y., Simpson H., Inspiration from Victorian times in Ultrasonic Surgical Tool Design, Modern Practice in Stress and Vibration Analysis, 2012.
- [2] Pan Z., Lucas M., Ganilova O.A., Study of an Ultrasonic Bone Cutting Blade for Orthopaedic Surgery, IEEE International Ultrasonics Symposium Proceedings, Dresden, 2012.
- [3] Robert James Wallace, Antonio Spadaccino, Andraay Leung, Zhongyin Pan, Olga Ganilova, Andrew Muir, Margaret Lucas, Hamish RW Simpson A Comparison of Past, Present and Future Bone Surgery Tools, International Journal of Orthopaedics, 2015, 2(3): 266-269.
- [4] Wallace R. J., Pan Z., Leung A., Muir A., Lucas M., Simpson H., 200 Years of Bone Cutting Technology, ORS 2015 Annual Meeting, Las Vegas, U.S.A., 2015.



## Reference

- [1] Cardoni A. and Lucas M., A Novel Multiple Blade Ultrasonic Cutting Device, *Ultrasonics*, 2004, **42**(1-9): 69-74.
- [2] Leclercq P., Zenati C., Amr S. and Dohan D. M., Ultrasonic Bone Cut: State-of-the-Art Technologies and Common Applications, *Journal of Oral and Maxillofacial Surgery*, 2008, **66**: 177-188.
- [3] Arnold G., Leiteritz L., Zahn S. and Rohm H., Ultrasonic Cutting of Cheese: Composition Affects Cutting Work Reduction and Energy Demand, *International Dairy Journal*, 2009, **19**(5): 314-320.
- [4] Chemat F., Zill-e-Huma and Khan M. K., Applications of Ultrasound in Food Technology: Processing, Preservation and Extraction, *Ultrasonics Sonochemistry*, 2011, **18**(4): 813-835.
- [5] Povey M. J. W. and Mason T. J., *Ultrasound in Food Processing*, Springer-Verlag New York, LLC, 2007.
- [6] O'Daly B. J., Morris E., Gavin G. P., O'Byrne J. M. and McGuinness G. B., High-Power Low-Frequency Ultrasound: A Review of Tissue Dissection And Ablation In Medicine And Surgery, *Journal of Materials Processing Technology*, 2008, **200**: 38-58.
- [7] Labanca M., Azzola F., Vinci R. and Rodella L. F., Piezoelectric Surgery: Twenty Years of Use, *British Journal of Oral and Maxillofacial Surgery*, 2008, **46**: 265-269.
- [8] Robiony M., Polini F., Costa F., Zerman N. and Politi M., Ultrasonic Bone Cutting for Surgically Assisted Rapid Maxillary Expansion (SARME) under Local Anaesthesia, *International Journal of Oral and Maxillofacial* 2007, **36**(3): 267269.
- [9] González-García A., Diniz-Freitas M., Somoza-Martín M., García-García A. and Compostela S. d., Ultrasonic Osteotomy in Oral Surgery and Implantology, *Oral and Maxillofacial Implants*, 2009, **108**(3): 360-367.
- [10] Beziat J.-L., Bera J.-C., Lavandier B. and Gleizal A., Ultrasonic Osteotomy as A New Technique in Craniomaxillofacial Surgery, *International Journal of Oral and Maxillofacial Surgery*, 2007, **36**: 493-500.
- [11] Lundskog J., Heat and Bone Tissue: An Experimental Investigation of the Thermal Properties of Bone and Threshold Levels for Thermal Injury, *Scandinavian Journal of Plastic and Reconstructive Surgery*, 1972, **9**: 1-80.
- [12] Cardoni A., MacBeath A. and Lucas M., Methods for Reducing Cutting Temperature in Ultrasonic Cutting of Bone, *Ultrasonics*, 2006, **44**: e37-e42.
- [13] Giraud J.-Y., Villemin S., Darmana R., Cahuzac J.-P., Autefage A. and Morucci J.-P., Bone cutting, *Clinical Physics and Physiological Measurement*, 1991, **12**(1): 1-19.
- [14] Cardoni A., *Characterising the Dynamic Response of Ultrasonic Cutting Devices*, University of Glasgow, Ph.D. Thesis, 2003.

- [15] Lucas M. and Mathieson A., In Power Ultrasonics, Applications of High-Intensity Ultrasound, Chapter 23, Ultrasonic Cutting for Surgical Applications, Woodhead Publishing, 2015.
- [16] go-Jua´rez J. A. G. and Graff K. F., In Power Ultrasonics, Applications of High-Intensity Ultrasound, Chapter 1, Introduction to Power Ultrasonics, Woodhead Publishing, 2015.
- [17] Gallego-Juarez J. A., High power ultrasound. In: Webster, John G. (Ed.), In: Encyclopedia of Electrical and Electronics Engineering, vol. 9., John Wiley & Sons, Inc., New York,, 1999.
- [18] Byl N. N., The Use of Ultrasound as an Enhancer for Transcutaneous Drug Delivery: Phonophoresis PHYS THER., 1995, **75**: 539-553.
- [19] Hueter T. F. and Bolt R. H., Sonics: Techniques for the Use of Sound and Ultrasound in Engineering and Science, Chapman & Hall, 1955.
- [20] Graff K., Ultrasonics: Historical Aspects, Ultrasonics Symposium, 1977: 1-10.
- [21] Shoh A., Welding of Thermoplastics by Ultrasound, Ultrasonics, 1976, **14**(5): 209-217.
- [22] Hulst A., Macrosonics in Industry 2: Ultrasonic Welding of Metals, Ultrasonics, 1972, **10**(6): 252-261.
- [23] Polyakov V. A., Nikolaev G. A., Volkov M. V., Loshchilov V. I. and Petrov V. I., Ultrasonic Bonding of Bones and Cutting of Live Biological Tissues, Mir Publishers, 1974.
- [24] Volkov M. V. and Shepeleva I. S., The Use of Ultrasonic Instrumentation for the Transection and Uniting of Bone Tissue in Orthopaedic Surgery, Reconstruction Surgery and Traumatology, 1974, **14**(0): 147-52.
- [25] Tsujino J., Recent Developments of Ultrasonic Welding, IEEE Ultrasonics Symposium, 1995: 1051-1060.
- [26] Pereira A. H. A., Ultrasonic Cleaning: Overview and State of the Art, ATCP Physical Engineering, São Carlos - Brazil 2010.
- [27] Lanin V. L., Ultrasonic Soldering in Electronics, Ultrasonics Sonochemistry, 2001, **8**(4): 379-385.
- [28] Feucht F., Ketelaer J., Wolff A., Mori M. and Fujishima M., Latest Machining Technologies of Hard-to-cut Materials by Ultrasonic Machine Tool, 6th CIRP International Conference on High Performance Cutting, HPC2014, 2014, **14**: 148-152.
- [29] Horton J. E., Tarpley T. M. and Jacoway J. R., Clinical Applications of Ultrasonic Instrumentation in the Surgical Removal of Bone, Oral Surgery, Oral Medicine, Oral Pathology, 1981, **51**(3): 236-242.
- [30] Bond L. J. and Cimino W. W., Physics of Ultrasonic Surgery using Tissue Fragmentation: Part II, Ultrasound Med. Biol., 1996, **22**(1): 101-117.
- [31] Hallez L., Touyeras F., Hihn J.-Y., Klima J., Guey J.-L., Spajer M. and Bailly Y., Characterization of HIFU Transducers Designed for Sonochemistry Application: Cavitation Distribution and Quantification, Ultrasonics, 2010, **50**(2): 310-317.

- [32] Jin M. and Murakawa M., Development of a Practical Ultrasonic Vibration Cutting Tool System, *Journal of Materials Processing Technology*, 2001, **113**(1-3): 342-347.
- [33] Dostrovsky S., Early Vibration Theory: Physics and Music in the Seventeenth Century, *Archive for History of Exact Sciences*, 1975, **14**(3): 169-218.
- [34] Mason W. P., *Physical Acoustics V15: Principles and Methods*, Academic Press Inc., 1981.
- [35] Wood R. W., *Supersonics (The Science of Inaudible Sounds)*, Brown University Press, 1939.
- [36] Wood R. W. and Loomis A. L., The Physical and Biological Effects of High Frequency Sound-Waves of Great Intensity, *Philosophical Magazine and Journal of Science*, 1927, **4**(22): 417-436.
- [37] Nyborg W., Basic Physics of Low Frequency Therapeutic Ultrasound, In: R.J. Siegel (Ed.), *Ultrasound Angioplasty (Developments in Cardiovascular Medicine)*, Kluwer Academic Publishers, Boston, 1996: 1-23.
- [38] Fong S. W., Klaseboer E., Turangan C. K., Khoo B. C. and Hung K. C., Numerical Analysis of a Gas Bubble Near Bio-materials in an Ultrasound Field, *Ultrasound in Medicine & Biology*, 2006, **32**(6): 925-942.
- [39] MacBeath A., *Ultrasonic Bone Cutting*, University of Glasgow, Ph.D. Thesis, 2006.
- [40] Cimino W. W., The Physics of Soft Tissue Fragmentation using Ultrasonic Frequency Vibration of Metal Probes, *Clin. Plast. Surg.*, 1999, **26**(3): 447-467.
- [41] Cimino W. W. and Bond L. J., Physics of Ultrasonic Surgery using Tissue Fragmentation: Part I, *Ultrasound Med. Biol.*, 1996, **22**(1): 89-100.
- [42] Lucas M., MacBeath A., McCulloch E. and Cardoni A., A Finite Element Model For Ultrasonic Cutting, *Ultrasonics*, 2006, **44**: 503-509.
- [43] Aro H., Kallioniemi H., Aho A. and Kellokumpu-Lehtinen P., Ultrasonic Device in Bone Cutting: A Histological and Scanning Electron Microscopical Study, *Acta Orthop. Scand*, 1981, **52**: 5-10.
- [44] Smith A., Nurse A., Graham G. and Lucas M., Ultrasonic Utting - A Fracture Mechanics Model, *Ultrasonics*, 1996, **34**(2-5): 197-203.
- [45] Neppiras E., *Macrosomics in industry 1: Introduction*, *Ultrasonics*, 1972, **10**(1): 9-13.
- [46] Babitsky V. I., Kalashnikov A. N., Meadows A. and Wijesundara A. A. H. P., Ultrasonically Assisted Turning of Aviation Materials, *Journal of Materials Processing Technology*, 2003, **132**(1-3): 157-167.
- [47] Babitsky V. I., Mitrofanov A. V. and Silberschmidt V. V., Ultrasonically Assisted Turning of Aviation Materials: Simulations and Experimental Study, *Ultrasonics*, 2004, **42**(1-9): 81-86.
- [48] Kim J.-D. and Choi I.-H., Micro Surface Phenomenon of Ductile Cutting in the Ultrasonic Vibration Cutting of Optical Plastics, *Journal of Materials Processing Technology*, 1997, **68**(1): 89-98.

- [49] Rawson F., *Ultrasound in Food processing*, London, UK, Blackie Academic & Professional, 1998.
- [50] Dolatowski Z. J., Stadnik J. and Stasiak D., *Applications of Ultrasound In Food Technology*, Acta Sci. Pol., Technologia Alimentaria, 2007, **6**(3): 89-99.
- [51] Schneider Y., Zahn S. and Linke L., *Qualitative Process Evaluation for Ultrasonic Cutting of Food*, Engineering in Life Sciences, 2002, **2**(6): 153-157.
- [52] Schneider Y., Zahn S. and Rohm H., *Power Requirements of the High-Frequency Generator in Ultrasonic Cutting of Foods*, Journal of Food Engineering, 2008, **86**(1): 61-67.
- [53] McCulloch E., *Experimental and Finite Element Modelling of Ultrasonic Cutting of Food*, University of Glasgow, Ph.D. Thesis, 2008.
- [54] Sinn G., Zettl B., Mayer H. and Stanzl-Tschegg S., *Ultrasonic-Assisted Cutting of Wood*, Journal of Materials Processing Technology, 2005, **170**(1-2): 42-49.
- [55] Deibel K.-R., Kaiser F., Zimmermann R., Meier L., Bolt P. and Wegener K., *Longitudinal Ultrasonic Vibration Assisted Guillotining of Stacked Paper*, Ultrasonics, 2014, **54**(6): 1585-1593.
- [56] U.S. Department of Health and Human Services, *Bone Health and Osteoporosis: A Report of the Surgeon General*. Rockville, MD: U.S. Department of Health and Human Services, Office of the Surgeon General, 2004.
- [57] <http://www.doitpoms.ac.uk/tlplib/bones/structure.php>, Accessed 29th, May, 2015.
- [58] Spence A. P., *Basic Human Anatomy*, Benjamin-Cummings Publishing Company, 1986.
- [59] Lee J., Ozdoganlar O. B. and Rabin Y., *An Experimental Investigation on Thermal Exposure during Bone Drilling*, Medical Engineering & Physics, 2012, **34**(10): 1510-1520.
- [60] Brisman D. L., *The Effect of Speed, Pressure, and Time on Bone Temperature during the Drilling of Implant Sites*, International Journal of Oral and Maxillofacial Implants, 1996, **11**(1): 35-37.
- [61] Iyer S., Weiss C. and Mehta A., *Effects of Drill Speed on Heat Production and the Rate and Quality of Bone Formation in Dental Implant Osteotomies. Part I: Relationship between Drill Speed and Heat Production*, International Journal of Prosthodontics, 1997, **10**(5): 411-414.
- [62] Abouzgia M. B. and James D. F., *Temperature Rise during Drilling Through Bone* International Journal of Oral and Maxillofacial Implants, 1997, **12**(3): 342-353.
- [63] Bachus K. N., Rondina M. T. and Hutchinson D. T., *The Effects of Drilling Force on Cortical Temperatures and Their Duration: An in Vitro Study*, Medical Engineering & Physics, 2000, **22**(10): 685-691.
- [64] Eriksson A. R., Albrektsson T. and Albrektsson B., *Heat Caused by Drilling Cortical Bone: Temperature Measured in Vivo in Patients and Animals*, Acta Orthopaedica, 1984, **55**(6): 629-631.

- [65] Sener B. C., Dergin G., Gursoy B., Kelesoglu E. and Slih I., Effects of Irrigation Temperature on Heat Control in Vitro at Different Drilling Depths, *Clinical Oral Implants Research*, 2009, **20**(3): 294-298.
- [66] Cordioli G. and Majzoub Z., Heat Generation during Implant Site Preparation: An in Vitro Study, *International Journal of Oral and Maxillofacial Implants*, 1997, **12**(2): 186-193.
- [67] Ark T. W., Neal J. G., Thacker J. G. and Edlich R. F., Influence of Irrigation Solutions on Oscillating Bone Saw Blade Performance, *Journal of Biomedical Materials Research*, 1998, **43**(2): 108-112.
- [68] Rashad A., Sadr-Eshkevari P., Heiland M., Smeets R., Hanken H., Gröbe A., Assaf A. T., Köhnke R. H., Mehryar P., Riecke B. and Wikner J., Intraosseous Heat Generation during Sonic, Ultrasonic and Conventional Osteotomy, *Journal of Cranio-Maxillofacial Surgery*, 2015, **43**(7): 1072-1077.
- [69] Lucas M., Cardoni A. and MacBeath A., Temperature Effects in Ultrasonic Cutting of Natural Materials, *CIRP Annals - Manufacturing Technology*, 2005, **54**(1): 195-198.
- [70] Abouzgia M. B. and Symington J. M., Effect of Drill Speed on Bone Temperature, *International Journal of Oral and Maxillofacial Surgery*, 1996, **25**(5): 394-399.
- [71] Hillery M. T. and Shuaib I., Temperature Effects in the Drilling of Human and Bovine Bone, *Journal of Materials Processing Technology*, 1999, **92-93**: 302-308.
- [72] Moritz A. R. and Henriques F. C., Studies of Thermal Injury II. The relative Importance of Lime and Surface Temperature in the Causation of Cutaneous Burns, *American Journal of Pathology*, 1947, **23**(5): 695-720.
- [73] Balamuth L., *Ultrasonics and Dentistry, Sound: Its Uses Control*, 1963, **2**: 15-19.
- [74] Catuna M. C., Sonic energy: A possible Dental Application, Preliminary Report of An Ultrasonic Cutting Method, *Ann. Dent.*, 1953, **12**: 100-101.
- [75] Postle H. H., Ultrasonic Cavity Preparation, *The Journal of Prosthetic Dentistry*, 1958, **8**(1): 153-160.
- [76] Amaral J., Ultrasonic Dissection, *Endosc. Surg. Allied Technol.*, 1994, **2**: 181-185.
- [77] Ebina K., Hasegawa H. and Kanai H., Investigation of Frequency Characteristics in Cutting of Soft Tissue using Prototype Ultrasonic Knives, *Jpn. J. Appl. Phys.*, 2007, **46**: 4793-4800.
- [78] Hoenig D. M., Chrostek C. A. and Amaral J. F., Laparoscopic Coagulating Shears: Alternative Method of Hemostatic Control of Unsupported Tissue, *Journal of Endourology*, 1996, **10**: 431-433.
- [79] Miller C. and McCarus S., Ultrasonic Cutting and Coagulation in Gynecologic Surgery, *The Journal of the American Association of Gynecologic Laparoscopists*, 1995, **2**(4, Supplement 1): S33.
- [80] Yaman Z. and Suer B. T., Piezoelectric Surgery in Oral and Maxillofacial Surgery, *Annals of Oral & Maxillofacial Surgery*, 2013, **1**(1): 1-9.

- [81] Schaeren S., Jaquiéry C., Heberer M., Tolnay M., Vercellotti T. and Martin I., Assessment of Nerve Damage Using a Novel Ultrasonic Device for Bone Cutting, *Journal of Oral and Maxillofacial Surgery*, 2008, **66**(3): 593-596.
- [82] Zinner D. D., Recent Ultrasonic Dental Studies Including Periodontia, without the Use of An Abrasive, *J. Dent. Res.*, 1955, **34**: 748-749.
- [83]
- [84] Mararow H., Bone Repair After Experimentally Produced Defects, *J. Oral Surg. Anesth. Hosp. Dent. Serv.*, 1960, **18**: 107-114.
- [85] McFall T., Yamane G. and Burnett G., Comparison of the Cutting Effect on Bone of An Ultrasonic Cutting Device and Rotary Burs, *J. Oral Surg. Anesth. Hosp. Dent. Serv.*, 1961, **19**: 200-209.
- [86] Horton J., Tarpley T. and Wood L., The Healing of Surgical Defects in Alveolar Bone Produced with Ultrasonic Instrumentation, Chisel, and Rotary Bur, *Oral Surg. Oral Med. Oral Pathol.*, 1975, **39**: 536-546.
- [87] Khambay B. S. and Walmsley A. D., Investigations Into the Use of An Ultrasonic Chisel to Cut Bone. Part 1: Forces Applied by Clinicians, *Journal of Dentistry*, 2000, **28**(1): 31-37.
- [88] Khambay B. S. and Walmsley A. D., Investigations Into the Use of An Ultrasonic Chisel to Cut Bone. Part 2: Cutting Ability, *Journal of Dentistry*, 2000, **28**(1): 39-44.
- [89] <http://www.mectron.com/>, Accessed 10th June, 2011.
- [90] <http://dental.mectron.com/>, Accessed 1st Oct, 2010.
- [91] Graff K. F., In *Power Ultrasonics, Applications of High-Intensity Ultrasound*, Chapter 6, *Power Ultrasonic Transducers: Principles and Design*, Woodhead Publishing, 2015.
- [92] Merkulov L. G., Design of Ultrasonic Concentrations, *Soviet Physics Acoustics*, 1957, **3**(3): 230-238.
- [93] Merkulov L. G. and Kharitonov A. N., Theory and Analysis of Sectional Concentrators, *Soviet Physics. Acoustics*, 1959, **5**: 183-190.
- [94] Rao J. S., The Fundamental Flexural Vibration of A Cantilever Beam of Rectangular Cross Section with Uniform Taper, *Aeronautical Quarterly*, 1965, **16**: 139-144.
- [95] Rao S. S., *Mechanical Vibrations (4th Edition)*, Prentice Hall Inc., 2003.
- [96] Clark S. K., *Dynamics of Continuous Elements*, Prentice Hall Inc., 1972.
- [97] Balamuth L., Mechanical Impedance Transformers in Relation to Ultrasonic Machining, *Transactions of the IRE Professional Group on Ultrasonic Engineering*, 1954, **2**(1): 23-33.
- [98] Eisner E. and Seager J. S., A Longitudinally Resonant Stub for Vibrations of Large Amplitude, *Ultrasonics*, 1965, **3**(2): 88-98.
- [99] Jakubowski M., Ultrasonic Horn Design: Translating an Art into Sound Principles, *Electromechanical Design*, 1972, **April**: 30-37.

- [100] Amza G. and Drimer D., The Design and Construction of Solid Concentrators for Ultrasonic Energy, *Ultrasonics*, 1976, **14**(5): 223-226.
- [101] Derks P. L., The Design of Ultrasonic Resonators with Wide Output Cross-Sections, Eindhoven University Of Technology, Ph.D. Thesis, 1984.
- [102] Adachi K., Ueha S. and Mori E., Modal Vibration Analysis of Ultrasonic Plastic Welding Tools using the Finite Element Method, *Proceedings of Ultrasonics International*, London, 1985: 727-732.
- [103] Adachi K. and Ueha S., Modal Vibration Control of Large Ultrasonic Tools with the Use of Wave-Trapped Horns, *Journal of Acoustic Society of America*, 1990, **87**(1): 208-214.
- [104] O'Shea K., Enhanced Vibration Control of Ultrasonic Tooling using Finite Element Analysis, *ASME Vibration Analysis - Analytical and computational*, 1991, **DE-37**: 259-265.
- [105] Koike Y. and Ueha S., A Finite-Element Analysis of Transient Vibration of An Ultrasonic Welding Tool, *Japanese Journal of Applied Physics*, 1993, **32**(5B): 2426-2429.
- [106] Chapman G. and Lucas M., Frequency Analysis of An Ultrasonically Excited Thick Cylinder, *International Journal of Mechanical Sciences*, 1990, **32**(3): 205-214.
- [107] Timoshenko S., *Vibration Problems in Engineering* (2nd Edition), New York, D. Van Nostrand, 1937.
- [108] Timoshenko S. and Young D. H., *Advanced Dynamics*, McGraw-Hall Book Company, Inc., 1948.
- [109] Rao S. S., *Engineering Optimization: Theory and Practice*, Fourth Edition, Hoboken, New Jersey, John Wiley & Sons, Inc., 2009.
- [110] Arora J., *Introduction to Optimum Design*, Third Edition, Waltham, Academic Press, 2011.
- [111] Brinkhuis J. and Tikhomirov V., *Optimization: Insights and Applications: Insights and Applications*, Princeton, Princeton University Press, 2005.
- [112] Deb K., *Optimization for Engineering Design: Algorithms and Examples*, Second Edition, New Delhi, PHI Learning Private Limited, 2012.
- [113] Amin S. G., Ahmed M. H. M. and Youssef H. A., Computer-Aided Design of Acoustic Horns for Ultrasonic Machining Using Finite-Element Analysis, *Journal of Materials Processing Technology*, 1995, **55**(3-4): 254-260.
- [114] Zhang Z. and Babitsky V. I., Finite Element Modeling of A Micro-Drill and Experiments on High Speed Ultrasonically Assisted Micro-Drilling, *Journal of Sound and Vibration*, 2011, **330**: 2124-2137.
- [115] Alam K., Mitrofanov A. V. and Silberschmidt V. V., Finite Element Analysis of Forces of Plane Cutting of Cortical Bone, *Computational Materials Science*, 2009, **46**: 738-743.
- [116] Gatti P. L. and Ferrar V., *Applied Structural and Mechanical Vibration: Theory, Methods and Measuring Instrumentation*, Taylor & Francis Group LLC, 2003.

- [117] Kumar B. M. and Sujith R. I., Exact Solutions for the Longitudinal Vibration of Non-Uniform Rods, *Journal of Sound and Vibration*, 1997, **207**(5): 721-729.
- [118] Eisenberger M., Exact Longitudinal Vibration Frequencies of a Variable Cross-Section Rod, *Applied Acoustics*, 1991, **34**(2): 123-130.
- [119] Li Q. S., Exact Solutions for Free Longitudinal Vibration of Stepped Non-Uniform Rods, *Applied Acoustics*, 2000, **60**(1): 13-28.
- [120] Ece M. C., Aydogdu M. and Task V., Vibration of A Variable Cross-Section Beam, *Mechanics Research Communications*, 2007, **34**: 78-84.
- [121] Naguleswaran S., A Direct Solution for the Transverse Vibration of Euler-Bernoulli Wedge and Cone Beams, *Journal of Sound and Vibration*, 1994, **172**(3): 289-304.
- [122] Tong X. and Tabarr B., Vibration Analysis of Timoshenko Beams with Non-Homogeneity and Varying Cross-Section, *Journal of Sound and Vibration*, 1995, **186**(5): 821-835.
- [123] Trabuco L. and Viañ J. M., A Derivation of Generalized Saint Venant's Torsion Theory From Three-Dimensional Elasticity by Asymptotic Expansion Methods, *Applicable Analysis*, 1988, **31**: 129-148.
- [124] Slivker V., *Mechanics of Structural Elements: Theory and Applications*, Springer, 2007.
- [125] Eisenberger M., Nonuniform Torsional Analysis of Variable and Open Cross-Section Bars, *Thin-Walled Structures*, 1995, **21**(2): 93-105.
- [126] Eisenberger M., Torsional Vibrations of Open and Variable Cross-Section Bars, *Thin-Walled Structures*, 1997, **28**(3-4): 269-278.
- [127] Vet M., Torsional Vibration of Beams Having Rectangular Cross Sections *The Journal of the Acoustical Society of America*, 1962, **34**(10): 1570-1575.
- [128] Vet M., Torsional Vibration of Beams of Rectangular Cross Section, M.S. Thesis, 1960.
- [129] Kulkarni S. V. and Subrahmanyam K. B., Reissner Method Calculations of Natural Frequencies of Torsional Vibrations of Tapered Cantilever Beams, *Journal of Sound and Vibration*, 1981, **75**(4): 589-592.
- [130] Augustyn E., Possibilities of Analytical Description of Torsional Vibrations of Prismatic Beams, *The 2nd Electronic International Interdisciplinary Conference*, 2013: 445-447.
- [131] Elwany M. H. S. and Barr A. D. S., Some Optimization Problems in Torsional Vibration, *Journal of Sound and Vibration*, 1978, **57**(1): 1-33.
- [132] Everstine G. C., *Numerical Solution of Partial Differential Equations: Finite Difference Methods*, The George Washington University, Lecture Note, 2010.
- [133] Lindsay K. A., *Numerical Solution of Partial Differential Equations*, University of Glasgow, Lecture Note, 2003.
- [134] Smith G. D., *Numerical Solution of Partial Differential Equations: Finite Difference Methods*, 3rd Edition, OUP Oxford, 1985.



- [135] LeVeque R. J., Finite Difference Methods for Ordinary and Partial Differential Equations: Steady-State and Time-Dependent Problems, Society for Industrial and Applied Mathematics, 2007.
- [136] Khalaji I., Patel R. V. and Naish M. D., Systematic Design of an Ultrasonic Horn Profile for High Displacement Amplification, The Fourth IEEE RAS/EMBS International Conference on Biomedical Robotics and Biomechatronics, Roma, Italy, 2012: 913-918.
- [137] Nanu A. S., Marinescu N. I. and Ghiculescu D., Study on Ultrasonic Stepped Horn Geometry Design and FEM Simulation, Nonconventional Technologies Review, 2011, **4**: 25-30.
- [138] Naguleswaran S., Comments on "Vibration of Non-Uniform Rods and Beams", Journal of Sound and Vibration, 1996, **195**(2): 331-337.
- [139] Naguleswaran S., Vibration of an Euler-Bernoulli Beam of Constant Depth and with Linearly Varying Breadth, Journal of Sound and Vibration, 1992, **153**(3): 509-522.
- [140] Sanger D. J., Transverse Vibration of a Class of Non-Uniform Beams., Journal of Mechanical Engineering Science, 1968, **16**: 111-120.
- [141] Wang H.-C., Generalized Hypergeometric Function Solutions on the Transverse Vibration of A Class of Non-Uniform Beams, Journal of Applied Mechanics, 1967, **34**(series E): 702-708.
- [142] Bishop R. E. D., The Mechanics of Vibration, Cambridge University Press, 1960.
- [143] Belvins R. D., Formulas for Natural Frequency and Mode Shape, D. Van Nostrand, New York 1979.
- [144] Downs B., Transverse Vibrations of Cantilever Beams Having Unequal Breadth and Depth Taper, Journal of Applied Mechanics, 1977, **44**(series E): 737-742.
- [145] Gorman D. J., Free Vibration Analysis of Beams and Shafts, Wiley, New York, 1975.
- [146] Abrate S., Vibration of Non-Uniform Rods and Beams, Journal of Sound and Vibration, 1995, **185**(703-716).
- [147] Conway H. D. and Dubil J. F., Vibration Frequencies of Truncated Cone and Wedge Beams, Journal of Applied Mechanics, 1965, **31**(329-330).
- [148] Naguleswaran S., Aspects of the Mode Shape Differential Equation of A class of Non-Uniform Beams, Proceedings of the IPENZ Annual Conference, 1996, **1996**: 9-13.
- [149] Gottlieb H. P. W., Comments on Vibrations of Non-Uniform Beams and Rods, Journal of Sound and Vibration, 1996, **195**(1): 139-141.
- [150] Meirovitch L., Analytical Methods in Vibration, Macmillan, New York, 1967.
- [151] Conway H. D., Becker E. C. H. and Dubil J. F., Vibration Frequencies of Tapered Bars and Circular Plates, Journal of Applied Mechanics, 1964, **31**(2): 329-331.

- [152] Bapat C. N., Vibration of Rods with Uniformly Tapered Sections, *Journal of Sound and Vibration*, 1995, **185**(1): 185-189.
- [153] Gere J. M., Torsional Vibrations of Beams of Thin Walled Open Cross Section, *Journal of Applied Mechanics*, 1954, **21**: 381-387.
- [154] Carr J. B., The Torsional Vibrations of Uniform Thin Walled Beams of Open Section, *The Aeronautical Journal of the Royal Aeronautical Society*, 1969, **73**: 672-674.
- [155] Rao C. K. and Mirza S., Free Torsional Vibrations of Tapered Cantilever I-Beams, *Journal of Sound and Vibration*, 1988, **123**(3): 489-496.
- [156] Prokić A., Bešević M. and Lukić D., A Numerical Method for Free Vibration Analysis of Beams, *Latin American Journal of Solids and Structures*, 2014, **11**(8): 1432-1444.
- [157] Krishnaswamy S. and Batra R. C., On Extensional Vibration Modes of Elastic Rods of Finite Length Which Include the Effect of Lateral Deformation, *Journal of Sound and Vibration*, 1998, **215**(3): 577-586.
- [158] Green A. E., Naghdi P. M. and Wenner M. L., On the Theory of Rods. I. Derivations from the Three-Dimensional Equations, *Proceedings of the Royal Society of London*, 1974, **A337**: 451-483.
- [159] Green A. E., Naghdi P. M. and Wenner M. L., On the Theory of Rods. II. On the Theory of Rods. II. Developments by Direct Approach, *Proceedings of the Royal Society of London*, 1974, **A337**: 485-507.
- [160] Zaretzky C. L. and Silva M. R. M. C. d., Experimental Investigation of Non-Linear Modal Coupling in the Response of Cantilever Beams, *Journal of Sound and Vibration*, 1994, **174**(2): 145-167.
- [161] Lucas M., Cardoni A., Lim F. C. N. and Cartmell M. P., Effects of Modal Interactions on Vibration Performance in Ultrasonic Cutting, *CIRP Annals - Manufacturing Technology*, 2003, **52**(1): 193-196.
- [162] Gallego-Juárez J. A., Riera E. and Acosta-Aparicio V. M., Modal Interactions in HighPower Ultrasonic Processing Transducers, *Nonlinear Acoustics-Fundamentals and Applications*, 18th International Symposium, Stockholm, 2008: 595-604.
- [163] Nayfeh A. H. and Mook D. T., *Nonlinear Oscillations*, Wiley, New York, 1979.
- [164] Nayfeh A. H. and Balachandran B., Modal Interactions in Dynamical and Structural Systems, *Applied mechanics review*, 1989, **42**(11): S175-S201.
- [165] Nayfeh S. A. N. a. A. H., Energy Transfer From High-to Low-Frequency Modes in a Flexible Structure via Modulation, *Journal of Vibration and Acoustics*, 1994, **116**(2): 203-207.
- [166] Mukhopadhyay V., Lateral Vibration of Thin Beam Under Vertical Excitation, MSc Thesis, 1970.
- [167] Dugundji J. and Mukhopadhyay V., Lateral Bending-Torsion Vibrations of a Thin Beam Under Parametric Excitation, *Journal of Applied Mechanics*, 1973, **40**: 693-698.

- [168] Cartmell M. P. and Roberts J. W., Simultaneous Combination Resonances in a Parametrically Excited Cantilever Beam, *Strain*, 1987, **23**(3): 117-126.
- [169] Cartmell M. P., The Equations of Motion for A Parametrically Excited Cantilever Beam, *Journal of Sound and Vibration*, 1990, **143**(3): 395-406.
- [170] Forehand D. I. M. and Cartmell M. P., On the Derivation of the Equations of Motion for A Parametrically Excited Cantilever Beam, *Journal of Sound and Vibration*, 2001, **245**(1): 165-177.
- [171] Ibrahim R. A. and Hijawi M., Deterministic and Stochastic Response of Nonlinear Coupled Bending-Torsion Modes in a Cantilever Beam, *Nonlinear Dynamics*, 1998, **16**: 259-292.
- [172] Su X. and Cartmell M. P., Modifications to the Response of a Parametrically Excited Cantilever Beam by Means of Smart Active Elements, *Proceedings of the Institution of Mechanical Engineers, Part C: Journal of Mechanical Engineering Science*, 2010, **224**: 1579-1591.
- [173] Oguamanam D. C. D., Free Vibration of Beams with Finite Mass Rigid Tip Load and Flexural-Torsional Coupling, *International Journal of Mechanical Sciences*, 2003, **45**(6-7): 963-979.
- [174] Bux S. L., *Vibrations of Coupled Beam Systems with Non-Linear Interactions*, Ph.D. Thesis, 1983.
- [175] Bux S. L. and Roberts J. W., Non-Linear Vibratory Interactions in Systems of Coupled Beams, *Journal of Sound and Vibration*, 1986, **104**(3): 497-520.
- [176] Warminski J., Cartmell M. P., Bochenski M. and Ivanov I., Analytical and Experimental Investigations of an Autoparametric Beam Structure, *Journal of Sound and Vibration*, 2008, **315**(3): 486-508.
- [177] Silva M. R. M. C. d. and Glynn C. C., Nonlinear Flexural-Flexural-Torsional Dynamics of Inextensional Beams. I. Equations of Motion, *Journal of Structural Mechanics*, 1978, **6**(4): 437-448.
- [178] Silva M. R. M. C. d. and Glynn C. C., Nonlinear Flexural-Flexural-Torsional Dynamics of Inextensional Beams. II. Forced Motions, *Journal of Structural Mechanics*, 1978, **6**(4): 449-461.
- [179] Scurtu P. R., Clark M. and Zu J. W., Coupled Longitudinal and Transverse Vibration of Automotive Belts under Longitudinal Excitations using Analog Equation Method, *Journal of Vibration and Control*, 2012, **18**(9): 1336-1352.
- [180] Jang I. and Lee U., Spectral Element Analysis of the Axial-Bending-Shear Coupled Vibrations of Composite Timoshenko Beams, *Journal of Composite Materials*, 2012, **46**(22): 2811-2828.
- [181] Krawczuk M., Coupled Longitudinal and Bending Forced Vibration of Timoshenko Cantilever Beam with a Closing Crack, *Journal of Theoretical and Applied Mechanics*, 1994, **32**(2): 463-482.
- [182] Darpe A. K., Gupta K. and Chawla A., Coupled Bending, Longitudinal and Torsional Vibrations of a Cracked Rotor, *Journal of Sound and Vibration*, 2004, **269**(1-2): 33-60.

- [183] Papadopoulos C. A. and Dimarogonas A. D., Coupled Longitudinal and Bending Vibrations of a Rotating Shaft with an Open Crack, *Journal of Sound and Vibration*, 1987, **117**(1): 81-93.
- [184] O'Reilly O. M., On Coupled Longitudinal and Lateral Vibrations of Elastic Rods, *Journal of Sound and Vibration*, 2001, **247**(5): 835-856.
- [185] Green A. E. and Laws N., A General Theory of Rods, *Proceedings of the Royal Society of London*, 1966, **A293**: 145-155.
- [186] Green A. E., Laws N. and Naghdi P. M., A linear theory of straight elastic rods, *Archive for Rational Mechanics and Analysis*, 1967, **25**(4): 285-298.
- [187] Naghdi P. M., Finite Deformation of Elastic Rods and Shells, *Proceedings of the IUTAM Symposium on Finite Elasticity*, D. E. Carlson and R. T. Shield, editors, 1982: 47-103.
- [188] Green A. E. and Naghdi P. M., A Unified Procedure for the Construction of Theories of Deformable Media II. Generalized Continua, *Proceedings of the Royal Society of London*, 1995, **A448**: 357-377.
- [189] Mancera P. F. and Hunt R., Numerical Solution of A Constricted Stepped Channel Problem Using A Fourth Order Method, *J. KSIAM*, 1999, **3**(2): 51-67.
- [190] Kim C. S. and Dickinson S. M., On The Analysis of Vibrating Slender Beams Subject to Various Complicating Effects, *Journal of Sound and Vibration*, 1988, **122**(441-455).
- [191] Zhou G., Zhang Y. and Zhang B., The Complex-Mode Vibration of Ultrasonic Vibration Systems, *Ultrasonics*, 2002, **40**(1-8): 907-911.
- [192] Parker T. S. and Chua L. O., *Practical Numerical Algorithms for Chaotic Systems*, Springer, New York, 1989.
- [193] Nayfeh A. H., *Introduction to Perturbation Techniques*, Wiley-VCH, 2011.
- [194] Nayfeh A. H., *Perturbation Methods*, Wiley-VCH, 2008.
- [195] Cartmell M. P., *Combination Instabilities and Nonlinear Vibratory Interactions in Beam-Systems*, Ph.D. Thesis, 1984.
- [196] Ashworth R. P. and Barr A. D. S., The Resonances of Structures with Quadratic Inertial Non-Linearity under Direct and Parametric Harmonic Excitation, *Journal of Sound and Vibration*, 1987, **118**: 47-68.
- [197] Ibrahim R. A. and Heo H., Autoparametric vibration of coupled beams under random support motion, *Journal of Vibration, Acoustics, Stress, and Reliability in Design*, 1986, **108**: 421-426.
- [198] Hamdan M. N., Al-Qaisia A. A. and Al-Bedoor B. O., Comparison of Analytical Techniques for Nonlinear Vibrations of A Parametrically Excited Cantilever, *International Journal of Mechanical Sciences*, 2001, **43**(6): 1521-1542.
- [199] Roberts J. W. and Cartmell M. P., Forced Vibration of a Beam System with Autoparametric Coupling Effects, *Strain*, 1984, **20**(3): 123-131.
- [200] Varoto P. S. and Silva D. G., Nonlinear Dynamic Behavior of a Flexible Structure to Combined External Acoustic and Parametric Excitation, *Shock and Vibration*, 2006, **13**(4-5): 233-254.

- [201] Ming Y., Levesley M. C. and Walker P. G., Transient Phenomenon of Longitudinal Flexural Coupled Vibrations in a Small Rectangular Piezoelectric Ceramic Plate, *Applied Physics Letters*, 2004, **84**(10): 1740-1741.
- [202] Katsikadelis J. T. and Tsiatas G. C., Non-Linear Dynamic Analysis of Beams with Variable Stiffness, *Journal of Sound and Vibration*, 2004, **270**(4-5): 847-863.
- [203] Kane T. R., Ryan R. and Banerjee A. K., Dynamics of a Cantilever Beam Attached to a Moving Base, *Journal of Guidance, Control, and Dynamics*, 1987, **10**(2): 139-151.
- [204] Leissa A. and Zhang Z.-D., On The Three-Dimensional Vibrations of the Cantilevered Rectangular Parallelepiped, *The Journal of the Acoustical Society of America* 1983, **73**(6): 2013-2021.
- [205] Lim C. W., Three-Dimensional Vibration Analysis of a Cantilevered Parallelepiped: Exact and Approximate Solutions, *The Journal of the Acoustical Society of America*, 1999, **106**(6): 3375-3383.
- [206] Ding L., Zhu H.-P. and Yin T., Wave Propagation in a Periodic Elastic-Piezoelectric Axial-Bending Coupled Beam, *Journal of Sound and Vibration*, 2013, **332**(24): 6377-6388.
- [207] Aoyagi M., Tomikawa Y. and Takano T., Ultrasonic Motors Using Longitudinal and Bending Multimode Vibrators with Mode Coupling by Externally Additional Asymmetry or Internal Nonlinearity, *Japanese Journal of Applied Physics*, 1992, **31**: 3077-3080.
- [208] Arafat H. N., Nayfeh A. H. and Chin C.-M., Nonlinear Nonplanar Dynamics of Parametrically Excited Cantilever Beams, *Nonlinear Dynamics*, 1998, **15**(1): 31-61.
- [209] Malatkar P., Nonlinear Vibrations of Cantilever Beams and Plates, Ph.D. Thesis, 2003.
- [210] Eftekhari M., Mahzoon M. and Ziaei-Rad S., Effect of Added Tip Mass on the Nonlinear Flapwise and Chordwise Vibration of Cantilever Composite Beam under Base Excitation, *International Journal of Structural Stability and Dynamics*, 2012, **12**(2): 285-310.
- [211] Aoyagi M. and Tomikawa Y., Ultrasonic Motor Based on Coupled Longitudinal-Bending Vibrations of a Diagonally Symmetric Piezoelectric Ceramic Plate, *Electronics and Communications in Japan, Part II: Electronics*, 2007, **79**(6): 60-67.
- [212] Cardoni A. and Lucas M., Strategies for Reducing Stress in Ultrasonic Cutting Systems, *Strain*, 2005, **41**(1): 11-18.
- [213] Cardoni A. and Lucas M., Enhanced Vibration Performance of Ultrasonic Block Horns, *Ultrasonics*, 2002, **40**(1-8): 365-9.
- [214] Rani M. R. and Rudramoorthy R., Computational Modeling and Experimental Studies of the Dynamic Performance of Ultrasonic Horn Profiles Used in Plastic Welding, *Ultrasonics*, 2013, **53**(3): 763-772.

- [215] Wang D.-A., Chuang W.-Y., Hsu K. and Pham H.-T., Design of A Bézier-Profile Horn for High Displacement Amplification, *Ultrasonics*, 2011, **51**(2): 148-156.
- [216] Wang D.-A. and Nguyen H.-D., A Planar Bézier Profiled Horn for Reducing Penetration Force in Ultrasonic Cutting, *Ultrasonics*, 2014, **54**(1): 375-384.
- [217] Roşca I. C., Chiriacescu S. T. and Creţu N. C., Ultrasonic Horns Optimization, *Physics Procedia*, 2010, **3**(1): 1033-1040.
- [218] Deibel K.-R. and Wegener K., Methodology for Shape Optimization of Ultrasonic Amplifier Using Genetic Algorithms and Simplex Method, *Journal of Manufacturing Systems*, 2013, **32**(4): 523-528.
- [219] Fu B., Hemsell T. and Wallaschek J., Piezoelectric Transducer Design via Multiobjective Optimization, *Ultrasonics*, 2006, **44**(Supplement): e747-e752.
- [220] Heikkola E., Miettinen K. and Nieminen P., Multiobjective Optimization of An Ultrasonic Transducer Using NIMBUS, *Ultrasonics*, 2006, **44**(4): 368-380.
- [221] Miettinen K. and Mäkelä M. M., Interactive Bundle-Based Method for Nondifferentiable Multiobjective Optimization: NIMBUS, *Optimization*, 1995, **34**(3): 231-246.
- [222] Miettinen K. and Mäkelä M. M., Interactive Multiobjective Optimization System WWW-NIMBUS on the Internet, *Computers & Operations Research*, 2000, **27**(7-8): 709-723.
- [223] Porto D., Bourquard A. and Perriard Y., Genetic Algorithm Optimization for a Surgical Ultrasonic Transducer, *Ultrasonics Symposium*, 2008: 1457-1460.
- [224] Murphy J., Porto D. and Perriard Y., Ultrasonic Transducer Model for Optimization of A Spinal Tissue Ablation System, *Industry Applications Conference, 41st IAS Annual Meeting, Conference Record of the 2006 IEEE*, 2006, **1**: 379-384.
- [225] Kazimi S. M. A., *Solid Mechanics*, Tata McGraw-Hill, 1982.
- [226] Nievergelt J., Exhaustive Search, *Combinatorial Optimization and Enumeration: Exploring the Potential of Raw Computing Power, SOFSEM 2000: Theory and Practice of Informatics, Lecture Notes in Computer Science*, 2002, **1963**(2000): 18-35.
- [227] Goldberg D. E., *Genetic Algorithms in Search, Optimization, and Machine Learning*, Addison-Wesley Publishing Company, Inc., 1989.
- [228] Matlab R2008a Help Documentation, Optimization Toolbox, The MathWorks. Inc.
- [229] Abaqus 6.12 User's Manual, Dassault Systèmes Simulia Corp.
- [230] Haslinger J. and Mäkinen R. A. E., *Introduction to Shape Optimization: Theory, Approximation, and Computation*, Philadelphia, Society for Industrial and Applied Mathematics, 2003.
- [231] Mitchell M., *An Introduction to Genetic Algorithms*, London, The MIT Press, 1998.

- [232] Bertsimas D. and Tsitsiklis J., Simulated Annealing, *Statistical Science*, 1993, **8**(1): 10-15.
- [233] Kirkpatrick S., Gelatt C. D. and Vecchi M. P., Optimization by Simulated Annealing, *Science*, 1983, **220**(4598): 671-680.
- [234] Reeves C. R., *Modern Heuristic Techniques for Combinatorial Problems*, Oxford, Blackwell Scientific Publications, 1993.
- [235] Katsikadelis J. T. and Tsiatas G. C., Regulating the Vibratory Motion of Beams using Shape Optimization, *Journal of Sound and Vibration*, 2006, **292**(1-2): 390-401.
- [236] Zang C., Friswell M. I. and Mottershead J. E., A Review of Robust Optimal Design and Its Application in Dynamics, *Computers & Structures*, 2005, **83**(4-5): 315-326.
- [237] Niordson F. I., On the Optimal Design of a Vibrating Beam, *Quarterly of Applied Mathematics*, 1965, **23**(1): 47-53.
- [238] Kamat M. P. and Simites G. J., Optimal Beam Frequencies by the Finite Element Displacement Method, *International Journal of Solids and Structures*, 1973, **9**(3): 415-429.
- [239] Thambiratnam D. P. and Thevendran V., Optimum Vibrating Shapes of Beams and Circular Plates, *Journal of Sound and Vibration*, 1988, **121**(1): 13-23.
- [240] Karihaloo B. L. and Niordson F. I., Optimum Design of Vibrating Cantilevers, *Journal of Optimization Theory and Applications*, 1973, **11**(6): 638-654.
- [241] Gill P. E. and Murray W., *Numerical Methods for Constrained Optimization*, Academic Press Inc., London, 1974.
- [242] Fiacco A. V. and McCormick G. P., *Nonlinear Programming: Sequential Unconstrained Minimization Techniques*, John Wiley, New York, 1968.
- [243] Thambiratnam D. P., Thevendran V., Chang S. L. and Lee S. L., Maximization of Natural Frequencies of Cylindrical Shells, *Engineering Optimization*, 1988, **13**(2): 85-97.
- [244] Kamat M. P., Effect of Shear Deformations and Rotary Inertia on Optimum Beam Frequencies, *International Journal for Numerical Methods in Engineering*, 1975, **9**(1): 51-62.
- [245] Doltsinis I. and Kang Z., Robust Design of Structures Using Optimization Methods, *Computer Methods in Applied Mechanics and Engineering*, 2004, **193**(23-26): 2221-2237.
- [246] Messac A. and Ismail-Yahaya A., Multiobjective Robust Design Using Physical Programming, *Structural and Multidisciplinary Optimization*, 2002, **23**(5): 357-371.
- [247] Treece G. M., Gee A. H., Mayhew P. M. and Poole K. E. S., High Resolution Cortical Bone Thickness Measurement from Clinical CT Data, *Medical Image Analysis*, 2010, **14**(3): 276-290.
- [248] Frauchiger L., Taborrelli M. and Descouts P., Structural Characterization of Ti90Al6V4 alloy and Sulphur Segregation, *Applied Surface Science*, 1997, **115**(3): 232-242.

- [249] Mason W. P. and Wehr J., Internal Friction and Ultrasonic Yield Stress of the Alloy 90Ti6Al4V, *Journal of Physics and Chemistry of Solids*, 1970, **31**(8): 1925-1933.
- [250] Puškár A., Cyclic Stress-Strain Curves and Internal Friction of Steel at Ultrasonic Frequencies, *Ultrasonics*, 1982, **20**(3): 118-122.
- [251] Macdonald D. E., Ultrasonic Frequency Metal Fatigue: A Review of the Investigations of the Institute for the Study of Fatigue (Fracture) and (Structural) Reliability, *Engineering Fracture Mechanics*, 1976, **8**: 17-29.
- [252] Stanzl-Tschegg S., Fatigue Crack Growth and Thresholds at Ultrasonic Frequencies, *International Journal of Fatigue*, 2006, **28**(11): 1456-1464.
- [253] <http://www.morganelectroceramics.com/resources/guide-to-piezoelectric-dielectric-ceramic/>, Accessed 5th April, 2014.
- [254] He J. and Fu Z.-F., *Modal Analysis*, Butterworth-Heinemann, 2001.
- [255] <http://www.sawbones.com/products/bio/testblocks/solidfoam.aspx>, Accessed 15th Sep, 2012.
- [256] C.M. Langton and Njeh C. F., *The Physical Measurement of Bone*, Bristol and Philadelphia, Institute of Physics Publishing, 2004.
- [257] Nafei A., Danielsen C. C., Linde F. and Hvid I., Properties of Growing Trabecular Ovine Bone, Part I: Mechanical and Physical Properties, *The Journal of Bone & Joint Surgery (British Volume)*, 2000, **82**(6): 910-920.
- [258] Cory E., Nazarian A., Entezari V., Vartanians V., Müller R. and Snyder B. D., Compressive Axial Mechanical Properties of Rat Bone as Functions of Bone Volume Fraction, Apparent Density and Micro-CT based Mineral Density, *Journal of Biomechanics*, 2010, **43**(5): 953-960.
- [259] Rogers G. J., Milthorpe B. K., Muratore A. and Schindhelm K., Measurement of the Mechanical Properties of the Ovine Anterior Cruciate Ligament Bone-Ligament-Bone Complex: A Basis for Prosthetic Evaluation, *Biomaterials*, 1990, **11**(2): 89-96.
- [260] Eriksson A. R. and Albrektsson T., Temperature Threshold Levels for Heat-Induced Bone Tissue Injury: A Vital-Microscopic Study in the Rabbit, *The Journal of Prosthetic Dentistry*, 1983, **50**(1): 101-107.
- [261] Frölke J. P., Peters R., Boshuizen K., Patka P., Bakker F. C. and Haarman H. J., The Assessment of Cortical Heat during Intramedullary Reaming of Long Bones, *Injury*, 2001, **32**(9): 683-688.
- [262] Suresh S., *Fatigue of materials*, 2nd Edition, Cambridge University Press, 1998.
- [263] Bhat S. and Patibandla R., *Metal Fatigue and Basic Theoretical Models: A Review*, Alloy Steel - Properties and Use, Dr. Eduardo Valencia Morales (Ed.), 2011.